Stability and receptivity of idealized detonations

by

Carlos Chiquete

A Dissertation Submitted to the Faculty of the

Program in Applied Mathematics

In Partial Fulfillment of the Requirements
For the Degree of

Doctor of Philosophy

In the Graduate College

The University of Arizona

2 0 1 1

THE UNIVERSITY OF ARIZONA
GRADUATE COLLEGE

As members of the Dissertation Committee, we certify that we have read the dissertation prepared by Carlos Chiquete entitled
"Stability and receptivity of idealized detonations"
and recommend that it be accepted as fulfilling the dissertation requirement for the Degree of Doctor of Philosophy.

_____ Date: 6/2/2011
Anatoli Tumin

_____ Date: 6/2/2011
Michael Tabor

_____ Date: 6/2/2011
Edward Kerschen

_____ Date: 6/2/2011
Moysey Brio

Final approval and acceptance of this dissertation is contingent upon the candidate's submission of the final copies of the dissertation to the Graduate College.

I hereby certify that I have read this dissertation prepared under my direction and recommend that it be accepted as fulfilling the dissertation requirement.

_____ Date: 6/2/2011
Anatoli Tumin

Statement by Author

This dissertation has been submitted in partial fulfillment of requirements for an advanced degree at The University of Arizona and is deposited in the University Library to be made available to borrowers under rules of the Library.

Brief quotations from this dissertation are allowable without special permission, provided that accurate acknowledgment of source is made. Requests for permission for extended quotation from or reproduction of this manuscript in whole or in part may be granted by the copyright holder.

Signed: Carlos Chiquete

Dedication

Judy, Elías, y toda mi familia y amigos.

Acknowledgments

Many, many thanks go to my advisor Anatoli Tumin. Much of what I have learned in this work has been learned through him; his patience has been endless and his knowledge has been irreplaceable.

The fifth chapter in this dissertation was work that was carried out at Los Alamos National Laboratory in the Summer of 2009 and 2010. This work work was done under the direction of Dr. Mark Short in the Detonation Theory and Modeling group. The work appearing in Chapter 5 has LANL release number `LA-UR 11-03111`.

Summer 2007, Spring 2008, Summer 2008, Fall 2008, Spring 2010, and Fall 2010 research assistantships were funded by a grant from the National Science Foundation VIGRE (Vertical InteGration in Research and Education) program #0602173. The remaining semesters of my PhD years were funded by teaching assistantships (Spring 2009, Fall 2009 and Spring 2011) and research assistantships (Fall 2005- Spring 2006).

Table of Contents

Table of Contents—*Continued*

Table of Contents—*Continued*

Table of Contents—*Continued*

List of Figures

LIST OF FIGURES—*Continued*

List of Figures—*Continued*

List of Tables

Abstract

The linear receptivity and stability of plane idealized detonation with one-step Arrhenius type reaction kinetics is explored in the case of three-dimensional perturbations to a Zel'dovich-von Neumann-Döring base flow. This is explored in both overdriven and explicitly Chapman-Jouguet detonation. Additionally, the use of a multi-domain spectral collocation method for solving the conventional stability problem is explored within the context of normal-mode detonation. An extension of the stability analysis to confined detonations in a slightly porous walled tube is also carried out. Finally, an asymptotic analysis of a detonation with two-step reaction kinetics in the limit of large activation energy and for general overdrive and reaction order is performed yielding a nonlinear evolution equation for perturbations that produce stable limit cycle solutions.

Stability and receptivity of idealized detonations

Carlos Chiquete, Ph.D.
The University of Arizona, 2011

Director: Anatoli Tumin

The linear receptivity and stability of plane idealized detonation with one-step Arrhenius type reaction kinetics is explored in the case of three-dimensional perturbations to a Zel'dovich-von Neumann-Döring base flow. This is explored in both overdriven and explicitly Chapman-Jouguet detonation. Additionally, the use of a multi-domain spectral collocation method for solving the conventional stability problem is explored within the context of normal-mode detonation. An extension of the stability analysis to confined detonations in a slightly porous walled tube is also carried out. Finally, an asymptotic analysis of a detonation with two-step reaction kinetics in the limit of large activation energy and for general overdrive and reaction order is performed yielding a nonlinear evolution equation for perturbations that produce stable limit cycle solutions.

Chapter 1
Introduction

Detonations are supremely violent combustion-driven shock waves that travel at supersonic speeds on the order of kilometers per second. The detonation wave front is self-propagating in liquid, solid and gaseous explosives and translates away from its ignition source transforming reactants into products and therefore releasing the potential energy stored in the molecular bonds of the reactants. The exothermic heat release of the reaction is transferred to both internal and kinetic energy and thus triggers sharp gradients in the thermodynamic state. These steep variations ultimately result in the self-propagation of the phenomenon.

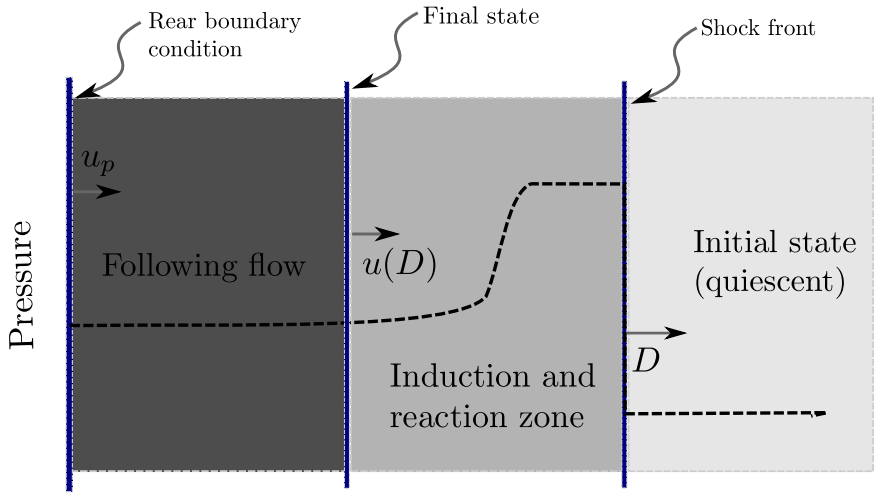

Figure 1.1. The structure for a largely planar detonation as it propagates into an explosive mixture. Note that the particle velocity of the products in the final state is in the direction of the overall motion of the wave. The following flow depends on the nature of the rear boundary condition.

The material that traverses the detonation wave undergoes a rapid transition from reactant to product. Specifically, the explosive material is in an initial state

unperturbed by the incoming supersonic detonation wave. Ignition of the reactants is achieved as the leading shock front adiabatically compresses the material greatly increasing the number of intra-molecular collisions. An "induction zone" follows the state that immediately follows the front where the reactants are disassociated and free radical species are produced. The variation in the thermodynamic state is usually small in this phase. Subsequently, recombination reactions occur which release the exothermic energy stored in the reacting material. The inevitable increase in temperature forces the pressure and density to decrease in this "reaction zone" which provides the forward thrust to the shock front. The detonation wave then continues to ignite fresh explosive material as it surges forward.

Every story has a beginning and for detonation it is in 1869 that Abel [1] measured the velocity of detonation in explosive charges of gun-cotton, or nitrocellulose. Some 14 years later, Berthelot and Vielle [2] systematically measured the velocity of detonations in various gaseous mixtures (usually consisting of fuel, oxidizer, and dilutant). The existence of various modes of combustion, i.e. transition from deflagration to detonation was observed by Mallard and Le Chatelier [3] in 1883. Thus, by the end of 19th century, the role of the adiabatic compression precipitated by the shock front was recognized and the clear distinction between deflagration (a subsonic combustion wave) and detonation was also identified.

1.1 The simplest theory

The main priority of early researchers of the phenomena was to obtain a criterion for selection the detonation velocity. The theoretical framework to find a suitable criterion was laid down by Donald L. Chapman [4] and Emile Jouguet [5] in the late 1800's and early in the subsequent century. These researchers based their approach on the pioneering work Rankine [6] and Hugoniot [7] carried out in analyzing the conservation equations across a non-reacting or inert shock wave. Chapman and

Jouguet modified this theory by including the chemical energy released due to the reaction. It is worth pointing out that Mikelson did much of the same work as Chapman and Jouguet but his dissertation work was largely unknown outside of Russia [8].

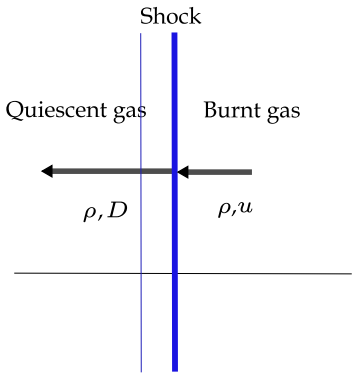

FIGURE 1.2. A schematic showing the Chapman-Jouguet (CJ) theory's main assumptions: leading compressive shock that immediately consumes the fuel or reactant directly preceding it. The process is assumed to occur instantaneously given the short observed detonation reaction zone thicknesses (on the order of millimeters) and the high velocity of the detonation (km/s).

The simplest theory relies on the conservation equations for fluids in the integral form. It is assumed that the material undergoes a three stage process: initial unperturbed state, compression to the post-shock state, and finally a transition to the reaction product final state. Using the schematic pictured in Fig. 1.2, the conservation of mass, momentum and energy can be written down across the shock connecting the different stages of the material that enters the detonation. The usual symbols are used, i.e. pressure, p, volume, v, density, ρ, and D is the velocity of the detonation and u is the particle velocity. The subscript "0" refers to the initial state in front the detonation.

- Mass

$$\rho_0 D = \rho(D - u)$$

- Momentum

$$p - p_0 = \rho_0 u D$$

- Energy
$$e + pv + \frac{1}{2}(D-u)^2 = e_0 + p_0 v_0 + \frac{1}{2}D^2$$
where the energy is assumed of the form appropriate for ideal gases, i.e. $e = pv/(\gamma - 1) - \lambda Q$.

In the preceding, the heat release is Q, γ is the specific heats ratio and $\lambda \in [0,1]$ is the reaction progress variable. Eliminating the particle velocity variable from the conservation relations leads to the hyperbolic Hugoniot curves and the Rayleigh line whose slope depends on the detonation velocity D. If the initial state is assumed known, the possible post-shock states and final post-reaction states can be determined from the following two equations involving the pressure and volume labeled as the Rayleigh line and the Hugoniot curve, respectively,

$$\mathcal{R} = \rho_0^2 D^2 - (p - p_0)/(v_0 - v) = 0, \text{ and} \tag{1.1.1}$$

$$\mathcal{H} = e(p, v, \lambda = 1) - e(p_0, v_0, \lambda = 0) - (1/2)(p + p_0)(v_0 - v) = 0. \tag{1.1.2}$$

Due to the increase in energy obtained via the heat release of the reaction (mathematically manifested as upward translation of the Hugoniot curves), there is a minimum value of D required to satisfy the conservation relations. The pv plane with the relevant curves are presented in Fig. 1.3. A continuous spectrum of detonation velocities above the minimum value is also revealed. The downstream state for pressure and density however is multivalued for the detonation velocities above the minimal value, and the two possible intersection points are termed 'strong' and 'weak' detonation whereby the higher density and pressure corresponds to the 'strong' case. Notably, in the case that the detonation velocity is the minimum then the strong and weak cases converge to a single state.

The main theoretical goal of the early researchers was to secure a criterion for selecting the correct detonation velocity. This was provided by both Chapman [4] and Jouguet [5] but through different avenues: Chapman simply posited that the detonation velocity should be the minimum and Jouguet discovered the minimum

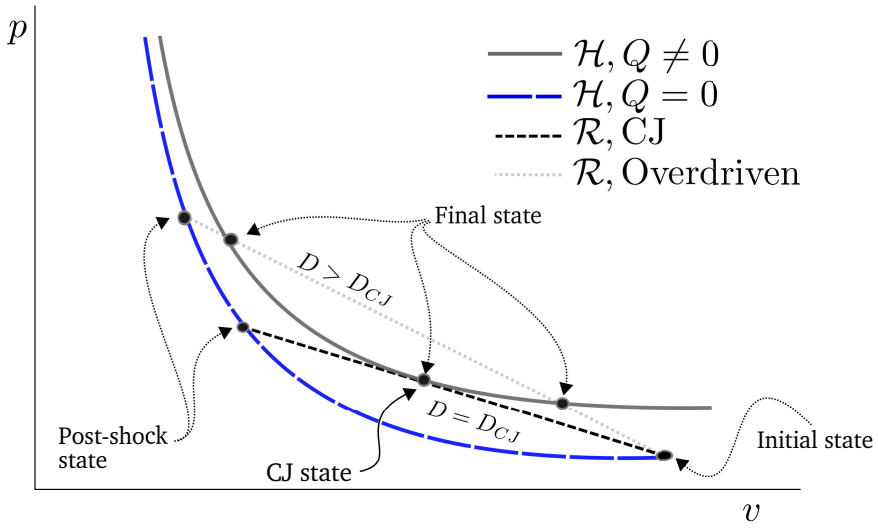

FIGURE 1.3. A schematic showing the Hugoniot and Rayleigh lines. Their intersection represents valid end and post-shock states. Note that for detonation speeds in excess of the D_{CJ} minimum have two valid possible end states on the upper Hugoniot curve. This is the origin of the *weak* and *strong* detonation distinction.

velocity was attached to the state corresponding to the minimum change in entropy. The corresponding end or product state becomes a sonic point in the CJ case. The remarkable result of these equivalent assumptions is that the detonation velocity agrees to within a few percent of observed experimental values [9]. It is however worthwhile to point out that the CJ criterion is not complete as it lacks a rigorous physical and mathematical argument.

Eliminating the strong detonation in the unsupported case. Specifically, the CJ criterion accurately predicts the detonation velocities observed in *freely propagating* or *unsupported* detonations. These are detonations where the following flow is not supported by a driving piston motion as in the case of a rigid wall in the rear of the detonation. How to eliminate the 'strong' or 'weak' detonations in favor of the CJ detonation in these cases was the object of much early investigation. Specific to the planar detonation case, a physical argument was developed in order to eliminate the *strong* branch of the detonation velocities. In the case of unsupported detonation,

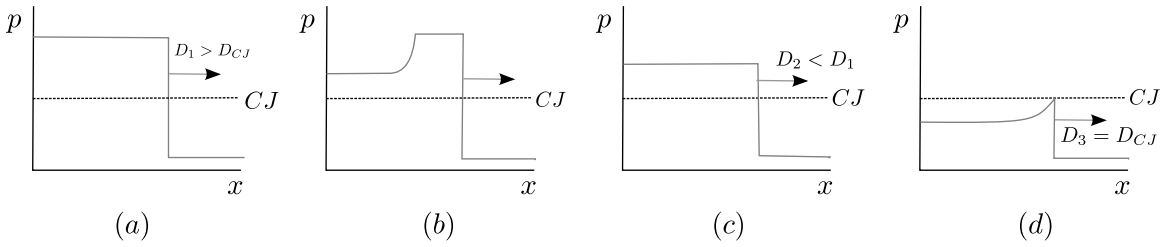

FIGURE 1.4. In the different stages above, D_1, D_2 and D_3 are the particular detonation velocities. (a) The pressure profile in an established 'strong' detonation wave with velocity greater than the CJ state. Note that the velocity at the front is subsonic. (b) Due to the subsonic product end state, expansion waves from the rear of the detonation in unsupported detonation can reach the shock front. (c) The expansion wave reduces the pressure to a new value in the end product state, necessarily modifying the detonation shock front velocity. (d) Further reductions end at the CJ state point since the expansion can no longer catch the end product state which is then sonic.

if a detonation has a speed greater than the CJ minimum then it has an associated final state which is subsonic (in the 'strong' intersection case). This fact exposes the detonation to expansion waves that travel from the rear of the detonation into the reaction zone directly behind the detonation (see Fig. 1.4). This necessarily affects the final state of the reaction zone and thus must modify the detonation velocity itself. After a certain transient period, the detonation velocity must be attenuated to match the new pressure brought about by the arriving expansion wave and this process continues until the minimal CJ velocity is reached. The corresponding CJ end state is sonic and any expansion wave can no longer surpass this point as no characteristic exists that can propagate towards the front. The strong detonation state therefore cannot persist. Eliminating the weak counterpart is more difficult and motivated subsequent work in incorporating a detailed reaction zone structure into the theory.

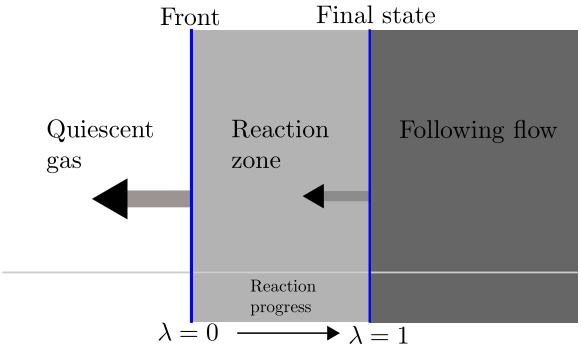

FIGURE 1.5. A schematic showing the ZND theory's main assumptions: leading compressive shock that initiates the reaction which is completed at a finite rate.

1.2 The Zel'dovich-von Neumann-Döring theory

Excluding the weak detonation. In 1942, John von Neumann [10] introduced the concept of a reaction progress variable which signifies the degree of completion of the reaction (commonly parametrized by λ). Von Neumann was able to show that unless these curves intersect in the pv plane then there is no path from the initial state of the explosive to the end weak state. In other words, if the reaction proceeds only in the forward direction then the partial Hugoniot curves do not intersect and graphing a selected number of these curves as in Fig. 1.6 shows that there is no possible path that leads from the post-shock state down to the weak intersection point. If these partial reaction states do intersect then one can then obtain a path to the weak state and then obtain a so-called pathological detonation but this latter case is only achievable for certain explosives. This argument essentially shows that the weak intersection is invalid for freely propagating detonations with a reaction that proceeds forward only i.e. $[Reactant] \rightarrow [Product]$. The pathological case is beyond the scope of the present work.

Along with von Neumann (1942) [10], both Yakov B. Zel'dovich (1940) [11] and Werner Döring (1943) [12] independently obtained a model incorporating the reaction zone structure following the compressive leading shock front. Zel'dovich specifically

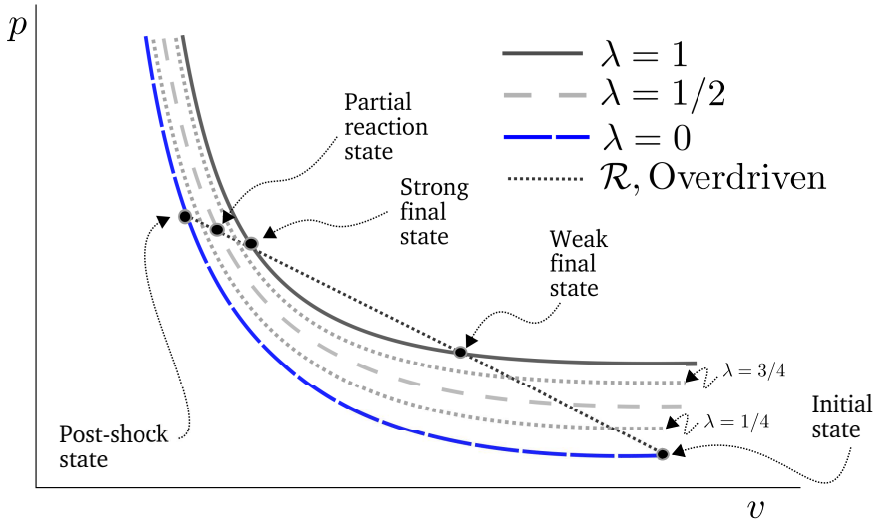

FIGURE 1.6. Adding partial reaction Hugoniot curves to the simple theory represented in Fig. 1.3 provides the criterion for elimination of the 'weak' solution since there is no path along the Rayleigh line from the post-shock state down to the weak state. The reaction is parametrized here by λ which progresses from 0 to 1 monotonically.

generalized the CJ criterion to a requirement of regularity at the sonic singularity inherent to the freely propagating detonation. Döring defined a model for the reaction and integrated the conservation equations in the reaction zone, obtaining the thermodynamic state profiles. The one-dimensional and steady model that incorporates a shock followed by a finite-rate chemical reaction is known as the Zel'dovich-von Neumann-Döring (ZND) model. The ZND model clarifies the mechanism for the propagation, i.e. an adiabatic compression brought about by the shock front which in turn is maintained by the thrust generated by the reaction zone expansion of the explosive fuel.

The possible configurations for a planar detonation are diagrammed in Fig. 1.7. In addition to the aforementioned CJ case, a detonation where the rear boundary condition includes a hypothesized piston prescribing a velocity greater than the minimal CJ final state velocity is termed overdriven detonation. In contrast to the freely propagating or unsupported detonation, the imposed rear boundary condition is con-

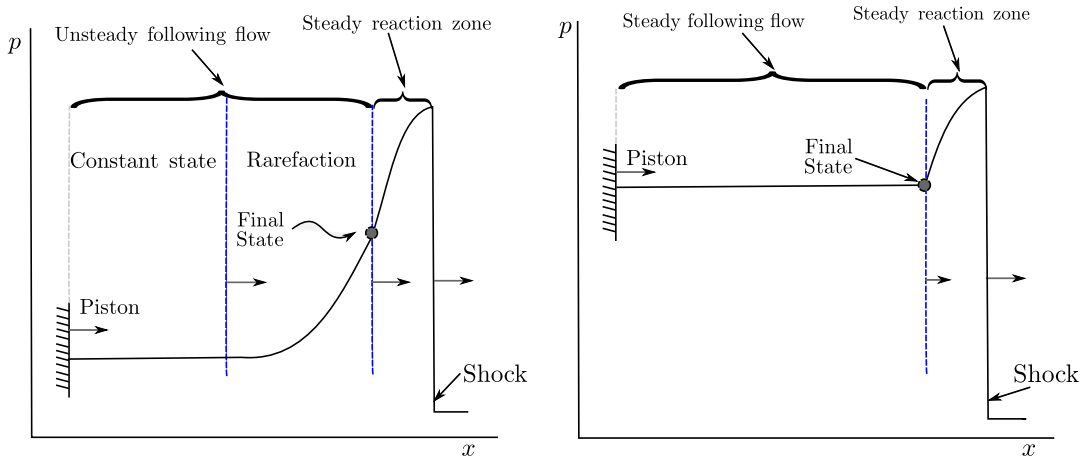

(a) Unsupported (b) Overdriven

FIGURE 1.7. (a) Diagram showing the detonation wave structure with the hypothetical piston following the steady flow. In this case the flow is sonic (and $D = D_{CJ}$) at the final state but a rarefaction wave connects the final state to the constant state that arises from the back boundary condition. (b) The overdriven case where the back boundary condition sets the pressure at the final state and thus the detonation velocity which is then larger than the minimum velocity, i.e. D_{CJ}.

nected to the final state of the reaction zone via a steady constant state. This imposes the velocity of the detonation so as to realize this prescribed reaction zone final state. The weak intersection is inaccessible based on the same argument used to exclude it in the unsupported case. The strong intersection is therefore accessible under the influence of this external forcing.

1.3 Estimate of reaction zone length and Reynolds number

In order the justify the forthcoming choice for the governing equation system for modeling the detonation phenomenon, the relevant scale of the reaction zone in such a process can be estimated in a simple way via an approximate order of magnitude argument. The relevant length scale can then be used to provide an estimate of the Reynolds number, a key indicator for the influence of diffusive processes. The full Navier-Stokes equations can then be considerably simplified in the event that the

Reynolds number is large.

Firstly then, one assumes that in order for two gas particles to release their stored chemical energy, a certain minimal energy collision is necessary. Assuming that the probability of a collision in a combustible gas mixture at a certain energy $\tilde{E}$ (kcal/mol), universal gas constant $\tilde{R}_u$, and temperature $\tilde{T}$ is calculable from the Boltzmann distribution law,

$$P \sim \exp(-\tilde{E}/\tilde{R}_u\tilde{T}), \tag{1.3.1}$$

then to obtain such an energetic event one would on average expect to wait for $N_{col} = \exp(\tilde{E}/\tilde{R}_u\tilde{T})$ molecular collisions. One can estimate the time $\tilde{\tau}_{col}$ required to observe N_{col} collisions by appealing to the mean free path $\tilde{a}_s$ and the average velocity of a gas molecule, $\bar{c}_{mol}$. Since the velocity of the molecules is on the order of the velocity of sound in the mixture $\tilde{c}_s$, then

$$\tau_{col} \sim N_{col}\frac{\tilde{a}_s}{\bar{c}_{mol}} \sim \frac{N_{col}\tilde{a}_s}{\tilde{c}_s}. \tag{1.3.2}$$

To obtain the relevant length scale $\tilde{\Delta}$ for the reaction zone length, one can determine the distance that will be traveled by a molecule in the time it will take to react, i.e.

$$\Delta \sim \bar{c}_{mol}\tilde{\tau}_{col} \sim \tilde{c}_s\frac{N_{col}\tilde{a}_s}{\tilde{c}_s} = N_{col}\tilde{a}_s = \tilde{a}_s\exp(\tilde{E}/\tilde{R}_u\tilde{T}). \tag{1.3.3}$$

The mean free path $\tilde{a}_s$ behind the shock can be correlated to the quiescent gas mean free path $\tilde{a}_{qg}$ as it depends inversely on density, $a_s \sim \frac{1}{\rho_s}$. The ratio of these lengths across the shock can be obtained, namely $\tilde{a}_s/\tilde{a}_{qg} = (\gamma-1)/(\gamma+1)$ (γ is the specific heats ratio). Therefore for a typical set of energy, temperature, γ and $\tilde{a}_{qg}$ scales,

$$\tilde{E} = 50 \text{ kcal/mol},\ \tilde{T} = 2000 \text{ K},\ \tilde{a}_{qg} = 10^{-5} \text{ m}, \text{and } \gamma = 1.2, \tag{1.3.4}$$

One estimates that $\tilde{\Delta} = 2.6$ mm. This estimate leads to the calculation of the relevant Reynolds number of the flow and thus, the proper approximation (if any) of the full Navier-Stokes equations that applies. Therefore,

$$Re = \frac{\bar{u}_s\tilde{\Delta}}{\tilde{\nu}_s} \sim \frac{\tilde{c}_s\tilde{\Delta}}{\tilde{\nu}_s} = \frac{\tilde{\Delta}}{\tilde{\nu}_s/\tilde{c}_s} \tag{1.3.5}$$

where $\tilde{u}_s$ is the speed of the mixture behind the shock. The relevant viscosity length scale $\tilde{\nu}_s/\tilde{c}_s$ is of order of the mean free path so it implies that

$$Re \sim \frac{\tilde{\Delta}}{\tilde{a}_s} = \mathcal{O}(10^5) \tag{1.3.6}$$

This large value means one can neglect viscosity or diffusion in the governing equations in the bulk of the fluid, and therefore the Euler equations of motion are chosen to model the detonation wave dynamics.

1.4 Stability analysis

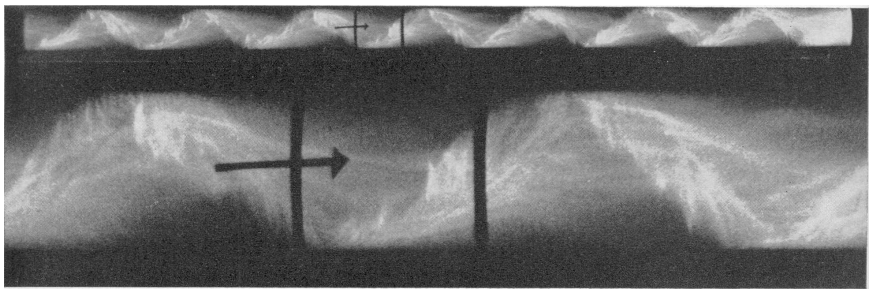

FIGURE 1.8. Photograph showing spinning detonation phenomenon as obtained by G.L. Schott in 1965[13] with its characteristic helical path.

The steady-state one-dimensional theory described up to this point only really holds in an approximate average sense. In actual experiments, most detonation fronts are observed to be intrinsically unstable having three-dimensional transient structure though the overall detonation velocity does maintain a remarkably close correspondence to the one-dimensional CJ equilibrium values that result from the theoretical analysis of the simple theory [9]. This unsteady fine structure began to be detected in the 1920's and 1930's owing to new high-speed streak photography. A remarkable phenomenon observed starting in 1926 by Campbell and Woodhead [14] is that of spinning detonation. The evidence gathered centered on an intense local chemical reaction near the tube wall which travels circumferentially and therefore traces a helical path as the detonation propagates. The frequency of the spin is close to constant

and further theoretical and experimental studies clarified its role in sustaining detonation near the "detonability limits", i.e. conditions that are close to extinguishing the detonation. As John H.S. Lee states, spinning detonation seems to be "nature's last resort for maintaining the detonation mode of combustion for most mixtures" [15]. The spin detonation regime only hints at the rich complexity of the detonation phenomenon. However, notwithstanding its simple nature, the stability analysis of the one-dimensional ZND model has provided valuable information in clarifying the array of experimental results.

The hydrodynamic stability analysis of detonations begins around 1960. Schelkin in 1959 [16] and subsequently Zaidel in 1961 [17] studied the stability properties of the so-called square-wave model of detonation. This model mimics the induction zone observed in detonations where a nearly constant thermodynamic state follows the leading shock. However, within this model, the reaction is then completed immediately after the induction zone, i.e. a reaction zone of negligible length. The stability analysis showed that the detonation was unstable in this limit as the eigenspectrum that defines the stability is composed of an infinite, enumerable set of unstable modes with large temporal growth rates. The simplicity of the square-wave model probably explains its early adoption in stability analysis of detonations.

The implementation of the general ZND model into stability studies was initiated by J. J. Erpenbeck in 1962 [18]. Therein, the author formulated the stability problem as an initial-value problem for the linearized reactive Euler equations, solved with the help of the Laplace transform with respect to time. Erpenbeck showed that the solution may have poles in the right-hand side of the Laplace variable plane, which means that the flow is unstable. Although the dispersion relation for the poles was formulated explicitly in terms of integrals and functions obtained from solutions of ordinary differential equations, the method has not been used for numerical studies of the spectrum. Instead of directly solving the dispersion relation numerically, Erpenbeck used the 'principle of the argument' in order to establish the existence of the

poles in the case of idealized one-reaction detonations [19] (more references relevant to the early stages of the stability theory of detonations are given by Fickett & Davis [9] and F.A. Williams [20]). Although Erpenbeck's solution of the initial-value problem for partial differential equations (PDE's) provides complete information about the flow physics (dispersion relation, properties of continuous and discrete spectra, initial amplitudes of the normal modes), the approach was not pursued after Erpenbeck's foundational work.

1.4.1 Instability mechanism

After Erpenbeck's work, a number of asymptotic studies in detonation stability were carried out, notably in the limit of large activation energy. G.E. Abouseif and T.Y. Toong [21] provide a description of the instability mechanism in this limit and is referred to as the wave-interaction model (also proposed in [22]). The concept is illustrated in Fig. 1.9. Essentially, acoustic perturbations are generated in the fast

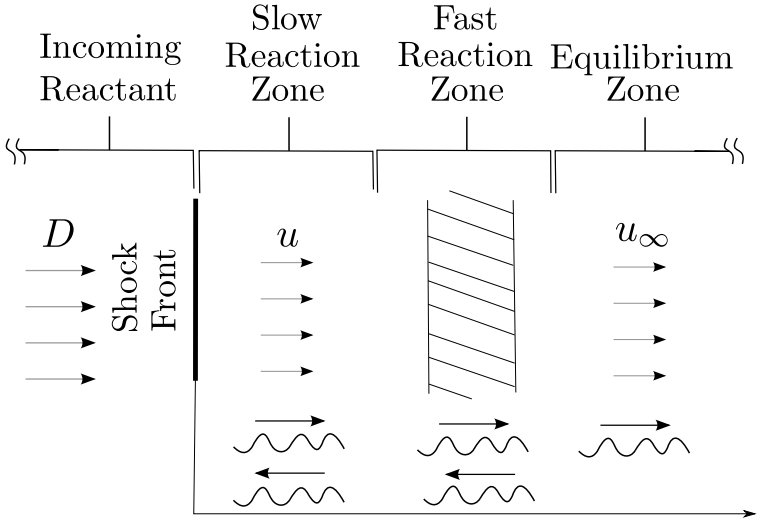

FIGURE 1.9. A representative schematic of the wave-interaction instability mechanism due to Abousief and Toong [21].

reaction zone that develops after the slowly reacting induction zone typical of most

detonations. These perturbations travel upstream and downstream of this zone and crucially towards the shock front where they are reflected as acoustic and irreversible temperature perturbations that travel back towards the fast reaction zone. These temperature perturbations are specially important in the reaction rate which is specially sensitive to temperature fluctuations and thus will generate yet more perturbations in the fast reaction zone. These in turn, generate yet more upstream acoustic disturbances that travel to the shock and the cycle of instability is complete. The analysis is carried out in the limit of high activation energy since there is a pronounced constant state in the induction zone and a thin reaction zone. This structure specifically facilitates the mathematical analysis of the traveling waves in the slow reaction zone with respect to calculating the reflection coefficients of the perturbations at the shock.

1.4.2 Normal modes

Systematic studies of the discrete spectrum in a variety of gaseous detonation stability problems started with the normal mode approach by Lee & Stewart [23] in 1990. (Pukhnachev [24] was probably the first to use the normal-mode analysis, particularly for the stability of Chapman-Jouguet detonation confined in a tube.) In the normal-mode analysis, the solution of the linearized Euler equations for a reacting gas is considered time dependent as $\exp(\tau t)$, where τ has to be determined. This leads to an inhomogeneous system of linear differential equations in the shock-wave coordinates. In [23], the system of conservation equations are integrated, starting with the post-shock values ($x = 0_+$) for the velocity, pressure, specific volume, and reaction progress variable perturbations. At the end of the reaction zone (formally $x \to \infty$ in a reaction governed by the first order Arrhenius rate), the solution's boundedness constraint was formulated as an algebraic relation for the perturbations. This constraint served as the dispersion relation, solved with the help of a shooting algorithm in order to find the eigenvalue τ. Later on, the normal-mode approach was utilized in a number of

problems [25, 26, 27] including detonations in pipes and a variety of reaction rates. A review of the literature appears in [28].

In terms of the conventional stability analysis, one should keep in mind the rationale underlying the normal-mode analysis. It is assumed that there is a complete set of eigenfunctions, and a solution of the PDE's (e.g., the linearized Euler equations for a reacting gas) can be presented as an eigenfunction expansion. If there is an unstable mode, one may expect that solution of the PDE may possess the unstable behavior as well. However, the projection of a specific initial perturbation on a basis comprised of the eigenfunctions may not necessarily include the unstable mode. In other words, the normal-mode analysis substitutes solving a real physical problem with a study of the elements of the basis (eigenfunctions) without a complete discussion as to their weights in an actual physical set-up (the study of this question is termed the receptivity problem). In addition, many hydrodynamic stability problems (including stability of detonations) are associated with a non-self adjoint operator, i.e. a non-Sturm-Liouville type of boundary-value problem. The latter means that in order to establish a completeness of the eigenfunction system and to find the coefficients in the eigenfunction expansion, one has to solve the original physical problem formulated in terms of PDE's.

The normal-mode analysis was the preeminent feature of conventional hydrodynamic stability theory before it was recognized that the receptivity problem is also an important element of the flow response [29, 30]. The analysis requires the solution of PDE's, and a possible formulation is the initial-value problem where one specifies the initial profile of the perturbation flow. Using the Laplace transform with respect to time leads to a simplified set of equations and a formal solution in the transformed space. Naturally, the inverse transform is needed in order to capture the time evolution of the perturbations. A detailed analysis of the inverse Laplace transform can provide expansion of the solution into normal modes of discrete and continuous spectra. This expansion ultimately shows that the two approaches are

equivalent in terms of determining the temporal stability. Furthermore, the weights of these discrete modes represent the receptivity of the flow to the particular initial perturbation field. As an example of this concept, Forgoston & Tumin [31] investigated the initial-value problem in hypersonic boundary layers. This type of analysis was not completed by Erpenbeck in [18] and [19] since the main interest at that time was in the singularities associated with the unstable modes. In the unbounded case, Tumin [32] completed the relevant receptivity analysis for 1D perturbations of the overdriven idealized detonation model.

1.5 Motivation and structure of dissertation

One of the main motivations of the present work is to rehabilitate the IVP approach for the stability analysis of idealized detonations. As Lee and Stewart state in their 1990 seminal paper [23],

> It is fair to say that Erpenbeck's method [IVP] is hard to implement and it does not give a computationally direct way to determine the stability boundaries or the dispersion relation that defines the unstable modes.

Chapter 1 is part of an effort to show that the IVP method does provide all the relevant stability information. Additionally, the work here aims to highlight the distinct advantage of the IVP approach which provides the initial amplitudes of the unstable modes and thereby can provide additional physical insight from the linear stability analysis. The first chapter of this dissertation defines the initial value problem for 3D perturbations in a planar unbounded detonation and explores several instances of the receptivity analysis. This work is published in [33].

The second chapter is an extension to CJ detonation of the IVP problem for transverse perturbations. Stability analyses often treat the CJ case as a special limiting case of overdriven detonation in order to avoid analytical difficulties that arise near the rear sonic state. The end of the reaction zone represents a singular point of the

governing equations for the perturbations. An explicit treatment of this was achieved in 1997 by G.J. Sharpe [34] in the normal mode context. There has been a long-standing confusion of the applicability of the IVP approach in this case as Sharpe states in his paper [34],

> Erpenbeck's method is not applicable to Chapman-Jouguet (CJ) detonation because of analytical difficulties involved in this case, and does not give any information about the linear growth rates and frequencies of the perturbations.

In Chapter 2, it is shown that the CJ case can indeed be treated via the IVP approach in the same manner as in overdriven detonation and provides the relevant stability information as well. The analytical difficulties that Sharpe highlights can be overcome in a similar manner to the normal-mode approach. This work appears in [35].

The conventional stability analysis in detonations relies heavily on shooting algorithms to solve two-point boundary value problems in determining the eigenvalues and eigenfunctions that define the stability of a specific detonation. There is an alternative method incorporating spectral decomposition of the perturbations which provides the entire spectrum in a single calculation eliminating the need to provide initial guesses or the "carpet-search" of the complex plane inherent in the shooting approach. There have been a handful of cases [36, 37] in detonation stability where these methods are applied but they have not found broad application. In Chapter 3, a multi-domain method is used in the calculation of the stability properties of a recent condensed phase reaction model of an idealized detonation. This work appears in [38].

In Chapter 4, a stability analysis is carried out taking into account slightly porous walls in an idealized detonation confined to a circular pipe. The analysis is carried out using the normal mode approach and corrections are obtained to the underlying impenetrable wall case stability results in the slight porous wall case. Experimental

[39, 40] and full numerical studies [41] have been carried out within this configuration showing that the porosity attenuates the transverse instability that often develops in confined detonations. To our knowledge, no linear stability analysis exists within this setting and Chapter 4 addresses this gap for slightly porous walls. This work appears in [42].

Finally, the analysis in the first four chapters is confined to a simple one-step Arrhenius reaction rate and to explicitly linearized governing equations. In Chapter 5, an asymptotic procedure is used to obtain nonlinear governing equations in time for perturbations to a detonation modeled with an explicit two-step reaction rate. The asymptotically derived set of PDE's are solved analytically through an iterative approximate procedure to yield a single evolution equation in time for the detonation velocity perturbation revealing decaying stable oscillations as well as bounded unstable 1D pulsations. The results appear in [43].

1.6 Summary

The current work takes place within the context of the hydrodynamic stability theory for detonation waves. The general hydrodynamic stability theory has its beginnings in the the shear flow studies of the mid-18th century with foundational contributions from Helmholtz, Kelvin, Rayleigh, Orr, and Sommerfeld (see Drazin and Reid [44]). Obtaining the unstable modes of these flows formed the main impetus for the theory for many years before it was recognized that the receptivity problem was also a key component of the flow dynamics. How unstable mode amplitudes are excited within a physical set-up forms the basic question of the receptivity analysis. A canonical receptivity analysis is that of the laminar boundary layer where it was found that the interaction between sound disturbances and leading edge roughness contributes to the growth of the downstream unstable modes known as Tollmien-Schlichting waves [45]. One of the major motivations and contributions of this work is the incorporation and

extension of this type of analysis to the case of idealized detonations.

In addition to the receptivity issue, the current work contributes to the conventional stability theory for detonations as well. The numerical advantages of multi-domain spectral collocation methods with respect to the conventional "carpet search" algorithm are demonstrated via the solution of the two-point boundary value problem that usually defines the stability of a detonation flow. A novel linear stability analysis is also performed in the context of an idealized detonation in a porous-walled circular pipe. The expected effect is to observe attenuation of the unstable transverse modes as observed in experiments. Finally, the non-linear stability of detonations is also treated via an evolution equation that reproduces the one-dimensional pulsating instability observed in numerics and experiments for varying reaction order and overdrive. This work helps in clarifying the instability mechanism of detonations having a two-tiered reaction kinetic structure. The unifying theme of the current work is an effort to use the hydrodynamic linear and non-linear stability theory to better understand the detonation phenomenon.

Chapter 2
Receptivity of 3D perturbations in an idealized detonation

2.1 Introduction

The stability of idealized one-reaction detonations with one-dimensional perturbations was revisited in Ref. [32]. The solution of the initial-value problem (IVP) was presented as an expansion into the modes of discrete and continuous spectra. The result provides a convenient tool for prediction of initial amplitudes of the unstable modes depending on the initial perturbation field. It was shown that the spectrum stemming from the solution of the initial-value problem is equivalent to the spectrum of the conventional normal-mode approach. In other words, the results of Ref. [32] rehabilitated Erpenbeck's approach to stability analysis of detonations.

The main objective of the present chapter is to extend the results of Ref. [32] to the case of three-dimensional perturbations in idealized plane one-reaction detonations. For clarity of presentation, the steady-state ZND solution that one can find, for example, in Refs. [18, 23, 25, 26] is repeated in the following and the alternative stability analysis based on the normal mode approach is introduced as well.

2.2 The governing equations

The present work focuses on a detonation propagating in an ideal gas that participates in a first-order, irreversible reaction without mole and specific heat change. It means that the gas constant, R_g, and the specific heat ratio or isentropic derivative, γ, are the same in the free quiescent gas and in the reaction zone. This is reasonable in the limit where explosive mixtures are diluted with non-reacting components such as

Argon. In the present work, three-dimensional perturbations will be sought to the one-dimensional base flow obtained through the ZND model of detonation with Arrhenius one-step reaction kinetics. The continuity, momentum, energy, and reaction progress equations in the lab frame are as follows:

$$\begin{aligned} &\frac{Dv}{Dt} - v\nabla_l \cdot \mathbf{u}^l = 0 \\ &\frac{D\mathbf{u}^l}{Dt} + v\nabla_l \cdot p = 0 \\ &\frac{De}{Dt} + p\frac{Dv}{Dt} = 0 \\ &\frac{D\lambda}{Dt} = r \end{aligned} \tag{2.2.1}$$

where, v,p and $\mathbf{u}^l$ are the specific volume, pressure and velocity respectively; $D/Dt = \partial/\partial t + \mathbf{u}^l \cdot \nabla$ is the substantial derivative; sub- or superscript "l" indicates the lab frame. The specific energy for an ideal polytropic gas is $e = pv/(\gamma - 1) - \lambda\tilde{Q}$, where λ is the reaction progress variable ($0 \leq \lambda \leq 1$) and $\tilde{Q}$ is the heat release. The reaction rate is assumed in the form $r = \tilde{k}(1-\lambda)\exp(-\tilde{E}/R_gT)$, where $\tilde{E}$ is the activation energy, T is the temperature, and $\tilde{k}$ is a constant. The system of equations is supplemented by the equation of state for an ideal gas, $pv = R_gT$. The shock wave is considered as a traveling discontinuity with Rankine-Hugoniot jump conditions for the thermodynamic variables.

The conventional scaling is used as in Refs. [23, 25, 26]. Specific volume, v_s, pressure, p_s, and speed of sound behind the shock, c_s, are used as the dimensional scales for the physical variables. The half-reaction zone length, l_c, is chosen as the characteristic length scale. The time scale is $t_c = l_c/c_s$.

2.2.1 Formulation of the ZND theory

The ZND theory is fundamentally a steady, one-dimensional model for planar detonation formulated in the shock frame of reference. The theory was developed in the early 1940's independently by Yakov B. Zel'dovich (1940), John von Neumann

(1942), and Döring (1943) as mentioned in the previous chapter. The detonation wave propagates in a combustible gaseous mixture with an Arrhenius reaction rate.

In general, the essential assumptions regarding the ZND theory that are used throughout this work are as follows:

- the flow is one-dimensional,
- the shock is considered as a discontinuous jump in the thermodynamic variables due to the neglect of transport effects such as conduction or diffusion,
- the gas or the thermodynamic variables are in equilibrium except for the chemical composition of the gas,
- and λ (a reaction progress variable) progresses from zero (ahead of the shock) at a finite rate through the reaction zone behind the shock. Additionally, the reaction will be irreversible and only progresses in one direction.

These assumptions produce the steady structure (in the detonation wave frame) throughout the region of space where the reaction takes place.

This structure of the steady state can be summarized for example in Fig. 1.5. The gaseous detonation is split into three major zones in the current context:

- the *quiescent* gas in front of the shock wave (which travels at some speed $\tilde{D}$ to the left in the schematic),
- the *reaction* zone immediately behind the shock,
- and the *burnt* gas zone which lies at the end of the reaction zone, i.e. the point where the fuel is finally and completely burnt.

One of the fundamental differences with the simplest or CJ theory is that the reaction takes place over a non-zero extent in length. Recall that the CJ model assumed that

the reaction was completed immediately following the shock. The incorporation of a finite reaction rate produces the three zones of the ZND model outlined above.

However, as in the simplest theory, the shock wave is considered as an infinitely thin, unbounded planar surface with Rankine-Hugoniot jump conditions which are due to the conservation of mass, momentum and energy across the shock surface. If one imagines attaching the coordinate system in the frame of reference moving along with the shock (say at speed $\tilde{D}$), one would see an in-flow of quiescent gas on a control surface slightly in front of the shock. Similarly, if one where to look slightly behind, there would be some flow away from the shock surface. These observations can be rewritten as conservation relations through some control volume that traverses the shock discontinuity (note that quantities with ($\tilde{}$) are considered dimensional) in the shock frame of reference:

- Conservation of mass:

$$\tilde{\rho}\tilde{u} = \tilde{\rho}_1\tilde{D}, \tag{2.2.2}$$

- Conservation of momentum:

$$\tilde{p} - \tilde{p}_1 = \tilde{\rho}(\tilde{D} - \tilde{u})\tilde{D}, \tag{2.2.3}$$

- Conservation of energy:

$$\tilde{e} + \tilde{p}/\tilde{\rho} + \frac{1}{2}\tilde{u}^2 = \tilde{e}_1 + \tilde{p}_1/\tilde{\rho}_1 + \frac{1}{2}\tilde{D}^2, \tag{2.2.4}$$

where $\tilde{p}$ is pressure, $\tilde{u}$ is velocity, $\tilde{v}$ is specific volume, $\tilde{e}$ is the specific energy (all quantities defined at some distance behind the shock) and $\tilde{D}$ is the speed of the shock. The subscript "1" refers the quiescent state quantities in front of shock. The specific energy $\tilde{e}$ is of the form appropriate for perfect gases,

$$\tilde{e} = \frac{\tilde{p}\tilde{v}}{\gamma - 1} - \lambda\tilde{Q} \tag{2.2.5}$$

where $\tilde{Q}$ is the heat release of the reaction and γ is the specific heats ratio. Here, the energy of the gas is written with help of the perfect gas equation of state i.e.

$$\tilde{p}\tilde{v} = \tilde{R}_g\tilde{T} \tag{2.2.6}$$

where $\tilde{R}_g$ is the gas constant. As in Ref. [23], one can find take Eqs. (2.2.2)-(2.2.4), and solve for the dimensionless (scaled with conditions just behind the shock) steady-state distributions of pressure, p^*, velocity, u^*, and specific volume, v^*, for a plane detonation wave in terms of λ^*:

$$p^* = a + (1-a)\sqrt{1-b\beta\lambda^*},\ u^* = \frac{1-p^*}{\gamma M_s} + M_s,\ v^* = \frac{u^*}{M_s} \tag{2.2.7}$$

where a and b are the constants

$$a = \frac{1+\gamma D^2}{2\gamma M_s^2 - (\gamma-1)},\ b = \frac{2\gamma M_s^2(\gamma-1)}{(1-a)^2(\gamma+1)} \tag{2.2.8}$$

and the "$*$" superscript refers to the dimensionless version of the quantity in question.

The steady dimensionless detonation velocity, D, is scaled with the speed of sound in the quiescent gas, and M_s is the Mach number of the flow immediately behind the shock in the frame moving with the shock wave (i.e. at $\lambda = 0$). The dimensionless heat release, $\beta = \tilde{Q}/\tilde{R}_g\tilde{T}_s$, is based on the temperature immediately behind the shock, T_s.

The specific form of the reaction kinetics follows the first-order one-step Arrhenius reaction rate. It is highly sensitive to temperature due to its exponential form:

$$\tilde{r} = \frac{D\lambda}{Dt} = \tilde{k}(1-\lambda)e^{-\tilde{E}/\tilde{R}_g\tilde{T}} \tag{2.2.9}$$

where $D/Dt = \partial/\partial\tilde{t} + \tilde{u}\partial/\partial\tilde{x}$ is the material derivative, $\tilde{E}$ is the activation energy of the specific reaction in question. The associated dimensionless version of the reaction rate is

$$r^* = k(1-\lambda^*)\exp(-\theta/T^*) \tag{2.2.10}$$

where θ is a dimensionless activation temperature, and k is a dimensionless constant,

$$\begin{aligned} \theta &= \tilde{E}/\tilde{R}_g\tilde{T}_s \\ k &= \int_0^{1/2} u^* \left(1-\lambda^*\right)^{-1} \exp\left(\theta/T^*\right) d\lambda^*. \end{aligned} \tag{2.2.11}$$

The relevant parameters of the flow so far are the activation energy, E, reaction heat release Q, and the specific heats ratio γ. However, a final parameter is needed to characterize the ZND flow completely and it is the overdrive factor f. It is a simple measure of the detonation velocity with respect to the limiting minimal value corresponding to the Chapman-Jouguet state and is defined as

$$f = (\tilde{D}/\tilde{D}_{CJ})^2 \tag{2.2.12}$$

Integration of Eq. (2.2.10) provides the reaction progress variable, λ^*, as a function of distance from the shock wave, x_1. Fig. 2.1 illustrates λ^* as a function of x at $\gamma = 1.2$, $E = \tilde{E}/\tilde{R}_g\tilde{T}_1 = 50$, $Q = 50$, and $f = 1.2$ as an example. The primary objective is to determine the stability characteristics of this type of flow. To accomplish this one needs to define the governing equations of the perturbations and this is done in the following sections.

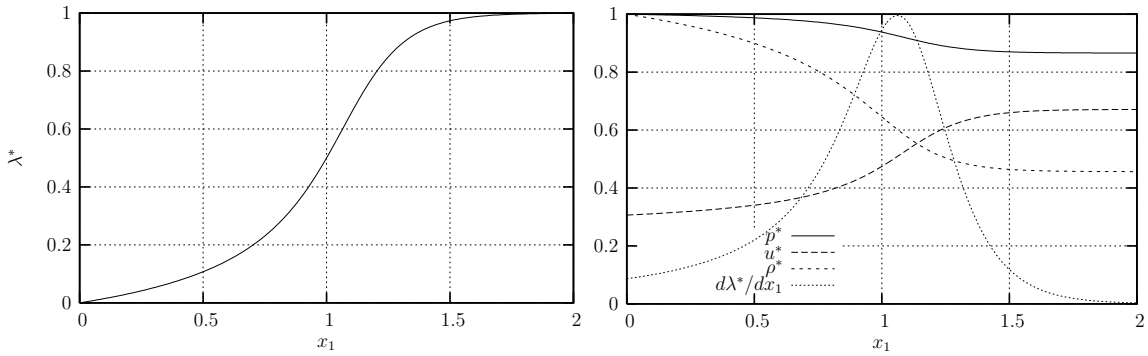

FIGURE 2.1. The reaction progress variable as a function of the distance from the shock wave (left). On the right, the rest of the thermodynamic variables and velocity along with the rate of change of λ^* with x. The case for $f = 1.2, \gamma = 1.2, E = 50$ and $Q = 50$.

2.2.2 Linearized governing equations for the perturbations.

Following the general procedure laid down by Erpenbeck [18], the governing equations for perturbations are obtained as a linearization of (2.2.1) and using the wave coordinate

$$x_1 = x_1^l - D_s t - \psi\left(x_2, x_3, t\right) \tag{2.2.13}$$

where D_s is the detonation shock velocity scaled with the speed of sound behind the shock and $\psi(x_2, x_3, t)$ is the shock displacement. The particle velocity is measured with respect to the unperturbed shock wave frame:

$$u_1 = u_1^l - D_s \tag{2.2.14}$$

One can derive the linearized equations as follows:

$$\frac{\partial \mathbf{z}'}{\partial t} + \mathbf{A}_1 \frac{\partial \mathbf{z}'}{\partial x_1} + \mathbf{A}_2 \frac{\partial \mathbf{z}'}{\partial x_2} + \mathbf{A}_3 \frac{\partial \mathbf{z}'}{\partial x_3} + \mathbf{C}\mathbf{z}' - \mathbf{g}_t \frac{\partial \psi}{\partial t} - \mathbf{g}_2 \frac{\partial \psi}{\partial x_2} - \mathbf{g}_3 \frac{\partial \psi}{\partial x_3} = 0 \tag{2.2.15}$$

where $\mathbf{z}' = (v', u_1', u_2', u_3', p', \lambda')^T$ is a vector comprised of specific volume, three-velocity components, pressure, and the reaction progress variable perturbations superscript T stands for transposed); $\mathbf{A}_1$, $\mathbf{A}_2$ and $\mathbf{A}_3$ are 6×6 matrices; $\mathbf{g}_t$, $\mathbf{g}_2$ and $\mathbf{g}_3$ are column vectors. The matrices and the vectors are presented in Appendix A.1. Since the objective of this chapter is to define the initial value problem approach and extol its virtues, the conventional normal mode approach is first presented in order to clarify the key difference between the two approaches.

2.3 The normal-mode approach

In 1990, Lee and Stewart systematically obtained stability boundaries for a wealth of parameter ranges for one-dimensional perturbations to the planar detonation flow [23]. It is notable that Pukhnachev was probably the first to use the normal mode approach for stability, in the case of Chapman-Jouguet detonation confined to a tube in 1963 [24]. However, the work by Lee and Stewart in [23] ushered in an proliferation

of stability research for detonations [26, 27]. An extensive review appears in Ref. [28]. The following is a brief summary of the approach followed therein.

The normal-mode approach begins with a simple hypothesis for the form of the perturbation vector solution $\mathbf{z}'$ and the perturbation to the shock position ψ:

$$\mathbf{z}' = \hat{\mathbf{z}} \exp(\tau t), \text{ and } \psi = \hat{\psi} \exp(\tau t). \tag{2.3.1}$$

Mathematically, the main feature is that the normal-mode approach presupposes the simple exponential in time dependence. The rest of the procedure for this 1D base flow is simply to reduce the system of equations to ODE's and formulate an eigenvalue problem for τ through a two-point boundary value problem. Assuming that the primed quantities are small perturbations to the base flow denoted by the superscript "$*$", one can derive the linearized equations from (2.2.1) as follows:

$$\tau \hat{\mathbf{z}} + \mathbf{A}_1 \frac{d\hat{\mathbf{z}}}{dx_1} + (i\alpha \mathbf{A}_2 + i\beta \mathbf{A}_3 + \mathbf{C})\, \hat{\mathbf{z}} - (\tau \mathbf{g}_t + i\alpha \mathbf{g}_2 + i\beta \mathbf{g}_3)\, \hat{\psi} = 0. \tag{2.3.2}$$

Note that a further reduction to ODE's is made possible by assuming that the 3D perturbations are proportional to $\exp(i\alpha x_2 + i\alpha_3 x_3)$. The matrices and vectors are presented in Appendix A.1. One can derive a boundary condition at the shock front for the above equations based on the perturbed shock relations which are specialized to the unsteady shock attached frame, i.e. $x = x^l - D_s t - \psi(t)$. On the front then

$$\hat{\mathbf{z}}\,(0_+) = (\tau \mathbf{h}_t + i\alpha \mathbf{h}_2 + i\beta \mathbf{h}_3)\, \psi \tag{2.3.3}$$

with each vector $\mathbf{h}_i$ being a function of the parameters of the flow such as M_s and D, the Mach number behind the shock and the velocity of the shock front scaled with the quiescent gas speed of sound, respectively.

Finally, a boundary condition must be defined at the end of the reaction zone or as $x_1 \to \infty$ to provide the closure for defining the temporal stability. The conventional choice is known as the "radiation condition" since it ensures no acoustic waves

propagate towards the shock. It was initially defined by Ludford and Buckmaster [46]:

$$\tau u_1' - i\kappa u_1^* u_2' + \frac{\rho_1^*}{\gamma c^*}\left[\tau^2 + k^2(c^{*2} - u_1^{*2})\right]^{1/2} p' = 0. \tag{2.3.4}$$

Eq. (2.3.2) together with Eqs. (2.3.3) and (2.3.4) define a two-point boundary value problem. Both $\mathbf{z}'$ and τ are complex. Most normal-mode analysis proceeds to the numerical phase where a shooting procedure is used starting at $x = 0$ and proceeding to the end of the reaction zone. A standard two-variable (for $\mathrm{Re}(\tau)$ and $\mathrm{Im}(\tau)$) Newton-Rhapson iteration is then used on the acoustic radiation condition to find the complete eigenvalue τ. The real part of this complex number determines the stability of the base flow.

2.4 The initial value problem

In what follows, the solution of the initial-value problem initially defined by Erpenbeck in Ref. [18] is presented with slight modifications in notation. Equation (2.2.15) has to be solved with the following initial condition:

$$t = 0: \;\; z'(x_1, x_2, x_3, 0) = z_0(x_1, x_2, x_3), \;\; \psi(x_2, x_3, 0) = 0 \tag{2.4.1}$$

Note that the condition on ψ can be relaxed to include a non-zero function of x_2, and x_3, the transverse coordinates. The contrast with the conventional normal-mode approach is that the perturbations are allowed to evolve from an initial physical state. The task is then to determine the conditions that determine whether the perturbations decompose into unstable modes or if these simply decay away. Additionally, in the IVP formulation, the perturbations are to obtained as solutions of PDE's.

As a first step, one applies the Fourier transform in the transverse coordinates x_2 and x_3,

$$\hat{\mathbf{z}}(x_1, \alpha, \beta, t) = \int_{-\infty}^{\infty}\int_{-\infty}^{\infty} e^{-i(\alpha x_2 + \beta x_3)} \mathbf{z}'(x_1, x_2, x_3, t)\, dx_2 dx_3 \tag{2.4.2}$$

since the detonation proceeds in an unbounded transverse domain and the perturbations are assumed to vanish as x_2 and $x_3 \to \pm\infty$. Likewise for $\hat{\psi}$,

$$\hat{\psi}(\alpha,\beta,t) = \int_{-\infty}^{\infty}\int_{-\infty}^{\infty} e^{-i(\alpha x_2+\beta x_3)}\psi(x_2,x_3,t)\,dx_2dx_3. \tag{2.4.3}$$

One arrives at the following system of equations:

$$\frac{\partial\hat{\mathbf{z}}}{\partial t} + \mathbf{A}_1\frac{\partial\hat{\mathbf{z}}}{\partial x_1} + (i\alpha\mathbf{A}_2 + i\beta\mathbf{A}_3 + \mathbf{C})\,\hat{\mathbf{z}} - \mathbf{g}_t\frac{\partial\hat{\psi}}{\partial t} - (i\alpha\mathbf{g}_2 + i\beta\mathbf{g}_3)\,\hat{\psi} = 0 \tag{2.4.4}$$

Appropriate for a linear PDE system with a prescribed initial state, one applies the Laplace transform with respect to time

$$\begin{aligned}\bar{\mathbf{z}}(x_1,\alpha,\beta,\tau) &= \int_0^{\infty}\hat{\mathbf{z}}(x_1,\alpha,\beta,t)\,e^{-\tau t}dt\\ \bar{\psi}(\alpha,\beta,\tau) &= \int_0^{\infty}\hat{\psi}(\alpha,\beta,t)\,e^{-\tau t}dt\end{aligned} \tag{2.4.5}$$

and so the initial state is incorporated via an inhomogeneous term in a system of now ordinary differential equations:

$$\mathbf{A}_1\frac{d\bar{\mathbf{z}}}{dx_1} + (i\alpha\mathbf{A}_2 + i\beta\mathbf{A}_3 + \mathbf{C} + \tau\mathbf{I})\,\bar{\mathbf{z}} - (\tau\mathbf{g}_t + i\alpha\mathbf{g}_2 + i\beta\mathbf{g}_3)\,\bar{\psi} = \hat{z}_0(x_1). \tag{2.4.6}$$

The linearized Rankine-Hugoniot conditions on the shock wave can be written in the vector form as

$$\mathbf{z}'(0_+,t) = \mathbf{Y}\mathbf{z}'(0_-,t) + \mathbf{h}_2\frac{\partial\psi}{\partial t} + \mathbf{h}_2\frac{\partial\psi}{\partial x_2} + \mathbf{h}_3\frac{\partial\psi}{\partial x_3}. \tag{2.4.7}$$

Matrix $\mathbf{Y}$ and vectors $\mathbf{h}_t$,$\mathbf{h}_2$ and $\mathbf{h}_3$ are presented in Appendix A.1.2. Note that any perturbation that may exist in the quiescent gas has input into the stability results via the boundary condition written above. Since the problem for perturbations in the quiescent gas can be solved easily (no reaction assumed therein), this vector $\mathbf{z}'(0,t)$ is considered known for the purposes of the forthcoming calculations. Under the Fourier and Laplace transforms the relevant condition becomes,

$$\bar{\mathbf{z}}(0_+) = \mathbf{Y}\bar{\mathbf{z}}(0_-) + (\tau\mathbf{h}_t + i\alpha\mathbf{h}_2 + i\beta\mathbf{h}_3)\,\bar{\psi}. \tag{2.4.8}$$

The solution of Eq. (2.4.6) has to be bounded as $x_1 \to \infty$ and also satisfy the shock boundary condition (2.4.8). Therefore, the fundamental solutions of the associated homogeneous system have to be analyzed (2.4.6) at $x_1 \to \infty$. For the moment, one considers overdriven detonation ($f > 1$) in order to avoid analytical difficulties related to an irregular singular point in the perturbation equations. This is manifested in the fact that the matrix's determinant, $\det(\mathbf{A}_1) \propto 1/(u_0^2 - c_0^2) \to \infty$ in the CJ case. Obtaining the asymptotic form of the fundamental solutions becomes therefore much more difficult. Unsupported CJ detonation is signaled by setting $f = 1$ in the ZND flow and is specifically addressed in Chapter 3. Assuming overdriven detonation however, one can find the fundamental solutions analytically as in [18],

$$\bar{\mathbf{z}}_j(x_1) = \bar{\mathbf{z}}_{j\infty} \exp(\mu_j x_1) \tag{2.4.9}$$

where

$$\begin{aligned}
\mu_1 &= \frac{u_\infty^* \tau + c_\infty \sqrt{\tau^2 + c_\infty^2 (1 - M_\infty^2)(\alpha^2 + \beta^2)}}{c_\infty^2 (1 - M_\infty^2)} \\
\mu_2 &= \frac{u_\infty^* \tau - c_\infty \sqrt{\tau^2 + c_\infty^2 (1 - M_\infty^2)(\alpha^2 + \beta^2)}}{c_\infty^2 (1 - M_\infty^2)} \\
\mu_3 &= \mu_4 = \mu_5 = -\frac{\tau}{u_\infty^*} \\
\mu_6 &= -\frac{\tau + C_{66}}{u_\infty^*}.
\end{aligned} \tag{2.4.10}$$

The quantity C_{66} in (2.4.10) is the element of matrix $\mathbf{C}$ that survives as $x_1 \to \infty$; u_∞^* is the gas velocity, c_∞ is the local speed of sound, and the Mach number, M_∞, corresponds to the flow parameters in the burnt gas.

For the overdriven case, $M_\infty < 1$, and one can see that the first fundamental solution, $\bar{\mathbf{z}}_j(x_1)$, is unbounded at $x_1 \to \infty$ ($\mu_1 > 0$ at $\mathrm{Re}(\tau) > 0$). The other fundamental solutions decay exponentially downstream from the shock wave. Using these properties of the fundamental solutions, one can write down solution of Eq.

(2.4.6) in the following form:

$$\begin{aligned}
\bar{\mathbf{z}} &= \sum_{j=2}^{6}\left(a_j + \int_0^{x_1} \mathbf{y}_j \cdot \mathbf{F} dx_1\right)\bar{\mathbf{z}}_j + \bar{\mathbf{z}}_1 \int_\infty^{x_1} \mathbf{y}_1 \cdot \mathbf{F} dx_1 \\
\mathbf{F} &= \mathbf{F}_1 + \mathbf{F}_2\bar{\psi} \\
\mathbf{F}_1 &= \mathbf{A}_1^{-1}\hat{z}_0,\ \mathbf{F}_2 = \mathbf{A}_1^{-1}\left(\tau\mathbf{g}_t + i\alpha\mathbf{g}_2 + i\beta\mathbf{g}_3\right)
\end{aligned} \tag{2.4.11}$$

where $\mathbf{y}_j$ is a fundamental solution of the adjoint system of equations:

$$\frac{d\mathbf{y}}{dx_1} - \left\{\mathbf{A}_1^{-1}\left(i\alpha\mathbf{A}_2 + i\beta\mathbf{A}_3 + \mathbf{C} + \tau\mathbf{I}\right)\right\}^T \mathbf{y} = 0 \tag{2.4.12}$$

The fundamental solution, $\mathbf{y}_j$, of Eq. (2.4.12) can be obtained as a vector comprised of cofactors of the j-th column of the matrix of the fundamental solutions $\mathbf{Z} = [\overline{\mathbf{z}}_1, \overline{\mathbf{z}}_2, \ldots, \overline{\mathbf{z}}_6]$ and divided by $\det(\mathbf{Z})$ [47]. At $x_1 \to \infty$, one can find $\mathbf{y}_j(x_1) = \mathbf{y}_{j\infty}(-\mu_j x_1)$. Particularly,

$$\mathbf{y}_{1\infty} = \begin{pmatrix}
0 \\
\tau \\
-i\alpha u_\infty^* \\
-i\beta u_\infty^* \\
-\frac{v_\infty^*}{\gamma c_\infty}\sqrt{\tau^2 + c_\infty^2\left(1 - M_\infty^2\right)k^2} \\
\frac{C_{56}u_\infty^* v_\infty^*\left[\tau^2 - u_\infty^{*2}k^2\right]}{\gamma\left[u_\infty^{*2}c_\infty^2 k^2 - \tau c_\infty^2 C_{66} - \tau^2 c_\infty^2 + C_{66}u_\infty^* c_\infty\sqrt{\tau^2 + c_\infty^2(1-M_\infty^2)k^2}\right]}
\end{pmatrix} \tag{2.4.13}$$

where $k^2 = \alpha^2 + \beta^2$. The coefficients $a_2, \ldots, a_6$ and the shock displacement $\overline{\psi}$ are found from the shock boundary conditions, Eq. (2.4.8). The relevant constants are as follows:

$$\begin{aligned}
\bar{\psi} &= -\frac{\mathbf{y}_1(0)\cdot\mathbf{Y}\bar{\mathbf{z}}(0_-) + \int_0^\infty\left(\mathbf{y}_1\cdot\mathbf{F}_1\right)dx_1}{V} \\
V(\tau,\alpha,\beta) &= \tau V_\tau + i\alpha V_2 + i\beta V_3 \\
V_\tau &= \left(\mathbf{y}_1(0)\cdot\mathbf{h}_t\right) + \int_0^\infty\left(\mathbf{y}_1\cdot\mathbf{A}_1^{-1}\mathbf{g}_t\right)dx_1 \\
V_2 &= \left(\mathbf{y}_1(0)\cdot\mathbf{h}_2\right) + \int_0^\infty\left(\mathbf{y}_1\cdot\mathbf{A}_1^{-1}\mathbf{g}_2\right)dx_1 \\
V_3 &= \left(\mathbf{y}_1(0)\cdot\mathbf{h}_3\right) + \int_0^\infty\left(\mathbf{y}_1\cdot\mathbf{A}_1^{-1}\mathbf{g}_3\right)dx_1
\end{aligned} \tag{2.4.14}$$

Having found the coefficients and the shock displacement, the transformed solution as a function of time of the initial-value problem can be written as

$$\hat{\mathbf{z}}\left(x_1,\alpha,\beta,t\right)=\frac{1}{2\pi i}\int_{\sigma-i\infty}^{\sigma+i\infty}\bar{\mathbf{z}}\left(x_1,\alpha,\beta,\tau\right)e^{\tau t}d\tau \tag{2.4.15}$$

The shock displacement $\overline{\psi}$ and the coefficients $a_2,\ldots,a_6$ may have singularities in the complex plane τ, where

$$V\left(\tau,\alpha,\beta\right)=0 \tag{2.4.16}$$

Zeros, τ_j, of this function were of the main interest for Erpenbeck [19]. The limited power of computers at the time should explain why he did not try to solve Eq. (2.4.16) directly. Although zeros of V in the complex plane τ were associated with unstable modes, Erpenbeck did not discuss closing of the path of integration in Eq. (2.4.15) to explain how the residue values at the poles will originate in the solution. Because the found solution (2.4.11) cannot be considered at $\mathrm{Re}(\tau)\leq 0$, the Bromwich's integral's path of integration can be closed only in the $\mathrm{Re}(\tau)\geq 0$ half-plane. It was pointed out in Ref. [32] that the path of integration can be closed with arcs of large radii that tend to infinity, and an imaginary axis of τ. Therefore, $\hat{\mathbf{z}}(x_1,\alpha,\beta,t)$ will be represented as a sum of the residue values associated with zeros of the denominator (2.4.16) and an integral along the imaginary axis, $\mathrm{Im}(\tau)$,

$$\hat{\mathbf{z}}\left(x_1,\alpha,\beta,t\right)=\sum_j R_j\hat{\mathbf{z}}_{dmj}\left(x_1,\alpha,\beta\right)e^{\tau_j t}+\frac{1}{2\pi i}\int_{-i\infty}^{i\infty}\bar{\mathbf{z}}\left(x_1,\alpha,\beta,\tau\right)e^{\tau t}d\tau \tag{2.4.17}$$

If a pole occurs on the imaginary axis, the path has to be deformed around the pole, keeping $\mathrm{Re}(\tau)\geq 0$. The choice of the path around the poles on the imaginary axis is crucial for constructing a solution consistent with the causality principle [32]. Clearly if zeros of the denominator function V exist and have real part greater than zero, i.e. $\mathrm{Re}(\tau_j)>0$, then these modes grow in t as shown in the residue contribution in (2.4.17).

2.4.1 Receptivity and stability criterion

The result, Eq. (2.4.17), can be interpreted as an expansion of the solution of the initial-value problem into the modes of discrete and continuous spectra. The vectors $\hat{\mathbf{z}}_{dmj}(x_1, \alpha, \beta)$ in Eq. (2.4.17) are the discrete modes, and their weights, R_j, are the receptivity coefficients

$$R_j = -\frac{\left[\mathbf{y}_1(0) \cdot \mathbf{Y}\overline{\mathbf{z}}(0_-) + \int_0^\infty (\mathbf{y}_1 \cdot \mathbf{F}_1)\, dx_1\right]_{\tau=\tau_j}}{(\partial V/\partial\tau)_{\tau=\tau_j}} \tag{2.4.18}$$

The modes of continuous spectrum are represented by $\mathbf{z}_1, \ldots, \mathbf{z}_6$ evaluated at $\tau = is$, where s is a real parameter (angular frequency). Their physical interpretation can be given based on the asymptotic behavior at $x_1 \to \infty$. For example, the fundamental solution $\overline{\mathbf{z}}_1$ represents the upstream acoustic mode. One can see that the solution, Eq. (2.4.11), does not have the upstream acoustic mode at $x_1 \to \infty$, whereas the mode does exist upstream of the introduced initial perturbation. The fundamental solution $\overline{\mathbf{z}}_2$ represents the downstream acoustic wave, whereas $\overline{\mathbf{z}}_3$,$\overline{\mathbf{z}}_4$ and $\overline{\mathbf{z}}_5$ represent two vorticity modes and the entropy mode. One can find discussion of the integral in Eq. (2.4.17) as an expansion into the modes of the continuous spectrum in Ref. [32], where a non-reacting gas model was used in order to evaluate the inverse Laplace transform analytically.

The dispersion relation that the IVP method provides is given in terms of known functions and a single adjoint homogeneous solution of the perturbation equations, i.e. $y_1(x_1; \tau)$ in the current notation. Therefore, in order to find a discrete mode, one could start at some large x_1 using the asymptotic representation (2.4.13) and integrate Eq. (2.4.12) toward shock to obtain $y_1(x_1; \tau)$. Subsequently, one could use the dispersion relation (2.4.16) to iterate for the eigenvalues τ_j. The method here is exactly equivalent to the normal-mode approach results and the proof is outlined in Appendix A.2.

2.4.2 The radiation boundary condition

In the conventional normal-mode analysis, the rear-boundary condition is required in an explicit form in order to formulate the two-point boundary value problem. Derivation of the condition was a subject of discussion in many publications (see for example Ref. [23]). Short [25] and Short and Stewart [26] used an approximate rear-boundary condition that can be written in our notation as

$$\tau z_2 - i\alpha u_\infty^* z_3 - i\beta u_\infty^* z_4 - \frac{v_\infty^*}{\gamma c_\infty}\sqrt{\tau^2 + c_\infty^2\left(1 - M_\infty^2\right)k^2}\, z_6 = 0 \tag{2.4.19}$$

where z_i are the elements of the normal mode eigenfunction. The condition (2.4.19) was derived by Buckmaster and Ludford [46] as a condition that there are no acoustic waves propagating upstream. Actually, derivation of the rear-boundary condition is a trivial problem if properties of the adjoint solution are taken into account. A bounded solution for discrete modes and absence of the upstream acoustic modes in the burnt gas stems from Eq. (2.4.11) and its inverse Laplace transform written as a sum of the discrete modes and modes of the continuous spectra (2.4.17). The main point is that solution (2.4.11) does not include the fundamental solution $\overline{\mathbf{z}}_1$ at $x_1 \to \infty$. Because the adjoint solution $\mathbf{y}_1$ is orthogonal to the other fundamental solutions, $\overline{\mathbf{z}}_2, \ldots$ and $\overline{\mathbf{z}}_6$, the rear boundary condition can be written straightforwardly as

$$\lim_{x_1 \to \infty} \mathbf{y}_1 \cdot \mathbf{z} = 0 \Rightarrow \mathbf{z} \cdot \mathbf{y}_{1\infty} = 0 \tag{2.4.20}$$

After substitution of $\mathbf{y}_{1\infty}$ into Eq. (2.4.20), the rear-boundary condition in (2.4.19) is obtained. This shows that the radiation condition is equivalent to the requirement of spatial boundedness.

2.5 Numerical examples of the stability analysis

2.5.1 1D spectrum

In the case of one-dimensional perturbations [48], a multi-domain spectral collocation (MDSC) method was utilized with the rear-boundary condition included into the algorithm. It was possible because the boundary condition was a linear function of the eigenvalue τ. The MDSC method requires a linear relationship in τ to formulate the problem as a generalized eigenvalue problem, i.e. $Kz = \tau Hz$ where H and K are matrices. The method is described in detail in Chapter 4.

Fig. 2.2 illustrates eigenvalue map for one-dimensional perturbations obtained with the help of three-domain method at $f = 1.2$, $\gamma = 1.2$, $E = Q = 50$. Number of polynomials for each domain in this example is $N = 100$. The eigenvalues in Fig. 2 are scaled with t_c (eigenvalues in Table 2 of Ref. [48] are scaled with the half-time reaction).

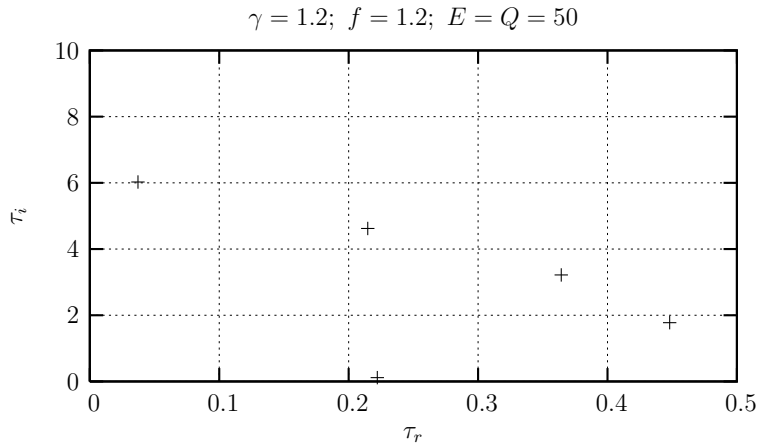

FIGURE 2.2. Eigenvalue map for one-dimensional perturbations obtained with the help of three-domain spectral collocation method [48].

2.5.2 3D spectrum

In the case of three-dimensional perturbations, the rear-boundary condition (2.4.19) is non-linear with respect to τ , and one must enforce homogeneous boundary conditions on the perturbation at some large distance x_{max}. Such a boundary condition brings the discretized continuous spectrum (along the imaginary axis) into the map together with spurious modes. Figure 2.3 illustrates eigenvalue map obtained with the help of a three-domain solver for three-dimensional perturbations at $k = \sqrt{\alpha^2 + \beta^2} = 0.001$. Due to the structure of the equations and a corresponding transformation of the transverse velocity perturbations $(\alpha/ku_2' + \beta/ku_3')$, one can obtain the stability results for the transverse perturbations by varying only k. The domain distribution was: $0 \le x_1 \le 4$, $4 \le x_1 \le 15$, and $15 \le x \le 120$. Number of polynomial s was equal to 200 in each domain. One can see from Fig. 2.3 that the method is reliable only for

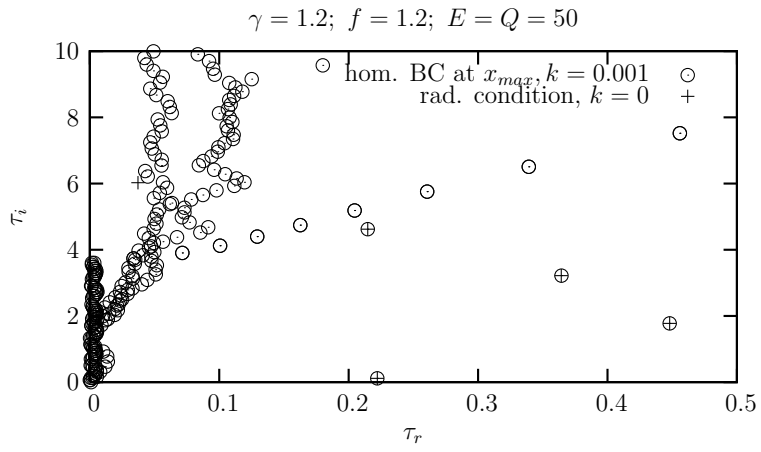

FIGURE 2.3. Comparison of eigenvalue maps when the homogeneous boundary conditions are enforced at x_{max} $(k = 0.001)$ and when the radiation condition is used at the end point.

moderate frequencies. At large frequencies, there are many spurious modes. This is a picture that is typical in stability analysis of boundary layers, where perturbations are required to be zero at some large distance from the wall. Since the modes that are close to neutral point decay very slowly, their resolution with a homogeneous

boundary condition is difficult, and they can be easily lost within the modes of the continuous spectrum that do not decay as $x_1 \to \infty$. However, Fig. 2.4 shows a plot of the radiation boundary condition as a function of x_1 for the first mode (having the lowest frequency, $\mathrm{Im}(\tau)$). This function can serve as an indicator that the eigenvalue is meaningful and there is a good convergence of the method if the function indeed decays.

In addition to the spectral method, the solution of the direct problem (2.3.2), (2.3.3) and (2.3.4) and the adjoint IVP method using (2.4.12), (2.4.13) and (2.4.16) was obtained with a shooting algorithm. In these cases, two different solvers were tried. In the first, the IMSL routine DIVPAG implementing Gear's BDF method with min(absolute error, relative error) $< 10^{-11}$ was utilized. The second one was based on DDASSL routine developed by L. R. Petzold [1]. Both solvers were found efficient for direct and adjoint problems. Integration of the differential equations was carried out with the help of the IMSL routine. The shooting procedure was used together with Newton's algorithm to find a root of Eqs. (2.4.19) (direct problem) and (2.4.16) (adjoint problem). Results obtained with the help of these methods were in good agreement.

For 3D perturbations, the following is a possible strategy for analysis of the spectrum.

1. Start with the one-dimensional perturbation using the MDSC method of Ref. [48] and use the found eigenvalues as starting points in the parametric study when parameter k is varied using a conventional method of solving equations (2.3.2) with initial data (2.3.3) together with the boundary condition (2.3.4).

2. Since increase in k can lead to the appearance of new modes [26], one can use the eigenvalue maps to catch them when they are well separated from the continuous spectrum.

[1] Downloaded from software repository of the National Institute of Standards and Technology

3. After that, the new mode can be included in the parametric study described in step 1.

Figure 2.5 illustrates the eigenvalue map at $k = 6$, when a new mode (the sixth mode) appears on the plot.

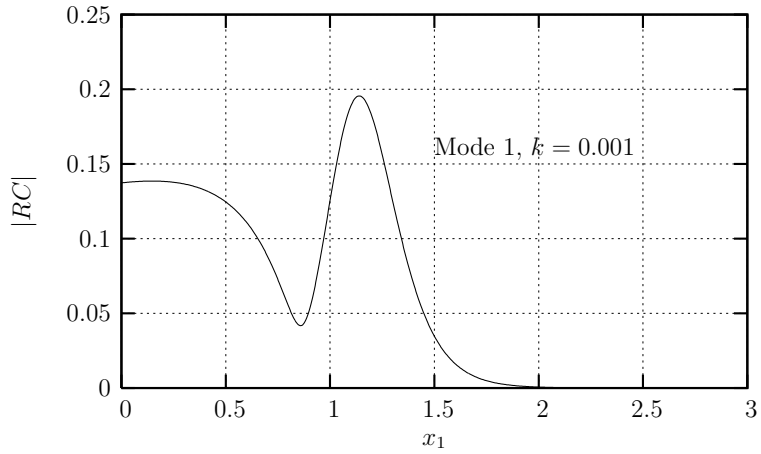

FIGURE 2.4. Function $RC(x)$ in the case of the first mode computed using the homogeneous boundary condition at x_{max}.

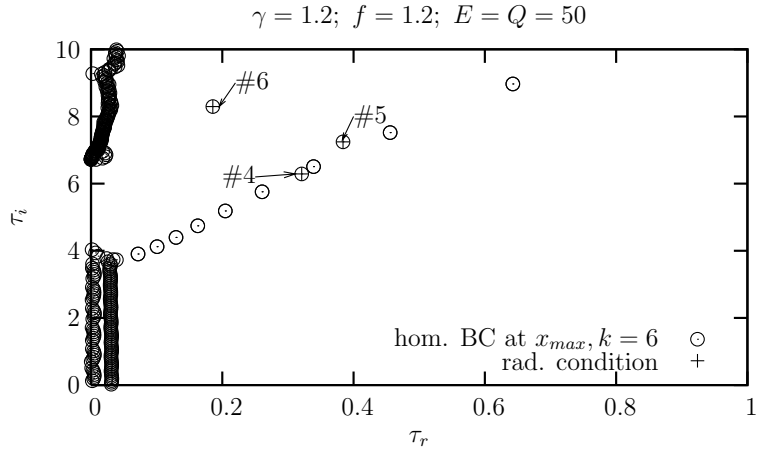

FIGURE 2.5. Appearance of a new mode (No. 6) on the eigenvalue map when parameter k is increased.

Following this strategy, the results of Ref. [26] for the nine unstable modes as shown in Fig. 2.6 are readily reproduced. One may compare these plots with Fig.

7(a) and 7(b) of Ref. [26], respectively. The symbols represent results obtained from the analysis of the direct problem, whereas lines in Fig. 2.6(b) represent the results obtained from the adjoint approach. Figure 2.7 show the real and imaginary parts

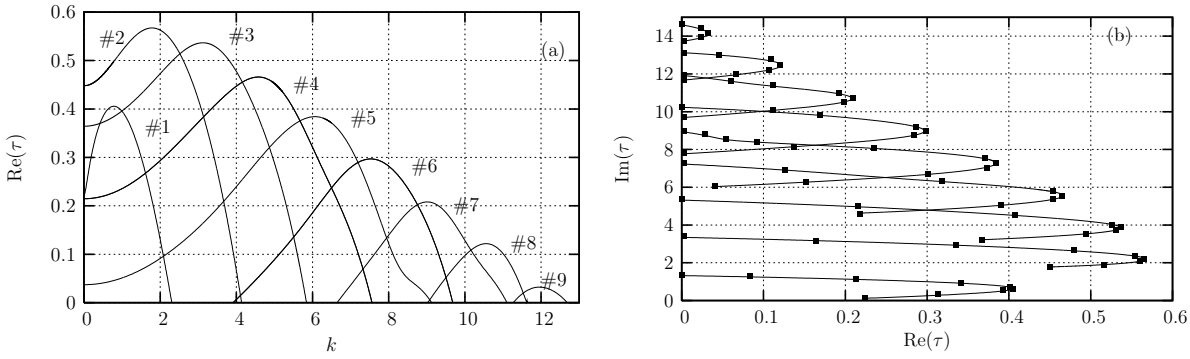

FIGURE 2.6. Stability spectrum showing (a) $\mathrm{Re}(\tau)$ vs k and (b) $\mathrm{Im}(\tau)$ vs $\mathrm{Re}(\tau)$ for the six unstable modes at $\gamma = 1.2$, $f = 1.2$, $E = Q = 50$. Lines − results from analysis of the direct problem; the symbols − results from the adjoint approach.

of the eigenfunction $\mathbf{z}$ corresponding to the first mode at $k = 0.78$ ($\tau = 0.40556 + i0.63176$). Numbers in the legends indicate components of the vector. One can compare Figs. 2.7a and 2.7b with plots in Figs. 8a and 8b of Ref. [26], respectively.

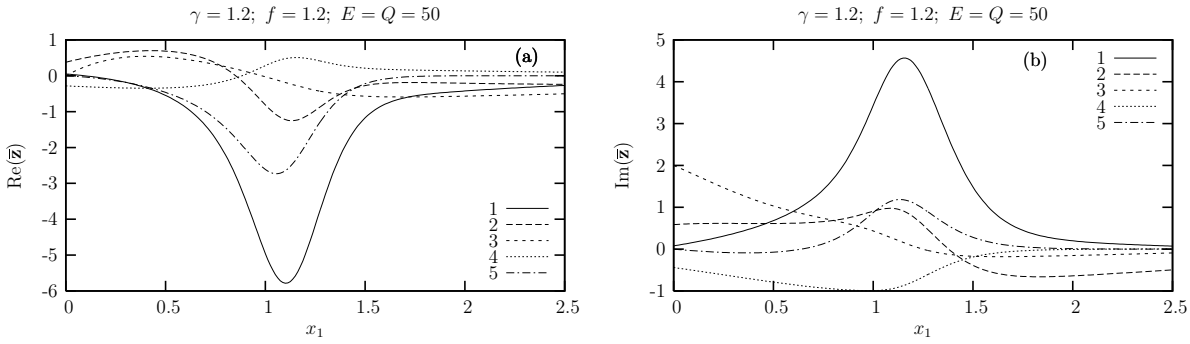

FIGURE 2.7. Real (a) and imaginary (b) parts of the eigenvector components for the first mode, $k = 0.78$. 1 - ρ', 2 u_1', 3 - $\alpha u_2' + \beta u_3'$, 4 - p' and 5 - λ'.

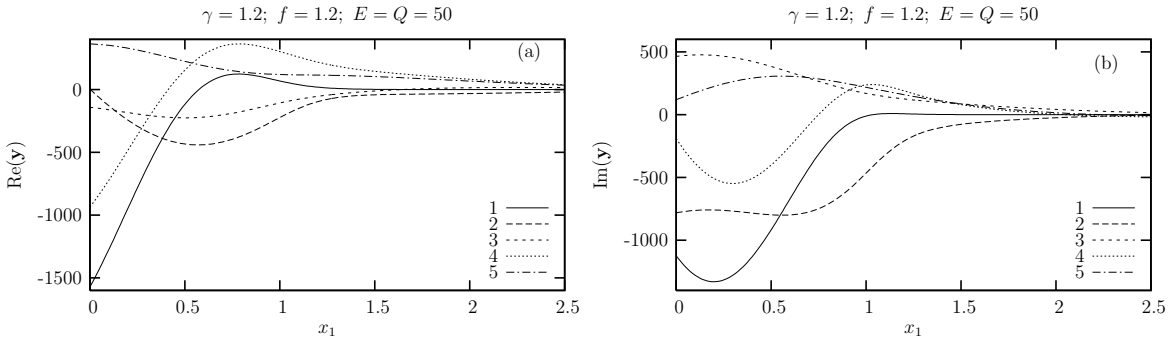

FIGURE 2.8. Real (a) and imaginary (b) parts of the adjoint solution corresponding to the first mode, $k = 0.78$

2.6 Examples of the receptivity analysis

2.6.1 Perturbations in the reaction zone

In the case of a perturbation introduced in the reaction zone, the receptivity coefficient (2.4.18) will not include the forcing term associated with perturbations incoming from the quiescent gas:

$$R_j = -\frac{\left[\int_0^\infty (\mathbf{y}_1 \cdot \mathbf{F}_1)\, dz\right]_{\tau=\tau_j}}{(\partial V/\partial\tau)_{\tau=\tau_j}} \tag{2.6.1}$$

The numerator in Eq. (2.6.1) depends on the initial data. One could evaluate the denominator numerically with the help of finite differences however it is possible to derive a formula instead for $(\partial V/\partial\tau)_{\tau=\tau_j}$.

By the definition of V in Eq. (2.4.14), one can write:

$$\begin{aligned}\frac{\partial V}{\partial\tau} = (\mathbf{h}_t, \mathbf{y}_1(0)) + \int_0^\infty \left(\mathbf{y}_1, A_1^{-1}\mathbf{g}_t\right) dx + \tau\left[\left(\frac{\partial \mathbf{y}_1(0)}{\partial\tau}, \mathbf{h}_t\right) + \int_0^\infty \left(\frac{\partial \mathbf{y}_1}{\partial\tau}, A_1^{-1}\mathbf{g}_t\right) dx\right] + \\ i\alpha\left[\left(\frac{\partial \mathbf{y}_1(0)}{\partial\tau}, \mathbf{h}_2\right) + \int_0^\infty \left(\frac{\partial \mathbf{y}_1}{\partial\tau}, A_1^{-1}\mathbf{g}_2\right) dx\right] + \\ i\beta\left[\left(\frac{\partial \mathbf{y}_1(0)}{\partial\tau}, \mathbf{h}_3\right) + \int_0^\infty \left(\frac{\partial \mathbf{y}_1}{\partial\tau}, A_1^{-1}\mathbf{g}_3\right) dx\right]\end{aligned} \tag{2.6.2}$$

Differentiation of the adjoint system (2.4.12) with respect to τ is the first step.

$$\frac{d}{dx_1}\frac{\partial \mathbf{y}_1}{\partial \tau} - \left\{A_1^{-1}\left(i\alpha A_2 + i\beta A_3 + C + \tau I\right)\right\}^T \frac{\partial \mathbf{y}_1}{\partial \tau} - \left\{A_1^{-1}\right\}^T \mathbf{y}_1 = 0 \tag{2.6.3}$$

and one evaluates the dot product of (2.6.3) with ζ:

$$\left(\zeta, \frac{d}{dx_1}\frac{\partial \mathbf{y}_1}{\partial \tau}\right) - \left(\zeta, \left\{A_1^{-1}\left(i\alpha A_2 + i\beta A_3 + C + \tau I\right)\right\}^T \frac{\partial \mathbf{y}_1}{\partial \tau}\right) - \left(\zeta, \left\{A_1^{-1}\right\}^T \mathbf{y}_1\right) = 0. \tag{2.6.4}$$

After integration of Eq. (2.6.4) with respect to x_1 from zero to infinity,

$$\begin{aligned}&\left(\zeta\left(0\right), \frac{\partial \mathbf{y}_1\left(0\right)}{\partial \tau}\right) + \int_0^\infty \left(A_1^{-1}\zeta, \mathbf{y}_1\right) dx_1 \\ &+ \int_0^\infty \left(\frac{d\zeta}{dx}, \frac{\partial \mathbf{y}_1}{\partial \tau}\right) dx_1 + \int_0^\infty \left(\left\{A_1^{-1}\left(i\alpha A_2 + i\beta A_3 + C + \tau I\right)\right\}\zeta, \frac{\partial \mathbf{y}_1}{\partial \tau}\right) dx_1 = 0.\end{aligned} \tag{2.6.5}$$

Taking into account that ζ satisfies Eq. (A.2.1) and initial conditions, Eq. (A.2.2), one can derived from (2.6.5)

$$-\left(\zeta\left(0\right), \frac{\partial \mathbf{y}_1\left(0\right)}{\partial \tau}\right) - \int_0^\infty \left(A_1^{-1}\left(\tau \mathbf{g}_t + i\alpha \mathbf{g}_2 + i\beta \mathbf{g}_3\right), \frac{\partial \mathbf{y}_1}{\partial \tau}\right) dx_1 - \int_0^\infty \left(A_1^{-1}\zeta, \mathbf{y}_1\right) dx_1 = 0. \tag{2.6.6}$$

Substitution (2.6.6) in (2.6.2) produces the following

$$\frac{\partial V}{\partial \tau} = \left(\mathbf{h}_t, \mathbf{y}_1\left(0\right)\right) + \int_0^\infty \left(\mathbf{y}_1, A_1^{-1}\mathbf{g}_t\right) dx_1 - \int_0^\infty \left(A_1^{-1}\zeta, \mathbf{y}_1\right) dx_1 \tag{2.6.7}$$

A trapezoidal formula on the interval $[0, x_{1max}]$ is used for integrals in Eq. (2.6.7) and their analytical evaluation on the interval $[x_{1max}, \infty)$ using the asymptotic solutions for ζ and $\mathbf{y}_1$ in the burnt gas.

As an example of the receptivity problem, an adiabatic initial perturbation is introduced at $x_1 = x_{10} > 0$

$$\mathbf{z}_0 = \mathbf{z}_{rc}\delta\left(x_1 - x_{10}\right)\delta\left(x_2\right)\delta\left(x_3\right) \tag{2.6.8}$$

where δ is the Dirac's delta-function. The vector $\mathbf{z}_{rc}$ is chosen as an adiabatic perturbation corresponding to

$$\mathbf{z}_{rc} = \begin{pmatrix} 1 \\ 0 \\ 0 \\ 0 \\ -\gamma p^*(x_{10})/v^*(x_{10}) \\ 0 \end{pmatrix} \tag{2.6.9}$$

The coefficient R_j in Eq. (2.4.18) represents weights of the discrete modes. One can change normalization of the eigenfunctions $\hat{\mathbf{z}}_{dmj}$ with a simultaneous change of the weights, whereas the product $R_j\hat{\mathbf{z}}_{dmj}$ remains the same. In other words, only the product retains physical meaning. In order to characterize amplitudes of the different modes generated by the initial data, Eq. (2.6.8), the maximum of the pressure perturbations, $\max|p_j|$, associated with each mode is used.

Figures 2.9-2.11 show $\max|p_j|$ for $j = 1, 3, 5$ and different values of parameter k. The modes' numbering and the flow parameters are the same as in Fig. 2.6. A possible explanation for the sensitivity to the initial position of the perturbation can be related to the instability mechanism due to Abousief and Toong [21] described in the introduction. Briefly, an upstream acoustic perturbation interacts with the shock and generates irreversible temperature perturbations. The temperature perturbations propagate downstream and introduce the reaction rate disturbance. This serves as a source term that produces more upstream and downstream acoustic waves. The generated upstream acoustic wave perturbs the shock front and completes the cycle. One can then expect that the initial perturbation at some locations x_{10} may be better synchronized with the instability cycle, and therefore that the flow receptivity is sensitive to the location of the initial perturbation.

The figures also illustrate that the flow is more receptive to three-dimensional perturbations in the case of the third and the fifth modes. This effect together with higher growth rates of three-dimensional perturbations should be responsible

for formation of three-dimensional structures in the flow. In all cases, the flow is more receptive to the perturbations introduced in the reaction zone, in the vicinity of the shock wave. Another example of the receptivity problem appears in Appendix A.

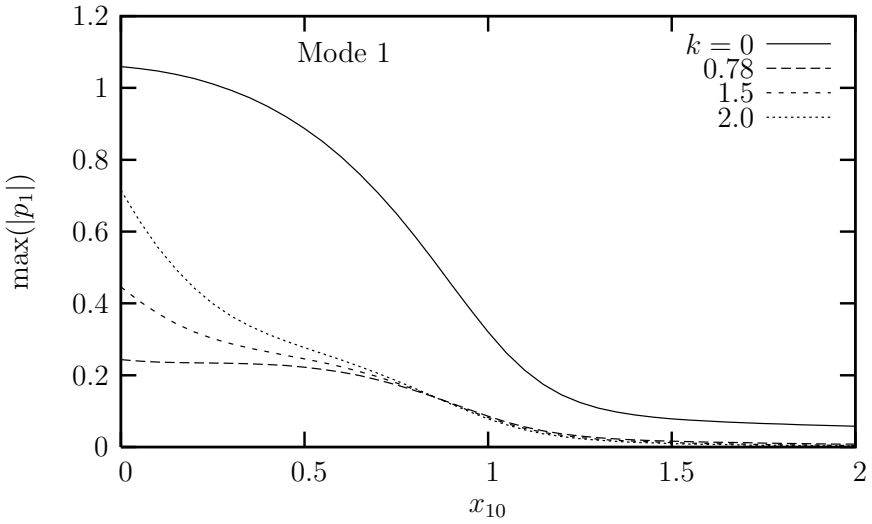

FIGURE 2.9. Maximum of the pressure perturbation in the discrete mode 1 when the initial perturbation is located at x_{10}. Adiabatic perturbation.

2.7 Conclusion

The initial-value problem for three-dimensional perturbations has been revisited. It is shown that the solution can be presented as an expansion into normal modes of discrete and continuous spectra. The discrete spectrum stemming from the solution is equivalent to the spectrum in the conventional normal-mode approach. It is demonstrated that the rear-boundary condition for perturbations in the burnt gas is a trivial consequence of the adjoint solution properties. The solution of the initial-value problem also provides initial amplitudes of the normal modes. An example of initial perturbations within the reaction zone demonstrate that the flow is can be more receptive to three-dimensional perturbations. In addition, three-dimensional unstable

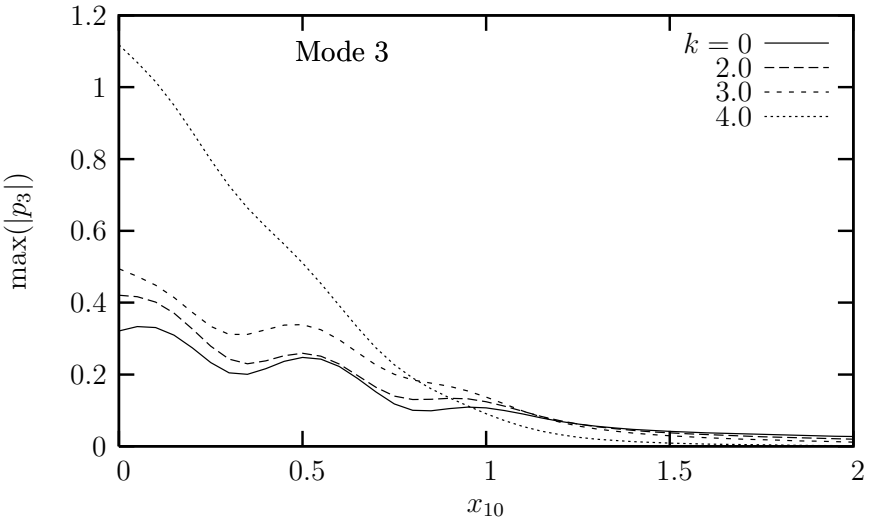

FIGURE 2.10. Maximum of the pressure perturbation in the discrete mode 3 when the initial perturbation is located at x_{10}. Adiabatic perturbation.

modes may have larger growth rates than one-dimensional modes. Both these factors are consistent with experimental observations that real detonation waves have three-dimensional structures.

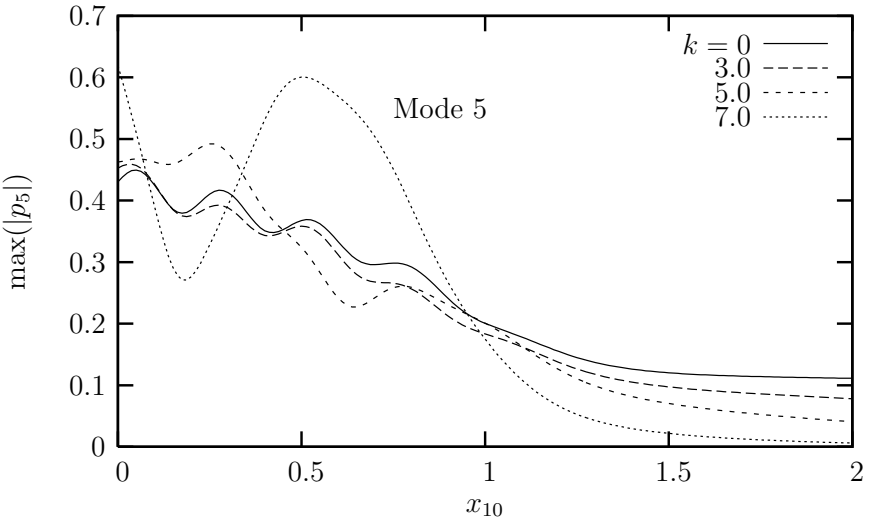

FIGURE 2.11. Maximum of the pressure perturbation in the discrete mode 5 when the initial perturbation is located at x_{10}. Adiabatic perturbation.

Chapter 3
The initial value problem in CJ detonation

3.1 Introduction

The initial value problem (IVP) approach pioneered by Erpenbeck was revisited in the previous chapter under the assumption of explicitly overdriven detonation and 3D perturbations to the planar unbounded ZND flow. It was also shown that the eigenfunctions and eigenvalues obtained through the normal-mode approach were equivalent to the discrete spectrum that naturally arises in the IVP formulation for 3D perturbations. Additionally, the issue of receptivity or the the question of how existing initial perturbations impact the amplitudes of the unstable modes was explored. The present chapter's aim is to close the gap with respect to the application of the IVP approach to the case of an idealized unbounded planar CJ detonation with a simple one-step reaction of unitary reaction order. In general, the CJ detonation is the commonly encountered experimental manifestation of the phenomenon. Mathematically, it involves obtaining asymptotic solutions of the *adjoint* linearized stability equations in the vicinity of an irregular singular point.

3.2 Governing equations

The usual symbols denote the velocity vector $\mathbf{u}$, pressure p, density ρ, reaction progress variable λ and specific internal energy e. The equations and subsequent dimensional scales are introduced following Sharpe in [34] for ease of comparison. The full set of governing equations (in the lab frame) are the Euler equations as in the previous chapter with an Arrhenius one-step reaction rate.

For an ideal polytropic gas, $e = p/(\gamma - 1)\rho - (1 - \lambda)Q$ where the reaction heat release is Q and λ represents the reaction progress variable, with $\lambda = 1$ denoting the

unburnt state and naturally, $\lambda = 0$ denoting a totally burnt state. Additionally, the Arrhenius form of the reaction rate is used and the ideal equation of state,

$$r = -K\lambda e^{-T_A/T},\ T = \frac{\mu p}{R\rho} \tag{3.2.1}$$

where T is the temperature, T_A is an activation temperature, μ is mean molecular weight of the gas, and finally R is the universal gas constant.

From this point forward, by convention, all over-lined quantities represent dimensional values and the "0" subscript represents the steady state distribution of the quantity in the reaction zone. In contrast to the previous chapter, the velocity scale is the detonation velocity. The equations can be made non-dimensional according to:

$$\rho = \frac{\bar{\rho}}{\bar{\rho}_+},\ \mathbf{u} = \frac{\bar{\mathbf{u}}}{\bar{D}},\ p = \frac{\bar{p}}{\bar{\rho}_+\bar{D}^2},\ T = \frac{p}{\rho} = \frac{\bar{R}\bar{T}}{\bar{\mu}\bar{D}^2}, \tag{3.2.2a}$$

$$\text{with } \tau = \frac{\bar{R}\bar{T}_A}{\bar{\mu}\bar{D}^2},\ t = \frac{\bar{K}\bar{t}}{\alpha}, Q = \frac{\bar{Q}}{\bar{D}^2} \tag{3.2.2b}$$

where D is the velocity of the detonation front, and α is a constant that is set by requiring the characteristic length scale in the problem to be the half-reaction zone width. With these dimensional scales in hand, the Arrhenius reaction rate takes the form

$$r = -\alpha\lambda e^{-\tau\rho/p}. \tag{3.2.3}$$

3.2.1 Linearization about the ZND flow

The ZND idealized detonation described in Chapter 2 is again employed as a base flow to small perturbations. In the present chapter, the CJ case is exclusively treated, i.e. $f = 1$. Several instances of the base flow are shown in 3.1. It should be stressed for the current work that Erpenbeck's previous formulation explicitly requires that the detonation wave be of the overdriven type i.e. $f > 1$. Presently, the governing equations will be linearized around the CJ ZND base flow and the the resulting

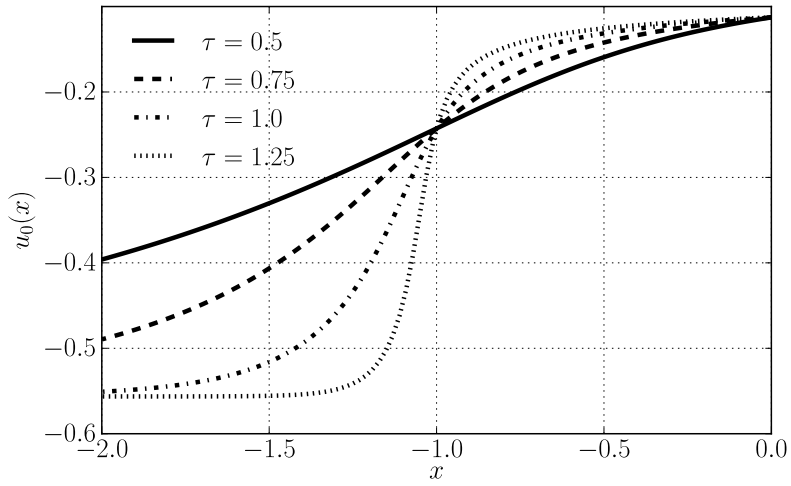

FIGURE 3.1. Steady state (u_0) in shock-attached coordinates for varying τ (dimensionless activation temperature) for $\gamma = 1.2$, $P = 0.02$ (non-dim. pressure in ambient material), and $f = 1$ (overdrive factor).

linearized stability equations will be investigated. The procedure for obtaining the IVP solution is similar to the overdriven case and is briefly repeated here.

In the following, only one transverse coordinate, y, appears for the sake of simplicity in the derivations. One could easily extend the analysis to the full 3D case. Firstly, to formulate the stability equations the reference frame is changed to the frame of the slightly perturbed shock,

$$x = x^l - t - \epsilon\psi(y, t) \tag{3.2.4}$$

where ϵ is a small constant in the subsequent expansion, and thus $\psi(y, t)$ is an $\mathcal{O}(1)$ quantity. Note that the end of the reaction zone is signaled when $x \to -\infty$ in contrast to the previous chapter. The coordinate y^l and time t^l are unchanged in the transformation but are renamed y and t. Also, the velocity in x^l direction is recast according to

$$u = u^l - 1 - \epsilon\frac{\partial\psi}{\partial t}. \tag{3.2.5}$$

The derivatives are transformed according to

$$\frac{\partial}{\partial x^l} \to \frac{\partial}{\partial x}, \ \frac{\partial}{\partial y^l} \to \frac{\partial}{\partial y} - \epsilon \frac{\partial \psi}{\partial y}\frac{\partial}{\partial x}, \frac{\partial}{\partial t^l} \to \frac{\partial}{\partial t} - \epsilon \frac{\partial \psi}{\partial t}\frac{\partial}{\partial x}. \tag{3.2.6}$$

Applying these transformations to the Euler equations and linearizing $\mathbf{z} = (\rho, u, v, p, \lambda)^T$ around the base flow, $\mathbf{z}_0(x) = (\rho_0, u_0, 0, p_0, \lambda_0)^T$, one obtains the following system of linearized stability equations in matrix form at $O(\epsilon)$,

$$\mathbf{A}_t \frac{\partial \mathbf{z}'}{\partial t} + \mathbf{A}_x \frac{\partial \mathbf{z}'}{\partial x} + \mathbf{A}_y \frac{\partial \mathbf{z}'}{\partial y} + \mathbf{B}\mathbf{z}' - \mathbf{s}_t \frac{\partial^2 \psi}{\partial t^2} - \mathbf{s}_y \frac{\partial \psi}{\partial y} = 0 \tag{3.2.7}$$

where $\mathbf{A}_t, \mathbf{A}_x, \mathbf{A}_y$ and $\mathbf{B}$ are 5×5 matrices and $\mathbf{s}_y$ and $\mathbf{s}_t$ are 5×1 column vectors. These are explicitly given in Appendix B.1.

Since the shock is considered as a discontinuous jump in the dependent variables of the system, one can define the Rankine-Hugoniot jump conditions at the shock. These are written with the convention that the subscript "$-$" denotes the area behind the front and "$+$" the area in front of the shock, i.e. the quiescent gas,

$$\begin{aligned}
&\Big(\rho(\mathbf{D}^l - \mathbf{u}^l)\Big)_- \cdot \mathbf{n} = \Big(\rho(\mathbf{D}^l - \mathbf{u}^l)\Big)_+ \cdot \mathbf{n} = m, \\
&p_+ - p_- = m^2\left(\frac{1}{\rho_-} - \frac{1}{\rho_+}\right), \\
&\left(e + \frac{p}{\rho} + \frac{1}{2}|\mathbf{D}^l - \mathbf{u}^l|^2\right)_+ = \left(e + \frac{p}{\rho} + \frac{1}{2}|\mathbf{D}^l - \mathbf{u}^l|^2\right)_-, \\
&\mathbf{u}_+ \cdot \mathbf{l} = \mathbf{u}_- \cdot \mathbf{l}, \ \lambda_+ = \lambda_-.
\end{aligned} \tag{3.2.8}$$

The resulting linearized equations can be summarized in the vector notation as the boundary condition,

$$\mathbf{z}'(0_-, y, t) = \mathbf{Y}\mathbf{z}'(0_+, y, t) + \mathbf{h}_y \frac{\partial \psi}{\partial y} + \mathbf{h}_t \frac{\partial \psi}{\partial t}. \tag{3.2.9}$$

The matrices and vectors are given in Appendix B.1. The vector of perturbations that appears in Eq. (3.2.9), $\mathbf{z}'(0_-, y, t)$, is the perturbation vector in the quiescent gas and is considered known since the problem for perturbations in the quiescent gas is straightforward.

3.2.2 Definition of the initial value problem and its general solution

The IVP is then prescribed by the following initial condition and boundary conditions,

$$\begin{aligned} t = 0: \ & \mathbf{z}'(x,y,0) = \mathbf{z}'_i(x,y), \\ & \psi(y,0) = 0, \left.\frac{\partial \psi}{\partial t}\right|_{t=0} = 0 \\ x = 0: \ & \mathbf{z}'(0_+,y,t) = \mathbf{Y}\mathbf{z}'(0_-,y,t) + \mathbf{h}_y \frac{\partial \psi}{\partial y} + \mathbf{h}_t \frac{\partial \psi}{\partial t} \\ x \to -\infty: \ & |\mathbf{z}'(x,y,t)| < \infty \end{aligned} \tag{3.2.10}$$

along with the linearized governing equation Eq. (3.2.7).

This defines a two-point boundary value problem as well as an initial value problem for perturbations in an idealized one-reaction detonation. The second stated boundary condition is a spatial boundedness constraint for the perturbation. Additionally, the conditions on $\psi(t=0)$ and $\partial\psi/\partial t|_{t=0}$ could be relaxed and generalized to non-zero values.

To facilitate the solution of the IVP by obtaining equations in only one variable, the Fourier transform is firstly performed in the transverse coordinate y,

$$\hat{\mathbf{z}}(x,k,t) = \int_{-\infty}^{\infty} e^{-iky}\mathbf{z}'(x,y,t)dy, \ \hat{\psi}(k,t) = \int_{-\infty}^{\infty} e^{-iky}\psi(y,t)dy. \tag{3.2.11}$$

Additionally, the Laplace transform is produced for both $\hat{\psi}$ and $\hat{\mathbf{z}}$, i.e.

$$\overline{\mathbf{z}} = \int_0^{\infty} e^{-\sigma t}\hat{\mathbf{z}}dt, \ \overline{\psi} = \int_0^{\infty} e^{-\sigma t}\hat{\psi}dt.$$

Finally, the resulting inhomogeneous system of ODE's in x is as follows

$$\mathbf{A}_x \frac{d\overline{\mathbf{z}}}{dx} + (ik\mathbf{A}_y + \mathbf{B} + \sigma\mathbf{A}_t)\overline{\mathbf{z}} - (\sigma^2\mathbf{s}_t + ik\mathbf{s}_y)\overline{\psi} = \mathbf{A}_t\hat{\mathbf{z}}_i. \tag{3.2.12}$$

where $\hat{\mathbf{z}}_i(x;k)$ is the transverse coordinate transform of the initial data $\mathbf{z}_i(x,y,z)$, and the equations depend on both k and σ. Defining the sonic parameter, $\eta_0 = u_0^2 - a_0^2$,

where the sound speed $a_0 = \sqrt{\gamma p_0/\rho_0}$, gives

$$\begin{aligned} &\eta_0 \frac{d\overline{\mathbf{z}}}{dx} = \mathbf{A}\overline{\mathbf{z}} + \eta_0 \mathbf{F} \\ &\begin{cases} \mathbf{A} = -\eta_0 \mathbf{A}_x^{-1}[ik\mathbf{A}_y + \mathbf{B} + \sigma \mathbf{A}_t] \\ \mathbf{F} = \mathbf{F}_1 + \mathbf{F}_2 \overline{\psi} \\ \mathbf{F}_1 = \mathbf{A}_x^{-1}\mathbf{A}_t \hat{\mathbf{z}}_i, \ \mathbf{F}_2 = \mathbf{A}_x^{-1}\left(\sigma^2 \mathbf{s}_t + ik\mathbf{s}_y\right) \end{cases} \end{aligned} \tag{3.2.13}$$

Both $\mathbf{F}$ and $\mathbf{A}$ depend on x, and on the transform variables.

The solution of the IVP contained in Eq. (3.2.13) will involve the method of variation of parameters. Thus, the fundamental solutions of the corresponding *direct* homogeneous problem to Eq. (3.2.13) will be crucial, i.e.

$$\eta_0 \frac{d\overline{\mathbf{z}}_h}{dx} = \mathbf{A}\overline{\mathbf{z}}_h. \tag{3.2.14}$$

The analytic asymptotic solutions as $x \to -\infty$ will be specially needed in determining how to apply the boundedness condition that is necessary to complete the IVP solution.

The solution method is the same as in the overdriven case so the specifics are omitted here. The crucial difference lies in the derivation of the appropriate asymptotic forms. After obtaining the weights of each direct fundamental solution through the use of the adjoint counterparts, the IVP solution in the general form is obtained:

$$\overline{\mathbf{z}} = \sum_{j=1}^{5} \left(a_j + \int_0^x (\mathbf{y}_j \cdot \mathbf{F}) dy' \right) \overline{\mathbf{z}}_j, \tag{3.2.15}$$

where the $\mathbf{y}_i$ are the fundamental solutions of the adjoint problem:

$$\eta_0 \frac{d\mathbf{y}_i}{dx} = -\mathbf{A}^T \mathbf{y}_i. \tag{3.2.16}$$

Note that in the solution above the boundary conditions of the problem have not been incorporated, i.e. the constants a_j are unknown. The first of the two boundary conditions that will be applied is the boundedness constraint at $x \to -\infty$. However, without information about the asymptotic form of the fundamental solutions it cannot

be determined which fundamental solution(s) need to be excluded as $x \to -\infty$. The focus of the next section is to obtain asymptotic versions of the fundamental solutions of the direct and adjoint problems.

3.3 Asymptotics of the direct and adjoint problems

3.3.1 Direct problem

As mentioned, to ensure the boundedness of the solution to the initial value problem it is necessary to obtain the asymptotic form of the fundamental solutions. Therefore, the method set out by Sharpe [34] will be applied to both the direct and adjoint equations. In Ref. [34], the outlined method to obtain the asymptotics in the vicinity of irregular fixed points is based on the work of Wasow [49] and Sharpe calculated the asymptotic expansions of the direct problem in the normal mode-context. These are described in the following.

The defining characteristic of Chapman-Jouguet (CJ) detonation is that the sonic parameter

$$\eta_0 = u_0^2 - a_0^2 \tag{3.3.1}$$

approaches zero at the end of the reaction zone (in this case as $x \to -\infty$). In other words, the flow is locally sonic as $x \to -\infty$. This introduces additional complication in obtaining the leading term for the asymptotic form of the fundamental solutions since the coefficient matrix becomes singular in this limit. The asymptotic analysis of the direct fundamental solutions within the normal mode approach which appears in [34] can be modified and applied in the IVP context. The asymptotic results are obtained with the change of variable,

$$w = u_0 - u_0^{\infty} \tag{3.3.2}$$

where w is the difference between the steady state velocity $u_0(x)$ and its asymptotic value u_0^∞. It can be shown to have the asymptotic form [34]

$$w \to \exp(\beta x), \quad \beta = -\frac{\alpha}{2u_0^\infty}\exp\left(\frac{\tau}{u_0^\infty(u_0^\infty + P + 1)}\right) > 0. \tag{3.3.3}$$

Therefore one can obtain asymptotic fundamental solutions denoted by the ∞ superscript,

$$\begin{aligned}
\overline{\mathbf{z}}_1^\infty &= \exp\left(\frac{2\sigma}{\beta(\gamma+1)w}\right) w^\phi(\mathbf{a}_0^1 + \mathbf{a}_1^1 w + \dots) \\
\overline{\mathbf{z}}_2^\infty &= w^{h_1}(\mathbf{a}_0^2 + \mathbf{a}_1^2 w + \dots) \\
\overline{\mathbf{z}}_3^\infty &= w^{h_1+2}(\mathbf{a}_0^3 + \mathbf{a}_1^3 w + \dots) \\
\overline{\mathbf{z}}_4^\infty &= w^{h_2}(\mathbf{a}_0^4 + \mathbf{a}_1^4 w + \dots) \\
\overline{\mathbf{z}}_5^\infty &= w^{h_1}\big((\mathbf{a}_0^5 + \mathbf{a}_1^5 w + \dots) + w^2 \ln w(\mathbf{b}_0 + \mathbf{b}_1 w + \dots)\big)
\end{aligned} \tag{3.3.4}$$

where

$$h_1 = -\frac{\sigma}{\beta u_0^\infty}, \; h_2 = -\frac{\sigma}{2\beta u_0^\infty} - \frac{k^2 u_0^\infty}{2\sigma\beta}, \tag{3.3.5}$$

and ϕ is a function of σ, k, u_0^∞ etc. The leading order vectors are as follows:

$$\begin{aligned}
\mathbf{a}_0^1 &= (1/(u_0^\infty)^2, 1, 0, 1, 0)^T, \\
\mathbf{a}_0^2 &= \left(1, \gamma\tau, -\frac{i\gamma\sigma\tau}{k u_0^\infty}, 0, 0\right)^T, \\
\mathbf{a}_0^3 &= \frac{(1+u_0^\infty)^2(\gamma+1)}{k^2 u_0^{\infty 2} + \sigma(4u_0^\infty\ \beta - \sigma)} \times \Bigg(-\frac{k^2 u_0^{\infty 2} - (\sigma - 2u_0^\infty\beta)^2}{2u_0^{\infty 3}}, \beta(2u_0^\infty\beta - \sigma), \dots \\
&\quad ik u_0^\infty\beta, 2u_0^\infty\beta^2, \frac{k^2 u_0^{\infty 2} + \sigma(4u_0^\infty\beta - \sigma)}{(1+u_0^\infty)^2(\gamma+1)}\Bigg)^T \\
\mathbf{a}_0^4 &= \left(1/u_0^{\infty 2}, \frac{k^2 u_0^{\infty 2} + \sigma^2}{k^2 u_0^{\infty 2} - \sigma^2}, -\frac{2i\sigma k u_0^\infty}{k^2 u_0^{\infty 2} - \sigma^2}, 1, 0\right)^T, \\
\mathbf{a}_0^5 &= \left(0, \frac{ik u_0^\infty}{\sigma}, 1, 0, 0\right)^T.
\end{aligned} \tag{3.3.6}$$

The asymptotic form reveals that the first fundamental solution is unbounded since the limit $w \to 0$ causes the exponential factor, $\exp\big(2\sigma/\big[\beta(\gamma+1)w\big]\big)$, to grow without

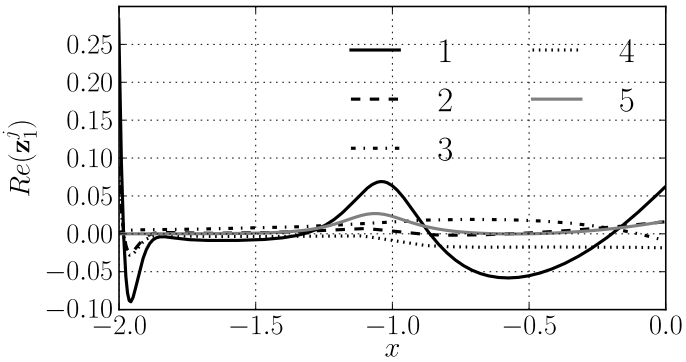

(a) Real

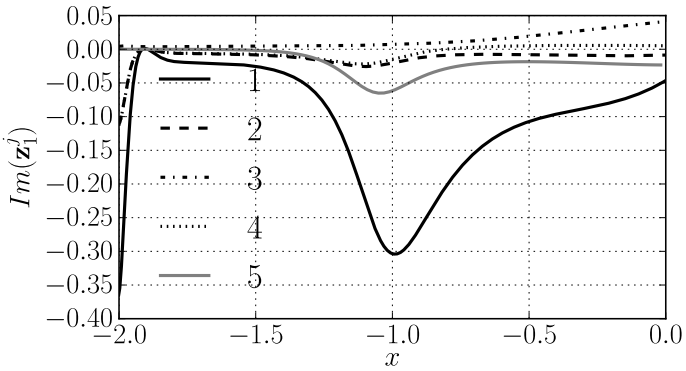

(b) Imaginary

FIGURE 3.2. The direct unbounded fundamental solution $\mathbf{z}_1$ for $\gamma = 1.2$, $P = 0.02$, $\tau = 1.0$ and $f = 1$ for the eigenvalue $\sigma^* = 0.17988 + 0.23341i$.

bound. Using the asymptotic version as a starting point one can then obtain the full numerical solution for $\overline{\mathbf{z}}_1$. The real and imaginary parts appear in Fig. 3.2. The question becomes then: how to eliminate this fundamental solution as $x \to -\infty$? Within the IVP approach, this requires the asymptotic form of the adjoint fundamental solutions in order to define the formal solution. Completing this analysis will lead to the solution of the IVP for the CJ case.

3.3.2 Adjoint asymptotics

Finding the adjoint fundamental solutions at the end of the reaction zone is critical in defining a bounded solution to the IVP. Therefore, one seeks asymptotic solutions to the problem encapsulated in (3.2.16). As a first step then, the independent variable is shifted from x to $w = u_0(x) - u_0^\infty \to \exp(\beta x)$. Clearly $x \to -\infty$ implies $w \to 0$ since $\beta x > 0$ as pointed out previously. In general, the superscript "∞" refers to the conditions at the end of the reaction zone. These transformations imply that one can transform the LHS of the adjoint homogeneous problem:

$$\eta_0 \frac{d\mathbf{y}}{dx} = -\mathbf{A}^T\mathbf{y} \tag{3.3.7}$$

to

$$\left(\eta_0 \frac{dw}{dx}\right)\frac{d\mathbf{y}}{dw} = -\mathbf{A}^T\mathbf{y}. \tag{3.3.8}$$

The derivative dw/dx is an explicit function of w only. Now, one can show that $\eta_0 \to w \to 0$ and $dw/dx \to w \to 0$ so that the problem becomes of the following type in the asymptotic limit

$$w^2 \frac{d\mathbf{y}^\infty}{dw} = -\mathbf{A}^T\mathbf{y}^\infty. \tag{3.3.9}$$

From the above it is clear that $w = 0$ is an irregular singular point of the underlying equations and there are additional complications compared to the overdriven case which is a *regular* singular point problem. To resolve the issue, a new variable is defined, $z = 1/w$, so that

$$\eta_0 \frac{d}{dx} = \frac{1}{2}\alpha(\gamma+1) \times \exp\left(\frac{\tau z^2}{(u_0^\infty z + 1)(1 + (u_0^\infty + P + 1)z)}\right)\frac{d}{dz}. \tag{3.3.10}$$

Dividing through by the factor multiplying d/dz on the RHS of Eq. (3.3.10) and expanding the resulting RHS of Eq. (3.3.7) in powers of $1/z$ one can define the expanded homogeneous problem,

$$\frac{d\mathbf{y}^\infty}{dz} = -\left(\mathbf{A}_0^T + \frac{1}{z}\mathbf{A}_1^T + \frac{1}{z^2}\mathbf{A}_2^T + \dots\right)\mathbf{y}^\infty. \tag{3.3.11}$$

For the CJ case the leading order matrix $\mathbf{A}_0$ is highly degenerate adding to the complication of obtaining asymptotic solutions. In particular the matrix

$$\mathbf{A}_0 = \frac{1}{(\gamma+1)\beta}\begin{pmatrix} 0 & \sigma/u_0^{\infty 2} & -ik/u_0^{\infty} & \sigma/u_0^{\infty 2} & -(\gamma+1)\beta(1+u_0^{\infty})^2/u_0^{\infty 2} \\ 0 & \sigma & -iku_0^{\infty} & \sigma & -(\gamma+1)\beta(1+u_0^{\infty})^2 \\ 0 & 0 & 0 & 0 & 0 \\ 0 & \sigma & -iku_0^{\infty} & \sigma & -(\gamma+1)\beta(1+u_0^{\infty})^2 \\ 0 & 0 & 0 & 0 & 0 \end{pmatrix}, \tag{3.3.12}$$

and so as a result the matrix, $-\mathbf{A}_0^T$, has the eigenvalues $-2\sigma/(\gamma+1)\beta$ and 0 (with multiplicity 4). Consequently, a series of transformations are required to obtain the fundamental solutions. These transformations are based on the methods outlined by Wasow [49], but modeled on the normal mode analysis of the asymptotics in Sharpe [34].

3.3.3 Derivation of asymptotic adjoint fundamental solutions

Firstly, a transformation $\mathbf{y}^{\infty} = \mathbf{T}\mathbf{w}$ is produced where $\mathbf{T}$ is the matrix of eigenvectors of $-\mathbf{A}_0^T$, and one can define $\mathbf{B}_0 = \mathbf{T}^{-1}(-\mathbf{A}_0^T)\mathbf{T}$ to produce the modified problem:

$$\frac{d\mathbf{w}}{dz} = \left(\mathbf{B}_0 + \frac{1}{z}\mathbf{B}_1 + \frac{1}{z^2}\mathbf{B}_2 + \dots\right)\mathbf{w} \tag{3.3.13}$$

Further, let

$$\mathbf{w} = \left(\mathbf{I} + \frac{1}{z}\mathbf{M}_1 + \frac{1}{z^2}\mathbf{M}_2 + \dots\right)\mathbf{v} \tag{3.3.14}$$

so that $\mathbf{v}$ satisfies the equation

$$\frac{d\mathbf{v}}{dz} = \left(\mathbf{D}_0 + \frac{1}{z}\mathbf{D}_1 + \frac{1}{z^2}\mathbf{D}_2 + \dots\right)\mathbf{v}. \tag{3.3.15}$$

Both $\mathbf{D}_i$ and $\mathbf{M}_i$ are defined to have a distinctive structure, i.e.

$$\mathbf{D}_i = \begin{pmatrix} D_i^{11} & \mathbf{0} \\ \mathbf{0} & \mathbf{D}_i^{22} \end{pmatrix}, \ \mathbf{M}_i = \begin{pmatrix} 0 & \mathbf{M}_i^{12} \\ \mathbf{M}_i^{21} & \mathbf{0} \end{pmatrix}. \tag{3.3.16}$$

Here, $\mathbf{D}_i^{22}$ is 4×4, $\mathbf{M}_i^{12}$ is 4×1, and $\mathbf{M}_i^{21}$ is 1×4. Equating the coefficients of $1/z^i$ term by term in Eq. (3.3.15), results in a series of equations for the unknown matrices. For example at order z^0 one obtains $\mathbf{D}_0 = \mathbf{B}_0$ and for further orders,

$$\begin{aligned} \mathbf{B}_1 + \mathbf{B}_1\mathbf{M}_1 &= \mathbf{D}_1 + \mathbf{M}_1\mathbf{D}_0 \\ \mathbf{M}_1 + \mathbf{B}_0\mathbf{M}_2 + \mathbf{B}_1\mathbf{M}_1 + \mathbf{B}_2 &= \mathbf{D}_2 + \mathbf{M}_1\mathbf{D}_1 + \mathbf{M}_2\mathbf{D}_0 \\ 2\mathbf{M}_2 + \mathbf{B}_0\mathbf{M}_3 + \mathbf{B}_1\mathbf{M}_2 + \mathbf{B}_2\mathbf{M}_1 + \mathbf{B}_3 &= \mathbf{D}_3 + \mathbf{M}_1\mathbf{D}_2 + \mathbf{M}_2\mathbf{D}_1 + \mathbf{M}_3\mathbf{D}_0. \end{aligned} \tag{3.3.17}$$

From the structure of $\mathbf{D}_i$ represented in Eq. (3.3.16) it can be seen that the first component of $\mathbf{v}$ is decoupled from the remaining elements,

$$\frac{dv_1}{dz} = \left(-\frac{2\sigma}{(\gamma+1)\beta} + \frac{1}{z}D_1^{11} + \frac{1}{z^2}D_2^{11} + \dots \right) v_1. \tag{3.3.18}$$

The rest of the components can be placed in the 4×1 vector, $\mathbf{v}^* = (v_2, v_3, v_4, v_5)^T$, and so $\mathbf{v}^*$ satisfies the reduced equation

$$\frac{d\mathbf{v}^*}{dz} = \left(\frac{1}{z}\mathbf{D}_1^{22} + \frac{1}{z^2}\mathbf{D}_2^{22} + \dots \right) \mathbf{v}^*. \tag{3.3.19}$$

It is possible to solve Eq. (3.3.18) directly by defining $v_1 = \exp(-2\sigma z/(\gamma+1)\beta) g(z)$. This then provides our first asymptotic fundamental solution in the transformed system, in terms of $w = 1/z = u_0 - u_0^\infty$,

$$\mathbf{v}_1 = \exp\left(-\frac{2\sigma}{\beta(\gamma+1)w} \right) w^{-\phi} \left(\mathbf{c}_0^1 + w\mathbf{c}_1^1 + w^2\mathbf{c}_2^1 + \dots \right) \tag{3.3.20}$$

where $\mathbf{c}_0^1 = (1, 0, 0, 0, 0)^T$ and $\phi = D_1^{11}$.

As for the rest of the components they will satisfy the reduced equations (now a 4×4 system). It is advantageous to again change the independent variable to $w = 1/z$. This will change the LHS of Eq. (3.3.19), according to,

$$\frac{d}{dz} = \frac{dw}{dz}\frac{d}{dw} = -w^2\frac{d}{dw}. \tag{3.3.21}$$

One can then define the modified problem:

$$w\frac{d\mathbf{v}^*}{dw} = -\left(\mathbf{D}_1^{22} + w\mathbf{D}_2^{22} + \dots \right) \mathbf{v}^*. \tag{3.3.22}$$

Clearly, $w = 0$ is a regular singular point of Eq. (3.3.22) (because w appears to the first power on the LHS).

The method for obtaining an asymptotic solution in the vicinity of a regular singular point employs a transformation, $\mathbf{v}^* = (\mathbf{I} + \mathbf{N}_1 w + \mathbf{N}_2 w^2 + \dots)\mathbf{m}$, which would produce a much simpler problem that only involves the leading order matrix, i.e.

$$w\frac{d\mathbf{m}}{dw} = -\mathbf{D}_1^{22}\mathbf{m}. \tag{3.3.23}$$

However, due to the fact that the eigenvalues of $-\mathbf{D}_1^{22}$ are such that two of them differ by a positive integer, then it is not yet possible to reduce the system to a form like Eq. (3.3.23). Specifically, the eigenvalues one obtains from the matrix, $-\mathbf{D}_1^{22}$, are $-h_1, -h_1, -h_2$ and $-h_1 - 2$. The following transformations reduce our problem to a point at which the leading order transformed matrix has the desired property.

Firstly, the eigenvectors of $-\mathbf{D}_1^{22}$ are used to diagonalize the leading order matrix by placing them into a matrix $\mathbf{Q}$ so that $\mathbf{v}^* = \mathbf{Q}\mathbf{q}$. Then as a result,

$$w\frac{d\mathbf{q}}{dw} = (\mathbf{E}_1 + \mathbf{E}_2 w + \dots)\mathbf{q} \tag{3.3.24}$$

with

$$\mathbf{E}_i = \mathbf{Q}^{-1}(-\mathbf{D}_i^{22})\mathbf{Q} \tag{3.3.25}$$

and in particular $\mathbf{E}_1 = \mathrm{diag}(-h_1, -h_1, -h_2, -h_1 - 2)$. One must now "shear" the leading order matrix, $\mathbf{E}_1$, with help of the matrix, $S(w)$,

$$S = \begin{pmatrix} 1 & & & \\ & 1 & & \\ & & 1 & \\ & & & w \end{pmatrix} \tag{3.3.26}$$

The transformation, $\mathbf{q} = (\mathbf{S}^{-1})^2\mathbf{p}$, produces an leading order matrix with the eigenvalues $-h_1, -h_1, -h_2$ and $-h_1$. At this point then, the leading order matrix has the

property that no two eigenvalues differ by a positive non-zero integer. Thus,

$$w\frac{d\mathbf{p}}{dw} = (\mathbf{F}_1 + \mathbf{F}_2 w + \dots)\mathbf{p} \tag{3.3.27}$$

with the leading order matrix

$$\mathbf{F}_1 = \begin{pmatrix} -h_1 & & & e_1 \\ & -h_1 & & e_2 \\ & & -h_2 & e_3 \\ & & & -h_1 \end{pmatrix} \tag{3.3.28}$$

where $e_i = (\mathbf{E}_3)_{4i}$. The matrix is no longer diagonal as there is a contribution from the third order matrix $\mathbf{E}_3$. The details of this transformation encapsulated by the matrix $\mathbf{S}$ appear in Appendix B.2. The final transformation, $\mathbf{p} = (\mathbf{I} + \mathbf{N}_1 w + \dots)\mathbf{m}$, will yield the matrix equation

$$w\frac{d\mathbf{m}}{dw} = \mathbf{F}_1\mathbf{m} \tag{3.3.29}$$

which is readily solvable since it has dependence only on $\mathbf{F}_1$ and not the entire series of matrices. The matrices $\mathbf{N}_i$ must satisfy a recursive relation similar to the matrices $\mathbf{D}_i$ and $\mathbf{M}_i$ encountered previously, specifically,

$$(\mathbf{F}_1 - \mathbf{I})\mathbf{N}_1 - \mathbf{N}_1\mathbf{F}_1 = -\mathbf{F}_2 \tag{3.3.30}$$

$$(\mathbf{F}_1 - 2\mathbf{I})\mathbf{N}_2 - \mathbf{N}_2\mathbf{F}_1 = -\mathbf{F}_3 - \mathbf{F}_2\mathbf{N}_1 \tag{3.3.31}$$

for $\mathbf{N}_1$ and $\mathbf{N}_2$. Solving Eq. (3.3.29) is straightforward and one obtain 4 fundamental solutions in this transformed system as follows

$$\begin{aligned} \mathbf{m}_2 &= w^{-h_1}(1,0,0,0)^T, \\ \mathbf{m}_3 &= w^{-h_1}(0,1,0,0)^T, \\ \mathbf{m}_4 &= w^{-h_2}(0,0,1,0)^T, \\ \mathbf{m_5} &= w^{-h_1}(e_1\log(w), e_2\log(w), e_3/(h_2-h_1), 1)^T. \end{aligned} \tag{3.3.32}$$

However, the fundamental solutions were sought in the original system involving $\mathbf{y}^\infty$ and so inversion of the transformation is needed. The first step in this inversion is as

follows,

$$\mathbf{v}^* = \mathbf{Q}(\mathbf{S}^{-1})^2(\mathbf{I} + w\mathbf{N}_1 + w^2\mathbf{N}_2 + \dots)\mathbf{m} \tag{3.3.33}$$

Recall that $\mathbf{v}^*$ solves a reduced system so the fundamental solutions corresponding to $\mathbf{v}$ are simply

$$\mathbf{v}_i = (0, \mathbf{v}_i^*)^T, \ i = 2, 3, 4, 5. \tag{3.3.34}$$

Given $\mathbf{v}_1$ as defined in Eq. (3.3.20) and the solutions defined by Eq. (3.3.34), one then has a complete set of fundamental solutions in the system defined by Eq. (3.3.15). Finally, the fundamental solutions in the original system are obtained from the transformation:

$$\mathbf{y}^\infty = \mathbf{T}(\mathbf{I} + w\mathbf{M}_1 + w^2\mathbf{M}_2 + \dots)\mathbf{v}. \tag{3.3.35}$$

In particular one obtains the set of asymptotic fundamental solutions (denoted by superscript ∞) of the form:

$$\begin{aligned}
\mathbf{y}_1^\infty &= \exp\left(-\frac{2\sigma}{(\gamma+1)\beta w}\right) w^{-\phi}(\mathbf{d}_0^1 + \mathbf{d}_1^1 w + \dots) \\
\mathbf{y}_2^\infty &= w^{-h_1}(\mathbf{d}_0^2 + \mathbf{d}_1^2 w + \dots) \\
\mathbf{y}_3^\infty &= w^{-h_1-2}\big((\mathbf{d}_0^3 + \mathbf{d}_1^3 w + \dots) + w^2 \ln w(\mathbf{f}_0 + \mathbf{f}_1 w + \dots\big) \\
\mathbf{y}_4^\infty &= w^{-h_2}(\mathbf{d}_0^4 + \mathbf{d}_1^4 w + \dots) \\
\mathbf{y}_5^\infty &= w^{-h_1}(\mathbf{d}_0^5 + \mathbf{d}_1^5 w + \dots)
\end{aligned} \tag{3.3.36}$$

with $h_1 = -\sigma/\beta u_0^\infty$ and $h_2 = -\sigma/2\beta u_0^\infty - k^2 u_0^\infty/2\sigma\beta$ and with leading term vectors

$$\begin{aligned}
\mathbf{d}_0^1 &= \left(0, \frac{1}{2}, -\frac{iku_0^\infty}{2\sigma}, \frac{1}{2}, -\frac{(1+u_0^\infty)^2\beta(\gamma+1)}{2\sigma}\right)^T, \\
\mathbf{d}_0^2 &= \left(1, 0, 0, -1/u_0^{\infty 2}, \frac{(1+u_0^\infty)^2(\gamma+1)}{2u_0^{\infty 3}}\right)^T, \\
\mathbf{d}_0^3 &= (0,0,0,0,1)^T, \\
\mathbf{d}_0^4 &= \left(0, -\frac{1}{2}, \frac{iku_0^\infty}{2\sigma}, \frac{1}{2}, \frac{(1+u_0^\infty)^2\beta(\gamma+1)(k^2u_0^{\infty 2}-\sigma^2)}{2\sigma(k^2u_0^{\infty 2}+(4u_0^\infty\beta-\sigma)\sigma}\right)^T \\
\mathbf{d}_0^5 &= \left(\frac{i\gamma\sigma\tau}{ku_0^\infty}, \frac{iku_0^\infty\sigma}{\sigma^2-k^2u_0^{\infty 2}}, \frac{\sigma^2}{\sigma^2-k^2u_0^{\infty 2}}, \frac{i\sigma(\gamma\sigma^2\tau+k^2u_0^{\infty 2}(u_0^{\infty 2}-\gamma\tau))}{u_0^{\infty 3}k(k^2u_0^{\infty 2}-\sigma^2)}, \ldots\right. \\
&\left.\frac{i(1+u_0^\infty)^2\gamma(\gamma+1)\sigma\tau}{2ku_0^{\infty 4}}\right)^T.
\end{aligned} \tag{3.3.37}$$

The only bounded adjoint fundamental solution is $\mathbf{y}_1^\infty$, clearly the counterpart to the unbounded $\overline{\mathbf{z}}_1^\infty$ for $\mathrm{Re}(\sigma) > 0$. As in the direct case, the asymptotic form can be used as a starting point in integrating the governing equation for the adjoint fundamental solution. This appears in Fig. 3.3. The rest of the adjoint fundamental solutions are unbounded for the same restriction, i.e. for $\mathrm{Re}(\sigma) > 0$. An additional property of the found adjoint system is that it indeed has the basic biorthogonality property that at leading order

$$\overline{\mathbf{z}}_i^\infty \cdot \mathbf{y}_j^\infty = \delta_{ij}. \tag{3.3.38}$$

3.3.4 Boundedness and the radiation boundary condition

Recall that the IVP solution presented in (3.2.15) has a number of undefined constants. Most importantly, the weight function corresponding to the unbounded first fundamental solution, $q_1(x)$ necessarily must vanish as $x \to -\infty$. In other words, the main consequence of the asymptotic form of the direct fundamental solutions is that $\overline{\mathbf{z}}_1$ must be excluded as $x \to -\infty$ in order to guarantee the spatial boundedness of the IVP solution,

$$\lim_{x\to-\infty} |\overline{\mathbf{z}}| < \infty \Rightarrow \lim_{x\to-\infty} (\overline{\mathbf{z}} \cdot \mathbf{y}_1) = 0 \Rightarrow \lim_{x\to-\infty} q_1(x) \to 0 \tag{3.3.39}$$

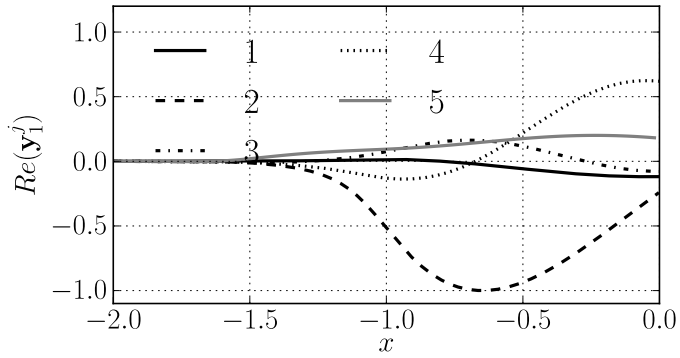

(a) Real

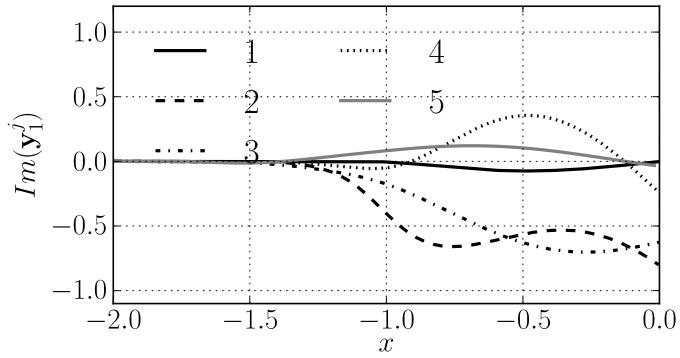

(b) Imaginary

FIGURE 3.3. The bounded adjoint fundamental solution $\mathbf{y}_1$ for $\gamma = 1.2$, $P = 0.02$, $\tau = 1.0$ and $f = 1$ for the eigenvalue $\sigma^* = 0.17988 + 0.23341i$.

In particular, one can guarantee this condition by effectively ensuring the projection of $\overline{\mathbf{z}}$ upon $\overline{\mathbf{z}}_1$ is zero with help of the adjoint fundamental solution $\mathbf{y}_1^\infty$, i.e. one can enforce that $\lim_{x\to-\infty}(\overline{\mathbf{z}}\cdot\mathbf{y}_1) = 0$ by using the asymptotic form of $\mathbf{y}_1$,

$$\lim_{x\to-\infty}(\overline{\mathbf{z}}\cdot\mathbf{y}_1) = 0 \Rightarrow \overline{\mathbf{z}}^\infty\cdot\mathbf{y}_1^\infty = 0 \tag{3.3.40}$$

and therefore to have that $\overline{\mathbf{z}}^\infty\cdot\mathbf{y}_1^\infty = 0$ it is enough to enforce $\overline{\mathbf{z}}^\infty\cdot\mathbf{d}_0^1 = 0$. One then obtains to leading order

$$\frac{\bar{u}}{2} - \frac{iku_0^\infty}{2\sigma}\bar{w} + \frac{1}{2}\bar{p} - \frac{(1+u_0^\infty)^2\beta(\gamma+1)}{2\sigma}\bar{\lambda} = 0 \tag{3.3.41}$$

Since the reaction progress perturbation can be shown smaller in the limit as $x \to -\infty$ than the other perturbations, one can obtain

$$\bar{u} - \frac{iku_0^\infty}{\sigma}\bar{w} + \bar{p} = 0 \tag{3.3.42}$$

which is the same radiation boundary condition obtained by Short et al. for the Chapman-Jouguet gaseous case [50][1]. Clearly, the radiation boundary condition can be thought of as the consequence of ensuring spatial boundedness.

3.4 The continuous and discrete spectrum

In the IVP context, Eq. (3.3.39) leads to the bounded form of $\overline{\mathbf{z}}$ as $x \to -\infty$ keeping $\mathrm{Re}(\sigma) > 0$:

$$\overline{\mathbf{z}}(x,t) = \sum_{j=2}^{5}\left(a_j + \int_0^x (\mathbf{y}_j \cdot \mathbf{F})dy'\right)\overline{\mathbf{z}}_j + \left(\int_{-\infty}^x (\mathbf{y}_1 \cdot \mathbf{F})dy'\right)\overline{\mathbf{z}}_1. \tag{3.4.1}$$

Applying the linearized Rankine-Hugoniot conditions on the shock ($x = 0$), the constants a_j can be defined and in particular the transformed perturbation in the shock position $\overline{\psi}$ is determined,

$$\begin{aligned} \overline{\psi} &= \frac{\mathbf{y}_1(0) \cdot \mathbf{Y}\overline{\mathbf{z}}(0_-) + \int_0^{-\infty}(\mathbf{y}_1 \cdot \mathbf{F}_1)dx}{-V} \\ V &= \left[ikV_k + \sigma V_\sigma\right], \end{aligned} \tag{3.4.2}$$

where

$$\begin{aligned} V_\sigma &= (\mathbf{y}_1(0) \cdot \mathbf{h}_t) + \sigma\int_0^{-\infty}(\mathbf{y}_1 \cdot \mathbf{A}_x^{-1}\mathbf{s}_t)dx', \\ V_k &= (\mathbf{y}_1(0) \cdot \mathbf{h}_y) + \int_0^{-\infty}(\mathbf{y}_1 \cdot \mathbf{A}_x^{-1}\mathbf{s}_y)dx'. \end{aligned} \tag{3.4.3}$$

Crucially, one finds that the constants a_j that appear in the solution, Eq. (3.4.1), also depend inverse proportionally to the function V defined above. The convergence of these integrals is discussed in Appendix B.3 using the asymptotic adjoint fundamental

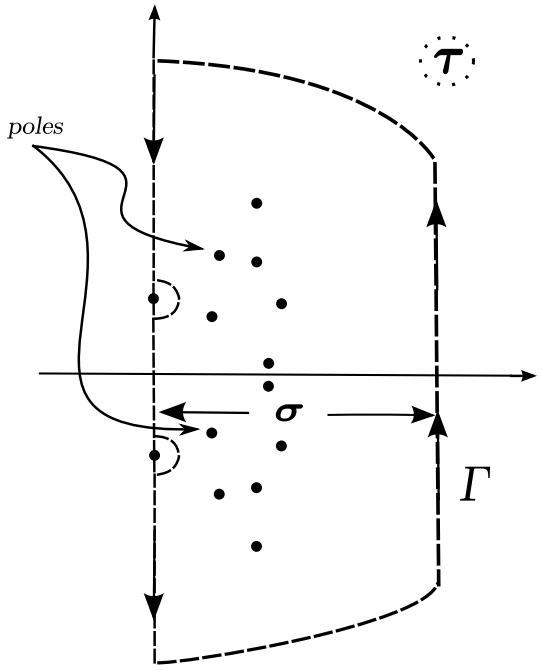

FIGURE 3.4. Schematic showing the relationship between the canonical inversion path Γ and the decomposition into residue and imaginary axis integrals.

solutions. One can then define the formal solution of the problem as the inverse Laplace transform:

$$\hat{\mathbf{z}}(x,t) = \frac{1}{2\pi i}\int_{\Gamma} \overline{\mathbf{z}} e^{\sigma t} d\sigma \tag{3.4.4}$$

where Bromwich's path of integration, i.e. Γ, is defined to be on the right hand side of any singularities in the complex plane of σ (see Figure 3.4). As noted, the coefficients $a_2, \ldots a_5$ and the shock displacement $\bar{\psi}$ may have singularities in the complex plane σ when $V(\sigma = \alpha_j) = 0$. The roots of this function were the primary interest in Erpenbeck's stability studies in the overdriven case [18]. Though Erpenbeck did not explain the closure of the Bromwich path of integration, the roots of this function are associated with the unstable modes. Similarly to the closure defined in [32], the

[1]However, note that different dimensional scales were used in [50]

present path Γ is closed with arcs of infinite radii and an integral over the imaginary axis keeping $\mathrm{Re}(\sigma) \geq 0$ in order to ensure boundedness as $x \to -\infty$. Therefore, one can represent the inverse Laplace transform as a sum of residues associated with the zeros of the function V and an integral over the imaginary axis of σ through the application of Cauchy's Residue Theorem:

$$\hat{\mathbf{z}}(x,t) = \frac{1}{2\pi i}\int_{\Gamma} \overline{\mathbf{z}} e^{\sigma t} d\sigma = \sum_{j} \mathrm{Res}\left(\overline{\mathbf{z}}(x,\sigma)e^{\sigma t}\right)\Big|_{\sigma=\alpha_j} + \frac{1}{2\pi i}\int_{-i\infty}^{i\infty} \overline{\mathbf{z}} e^{\sigma t} d\sigma \tag{3.4.5}$$

Further, the residue from the poles, α_j, can be rewritten as discrete modes with specific initial amplitudes R_j,

$$\hat{\mathbf{z}}(x,t) = \sum_{j} R_j(\alpha_j)\mathbf{z}_{dmj}(x;\alpha_j)e^{\alpha_j t} + \frac{1}{2\pi i}\int_{-i\infty}^{i\infty} \overline{\mathbf{z}} e^{\sigma t} d\sigma. \tag{3.4.6}$$

It is clear from the factor, $\exp(\alpha_j t)$, in the discrete mode terms that a temporal growth of the perturbation will result if $\mathrm{Re}(\alpha_j) > 0$. Therefore, looking for the roots of the function V provides a method for determining the instability of the CJ ZND flow within the IVP context.

Additionally, one can study the how the initial amplitudes of the unstable modes, R_j,

$$R_j = -\frac{1}{\partial V/\partial\sigma|_{\alpha_j}}\left[\mathbf{Y}\overline{\mathbf{z}}(0_-,\sigma)\cdot\mathbf{y}_i(0) + \int_0^{-\infty}(\mathbf{y}_1\cdot\mathbf{A}_x^{-1}\mathbf{A}_t\hat{\mathbf{z}}_i)\ dx\right]_{\sigma=\alpha_j}, \tag{3.4.7}$$

vary as a function of the introduced reaction zone perturbation, $\hat{\mathbf{z}}_i(x)$, and also the perturbation incoming from the quiescent gas, $\overline{\mathbf{z}}(0,\sigma)$, in front of the traveling shock. This is the so-called receptivity analysis.

3.5 Conclusions

The initial value problem approach for the CJ case in an idealized planar detonation is defined here by completing the analysis of the adjoint fundamental solutions of the underlying stability equations. This was done by applying the methods of Wasow in

the manner presented by Sharpe [49, 34]. The resulting solution retains the structure found in the overdriven case [18, 32]. As a result, the IVP approach in the CJ case provides the means for the receptivity analysis and a method for determining the unstable mode eigenfunctions and eigenvalues.

Chapter 4
Multi-domain spectral collocation methods in detonation stability

4.1 Introduction

The conventional stability analysis in detonation has utilized the normal-mode approach along with a shooting procedure to solve the two-point boundary value problem that defines the stability of the flow. The shooting procedure is sensitive to the initial guess for the eigenvalue controlling the temporal stability of the detonation wave, and therefore the method requires a "carpet search" of the complex plane. In other problems in hydrodynamic stability, the eigenvalue problem is solved with help of the spectral collocation method. This method has not been widely applied in studies of detonation stability though Namah et al. [36] and Buckmaster and Neves [37] did apply spectral collocation methods in the early 1990's. Their example however was not taken up in subsequent detonation stability studies for instance in [23, 26].

Recently, Tumin [48] explored the use of the spectral method in studying the one dimensional stability of overdriven detonation with Arrhenius kinetics. The purpose here is to extend the spectral collocation method's application to the case of three dimensional stability of Chapman-Jouguet detonations with an idealized gaseous and condensed phase reaction rate. This particular model's stability was recently investigated by Short et al. [50] using the aforementioned shooting algorithm.

4.2 Problem set-up

4.2.1 Governing equations and reaction rate model

The usual symbols denote the lab frame velocity vector $\mathbf{u}^l = (u^l, w^l)^T$, pressure p, specific volume v, reaction progress variable λ and specific internal energy e. The equations and subsequent dimensional scales are introduced following Short et al. [50]. The full set of governing equations (in the lab frame denoted by "l") for idealized one reaction detonation are the Euler equations as in the previous chapters. For an ideal polytropic gas one has

$$e = pv/(\gamma - 1) - \lambda\tilde{Q}, \text{ and } c^2 = \gamma pv \tag{4.2.1}$$

where $\tilde{Q}$ is the reaction heat release, λ represents the reaction progress variable, with $\lambda = 1$ denoting the burnt state and naturally, $\lambda = 0$ denoting a totally unburnt initial state. The main difference from the following analysis and the previous work lies in the reaction rate. In the current chapter, the reaction rate is as follows:

$$r = \begin{cases} kp^n(1-\lambda)^\nu \exp\left(-\dfrac{\theta}{pv}\right), & 0 \le \lambda \le 1 \\ 0, & \lambda = 1 \end{cases} \tag{4.2.2}$$

where k is the reaction rate constant. There are three parameters in the reaction rate: n (controls the pressure sensitivity of the reaction), θ (Arrhenius temperature sensitivity), and ν (reaction or depletion order). This reaction rate is meant to model not only first order Arrhenius gaseous explosives (with $\nu = 1$ and $n = 0$) but condensed phase explosives as well. The lack of accurate equations of state (as well as their complexity) for non-gaseous explosives hampers the modeling of these explosives. However, the irreversible one-step reaction given above can provide realistic pressures at the end of the reaction zone [50] and has been used previously in theoretical studies of condensed phase detonations [9].

By convention, all over-lined quantities represent dimensional values and the "0" subscript represents the steady state distribution of the quantity in the reaction zone.

The equations can be made non-dimensional as in [50] according to:

$$\begin{aligned} \rho = \frac{\bar{v}}{\bar{v}_u},\ \mathbf{u} = \frac{\bar{\mathbf{u}}}{\bar{D}},\ p = \frac{\bar{p}}{\bar{D}^2/\bar{v}_u},\ \mathbf{x} = \bar{\mathbf{x}}/\bar{l},\ t = \frac{\bar{t}}{\bar{l}/\bar{D}}, \\ Q = \frac{\bar{Q}}{\bar{D}^2},\ \theta = \frac{\bar{E}}{\bar{D}^2},\ c^2 = \frac{\bar{c}^2}{\bar{D}^2} \end{aligned} \tag{4.2.3}$$

where $\bar{v}_u$ refers to the quiescent gas specific volume. The length scale $\bar{l}$ is the characteristic length scale in the problem and it is defined to be the half-reaction zone width.

Rather than using the simple reaction rate variable used up to this point in this dissertation, a change of variable to β is effected whereby

$$\beta = (1 - \lambda)^{1/2} \tag{4.2.4}$$

so that $\beta = 0$ represents a fully depleted state, and conversely, $\beta = 1$ represents a fully fueled one. With this in mind, the reaction rate is suitably transformed,

$$\frac{D\beta}{Dt} = -\frac{1}{2} k p^n \beta^{2n-1} \exp(-\theta/pv) = W \tag{4.2.5}$$

A final parameter is defined, δ which represents an inverse square of the Chapman-Jouguet (CJ) velocity scaled with the upstream sound speed, i.e.

$$\delta = \frac{\bar{c}_u^2}{\bar{D}_{CJ}^2} \tag{4.2.6}$$

The CJ detonation is the particular case that arises when the flow is acoustically isolated, i.e. the final point of the reaction zone is sonic. Therefore, no acoustic signal can reach the shock front from the region behind the final point in the reaction zone. Additionally, in CJ detonation, the velocity of the shock front is exactly the minimally allowed value that can satisfy the conservation of mass, momentum and energy between the undisturbed fuel in front of the shock and the end of the reaction zone behind the front. Mathematically, the minimal velocity, $\bar{D}_{CJ}$ is obtained by requiring that the flow terminate in the sonic point, i.e.

$$M_\infty^2 = 1 \tag{4.2.7}$$

where M_∞ is the Mach number at the end of the reaction zone.

4.2.2 ZND model and linearization

As in previous chapters, the base flow considered in this stability study is the the well-known ZND model of an idealized planar detonation. Specifically, by switching the frame of reference of the governing equations to the moving frame, i.e. $x = x^l - t$ and $u = u^l - 1$, and solving the time-independent version of the equations, one can obtain the ZND base flow. The resulting solution for the base flow is given a subscript 0, i.e. $v_0(x), u_0(x), p_0(x)$ and $\beta_0(x)$. The resulting flow then depends on the parameters: overdrive factor f, δ, γ, n, ν, θ, and also the heat release of the reaction, Q. See the graph in Fig. 4.1 for an example of the pressure profile in the ZND flow for a condensed phase detonation. The main feature of this model is that the bulk of the heat release occurs at the shock. As before, the overdrive factor is defined as the square of the ratio between the actual velocity of the detonation wave and the minimally allowed velocity corresponding to the CJ state, i.e.

$$f = \left(\frac{\bar{D}}{\bar{D}_{CJ}}\right)^2.$$

In the present work, the Chapman-Jouguet case, i.e. $f = 1$ will be considered as well as overdriven detonation. The following wave coordinate is used,

$$x = x^l - t - \epsilon\psi(y, t) \tag{4.2.8}$$

where ϵ is a small constant in the subsequent expansion, and thus $\psi(y, t)$ is an $O(1)$ quantity. The coordinate y^l and time t^l are unchanged in the transformation but are renamed y and t. Also, the gas velocity u is measured according to

$$u = u^l - 1 \tag{4.2.9}$$

These transformations are applied to to the governing equation and a linearization of $\mathbf{z} = (v, u, w, p, \lambda)^T$ about the base flow, $\mathbf{z}_0(x) = (v_0, u_0, 0, p_0, \lambda_0)^T$ (in matrix-vector

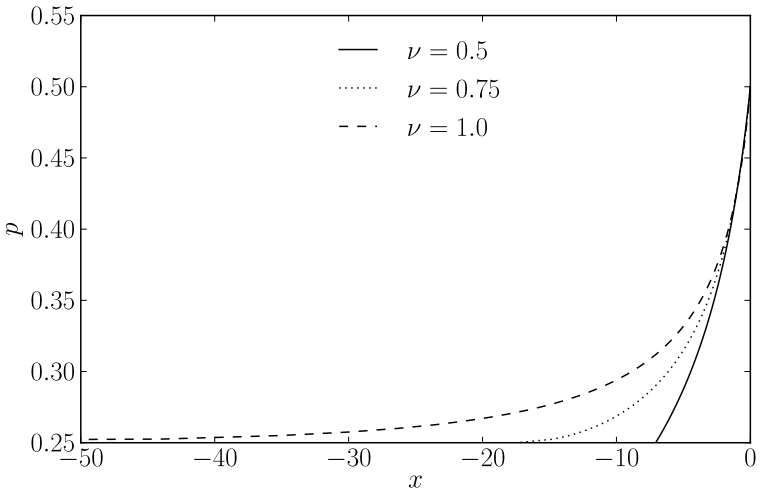

FIGURE 4.1. The ZND pressure profile for condensed flow parameters as ν is varied and $f = 1.0$, $\gamma = 3.0$, $\tau = 0.5$, $n = 2$ and $\delta = \theta = 0$. Note that the reaction rate reaches its maximum at the shock front in contrast to the temperature sensitive gaseous case.

form) is performed in the following manner,

$$\begin{aligned} \mathbf{z} &= \mathbf{z}_0(x) + \psi_0 \mathbf{z}'(x) \exp(iky + \alpha t), \\ \psi &= \psi_0 \exp(iky + \alpha t) \end{aligned} \tag{4.2.10}$$

Note that the sign of $\mathrm{Re}(\alpha)$ will determine whether the perturbations grow in time and thus determine the stability of the flow. Inserting this scheme into the governing equations then produces the following system of linearized stability equations in matrix form at $O(\epsilon)$,

$$\eta_0 \frac{d\mathbf{z}'}{dx} = \mathbf{A}_0 \mathbf{z}' + \mathbf{s}_0 \tag{4.2.11}$$

where $\eta_0 = u_0^2 - c_0^2$ and $\mathbf{A}_0$ is 5×5 and $\mathbf{s}_0$ is a column vector of size 5×1. These are defined in Appendix C.1. The subscript denotes the quantities depend on the base flow. The boundary condition at the shock, i.e. $x = 0$ can be obtained from the Rankine Hugoniot conditions, and written as

$$\mathbf{z}'(x = 0) = \mathbf{z}'(\beta = 1) = \alpha \mathbf{h} \tag{4.2.12}$$

However, there is an additional condition needed to close the system which then can be solved to obtain α. The chosen condition is that of simple spatial boundedness of the perturbations, i.e.

$$\lim_{x\to-\infty}|\mathbf{z}'(x)| = \lim_{\beta_0\to 0}|\mathbf{z}'(\beta_0)| < \infty \tag{4.2.13}$$

As $x \to -\infty$ the base flow quantities quickly reach their asymptotic, constant values. Therefore, near the rear boundary condition, the solution to (4.2.11) can be readily obtained as a linear superposition of the set of the corresponding asymptotic fundamental solutions of (4.2.11). The boundedness condition is then reduced to the condition that the superposition *excludes* the lone unbounded fundamental solution as $x \to -\infty$. This condition is termed the radiation boundary condition since this particular unstable mode is associated with an acoustic signal traveling *towards* the shock from the rear of the reaction zone. The radiation boundary condition was obtained for the present reaction rate model in Short et al. [50] and previously for an exclusively Arrhenius reaction rate in Sharpe [34]:

$$\begin{aligned}
&\textit{Gaseous case: } (\nu = 1, n = 0, \theta \neq 0, \gamma = 1.2)\\
&\quad \alpha u' + \alpha p' - iku_0w' + \mathcal{O}(\beta_0\log(\beta_0)) = 0\\
&\textit{Condensed phase case: } (1/2 \leq \nu < 1, n \neq 0, \theta = 0)\\
&\quad \alpha u' + \alpha p' - iku_0w' + \beta_0^{2\nu-1}\left[\frac{W_0u_1}{u_0}\left(v' - 2\alpha + \frac{(3-\gamma)}{2}u' + \ldots\right.\right.\\
&\quad \left.\left.\frac{\gamma-1}{2}p' + ik\frac{\gamma+1}{2\alpha}u_0w'\right)\right] = 0
\end{aligned} \tag{4.2.14}$$

For the purposes of the forthcoming numerical implementation, the main feature of the boundary conditions above is that in either case, the eigenvalue α appears *linearly* with respect to the perturbations.

The equations defined in (4.2.10), (4.2.11), (4.2.12) and (4.2.14) represent the so-called normal mode approach. It is equivalent to obtaining the eigenfunctions and eigenvalues of the underlying stability equations that result from the linearization

about the base flow $\mathbf{z}_0$. Mathematically, the problem that is produced is a two-point boundary value problem for the eigenvalue α. For the present numerical implementation it is advantageous to derive a system of equations with the reaction progress β_0 as the independent variable. To that end, one holds that

$$\frac{d}{dx} \rightarrow \frac{W_0}{u_0}\frac{d}{d\beta_0} \tag{4.2.15}$$

The governing equation then follows

$$\frac{W_0\eta_0}{u_0}\frac{d\mathbf{z}'}{d\beta_0} = \mathbf{A}_0\mathbf{z}' + \mathbf{s}_0 \tag{4.2.16}$$

The eigenvalue α is embedded in both $\mathbf{A}_0$ and $\mathbf{s}_0$. In Short et al [50], the boundary conditions and governing equation above are solved using a shooting method which is initialized at the shock boundary and *shot* towards the end of the reaction zone ($\beta \rightarrow 0$). In that case, the rear condition serves as a dispersion relation for the eigenvalue α. The eigenvalue map is thus built up from sampling the complex plane of α and iterating from a particular initial guess until the dispersion relation is reduced past some small threshold value. This, of course, introduces the possibility of bypassing some eigenvalues altogether. In the spectral collocation method described in the following, this *carpet search* is replaced with an algorithm that obtains the entire set of eigenvalues from solving a single generalized eigenvalue problem.

4.3 Multi-domain spectral collocation method

The SCM method employs an expansion of the unknown solution into a basis composed of Chebyshev polynomials whose natural domain is the interval $[-1, 1]$. An orthogonality condition involving these polynomials is imposed by an integral over this same interval. Within this framework, derivatives are computed not as finite differences, but by explicit differentiation of the underlying basis functions. Further details can be found in Ref. [51].

The sought-after solution is collocated at the so-called Chebyshev points which tend to concentrate on the endpoints of the Chebyshev interval. Because of this clustering near the endpoints, three separate Chebyshev domains are utilized for improved control of the placement of collocation points. These Chebyshev intervals have to be algebraically stretched to the actual computational domain in β following Fig. 4.2.

The boundedness constraint is imposed at some β_0 which will slightly greater than zero. The following describes the implementation for three subdomains:

1. $\beta_2 \leq \beta \leq 1$,
2. $\beta_1 \leq \beta \leq \beta_2$,
3. $\beta_0 \leq \beta \leq \beta_1$.

The intervals are transformed to the computational domain corresponding to the Chebyshev interval $-1 \leq \xi \leq 1$ using algebraic stretching:

- Domain 1:

$$\begin{aligned} \beta =& \beta_2 + a_1 \frac{1+\xi}{b_1 - \xi},\ a_1 = \frac{(\beta_{01} - \beta_2)(1-\beta_2)}{(1-\beta_2) - 2(\beta_{01} - \beta_2)}, \\ b_1 =& 1 + \frac{2a_1}{1-\beta_2} \end{aligned} \tag{4.3.1}$$

- Domain 2:

$$\begin{aligned} \beta =& \beta_1 + a_2 \frac{1+\xi}{b_2 - \xi},\ a_2 = \frac{(\beta_{02} - \beta_1)(\beta_2 - \beta_1)}{(\beta_2 - \beta_1) - 2(\beta_{02} - \beta_1)}, \\ b_2 =& 1 + \frac{2a_2}{\beta_2 - \beta_1} \end{aligned} \tag{4.3.2}$$

- Domain 3:

$$\begin{aligned} \beta =& \beta_0 + a_3 \frac{1+\xi}{b_3 - \xi},\ a_3 = \frac{(\beta_{03} - \beta_0)(\beta_1 - \beta_0)}{(\beta_1 - \beta_0) - 2(\beta_{03} - \beta_0)}, \\ b_3 =& 1 + \frac{2a_3}{\beta_1 - \beta_0} \end{aligned} \tag{4.3.3}$$

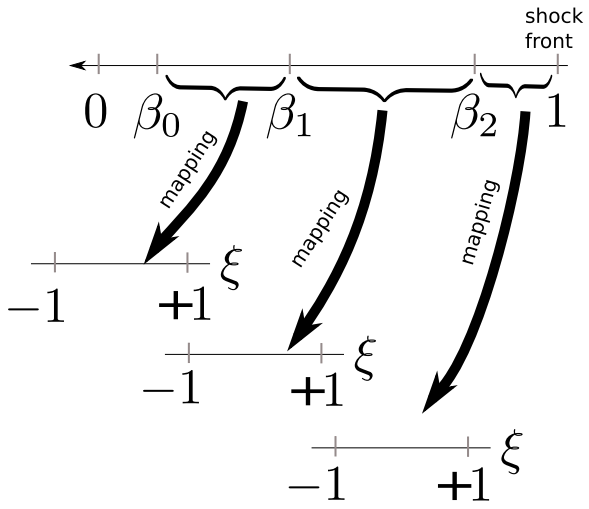

FIGURE 4.2. The variable transformation scheme from β to the 3 Chebyshev domains.

The parameters β_{0j} for $j = 1, 2, 3$ control the location of the collocation points within each interval. For the m-th domain, the Chebyshev points are given by

$$\xi_j^m = -\cos\frac{\pi j}{N_m}, (j = 0 \dots N_m) \tag{4.3.4}$$

The number of collocation points within each interval is specified by N_m though for the results presented here, the number of collocation points was uniform across the three domains. At the introduced interfaces, additional conditions are needed which are simply continuity of the solution and its derivative, i.e.

$$\begin{aligned} \mathbf{z}^1|_{\beta=\beta_2} &= \mathbf{z}^2|_{\beta=\beta_2}, \ \left.\frac{d\mathbf{z}^1}{d\beta}\right|_{\beta=\beta_2} = \left.\frac{d\mathbf{z}^2}{d\beta}\right|_{\beta=\beta_2} \\ \mathbf{z}^2|_{\beta=\beta_1} &= \mathbf{z}^3|_{\beta=\beta_1}, \ \left.\frac{d\mathbf{z}^2}{d\beta}\right|_{\beta=\beta_1} = \left.\frac{d\mathbf{z}^3}{d\beta}\right|_{\beta=\beta_1} \end{aligned} \tag{4.3.5}$$

A discretized solution vector $\mathbf{Z}$ is composed of $5N_1 + 5N_2 + 5N_3 + 16$ as follows:

$$\begin{aligned} \mathbf{Z} = (&z_{10}^1, \dots, z_{1N_1}^1, \dots, z_{50}^1, \dots, z_{5N_1}^1, \\ &z_{10}^2, \dots, z_{1N_1}^2, \dots, z_{50}^2, \dots, z_{5N_1}^2, \\ &z_{10}^3, \dots, z_{1N_1}^3, \dots, z_{50}^3, \dots, z_{5N_1}^3, \psi)^T \end{aligned} \tag{4.3.6}$$

The required derivatives at the interface are evaluated using the derivative matrix associated with the Chebyshev polynomials (see [51]). The governing equation for

the system provides $5N_1 + 5N_2 + 5N_3 - 15$ for the interior points of the the three domains. The governing equation also applies at β_0 so that 5 additional equations are obtained for a total of $5N_1 + 5N_2 + 5N_3 - 10$. The remaining necessary equations are obtained from the interface conditions (20 equations) in (4.3.5), radiation condition provides one and the boundary condition at $\beta = 1$ provides 5 additional equations for a total of $5N_1 + 5N_2 + 5N_3 + 16$. All of these equations can be written in vector-matrix form:

$$\mathbf{QZ} = \alpha \mathbf{SZ} \tag{4.3.7}$$

where $\mathbf{Q}$ and $\mathbf{S}$ are square matrices of size $5N_1 + 5N_2 + 5N_3 + 16$. This defines a so-called generalized eigenvalue problem (GEP). Note that the linear nature of the rear boundary condition with respect to α allows the GEP to be formulated in the manner presented in (4.3.7). A GEP solver ZGGEV included in the numerical algebra package LAPACK was used to solve the problem. The corresponding computer code relies heavily on various other LAPACK routines and it is written in Fortran.

Alternatively, a different approach which can be termed the "invert" or "INV+EP" strategy was utilized as well. It involves inverting the matrix $\mathbf{Q}$ and solving the resulting *regular* eigenvalue problem. Specifically one finds that solving this eigenvalue problem

$$(\mathbf{Q}^{-1}\mathbf{S})\mathbf{Z} = \frac{1}{\alpha}\mathbf{Z} \tag{4.3.8}$$

produces eigenvalues of nearly identical accuracy and at half the cost in computation time when compared to solving the GEP directly. A comparison of the results is shown in the table below for the following set of parameters: $\delta = \theta = 0, n = 6, \gamma = 3, \nu = 1/2, k \approx 0$. The table shows the real part of an unstable eigenvalue and the computation time for the two methods as the salient computational parameters N and β_0 are varied. Here N is the number of collocation points in *each* interval.

Finally, it should be noted that though the matrix $\mathbf{S}$ is singular and both schemes produce the sought spectrum without additional difficulty.

Method	Time	β_0	N	$\alpha_r \times 10^3$
INV.+EP	7.73 min.	2×10^{-4}	100	2.1643983130
GEP	16.04 min.	2×10^{-4}	100	2.1643983382
INV.+EP	7.70 min.	2×10^{-6}	100	2.2739044004
GEP	16.12 min.	2×10^{-6}	100	2.2739091580
INV.+EP	62.43 min.	2×10^{-7}	200	2.2284431882
GEP	138.1 min.	2×10^{-7}	200	2.2284683237

TABLE 4.1. Convergence comparison between the two methods of solution for the GEP. The computer used for the comparison of the schemes was *Dell Dimension 8400* 3.6GHz desktop.

4.4 Some results of the numerical method

The results presented here are organized in the following manner:

- a validation of the numerical method for a gaseous idealized detonation,
- convergence studies for a CJ one-dimensional spectrum simulating a condensed phase detonation,
- another example of a CJ one-dimensional eigenspectrum and eigenfunctions for condensed phase near the neutral stability threshold,
- and two examples of 3D spectrum for condensed phase detonation. ($k = 1/2, 2\pi/6$).

To reiterate, the parameter N represents the number of collocation points in *each* of the intervals and *not* the total number. Also, apart from the validation case, the ZND flow parameters were set to condensed phase values (i.e. $\theta = \delta = 0$). Since the code was set up for 3D perturbations ($k \neq 0$), the one-dimensional spectrum was recovered by the 3D code by simply specifying a very small transverse wave number, i.e. $k = 1 \times 10^{-7}$. The matrices are singular if k is made to be zero explicitly. Additionally, the three domains are separated by $[\beta_0, 0.03, 0.7, 1.0]$ where β_0 was varied among the different instances presented here.

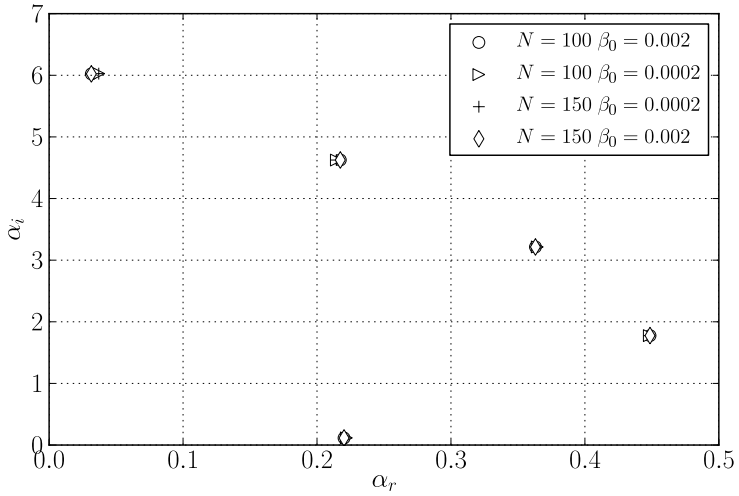

FIGURE 4.3. A validation of the code for differing β_0 and N (the three domains had the same number of collocation points). The other parameters are $E = 50, Q = 50, \gamma = f = 1.2$ with $n = 0$.

Validation. The code was validated for the gaseous case obtained by setting $E = Q = 50$, $f = \gamma = 1.2$, $\nu = 0$ and $n = 0$. The one-dimensional spectrum (set by holding that $k = 1 \times 10^{-7} \approx 0$) for this case is well known and as shown in Fig. 4.3, the code converges to the previously identified results.

1D Convergence test. A convergence test for the was performed for the case where $f = 1, n = 6, \gamma = 3, \nu = 1/2, \delta = 0$ and $\theta = 0$. The parameter β_0 and N were varied and as shown in Fig. 4.4, the single unstable eigenvalue is more sensitive to increasing the number of collocation points than to decreasing the lower bound for β, i.e. β_0. This was done for the one-dimensional perturbation case $k \approx 0$.

CJ 1D neutral spectrum and eigenfunctions. For the set of parameters $\theta = \delta = 0$ and $\gamma = 3, n = 5.904, \nu = 1/2$, the resulting one-dimensional spectrum is reproduced in Figure 4.5. Additionally, one can obtain the eigenfunctions (real part and imaginary part in Figure 4.6).

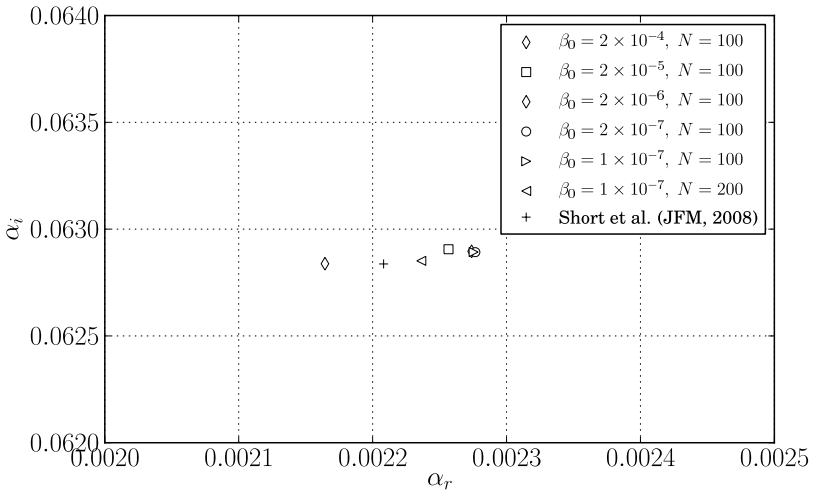

FIGURE 4.4. Convergence study for condensed phase detonation as β_0 and N is varied. The addition of collocation points has the largest effect on the convergence of the method. Note the jump from the + and $\times$ results when N is increased from 100 to 200.

β_0	N	α
2×10^{-4}	100	$0.002164400 + i0.06283807$
2×10^{-5}	100	$0.002256670 + i0.06290583$
2×10^{-6}	100	$0.002273917 + i0.06289576$
2×10^{-7}	100	$0.002276713 + i0.06289218$
1×10^{-7}	100	$0.002275425 + i0.06289266$
1×10^{-7}	200	$0.002236349 + i0.06285158$

TABLE 4.2. Evolution of eigenvalue as β_0 and N is varied.

Overdriven 1D spectrum and eigenfunctions. For the set of parameters simulating a slightly overdriven detonation, $f = 1.05$, and $\theta = \delta = 0$ and $\gamma = 3, n = 6.0, \nu = 1/2$, the resulting one-dimensional spectrum is reproduced in Figure 4.7. There are three modes that appear. Additionally, one can obtain the eigenfunctions for each of these (real part and imaginary part in Figure 4.8).

3D spectrum case I. For case the case where $\gamma = 3$, $\delta = \theta = 0$, $n = 2.4, \nu = 1/2$, and most importantly, $k = 0.5$, the three-dimensional spectrum produces one eigenvalue as shown in Fig. 4.9. The eigenfunction for this case is presented in Fig. 4.10.

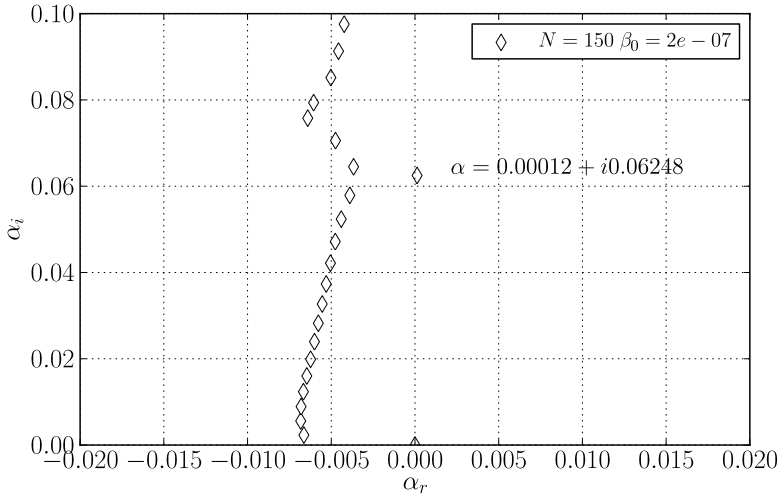

FIGURE 4.5. The one-dimensional spectrum produced for a set of parameters simulating a condensed phase detonation. There is only one relevant unstable eigenvalue. The eigenvalues that appear on the left hand side of the complex plane have no physical significance.

β_0	α
2×10^{-5}	$0.009191221 + i0.7306728$
2×10^{-6}	$0.008929646 + i0.7306370$
2×10^{-7}	$0.008903319 + i0.7306360$

TABLE 4.3. Convergence for the 3D spectrum for $k = 2\pi/6$ and $\beta_1 = 0.1$, $N = 200$.

3D spectrum case II. For the set of parameters $\gamma = 3, \theta = 0, \delta = 0, \nu = 0.5, n = 2.4$, setting $k = 2\pi/6$ produces the three-dimensional spectrum shown in Fig. 4.11. For comparison, the convergence as β_0 is decreased is shown. The eigenfunctions appear in Fig. 4.12.

4.5 Conclusions

The multidomain SCM is well suited for stability analysis of 3D perturbations in the case of CJ detonations. It is shown here that it works well in obtaining the entire spectrum by solving the generalized eigenvalue problem only once. The "invert"

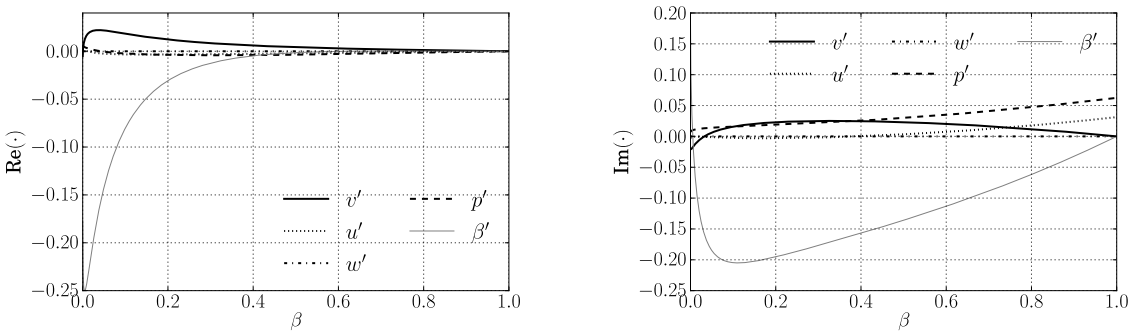

FIGURE 4.6. The real and imaginary part of the eigenfunctions for the unstable mode shown in Figure 4.5.

strategy is most efficient in the solution of the GEP. In the present work, this is done with help of LAPACK (SCALAPACK in the case of parallel computations) routines. Plotting the eigenfunctions for the unstable modes of interest may reveal a "jitter" of the eigenfunctions that can serve as indicator of convergence problems. Finally, resolution of the domain at the end of the reaction zone has the strongest effect on the convergence of the numerical method.

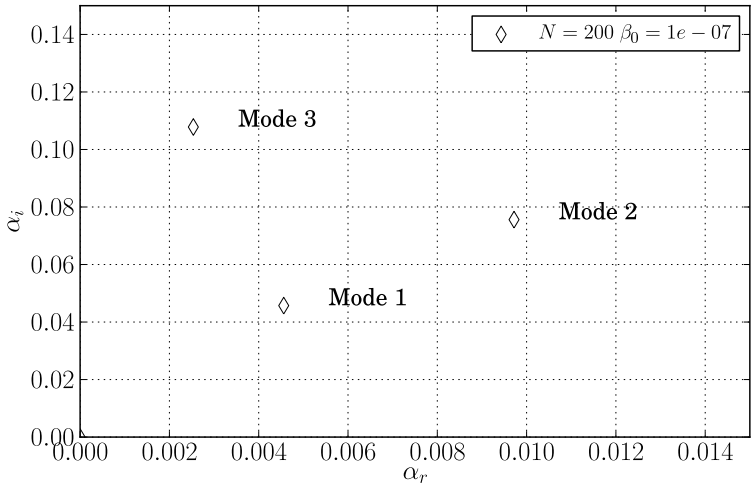

FIGURE 4.7. The one-dimensional spectrum produced for a set of parameters simulating an overdriven condensed phase detonation. There are three relevant unstable eigenvalues.

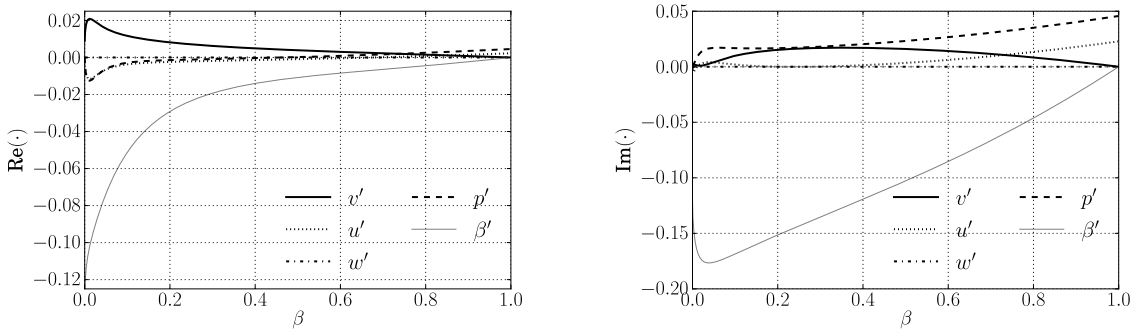

FIGURE 4.8. The real and imaginary part of the eigenfunctions for the first unstable modes shown in Figure 4.7. The other eigenfunctions are similar in form.

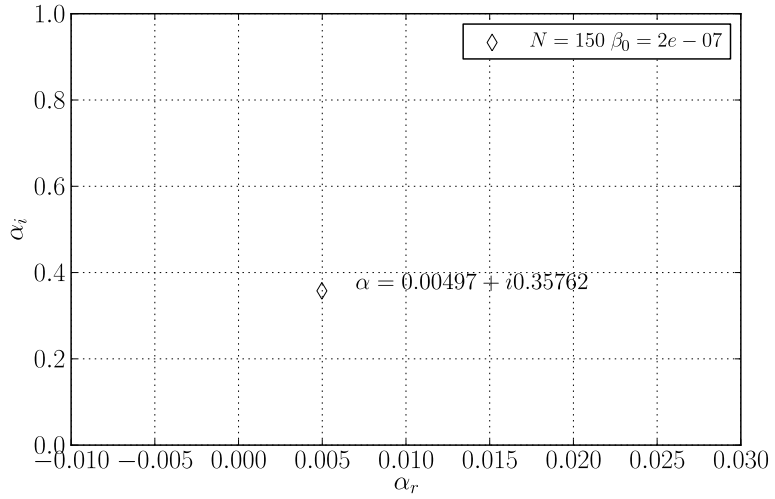

FIGURE 4.9. The three-dimensional spectrum ($k = 1/2$) produced by solving the GEP for a set of parameters simulating a CJ condensed phase detonation.

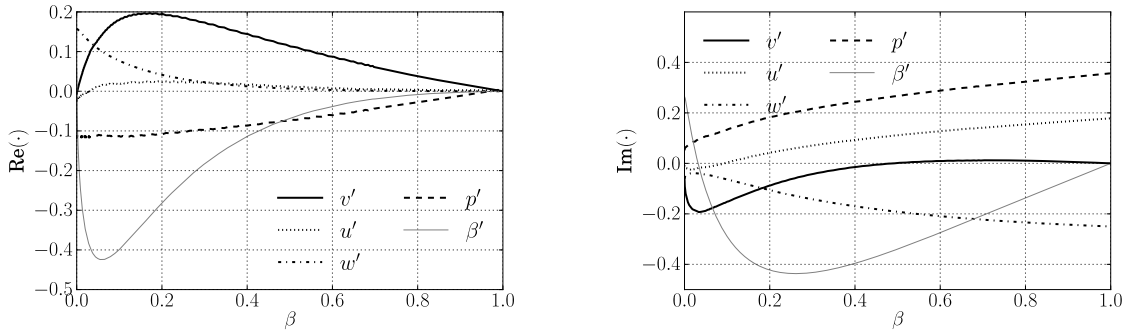

FIGURE 4.10. The three-dimensional eigenfunctions ($k = 1/2$) produced by solving the GEP for a set of parameters simulating a condensed phase detonation $f = 1.0$, $\gamma = 3.0$, $n = 2.4$, $\nu = 1/2$, $k = 1/2$ with $N = 200$.

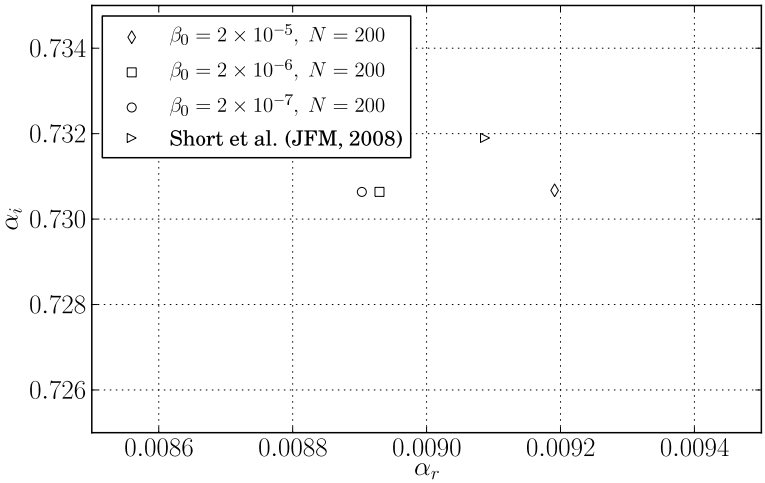

FIGURE 4.11. Convergence for CJ condensed phase detonation for a three-dimensional perturbation with $k = 2\pi/6$.

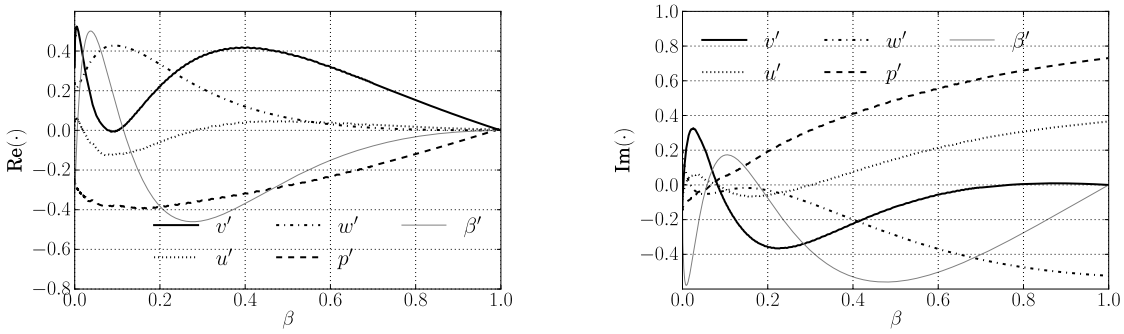

FIGURE 4.12. Convergence study for condensed phase detonation for a three-dimensional perturbation pertaining to $k = 2\pi/6$.

Chapter 5
A normal mode stability analysis of a detonation in an porous walled circular pipe

5.1 Introduction

Experimental studies of detonations often take place within the confining pipe geometry. In addition to the conventional impenetrable pipes, studies involving detonations in porous walled tubes have been carried out as well, notably Teodorczyk & Lee [40]. They found that the porous wall is crucial in the attenuation of transverse waves which have been observed to contribute to the persistence near the detonability limits of the propagating detonation wave. Radulescu & Lee [39] provided further insight: deto-

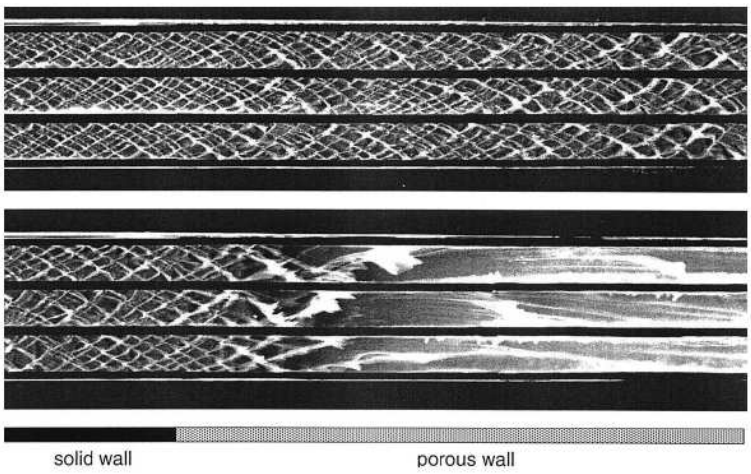

Figure 5.1. This reproduction (from Matei I. Radulescu, John H.S. Lee, Combustion and Flame 131 (2002) 29-46) depicts the effect of the porous wall on the transverse wave structure as evidenced by the soot foil records in a 2D thin channels. The porous wall sections attenuate the detonation of $C_2H_2 + 2.5O_2$ with initial unperturbed pressure $P_0 = 3.6$ kPa in the top three pictures and completely quench the detonation in the lower pictures ($P_0 = 2.6$ kPa).

nations in highly unstable mixtures confined by porous walls fail primarily through

the corresponding attenuation of these transverse waves. Fig. 2 from their work shows the effect of a porous wall section and is reproduced in Fig. 5.1. Conversely, detonations in weakly unstable mixtures fail due to global curvature effects caused by the mass divergence into the porous wall. The attenuation of the transverse waves is observed in numerical simulation as well [41]. The primary motivation in understanding the attenuating properties of these porous-walled pipes is their observed ability to quench unwanted detonations that can develop in explosive gas mixtures that occur in certain chemical industrial settings [40].

To our knowledge, there has been no stability analysis carried out within the porous walled tube configuration. The effect of a porous wall surrounding a cylindrical pipe on the stability problem for detonations will therefore be explored in the present work within the linearized stability framework. The porosity is modeled through the use of so-called acoustic boundary condition where the normal velocity component of the perturbation flow is no longer zero at the boundary but proportional to the pressure component. As a first order approximation, the analysis is restricted to the case where the pipe walls are only slightly porous in order to maintain the basic mathematical structure of the limiting case of the non-porous wall and facilitate a comparison between the two cases. Crucially, the approximation allows the definition the stability problem as a two-point boundary value problem as in the non-porous setting and thus enables the use of the standard numerical methods with only slight modification.

5.2 Governing equations

The full set of governing equations (in the lab frame) for idealized one reaction detonation are the Euler equations supplemented by an equation governing the reaction kinetics (as in the previous chapters). However, the Cartesian system of coordinates is replaced with the more appropriate cylindrical system. The velocity vector

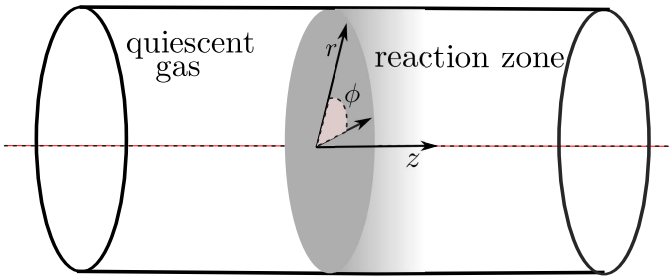

FIGURE 5.2. Schematic showing cylindrical coordinate system.

$\mathbf{u} = (u, w, v)^T$ encapsulates the radial, azimuthal, and axial velocities. The usual symbols denote pressure, p, specific density, ρ, reaction progress variable, λ and specific internal energy e. The internal energy $e = p/((\gamma - 1)\rho) - (1 - \lambda)\tilde{Q}$ is appropriate for an ideal gas, and here λ represents the reaction progress variable, with $\lambda = 1$ denoting the unburned state and naturally, $\lambda = 0$ denoting a totally burned state. The reaction rate r is the first order Arrhenius form, $r = -k(1 - \lambda)\exp(-\bar{E}/\bar{R}_g\bar{T})$ where T is the temperature, E is an activation temperature, and finally R_g is the specific gas constant. Additionally, the ideal gas equation of state allows one to define the sound speed via the equation, $c^2 = \gamma p/\rho$. The Rankine-Hugoniot jump conditions hold at the shock front surface.

One can then posit that there is a steady one-dimensional (1D) in the frame of reference moving with the shock, i.e. ZND idealized detonation model. This base flow holds in the confining cylindrical pipe that is proposed here. Note that the scales are also consistent with Kasimov & Stewart [27], i.e. half reaction length and post-shock values of density, pressure and sound speed. With these dimensional scales in mind, there are four dimensionless parameters that characterize the ZND flow which are the overdrive factor, f, measuring the extent by which the detonation speed exceeds the minimally allowed Chapman-Jouguet velocity $\bar{D}_{CJ}$, E is the activation energy scaled with quiescent gas value of the square of the sound speed, Q is the heat release scaled with the quiescent gas sound speed and γ is the specific heats ratio.

5.2.1 Stability analysis

In the following, the standard stability analysis is performed using the normal mode approach. Firstly, one proposes a change of coordinate to the moving *perturbed* shock, and the particle velocity is measured with respect to the unperturbed shock:

$$z = z^l - D_s t - \psi'(t, r, \phi), \; v = v^l - D_s, \tag{5.2.1}$$

where ψ' is a small perturbation to the shock position and D_s is the detonation velocity scaled with the post-shock sound speed. The detonation is assumed to be propagating to the right in only one spatial direction, z^l. One supposes that the ZND base flow is modified by first order perturbations which fully depend on axial coordinate z, radial coordinate r, azimuthal angle ϕ, and time, t.

The standard linearizing procedure is followed and as a result of these transformations one obtains the system of PDE's:

$$\frac{\partial \mathbf{q}'}{\partial t} + \mathbf{A}_r \frac{\partial \mathbf{q}'}{\partial r} + \mathbf{A}_\phi \frac{1}{r}\frac{\partial \mathbf{q}'}{\partial \phi} + \mathbf{A}_z \frac{\partial \mathbf{q}'}{\partial z} + \mathbf{C}\mathbf{q}' = \mathbf{g}_t \frac{\partial \psi'}{\partial t} + \mathbf{g}_r \frac{\partial \psi'}{\partial r} + \mathbf{g}_\phi \frac{1}{r}\frac{\partial \psi'}{\partial \phi} \tag{5.2.2}$$

where $\mathbf{q}' = (\rho', u', w', v', p', \lambda')^T$ is the relevant vector of perturbations and the coefficient matrices and vectors are functions of the base flow. The appropriate boundary condition on the shock front ($z = 0_+$) are derived from the linearized Rankine-Hugoniot jump conditions,

$$\mathbf{q}'(r, z = 0_+, \phi, t) = \mathbf{h}_t \frac{\partial \psi'}{\partial t} + \mathbf{h}_r \frac{\partial \psi'}{\partial r} + \mathbf{h}_\phi \frac{1}{r}\frac{\partial \psi'}{\partial \phi} \tag{5.2.3}$$

At the end of the reaction zone a spatial boundedness constraint is imposed,

$$\lim_{z \to \infty} \left| \mathbf{q}' \right| < \infty. \tag{5.2.4}$$

This is formally required as $z \to \infty$ but practically, only a few reaction lengths are sufficient to reach the end of the reaction zone. The normal mode approach to determining stability relies on the following ansatz:

$$\mathbf{q}' = \mathbf{z}(r, z, \phi; \tau) \exp(\tau t). \tag{5.2.5}$$

As a result of this choice, one encapsulates the temporal instability of the flow in the real part of τ and its corresponding frequency in the imaginary part. Under this assumption, the task becomes to obtain a reduced eigenvalue problem that will determine τ for the particular detonation in question. Ideally, one would hope for the governing equations of this eigenvalue problem to be a set of ordinary differential equations (ODE's). To that end, the procedure continues via a Fourier series expansion in the azimuthal variable in order to eliminate the explicit variable dependence on ϕ,

$$\mathbf{z}(r,z,\phi;\tau) = \frac{1}{2\pi}\sum_{n}\mathbf{z}_n(r,z;\tau,n)\exp(in\phi). \tag{5.2.6}$$

These transformations lead to a system of PDE's in r and z but now lacking derivatives in t and ϕ for the reduced 2D *eigenfunctions* $\mathbf{z}_n$ and ψ_n:

$$\tau\mathbf{z}_n + \mathbf{A}_r\frac{\partial\mathbf{z}_n}{\partial r} + \mathbf{A}_\phi\frac{in}{r}\mathbf{z}_n + \mathbf{A}_z\frac{\partial\mathbf{z}_n}{\partial z} + \mathbf{C}\mathbf{z}_n = +\tau\mathbf{g}_t\psi_n + \mathbf{g}_r\frac{\partial\psi_n}{\partial r} + in\mathbf{g}_\phi\frac{in}{r}\psi_n \tag{5.2.7}$$

The transformed boundary conditions in the z direction are, specifically,

$$\mathbf{z}_n(r,z=0_+) = \tau\mathbf{h}_t\psi_n + \mathbf{h}_r\frac{d\psi_n}{dr} + \mathbf{h}_\phi\frac{in}{r}\psi_n, \text{ and } \lim_{z\to\infty}|\mathbf{z}_n| < \infty. \tag{5.2.8}$$

5.2.2 The eigenfunctions in non-porous case

The problem is not fully formulated until an additional boundary condition is defined on the wall. The governing equations depend on both r and z and formally, the resulting eigenvalue problem is paired to two-dimensional (2D) eigenfunctions. Ideally, a further step should produce a reduced set of ODE's to define the eigenvalue problem rather than the more complex set of PDE's in (5.2.7). This *separation* scheme should of course depend on the boundary condition in r. Specifically for the conventional non-porous pipe case there is a standard no-penetration boundary condition in the radial velocity on the walls ($r = a$):

$$u'(r=a,z,\phi,t) = 0. \tag{5.2.9}$$

$l\backslash n$	0	1	2	3	4	5	6	7
1	3.8317	1.8412	3.0542	4.2012	5.3176	6.4156	7.5013	8.5778
2	7.0156	5.3314	6.7061	8.0152	9.2824	10.5199	11.7349	12.9324
3	10.1735	8.5363	9.9695	11.3459	12.6819	13.9872	15.2682	16.5294
4	13.3237	11.706	13.1704	14.5859	15.9641	17.3128	18.6374	19.9419

TABLE 5.1. Zeros x_{nl} of the first derivative of the Bessel functions of the first kind, i.e. $J_n'(x_{nl}) = 0$ for the first four orders.

The boundary condition above specifically allows the definition of the following separation scheme based on Bessel functions and its derivatives (where J_n refers to the Bessel function of the first kind of order n) found by Kasimov & Stewart [27], i.e.

$$\hat{\mathbf{q}}_n(r,z,\tau_j) = \begin{pmatrix} \rho_{n,j}(z)J_n(k_{nj}r) \\ u_{n,j}(z)\dfrac{d}{dr}(J_n(k_{nj}r)) \\ v_{n,j}(z)J_n(k_{nj}r)/r \\ w_{n,j}(z)J_n(k_{nj}r) \\ p_{n,j}(z)J_n(k_{nj}r) \\ \lambda_{n,j}(z)J_n(k_{nj}r) \end{pmatrix} \tag{5.2.10}$$

$$\psi_n = \psi_{n,j}J_n(k_{nj}r). \tag{5.2.11}$$

The eigenvalues k_{nj} come about from the boundary condition at $r = a$,

$$u_n(r=a,z;n,\tau) = 0 \Rightarrow \frac{d}{dr}J_n(kr)\bigg|_{r=a} = 0. \tag{5.2.12}$$

In our previous work in the linear stability of the ZND flow in the unbounded case, the wave number k in the transverse direction belonged to a real, continuous set. Conversely, in the restricted finite domain of a pipe geometry, the parameter becomes a discrete number and is obtained from the no penetration wall condition. However, note that Shalaev & Tumin [52] show that the stability of the confined case is equivalent to the unbounded case via a transformation of variables. Additionally, they find that the unstable modes carry no axial vorticity by definition, pointing to the importance of the continuous spectrum that arises in the IVP approach but not within the normal-mode analysis of the discrete spectrum.

The discrete set of radial wave numbers k_{nj} introduces the orthogonality relation:

$$\int_0^a r J_n(k_{nj}r) J_n(k_{nl}r) dr = Q_l \delta_{jl}$$
$$Q_l = \frac{k_{nl}^2 a^2 - n^2}{2k_{nl}^2} J_n^2(k_{nl}a) \tag{5.2.13}$$

and this leads to a system of ODE's in z for the quantities $\rho_{nj}(z), \ldots, \lambda_{n,j}(z)$. Each of these can then be placed into a vector $\mathbf{p}_j$ and one can then obtain the two-point boundary value problem,

$$\frac{d\mathbf{p}_j}{dz} + \mathbf{T}\mathbf{p}_j = \mathbf{F} \tag{5.2.14}$$

where $\mathbf{T}$ and $\mathbf{F}$ depend explicitly on the base flow quantities, k_{nj} and n. These eigenfunctions $\mathbf{p}_j$ and their corresponding eigenvalues τ_j determine the stability of the ZND base flow subject to their compliance with the previously expressed boundary conditions. This particular stability problem is solved in [27] and also subsequently treated via the IVP approach in [52].

5.3 The porous wall and the acoustic boundary condition

The focus of the present work is to model the effect of a porous wall on detonations within the framework of the linearized stability analysis. The model involves incorporating an acoustic absorbing boundary condition on the wall (i.e. $r = a$) in lieu of the no-penetration condition used up to this point in order to model surfaces that are neither rigid nor impenetrable. The boundary condition is built on the assumption that the perturbation pressure should track linearly with the normal velocity at the surface in question [53]. The specific acoustic impedance is the quantity that links these two components and its introduction to acoustics dates to A.G. Webster [54] in 1914. Therefore each component perturbation of a prescribed frequency is uncoupled from the rest via this linear relationship [53], i.e. one has for each of these temporal

modes the following:

$$\left(\frac{\hat{p}}{\hat{v}_{in}}\right)_{S_0} = Z_s(\omega) \tag{5.3.1}$$

where $\hat{p}$ and $\hat{v}_{in}$ denote the pressure and normal velocity component mode for each defined time frequency ω at the normal surface, S_0 is the normal surface in question, and $Z_s(\omega)$ is the frequency dependent specific impedance (complex number in general). The formulation of the acoustically absorbing BC similar to (5.3.1) first appeared in 1921 and it is due to Kennelly and Kurokawa [55].

Matching the acoustic boundary condition that results from the analysis of the porous layer to the outer inviscid flow where the ZND flow applies remains to be examined. In problems involving acoustic perturbation propagation in ducts, the conventional approach has been to model the boundary layer as a thin vortex sheet and where appropriate jump conditions are found across the thin interface. This condition was originally utilized and derived by K. Taylor in 1979 [56] and later, more formally derived by M.K. Myers [57]. It involves matching the perturbation normal velocity to the normal velocity of the surface at each point and thereby ensuring continuity of *particle displacement*. One obtains then the boundary condition of the form (following the notation used by Farassat and Dunn in [58]) :

$$\mathbf{u}_1 \cdot \mathbf{n}_0 = \frac{\partial g}{\partial t} + \mathbf{u}_0 \cdot \nabla g + g\mathbf{n_0} \cdot (\mathbf{n}_0 \cdot \nabla)\mathbf{u}_0 \text{ on } S(t) \tag{5.3.2}$$

where $\mathbf{u}_1$ is the normal velocity perturbation in the inviscid flow and $\mathbf{u}_0$ is the base flow in the same region. The surface $S(t)$ assumed to vary weakly away from a mean surface S_0 where $g(\mathbf{x}, t)$ is the perturbation to the normal displacement of the surface and for the current case and $\mathbf{n}_0$ is the normal vector to the mean surface. In the current work, the normal direction to the surface is parallel the radial coordinate and the mean surface lies at $r = a$. In the one-dimensional ZND flow, there is only a base velocity in the axial direction,

$$\mathbf{u}_0 = (0, 0, v^*(z))^T, \tag{5.3.3}$$

and it is held that the normal velocity "below" the thin boundary layer surface tracks with the perturbation pressure according to (5.3.1), i.e. in the porous layer, $u_n^{porous} = p_n^{porous}/Z$. The time dependence of each of the relevant quantities is assumed proportional to $\exp(\tau t)$. Since $u_n^{porous} = \partial g/\partial t$, it follows that $g = p_n^{porous}/\tau Z$. Continuity of pressure across the interface is also held so that the perturbation pressure in the porous and inviscid flow are equal. In the shock frame of reference then,

$$u_n = p_n/Z + \frac{v^*}{\tau}\frac{\partial}{\partial z}\left[p_n/Z\right] \text{ at } r = a. \tag{5.3.4}$$

The impedance Z will be slowly varying in the axial variable z and therefore the term stemming from its gradient is negligible for the current case. The boundary condition for the inviscid perturbations is therefore,

$$u_n - \frac{p_n}{Z} - \frac{v^*}{Z\tau}\frac{\partial}{\partial z}\left[p_n\right] = 0 \text{ at } r = a. \tag{5.3.5}$$

The specific geometry of the walls will affect the impedance Z and additionally, the eigenvalue (i.e. τ) of the normal-mode perturbation. Finally, note that in the case of infinite impedance the impenetrable wall case boundary condition is recovered.

As a result of this new boundary condition, the stability is formally determined by solution of a PDE system in r & z for 2D eigenfunctions and eigenvalue τ, all parametrized by the azimuthal wave number n. Clearly, both the computational complexity and cost of the numerical implementation for the stability problem solution increases with respect to the non-porous case. However, as a first step, an approximate analysis of the stability problem was undertaken in order to ascertain the effect of slight porosity on the stability problem.

5.3.1 Mathematical approach to the stability question

The overriding philosophy to determine the stability of the reduced problem for a *slightly* porous wall is through an eigenfunction expansion in r (as described in general, for example, by Zauderer [59]). In the current case then, the j-th normal-mode is

expanded in the radial variable using the eigenfunctions obtained from the non-porous case,

$$\mathbf{z}_n^j = \begin{pmatrix} \rho_n^j(r,z) \\ u_n^j(r,z) \\ w_n^j(r,z) \\ v_n^j(r,z) \\ p_n^j(r,z) \\ \lambda_n^j(r,z) \end{pmatrix} = \sum_m^\infty \begin{pmatrix} \rho_{n,m}^j(z) J_n(k_{nm}r) \\ u_{n,m}^j(z) \dfrac{d}{dr}(J_n(k_{nm}r)) \\ v_{n,m}^j(z) J_n(k_{nm}r)/r \\ w_{n,m}^j(z) J_n(k_{nm}r) \\ p_{n,m}^j(z) J_n(k_{nm}r) \\ \lambda_{n,m}^j(z) J_n(k_{nm}r) \end{pmatrix}, \tag{5.3.6}$$

$$\text{and } \psi_n = \sum_m^\infty \psi_{n,m}^j J_n(k_{nm}r). \tag{5.3.7}$$

In order to obtain the 'weight', $\rho_{n,m}^j(z), u_{n,m}^j(z)$, etc., for each radial eigenfunction, one incorporates a type of integral inner product over the radial domain. This inner product is incorporated equation by equation by integrating against the appropriate radial eigenfunction. For example, one has for the continuity equation

$$\begin{aligned} \rho^*\left(\frac{\partial u_n^j}{\partial r} + \frac{u_n^j}{r} + \frac{in}{r} w_n^j\right) + \tau_j \rho_n^j + \rho^* \frac{\partial v_n^j}{\partial z} + \frac{d\rho^*}{dz} v_n^j + \\ v^* \frac{\partial \rho_n^j}{\partial z} + \frac{dv^*}{dz}\rho_n^j - \frac{d\rho^*}{dz}\tau \psi_n^j = 0, \end{aligned} \tag{5.3.8}$$

parametrized by n, the azimuthal wave number, and obtained subsequent to the implementation of the exponential time-dependence prescribed by the normal mode approach. One proceeds by multiplying through by the function $J_n(k_{nj}r)r$ and integrating from $r \in [0, a]$,

$$\begin{aligned} &\int_0^a J_n(k_{nj}r) r \left(\rho^* \frac{\partial u_n^j}{\partial r}\right) dr + \int_0^a \rho^* J_n(k_{nj}r) r \left(\frac{u_n^j}{r} + \frac{in}{r} w_n^j\right) dr + \\ &\int_0^a J_n(k_{nj}r) r \left(\tau \rho_n^j + \rho^* \frac{\partial v_n^j}{\partial z} + \frac{d\rho^*}{dz} v_n^j + v^* \frac{\partial \rho_n^j}{\partial z} + \frac{dv^*}{dz}\rho_n^j - \frac{d\rho^*}{dz}\tau_j \psi_n^j\right) dr = 0 \end{aligned} \tag{5.3.9}$$

Integration by parts explicitly introduces the boundary condition at $r = a$:

$$\begin{aligned} &\rho^* \Big[J_n(k_{nj}r) r u_n^j\Big]\Big|_{r=0}^{r=a} - \rho^* \int_0^a \frac{d}{dr}\big[J_n(k_{nj}r)r\big] u_n^j dr + \\ &\int_0^a \rho^* J_n(k_{nj}r) r \left(\frac{u_n^j}{r} + \frac{in}{r} w_n^j\right) dr + \int_0^a J_n(k_{nj}r) r \Big(\tau_j \rho_n^j + \\ &\rho^* \frac{\partial v_n^j}{\partial z} + \frac{d\rho^*}{dz} v_n^j + v^* \frac{\partial \rho_n^j}{\partial z} + \frac{dv^*}{dz}\rho_n^j - \frac{d\rho^*}{dz}\tau_j \psi_n^j\Big) dr = 0. \end{aligned} \tag{5.3.10}$$

Applying the acoustic boundary condition:

$$\frac{\rho^* J_n(k_{nj}a)a}{Z}\left[p_n^j(a,z)+\frac{v^*}{\tau}\frac{\partial}{\partial z}p_n^j(a,z)\right]-\rho^*\int_0^a\frac{d}{dr}\big[J_n(k_{nj}r)r\big]u_n^j dr+ \\ \int_0^a\rho^* J_n(k_{nj}r)r\left(\frac{u_n^j}{r}+\frac{in}{r}w_n^j\right)dr+\int_0^a J_n(k_{nj}r)r\Bigg(\tau_j\rho_n^j+ \\ \rho^*\frac{\partial v_n^j}{\partial z}+\frac{d\rho^*}{dz}v_n^j+v^*\frac{\partial\rho_n^j}{\partial z}+\frac{dv^*}{dz}\rho_n^j-\frac{d\rho^*}{dz}\tau_j\psi_n^j\Bigg)dr=0. \tag{5.3.11}$$

Clearly, as $Z\to\infty$, the equivalent equation to the solid-wall case is recovered and the eigenfunction expansion collapses to a single element of the radial eigenfunction set, in this case, the j-th such element.

The weight functions such as $\rho_{n,m}^j(z)$ are functions only of z. Note that the eigenfunction expansion leads to an infinite sum over the radial eigenfunction indexed by m since replacing p_n^j in equation (5.3.11) with the eigenfunction expansion leads to the following:

$$-\rho^* k_{nj}^2 u_{nj}^j(z)+\sum_m^\infty\frac{\rho^* J_n(k_{nj}a)a}{Q_j Z}J_n(k_{nm}a)\left[p_{nm}^j(z)+\frac{v^*}{\tau}\frac{d}{dz}p_{nm}^j(z)\right]+\tau_j\rho_{nj}^j(z)+\rho^*\frac{dv_{nj}^j}{dz}+ \\ \frac{d\rho^*}{dz}v_{nj}^j+v^*\frac{d\rho_{nj}^j}{dz}+\frac{dv^*}{dz}\rho_{nj}^j-\tau_j\frac{d\rho^*}{dz}\psi_{nj}^j=0. \tag{5.3.12}$$

The sum is well defined and converges uniformly and absolutely as long as $p_n^j(r,z)$ is smooth (minimally: first two derivatives in r must exist according to [60]). The integrals in equation (5.3.11) disappear due to the orthogonality of the underlying radial eigenfunctions and so one obtains equations that depend only on z.

The derivations of the other relevant conservation equations proceed similarly. The salient aspect is that the evolution of the j-th unstable normal mode will depend directly on all the radial eigenfunctions from the non-porous case. For the case where $1/Z$ is small, this can be improved upon as follows. As $Z\to\infty$, one expects that the

eigenfunction expansion reverts to the simple form in the non-porous case. Therefore,

$$\begin{aligned}\underbrace{p_n^j(r,z)}_{\text{porous case}} &= \sum_m^{\infty} p_{n,m}^j(z) J_n(k_{nm} r) \overset{Z\to\infty}{\Longrightarrow} \underbrace{p_n^j(r,z)}_{\text{non-porous}} = p_{nj}^j(z) J_n(k_{nj} r) \\ &\Rightarrow \text{for } m \neq j,\ p_{n,m}^j = \mathcal{O}(1/Z)\end{aligned} \tag{5.3.13}$$

This in effect forces the eigenfunction expansion weights different from j to be $\mathcal{O}(1/Z)$ or more generally, vanish in the limit. The input from the other radial eigenfunctions is thus a higher order effect within the governing equations,

$$\begin{aligned}&-\rho^* k_{nj}^2 u_{nj}^j(z) + \frac{1}{Z}\frac{\rho^* J_n(k_{nj}a)a}{Q_j} J_n(k_{nj}a)\left[p_{nj}^j(z) + \frac{v^*}{\tau}\frac{d}{dz}p_{nj}^j(z)\right] + \mathcal{O}\left(\frac{1}{Z^2}\right) + \tau_j \rho_{nj}^j(z) + \\ &\quad v^*\frac{d\rho^*}{dz}v_{nj}^j + \frac{d\rho_{nj}^j}{dz} + \frac{dv^*}{dz}\rho_{nj}^j - \tau_j\frac{d\rho^*}{dz}\psi_{nj}^j = 0.\end{aligned} \tag{5.3.14}$$

Dropping the higher order $\mathcal{O}(1/Z^2)$ terms leads to a system of ODE's that can be written in the form:

$$\left[\mathbf{A} + \frac{1}{Z}\mathbf{D}_n^{jj}\right]\frac{d\mathbf{R}_n^j(z)}{dz} + \mathbf{B}_n^j \mathbf{R}_n^j(z) + \frac{1}{Z}\mathbf{C}_n^{jj}\mathbf{R}_n^j(z) = \mathbf{g}_n \tag{5.3.15}$$

where the eigenfunction vector $\mathbf{R}_n^j(z) = (\rho_{n,j}^j, \ldots \lambda_{n,j}^j)^T$. The boundary conditions are correspondingly obtained as a matrix-vector system,

$$\begin{aligned}&\mathbf{R}_n^j(z = 0_+) = (\tau_j \mathbf{h}_t + \mathbf{h}_r + in\mathbf{h}_\phi) \\ &\lim_{z\to\infty} |\mathbf{R}_n^j(z)| < \infty.\end{aligned} \tag{5.3.16}$$

The stability problem is thus a 1D two-point boundary value problem in z as in the non-porous wall case. The procedure described here is illustrated in a simpler though related model problem in Appendix D.1.

5.3.2 Model for the acoustic impedance

In the current work, a relatively thin porous layer lines the walls of the cylindrical tube. The schematic is shown from both a top view (Fig. 5.3) and a side (Fig.

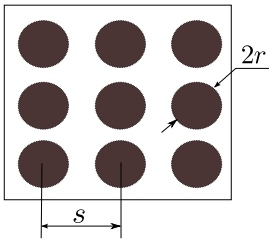

FIGURE 5.3. Schematic of porous layer from a top view

5.4). For the specific case presented here, one imagines a layer containing a series of cylindrical cavities of a specified radius $\bar{r}$ separated by a certain distance $\bar{s}$. Note that other cavity cross-sections could be used as well. With the geometry of the

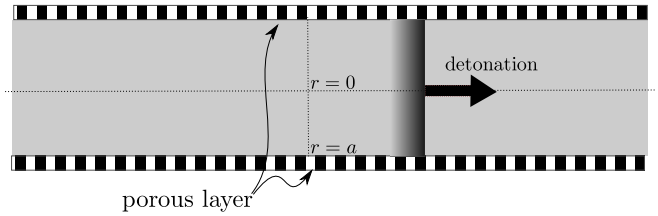

FIGURE 5.4. Schematic of porous layer (side view).

porous layer defined, the remaining task is to determine the nature of the specific impedance Z produced by this specific layer which then determines the modified boundary condition,

$$u_n\big|_{r=a} - \frac{1}{Z}\left(p_n + \frac{v^*}{\tau}\frac{dp_n}{dz}\right)\bigg|_{r=a} = 0. \tag{5.3.17}$$

The specific impedance Z depends on the geometry, characteristics of the ambient base flow, and crucially, on the time-dependence encapsulated in τ_j of the perturbation itself. Stinson and Champoux [61] obtained this quantity for the configuration above for each specific cavity and also as a bulk material. Their method relies on solving the continuum fluid equations in each cavity for perturbations to a steady thermodynamic state. In the case that the cavities are indeed on the order of the molecular mean-free

path, Kozlov et al. [62] provide the same quantities for non-zero Knudsen number. In the present work, the size of the cavities are assumed to be within the former regime.

The method of Stinson and Champoux [61] involves solving perturbation equations in the cavity assuming a perfect gas with a constant equilibrium flow and with finite dynamic viscosity. The solution for the perturbations in this restricted domain are used to obtain the constant of proportionality between the normal velocity and pressure perturbations at the surface. The result for each cavity was then integrated in order to obtain the effective specific acoustic impedance for the surface as a whole.

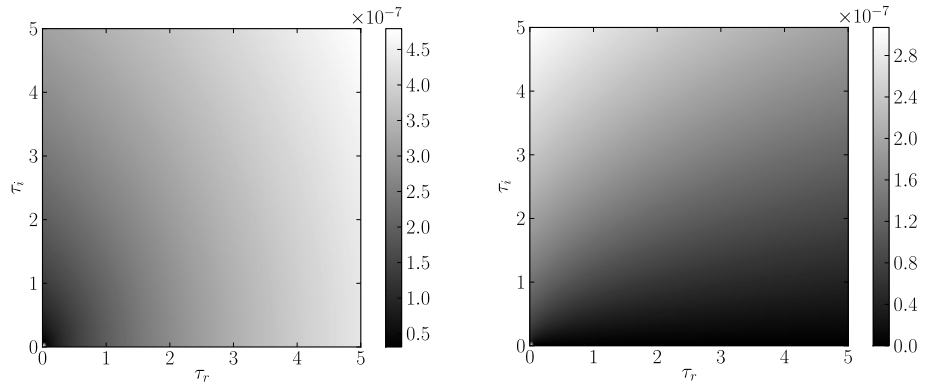

FIGURE 5.5. Typical values for real (a) and imaginary (b) parts of $1/Z$ as a function of the input unstable mode eigenvalue $\tau = \tau_r + i\tau_i$ for small porosity $n_p = \mathcal{O}(10^{-6})$ and values consistent with a highly unstable idealized detonation (detailed in §5.4(5.4.2)).

In the specific case considered here, the radius of the pipe is considered much larger than the characteristic size of the porous walled holes yet large enough that the continuum equations hold in these cavities. Using the appropriate characteristic scaling from the ZND detonation flow (i.e. quantities directly behind the detonation flow among others) and based on the analysis described to this point, one obtains in non-dimensional units,

$$Z = -\frac{i\rho^* c^*}{n_p}\sqrt{\frac{J_0(k_v)/J_2(k_v)}{\gamma + (\gamma-1)J_2(k_t)/J_0(k_t)}} \tag{5.3.18}$$

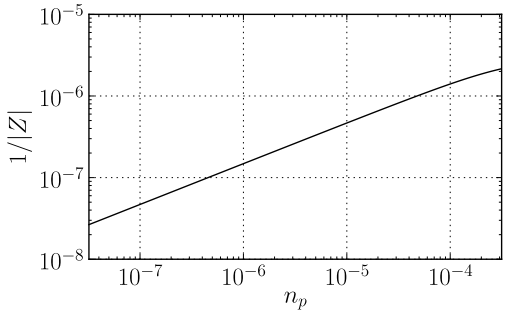

FIGURE 5.6. The magnitude of Z as a the porosity is varied for a highly unstable idealized detonation as in Fig. 5.5

with

$$n_p = \pi\left(\frac{\bar{r}}{\bar{s}}\right)^2,\ k_v = \xi i\sqrt{\rho^*\tau_j},\ k_t = \sqrt{Pr}k_v,\ \xi = \sqrt{\frac{\bar{r}^2\bar{\rho}_s\bar{c}_s}{\bar{\mu}_w\bar{l}_c}}. \tag{5.3.19}$$

Though the equilibrium base flow varies through the reaction zone, one assumes an constant equilibrium state in each cavity assuming that the variation of the base flow is large compared with the size of each cavity. In terms of the quantities that appear in the formulas, the J_0 and J_2 refer to the zero and second order Bessel functions of the first kind, Pr is the Prandtl number, and $\bar{r}$ and $\bar{s}$ are the dimensional quantities representing the radius of the cavity and the separation of the cavities, respectively. Additionally, n_p is a measure of the porosity or the ratio of cavity volume to the overall volume of the layer. The constant ξ depends on the dimensional detonation quantities $\bar{\rho}_s$ and $\bar{c}_s$, and $\bar{l}_c$ (respectively density, speed of sound directly behind the shock and the characteristic reaction zone length). The constant $\bar{r}$ is the characteristic size of the holes in the porous media that make up the pipe's walls. Furthermore, $\bar{\mu}_w$ is the dynamic viscosity of the gas. Note that the porosity parameter n_p basically constrains the magnitude of the overall effect of the acoustic boundary condition since $n_p = \pi(\bar{r}/\bar{s})^2$ and $1/Z \propto n_p$. The main goal of the present study was to determine the effect of this modeled boundary condition on the growth rate of the perturbations as the porosity is increased from zero, i.e. the impenetrable wall case.

5.4 Numerical results

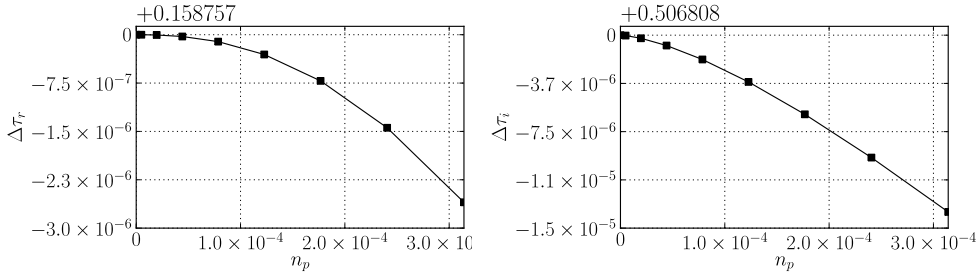

(a) Real part (b) Imaginary

FIGURE 5.7. Evolution of unstable mode eigenvalue for parameters consistent with $2H_2 + O_2 + 12Ar$ as n_p increases for both growth rate and frequency. The real and imaginary parts of the eigenfunctions appear on the bottom row.

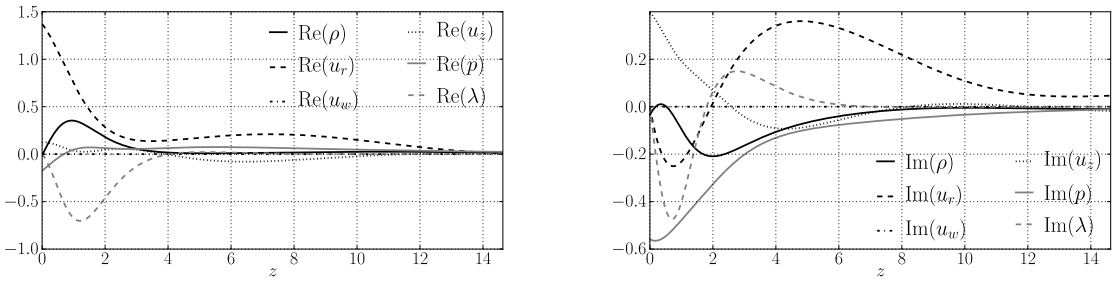

(a) Real part (b) Imaginary

FIGURE 5.8. The real and imaginary parts of the eigenfunctions for mode 1 at $n_p = \mathcal{O}(10^{-3})$.

5.4.1 The method

The numerical method for obtaining the evolution of the growth rate and frequency of the perturbations comprises several steps which are detailed below. The numerical methods employed to find the eigenvalues are implemented in Fortran using the numerical libraries LAPACK and SLATEC.

1. A multi-domain spectral collocation method ([48], [38]) is utilized to obtain the entire spectrum for the related 1D perturbation system without the porous

Constant	Description	weakly unstable	strongly unstable
Pr	Prandtl number	0.885	0.7980
f	overdrive factor	1.1	1.05
γ	specific heats ratio	1.6	1.4
E	Activation energy	77.24	202.23
Q	Heat release	24.2	56.9
a	Radius of pipe	7.663	10.382

TABLE 5.2. Parameters for numerical implementations

wall (i.e. $n_p = 0$). The method is not appropriate for higher dimensional perturbation problems due to the requirement of a linear boundary condition in τ_j at the end of the reaction zone. However, due to the spectral expansion, the entire spectrum is determined at once.

2. These seed values for the τ_j are used as initial guesses for the Newton-Raphson shooting method used by Lee & Stewart [23], i.e. one starts from the known values at the shock front and *shoots* towards the end of the reaction zone using the boundary condition as a "dispersion relation".

3. As n_p is increased, this Newton-Raphson method is used to track the resulting eigenvalue and eigenfunctions. Note that as this parameter is increased the inverse specific impedance, $1/Z$, is increased and thus the effect of the porosity.

5.4.2 Examples

Explosives can be broadly characterized as 'highly' and 'weakly' unstable depending on the amount of dilution of the reactive elements. The following examples are obtained with help from data obtained from J. Austin [41] and aim to mimic a highly and weakly unstable detonation. However, the physical values of the constants should still be considered largely approximate.

Weakly unstable case This particular case is aimed at testing a weakly unstable case, and the parameters were chosen to be consistent with an Argon diluted mixture with formula $2H_2 + O_2 + 12Ar$. There is only one unstable mode, $\tau = 0.1587284 + 0.5068546i$, and for the case at hand, the stability of this 3D unstable mode is tested with $k_{01} = 0.5$ and $f = 1.05$ (slightly overdriven). Additionally, the ZND flow parameters are $\gamma = 1.6, Q = 24.2$, and $E = 77.25$ and the radius of the tube is considered to be 7.663 times the reaction zone length. The evolution as n_p is increased from 0 to about 3×10^{-4} is shown in Fig. 5.7. The eigenfunctions are pictures in Fig. 5.8. Different Bessel function orders, n, and wave numbers k_{nm} affect the growth rate term in the same qualitative manner as in the $n = 0$ case (see Fig. 5.9).

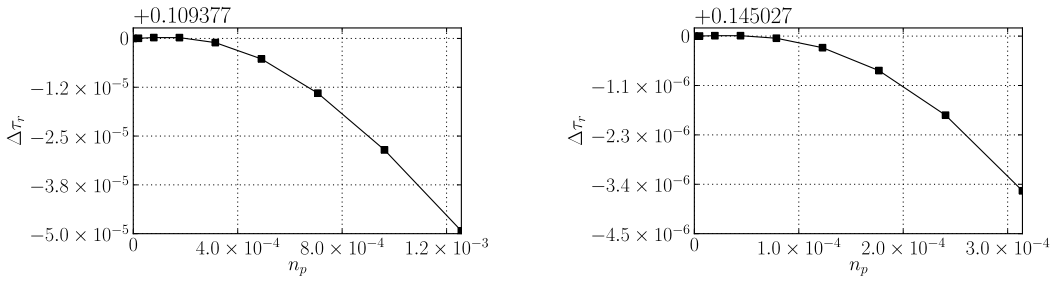

(a) $k_{11} = 0.2402$ (b) $k_{21} = 0.3985$

FIGURE 5.9. The deviation in the unstable mode growth rate for the weakly unstable case as n_{porous} increases for various Bessel function orders and radial wave number k_{nm}.

Highly unstable case The eigenfunctions, frequencies and the growth rates were obtained for parameters consistent with the mixture $C_2H_4 + 3O_2 + 10.5N_2$ for varying degrees of porosity. This case has more unstable modes and are of a higher growth rate (see Fig. 5.10) than the weakly stable case presented previously. Each mode is labeled in order of increasing frequency and note that mode 2 is the unstable element with largest growth rate in this case. The porosity is varied between 0 and about 3×10^{-4} for each case. The growth rates are shown for the non-zero frequency modes appear in Fig. 5.11 and 5.12. The corresponding eigenfunction appear in Figs. 5.13,

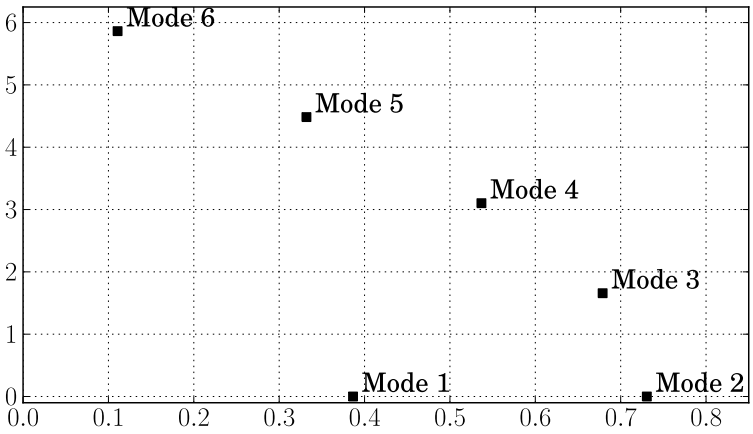

FIGURE 5.10. Example of overdriven, 1D spectrum with $f = 1.1$, $E = 202.23$, $Q = 56.9$ and $\gamma = 1.403$. These values are meant to be consistent with the gas mixture $C_2H_4 + 3O_2 + 10.5N_2$. E and Q are obtained from [41].

5.14, 5.15 and 5.16.

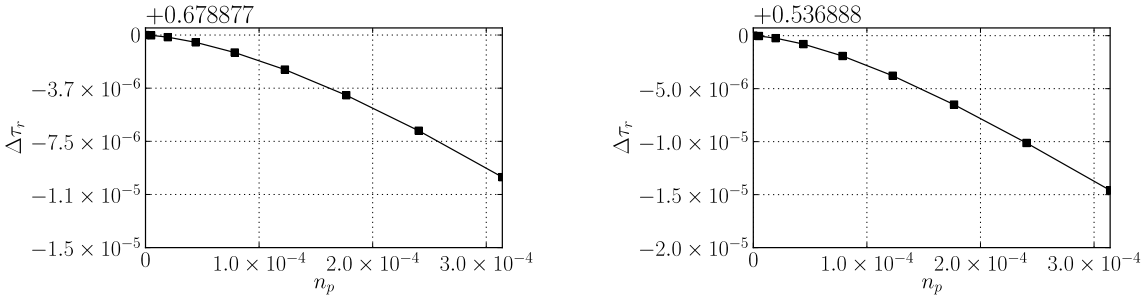

(a) Mode 3 (b) Mode 4

FIGURE 5.11. Deviation in growth rate for modes 3 and 4.

5.5 Conclusion

An extension of the non-porous pipe stability analysis is considered where the wall is allowed to take on a slight porosity. The effect is modeled as an acoustic boundary condition for transverse first order perturbations to the idealized ZND flow in the pipe. A model for the acoustic impedance is incorporated to determine the impedance which

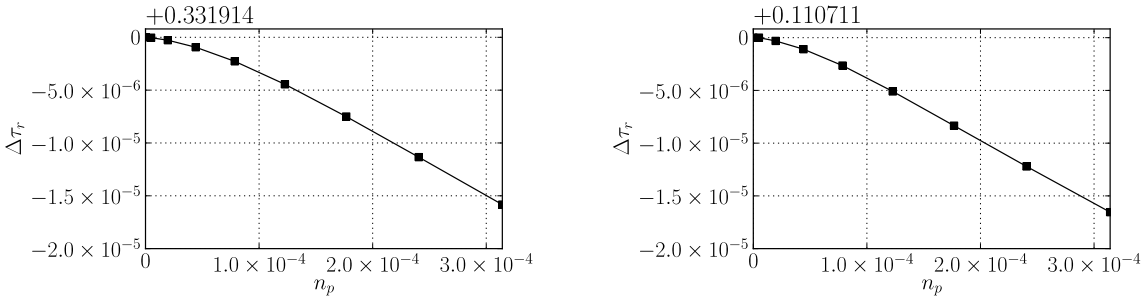

(a) Mode 4 (b) Mode 6

FIGURE 5.12. Deviation in growth rate for the highly oscillatory modes 5 and 6.

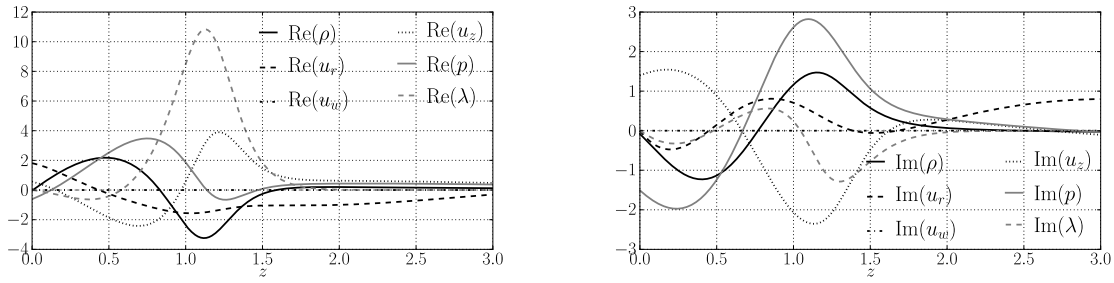

FIGURE 5.13. Eigenfunctions for $n_{porous} = \mathcal{O}(10^{-4})$ (mm) for mode 3 for both real and imaginary parts.

is then, crucially, a function of the perturbation frequency. Modified equations are then obtained incorporating the acoustic boundary condition, and the perturbation eigenfunctions and temporal eigenvalue containing the growth rate and frequency are sought. The method of solution is a radial expansion using the Bessel function derived eigenfunctions of the impenetrable wall case. The leading order effect of the slight porosity is retained allowing the definition of a modified two-point boundary value problem is then to determine the corresponding stability information. This allows the use of the numerical method used to determine stability in the more conventional case.

Two different detonable gases are approximated via the ZND 1D model, one representing a highly unstable Nitrogen gas mixture and a weakly unstable Argon gas mixture. It is found that the slight porosity attenuates or dampens the growth rate

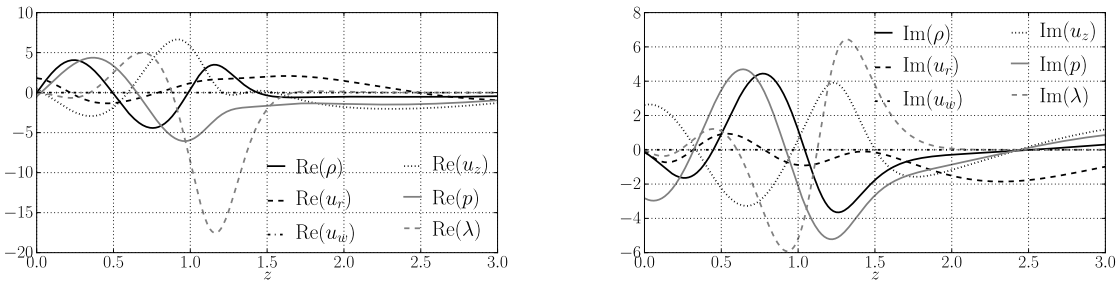

FIGURE 5.14. Eigenfunctions for $n_{porous} = \mathcal{O}(10^{-4})$ (mm) for mode 4 for both real and imaginary parts.

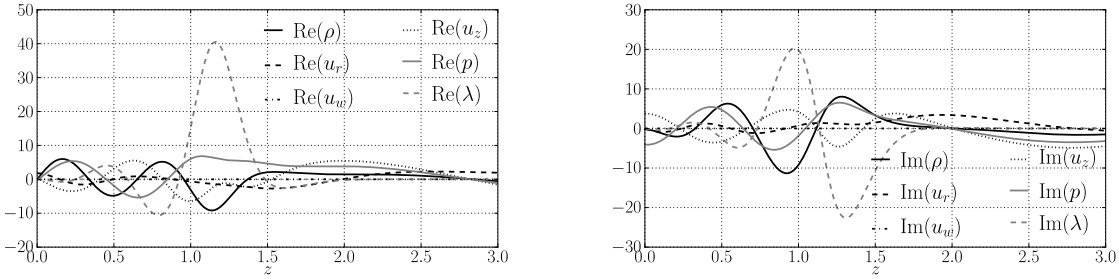

FIGURE 5.15. Eigenfunctions for $n_{porous} = \mathcal{O}(10^{-4})$ (mm) for mode 5 for both real and imaginary parts.

of perturbations for different radius, and eigenfunction wave numbers in both radial and azimuthal directions. Also, the temporal frequency of the perturbations is decreased and therefore reduces the azimuthal velocity of the transverse waves at the wall. The reduction in the growth rate of the transverse perturbations seems consistent with experimental evidence of transverse wave attenuation. However, it should be stressed the effects modeled here correspond to the initial, linear stages of the transverse perturbation's growth.

In the introduction to this work, the phenomenon known as spinning detonation was described. Crucially, the transverse waves propagate azimuthally, and leave soot foil trails on the walls of the confining tubes due to the specially intense pressures at the wall that they produce. In experiments, the pitch to diameter ratio of the

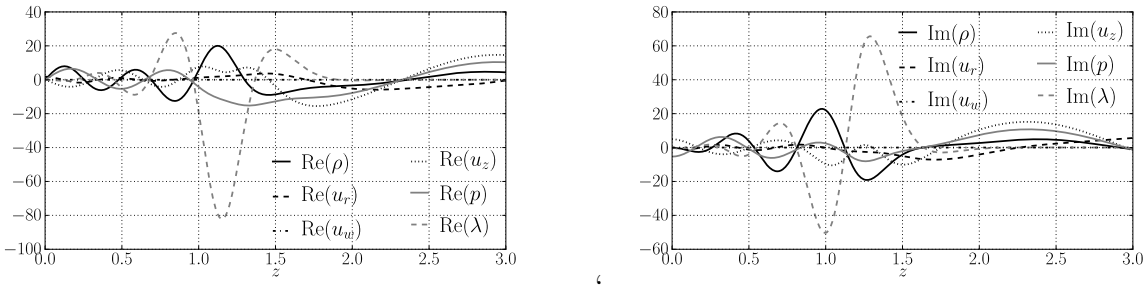

FIGURE 5.16. Eigenfunctions for $n_{porous} = \mathcal{O}(10^{-4})$ (mm) for mode 6 for both real and imaginary parts.

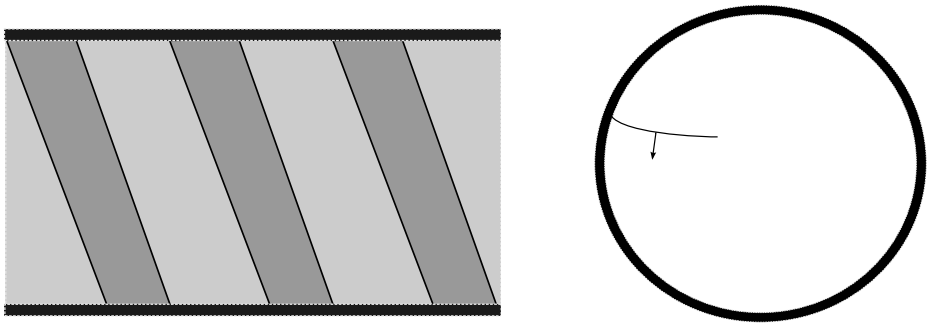

(a) (b)

FIGURE 5.17. (a) The spinning instability (single-headed or composed only of one angular frequency) leaves a soot foil record on the walls of the pipe. Sketched here, is the path of this the record viewed from the side on. (b) The same picture showing the azimuthal propagation of the spinning instability which extends from the wall to a point close to half the radius. The segment shown is represents the line of tripe-shock intersection created by the extraordinary intensity of the spinning instability.

propagating spinning modes is measured and found to be remarkably constant and is a measure of the "tilt" of these helically rotating transverse waves. The pitch to diameter ratio is for most near-limit mixtures found to be about 3, with other mixtures ranging between 2 and 6 [63]. In Kasimov & Stewart's work on the detonation stability in a pipe with impenetrable walls [27], the imaginary part of the normal mode eigenvalue was linked to the pitch versus diameter ratio of the spinning modes

(See Fig. 5.17), i.e

$$\frac{p}{d} = \frac{2\pi n D_s}{\tau_i d} \tag{5.5.1}$$

where the $\tau_i = \mathrm{Im}(()\tau)$ is the imaginary part of the unstable normal mode eigenvalue whose real part is the largest and therefore most likely to be manifested in the non-linear stage of the perturbation evolution. The constants D_s and d are the detonation velocity and diameter in non-dimensional units. It is well-known that the frequencies of perturbations obtained from the linear stability analysis tend to be maintained in the non-linear manifestation of the instability and this has been shown initially in 1979 [9] and more recently as well [64]. Therefore, the suppressive or attenuating effect of the acoustic boundary condition on the frequency would suggest that this ratio is increased in the event of a slightly porous wall.

Chapter 6
Asymptotic analysis of pulsating chain-branching detonation

6.1 Introduction

Unsteady one dimensional detonations are known to develop a pulsating instability [65, 22, 66, 67]. Elucidating the coupling between the nonlinear gas-dynamic wave propagation and the exothermic reaction chemistry that produces this instability is therefore of high importance. However, the general mathematical description of the phenomenon is of high complexity as well and one has to exploit asymptotic forms of the problem to make significant analytical progress. This is is the approach taken presently where a non-linear evolution equation is obtained for detonations incorporating chain-branching reaction kinetics.

The specific two-step chain-branching kinetic model revisited here was used extensively in numerical computations by Oran and Boris [68]. M. Short [69] analyzed an asymptotic form of this reaction for Chapman-Jouguet detonations through the derivation of an evolution equation for the shock velocity. Subsequently, the model was utilized in Short and Bdzil [70] and again by Short and Sharpe [71] where the asymptotic results in Ref. [69] are compared to full numerical simulations. The considered model is meant to mimic the essential attributes that chemical reactions typically exhibit, i.e., a chain-initiation zone where there is little heat release, a chain-branching zone where fuel is converted into chain-radical and finally, a subsequent chain-termination zone where the chain-radical is converted into product.

Specifically, it is assumed here that there is an initial induction zone that is temperature insensitive due to a high activation energy (chain-initiation). The chain-

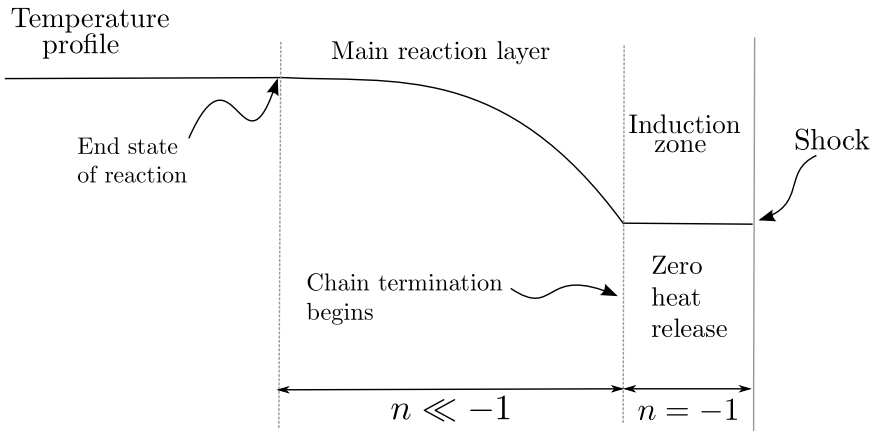

FIGURE 6.1. The general structure of the steady detonation wave within the considered model.

branching step is constrained to occur instantaneously immediately after the induction zone. A gas state-independent reaction which releases the bulk of the heat stored in the fuel (chain-termination step) ends the reaction. These assumptions lead to an overall structure of an initial short induction zone and a following spatially distributed reaction zone. The lengths of zones depend on the rate constants of each reaction and their relative proportion was found to be an important parameter for determining the temporal stability of the CJ detonation [69].

The reactive Euler equations are used to model the evolution of the perturbations to the fluid density, velocity, pressure, reaction progress, and also to the shock velocity. Furthermore, it is assumed that the instabilities develop on a slow time scale tied to the inverse activation energy which is considered to be very small. An asymptotic expansion in this parameter, ϵ, produces a set of PDE's for the perturbations which are solved in two stages, firstly in the induction and subsequently the main reaction zone. A nonlinear evolution equation is then obtained for the shock velocity exploiting an iterative asymptotic procedure. The resulting equation is second order and autonomous and its dynamics produce bounded nonlinear oscillations as seen in full numerical solution of the problem [71]. The work presented here generalizes the

evolution equation in [69] which was confined to $\nu = 1/2$ and CJ detonation to any overdrive and any reaction order, both essential parameters that prescribe the detonation steady state structure. The method relies on imposing a radiation boundary condition rather than a regularity condition as was the case in [69].

6.2 The detonation model

6.2.1 Governing equations and constitutive relations

As before, the governing equations for the detonation flow are the reactive Euler equations in the form:

$$\frac{D\rho}{Dt} + \rho\nabla\cdot\mathbf{u} = 0,\ \frac{D\mathbf{u}}{Dt} + \frac{1}{\rho}\nabla p = 0\ \frac{De}{Dt} + p\frac{D}{Dt}\left(\frac{1}{\rho}\right) = 0. \tag{6.2.1}$$

The reaction is parametrized by the reaction progress variables λ_1 and λ_2 and the consumption equation determines their evolution,

$$\frac{D\lambda_i}{Dt} = r_i \quad \text{with} \quad \begin{cases} r_1 = k_1 H(1-\lambda_1)\exp\left(\frac{1}{\epsilon}\left(\frac{1}{RT_0} - \frac{1}{RT}\right)\right) \\ r_2 = k_2(1 - H(1-\lambda_1))(1-\lambda_2)^\nu \end{cases} \tag{6.2.2}$$

where T_0 denotes the post-shock temperature, and R is the gas constant. This particular form of the reaction rates ensures that the induction zone is governed by a single reaction progress variable, i.e. λ_1. This is imposed by the Heaviside function $H(\cdot)$. Note that $\lambda_i \in [0,1]$. Furthermore, the model assumes an ideal gas equation of state, associated sound speed, and internal energy, e, specifically

$$\frac{p}{\rho} = RT \Rightarrow c^2 = \gamma p/\rho,\ e = \frac{1}{\gamma - 1}\frac{p}{\rho} - \sum_i Q_i\lambda_i. \tag{6.2.3}$$

6.2.2 Reduction to one-dimension and moving frame of reference

The governing equations are restricted to consider a detonation propagating in only one spatial direction (in the positive direction in x). The detonation is thus assumed

to propagate at a constant velocity to leading order i.e. D. It is advantageous for the analysis to change the frame of reference attached to the shock front. Therefore, a variable n determines the distance from the shock in terms of the lab coordinate x in the following manner,

$$n = x - Dt. \tag{6.2.4}$$

Note that if $x < Dt$ this implies that the point in question lies behind the shock, and thus the detonation structure corresponds to $n < 0$ in the new variable. These change of variable follows such that

$$\frac{\partial}{\partial x} \to \frac{\partial n}{\partial x}\frac{\partial}{\partial n} = \frac{\partial}{\partial n}, \ \frac{\partial}{\partial t} \to \frac{\partial n}{\partial t}\frac{\partial}{\partial n} + \frac{\partial}{\partial t} = \frac{\partial}{\partial t} - D\frac{\partial}{\partial n}. \tag{6.2.5}$$

In order to measure the velocity with respect to the shock position one holds that

$$u = u_n + D \tag{6.2.6}$$

where the subscript n is meant to denote the new shock frame velocity. Under these transformations, the Euler reactive equations in the shock frame become

$$\begin{aligned}
&\frac{\partial \rho}{\partial t} + \frac{\partial}{\partial n}\big(\rho u_n\big) = 0 \\
&\frac{\partial}{\partial t}(\rho u) + \frac{\partial}{\partial n}\big(\rho u_n^2 + p\big) = 0 \\
&\frac{\partial u}{\partial t} + \frac{1}{u}\bigg(\frac{1}{(\gamma-1)\rho}\frac{\partial p}{\partial t} - \frac{\gamma p}{(\gamma-1)\rho^2}\frac{\partial \rho}{\partial t} - \sum_i Q_i \frac{\partial \lambda_i}{\partial t}\bigg) + \\
&\qquad \frac{\partial}{\partial n}\bigg(\frac{\gamma}{\gamma-1}\frac{p}{\rho} + \frac{u_n^2}{2} - \sum_i Q_i \lambda_i\bigg) = 0 \\
&\frac{\partial \lambda}{\partial t} + u\frac{\partial \lambda_i}{\partial n} = r_i.
\end{aligned} \tag{6.2.7}$$

Further it is assumed a steady solution in this frame, the ZND detonation structure can be found. The resulting equations are as follows (in conservation form):

$$\begin{aligned}
&\frac{\partial}{\partial n}\left(\rho u_n\right) = 0 \\
&\frac{\partial}{\partial n}\left(\rho u_n^2 + p\right) = 0 \\
&\frac{\partial}{\partial n}\left(\frac{\gamma}{\gamma-1}\frac{p}{\rho} + \frac{u_n^2}{2} - \sum_i \beta_i \lambda_i\right) = 0 \\
&\frac{\partial \lambda_i}{\partial n} = \frac{r_i}{u}
\end{aligned} \tag{6.2.8}$$

The first three equations can be used to solve for the unknown u_n, ρ and p in terms of $\lambda_{1,2}$. Thus, simultaneously integrating the reaction equations with respect to n leads to obtaining the steady state quantities. Particularly, one can find the following dependence of each variable on λ_i (where the subscript 0 denotes the value of each quantity directly behind the shock front, i.e. $n = 0^-$),

$$\begin{aligned}
\rho &= \frac{U_{n0}\rho_0}{U_n} \\
U_n &= \frac{\rho_0 U_{n0}^2 + p_0 - p}{\rho_0 U_{n0}} \\
p &= a + (p_0 - a)\sqrt{1 - b\sum_i Q_i \lambda_i}
\end{aligned} \tag{6.2.9}$$

where

$$a = \frac{\rho_0 U_{n0}^2 + p_0}{\gamma + 1},\ b = \frac{2(\gamma^2 - 1)\rho_0^2 U_{n0}^2}{(\rho_0^2 U_{n0}^2 - \gamma p_0)^2}. \tag{6.2.10}$$

A set of steady states appear for different D, ν and k in Fig. 6.2 where the distance n is scaled with the induction zone length, $\tilde{l}_I$. Clearly, there is more than one way acquire a dimensionless system of equations. In Ref. [69], a system of reference is built upon the post-shock values. In the more recent Refs. [70, 71], a system of reference is built upon the minimum propagation velocity, D_{CJ}, and the density in the pre-shocked area, ρ_u. Additionally the length and time scales are linked, i.e. the relevant length scale is the length of the induction zone, l_I, and the time scale is the

corresponding transit time of a particle with a velocity on the order of the CJ velocity through this length, i.e. l_I/D_{CJ}.

The scalings are summarized in the following:

$$\rho = \frac{\tilde{\rho}}{\tilde{\rho}_u},\ U_n = \frac{\tilde{U}_n}{\tilde{D}_{CJ}},\ p = \frac{\tilde{p}}{\tilde{\rho}_u \tilde{D}_{CJ}^2},\ T = \frac{\tilde{T}}{D_{CJ}^2/(\gamma \tilde{R})},\ \beta_i = \frac{\tilde{Q}_i}{D_{CJ}^2}, \epsilon = \frac{\tilde{\epsilon}}{\gamma \tilde{R}/\tilde{D}_{CJ}^2}$$
$$x = \frac{\tilde{x}}{\tilde{l}_I},\ t = \frac{\tilde{t}}{t_I} = \frac{\tilde{t}}{\tilde{l}_I/\tilde{D}_{CJ}}. \tag{6.2.11}$$

The unannotated symbols above henceforth refer to dimensionless quantities for ease of notation. Additionally, the tilde appearing above a quantity will also denote a dimensional quantity in order to differentiate between dimensional and non-dimensional quantities. The governing equations that appear in Eq. (6.2.7) are mathematically unchanged with the new introduced scalings with one exception, the new scaled heat release β_i replaces Q_i.

The minimal velocity $\bar{D}_{CJ}$ is used to obtain the dimensionless system as well as characterize whether the detonation is of the supported (overdriven) type or unsupported (CJ). As previously described, the CJ condition is met when the flow at the end of the reaction zone, i.e. $\lambda_{1,2} \to 1$, ends in a sonic point (w.r.t. to the shock front). In other words, $U_n^2 \to c^2 = \gamma p/\rho$. Therefore, setting $\lambda_{1,2} = 1$, $\tilde{U}_n^2 = \tilde{c}^2$, and using the relations found in Eq. (6.2.9) in their dimensional form, one can obtain

$$\tilde{D}_{CJ} = \tilde{c}_u \left(\sqrt{\frac{(\tilde{Q}/(\tilde{c}_u^2/\gamma))(\gamma^2-1)}{2\gamma}} + \sqrt{\frac{(\tilde{Q}/(\tilde{c}_u^2/\gamma))(\gamma^2-1)}{2\gamma} + 1} \right) \tag{6.2.12}$$

or in non-dimensional units, one defines $\delta = (\tilde{c}_u/\tilde{D}_{cj})$ as the inverse Mach number of the CJ detonation wave.

$$\delta = \left(\sqrt{\frac{Q(\gamma^2-1)}{2\gamma}} + \sqrt{\frac{Q(\gamma^2-1)}{2\gamma} + 1} \right)^{-2} \tag{6.2.13}$$

where $\tilde{Q} = \sum_i \tilde{Q}_i$ and both $\tilde{D}_{CJ}$ and $\tilde{Q}$ are scaled with help from the upstream velocity of sound, $\tilde{c}_u$. Thus, the CJ detonation velocity is set if the upstream conditions and the total heat release are known.

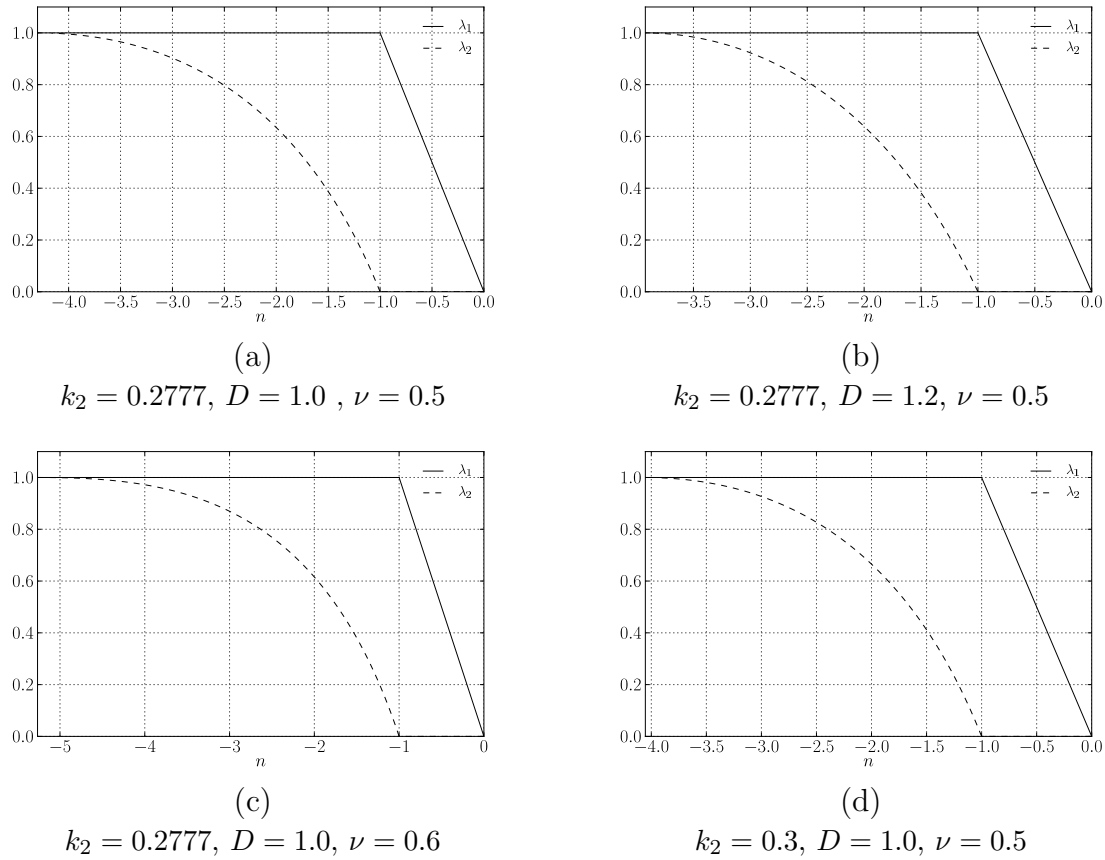

(a) $k_2 = 0.2777,\ D = 1.0\ ,\ \nu = 0.5$

(b) $k_2 = 0.2777,\ D = 1.2,\ \nu = 0.5$

(c) $k_2 = 0.2777,\ D = 1.0,\ \nu = 0.6$

(d) $k_2 = 0.3,\ D = 1.0,\ \nu = 0.5$

FIGURE 6.2. Reaction progress variables λ_1 and λ_2 as function of non-dimensional distance from shock n (scaled with induction zone length, l_I) for $\gamma = 1.4$ and $Q = 4.0$.

6.2.3 Rankine Hugoniot conditions

The immediate post-shock state denoted by the subscript "0" (known as the von Neumann state) can be defined in terms of the pre-shocked quantities and the detonation velocity D. This is done with help of the Rankine-Hugoniot jump conditions at the shock. The resulting equations provide expressions for the three assumed unknowns (i.e. post-shock state) which are p_0, ρ_0 and U_{n0} (denoted by the subscript 0). The algebraic equations result from integrating Eq. (6.2.9) in dimensionless form across

the shock

$$\rho_0 U_{n0} = -D \tag{6.2.14}$$

$$\rho_0 U_{n0}^2 + p_0 = D^2 + \frac{\delta}{\gamma} \tag{6.2.15}$$

$$\frac{\gamma}{\gamma-1}\frac{p_0}{\rho_0} + \frac{U_{n0}^2}{2} = \frac{\delta}{(\gamma-1)} + \frac{D^2}{2} \tag{6.2.16}$$

where it has been introduced that $D = \tilde{D}/\tilde{D}_{CJ}$ and $\delta = \gamma(\tilde{p}_u/\tilde{\rho}_u)/\tilde{D}_{CJ}^2 = \tilde{c}_u^2/\tilde{D}_{CJ}^2$ as defined in (6.2.13). Therefore D is a measure of the "overdrive", i.e. the extent by which the detonation velocity exceeds the minimum. In contrast to the the previous chapters, the overdrive was defined by the square of this ratio. These relations can be solved precisely:

$$\rho_0 = \frac{(\gamma+1)D}{(\gamma-1)D + 2\delta/D}, \tag{6.2.17}$$

$$U_{n0} = \frac{(\gamma-1)D + 2\delta/D}{-(\gamma+1)}, \tag{6.2.18}$$

$$p_0 = \frac{2}{\gamma+1}D^2 - \frac{\gamma-1}{\gamma(\gamma+1)}\delta. \tag{6.2.19}$$

These new relations have implications for the steady state relations, i.e.

$$\begin{aligned} \rho &= -\frac{D}{U_n} \\ U_n &= \frac{p - D^2 - \delta/\gamma}{D} \\ p &= a + (p_0 - a)\sqrt{1 - b\sum_i \beta_i \lambda_i} \end{aligned} \tag{6.2.20}$$

where

$$a = \frac{D^2 + \delta/\gamma}{\gamma+1},\ b = \frac{2(\gamma^2-1)}{(\delta/D - D)^2}. \tag{6.2.21}$$

With U_n, p and ρ known as functions of λ_i, one can integrate the reaction equations and obtain their dependence on n, and thus obtain the steady state profile for each of the variables of interest here. This is done in Fig. 6.2 for various rate constant in the main reaction layer.

6.3 The perturbation expansion

The preceding analysis dealt with a detonation propagating at an exactly constant value and to leading order a steady flow assumption was employed as well in the shock frame of reference. In the following, solutions will be sought for slowly-evolving dynamics of the perturbation as hinted by full numerical simulations of the underlying reaction kinetic model [64]. One can then assume that the flow is steady to leading order, but also having a small slowly time-varying component. In the present work this is introduced as a perturbation in the shock velocity of the form

$$D_n = D_n^{(0)} + \epsilon D_n^{(1)} \tag{6.3.1}$$

where ϵ is the inverse activation energy and is considered to be very small, $\epsilon \ll 1$, and thus signifying the high temperature sensitivity of the initial induction zone reaction parametrized by λ_1. It also provides the "slow" time scale i.e. $\tau = \epsilon t$ so that $\tau = O(1)$ implies $t = O(1/\epsilon) \gg 1$.

This necessarily modifies the equations in the moving frame so that the position of the shock front, $h(t, \tau)$, will then depend weakly on time as well. One has that

$$n = x - h(t, \tau) \tag{6.3.2}$$

where $h(t, \tau) = D_n^{(0)} t + H(\tau)$ and H is a slowly evolving function of time. Therefore changing the system of coordinates to this perturbed shock one finds

$$\frac{\partial}{\partial t} \to \frac{\partial n}{\partial t}\frac{\partial}{\partial n} + \frac{\partial}{\partial t} = -\frac{\partial h}{\partial t}\frac{\partial}{\partial n} + \frac{\partial}{\partial t} \tag{6.3.3}$$

and due to the slow time dependence of H,

$$\frac{\partial h}{\partial t} = D_n^{(0)} + \epsilon D_n^{(1)}, \text{ with } D_n^{(1)}(\tau) = \frac{\partial H}{\partial \tau}. \tag{6.3.4}$$

As a result of these transformations,

$$\frac{\partial}{\partial t} \to -(D_n^{(0)} + \epsilon D_n^{(1)})\frac{\partial}{\partial n} + \frac{\partial}{\partial t}, \ \frac{\partial}{\partial x} \to \frac{\partial}{\partial n}. \tag{6.3.5}$$

Finally, the velocity is modified with respect to leading order $D_n^{(0)}$ only, i.e. $u \to u_n + D_n^{(0)}$. The modified set of conservation equations in the transformed system are:

$$\begin{aligned}
&\frac{\partial \rho}{\partial t} + \frac{\partial}{\partial n}\big((u_n - \epsilon D_n^{(1)})\rho\big) = 0 \\
&\frac{\partial}{\partial t}(\rho u_n) + \frac{\partial}{\partial n}\big(\rho(u - \epsilon D_n^{(1)})u_n + p\big) = 0 \\
&\frac{1}{u_n - \epsilon D_n^{(1)}}\left(\frac{\partial e}{\partial t} - \frac{p}{\rho^2}\frac{\partial \rho}{\partial t}\right) + \frac{\partial u}{\partial t} + \frac{\partial}{\partial n}\left(\frac{u_n^2}{2} + e + \frac{p}{\rho}\right) = 0 \\
&\frac{1}{u_n - \epsilon D_n^{(1)}}\frac{\partial \lambda}{\partial t} + \frac{\partial \lambda}{\partial n} = \frac{r_i}{u_n - \epsilon D_n^{(1)}}.
\end{aligned} \tag{6.3.6}$$

6.3.1 Asymptotic series

To solve this system of PDE's, each quantity is expanded in powers of ϵ, i.e.

$$\begin{aligned}
&\rho = \rho^{(0)} + \epsilon\rho^{(1)} + O(\epsilon^2),\ u_n = u_n^{(0)} + \epsilon u_n^{(1)} + O(\epsilon^2), \\
&p = p^{(0)} + \epsilon p^{(1)} + O(\epsilon^2),\ \text{and } \lambda_i = \lambda_i^{(0)} + \epsilon\lambda_i^{(1)} + O(\epsilon^2).
\end{aligned} \tag{6.3.7}$$

The leading order perturbations are steady with respect to time, and so the leading order equations that result from substituting Eq. (6.3.7) into Eq. (6.3.6) are

$$\begin{aligned}
&\frac{\partial}{\partial n}\big(\rho^{(0)}u_n^{(0)}\big) = 0, \\
&\frac{\partial}{\partial n}\big(\rho^{(0)}(u_n^{(0)})^2 + p^{(0)}\big) = 0, \\
&\frac{\partial}{\partial n}\left(\frac{\gamma}{\gamma - 1}\frac{p^{(0)}}{\rho^{(0)}} + \frac{(u_n^{(0)})^2}{2} - \sum_i \beta_i \lambda_i^{(0)}\right) = 0, \\
&\frac{\partial \lambda_i^{(0)}}{\partial n} = \frac{r_i^{(0)}}{u_n^{(0)}}.
\end{aligned} \tag{6.3.8}$$

Note that the current spatial reference scale is l_I, the induction zone length. Further, the model assumes that the heat release in this zone is negligible, i.e. $\beta_1 = 0$. Due to the sequential nature of the reaction rates, the first reaction step must complete before the second step can proceed. These last two facts imply that $\sum_i \beta_i \lambda_i = 0$ for $0 < \lambda_i^{(0)} < 1$ in the induction zone. The first three equations can be solved separately

from the reaction rate equations in the induction zone and so the steady relations give automatically that

$$\rho^{(0)} = \rho_0,\ u_n^{(0)} = \rho_0,\ p^{(0)} = \rho_0. \tag{6.3.9}$$

The first order perturbation solution is really just the post-shock state values.

6.3.2 Expansion of Rankine-Hugoniot conditions

As in the steady case, one can imagine drawing a rectangle across the shock so that the conservation of mass across each face of our imaginary control volume can be written. Firstly, the conservation of mass in the shock moving frame dictates

$$\big(\rho(u_n - \epsilon D_n^{(1)})\big)\Big|_{n=0^-}^{\text{upstream}} = 0. \tag{6.3.10}$$

The quantities above must be perturbed according to our scheme and so

$$\begin{aligned}(\rho_0^{(0)} + \epsilon\rho_0^{(1)})(u_{n0}^{(0)} + \epsilon u_{n0}^{(1)})(1) + \epsilon D_n^{(1)})(1) + O(\epsilon^2) = \\ - (D_n^{(0)} + \epsilon(D_n^{(1)} + U_u^{(1)}))(1 + \epsilon\rho_u^{(1)}) + O(\epsilon^2).\end{aligned} \tag{6.3.11}$$

Note that in the preceding equation, the perturbations in the upstream velocity or density, denoted as $U_u^{(1)}$ or $\rho_u^{(1)}$, are included for the sake of generality but in the following, these are dropped for the sake of simplicity of the derivations. Equating both sides at each order in ϵ

$$\begin{aligned}O(\epsilon^0) &: \rho_0^{(0)} u_{n0}^{(0)} = -D_n^{(0)} \\ O(\epsilon^1) &: u_{n0}^{(0)}\rho_0^{(1)} + \rho^{(0)} u_{n0}^{(1)} = (\rho_0 - 1)D_n^{(1)}.\end{aligned} \tag{6.3.12}$$

The momentum and energy equations can be similarly treated and produce at the relevant order $\mathcal{O}(\epsilon)$,

$$\begin{aligned}&2u_{n0}^{(0)}\rho_0^{(0)}u_0^{(1)} + (u_{n0}^{(0)})^2\rho_0^{(1)} + p_0^{(1)} = 0 \\ &u_{n0}^{(0)}u_0^{(1)} + \frac{\gamma p_0^{(1)}}{(\gamma-1)\rho_0^{(0)}} - \frac{\gamma p_0^{(0)}\rho_0^{(1)}}{(\gamma-1)(\rho_0^{(0)})}{}^2 = (u_0 + D_n^{(0)})D_n^{(1)}.\end{aligned} \tag{6.3.13}$$

These three equations can be rewritten in a vector formulation,

$$\begin{pmatrix} u_{n0}^{(0)} & \rho^{(0)} & 0 \\ (u_{n0}^{(0)})^2 & 2u_{n0}^{(0)}\rho_0^{(0)} & 1 \\ -\frac{\gamma p_0^{(0)}}{(\gamma-1)(\rho_0^{(0)})^2} & u_{n0}^{(0)} & \frac{\gamma}{(\gamma-1)\rho_0^{(0)}} \end{pmatrix} \begin{pmatrix} \rho_0^{(1)} \\ u_{n0}^{(1)} \\ p_0^{(1)} \end{pmatrix} = \begin{pmatrix} \rho_0 - 1 \\ 0 \\ u_0 + D_n^{(0)} \end{pmatrix} D_n^{(1)}. \tag{6.3.14}$$

The determinant of the matrix, denoted $\mathbf{Y}$, is inversely proportional to $(u_{n0}^{(0)})^2 - \gamma p_0^{(0)}/\rho_0^{(0)} \neq 0$. Via the inversion of this matrix, one obtains

$$\begin{aligned} \rho_0^{(1)} &= k_\rho D_n^{(1)}, \\ k_\rho &= \frac{(\gamma-1)D_n^{(0)}\rho_0^{(0)} - 2D_n^{(0)}\gamma - (\gamma+1)u_{n0}^{(0)}}{(u_{n0}^{(0)})^2 - (c_0^{(0)})^2}, \end{aligned} \tag{6.3.15}$$

and the parameter k_ρ can be vastly simplified using the leading order steady solutions. This simplification applies to the other perturbation quantities, i.e. $u_{n0}^{(1)} = k_{u_n} D_n^{(1)}$ and $p_0^{(1)} = k_p D_n^{(1)}$ and specifically,

$$\begin{aligned} k_\rho &= \frac{4(\gamma+1)\delta}{D_n^{(0)}((\gamma-1)D_n^{(0)} + 2\delta/D_n^{(0)})^2}, \\ k_{u_n} &= \frac{2\delta - (D_n^{(0)})^2(\gamma-1)}{(D_n^{(0)})^2(\gamma+1)}, \\ k_p &= \frac{4D_n^{(0)}}{\gamma+1}. \end{aligned} \tag{6.3.16}$$

6.3.3 Leading order reaction progress and first order solution

The leading order solution is constant with respect to n and t so that only $\lambda_1^{(0)}$ must change in n. A more careful analysis must be done for the first reaction equation, i.e.

$$\frac{\partial \lambda_1^{(0)}}{\partial n} = \frac{r_1^{(0)}}{u_n^{(0)}} \quad \text{with } r_1 = k_1 \exp\left(\frac{1}{\epsilon}\left(\frac{1}{T_0} - \frac{1}{T}\right)\right). \tag{6.3.17}$$

In the dimensionless system $T = c^2 = \gamma p/\rho$ so this quantity must be expanded as well,

$$\begin{aligned}
\frac{1}{T} = \frac{1}{c^2} &= \frac{1}{\gamma}\big(\rho^{(0)} + \epsilon\rho^{(1)} + O(\epsilon^2)\big)\big(p^{(0)} + \epsilon p^{(1)} + O(\epsilon^2)\big)^{-1} \\
\frac{1}{c^2} &= \frac{1}{\gamma}\big(\rho^{(0)} + \epsilon\rho^{(1)} + O(\epsilon^2)\big)\left(\frac{1}{p^{(0)}} - \epsilon\frac{p^{(1)}}{(p^{(0)})^2} + O(\epsilon^2)\right) \\
\frac{1}{c^2} &= \frac{\rho^{(0)}}{\gamma p^{(0)}} + \epsilon\frac{1}{\gamma}\left(\frac{\rho^{(1)}}{p^{(0)}} - \frac{\rho^{(0)}p^{(1)}}{(p^{(0)})^2}\right) + O(\epsilon^2).
\end{aligned} \tag{6.3.18}$$

Since $\dfrac{\rho^{(0)}}{\gamma p^{(0)}} = \dfrac{1}{T^{(0)}} = \dfrac{1}{T_0}$,

$$\begin{aligned}
r_1^{(0)} + O(\epsilon) &= k_1 \exp\left(\frac{1}{\epsilon}\left(\frac{1}{T_0} - \left(\frac{\rho^{(0)}}{\gamma p^{(0)}} + \epsilon\left(\frac{\rho^{(1)}}{\gamma p^{(0)}} - \frac{\rho^{(0)}p^{(1)}}{\gamma(p^{(0)})^2}\right) + O(\epsilon^2)\right)\right)\right) \\
\Rightarrow r_1^{(0)} &= k_1 \exp\left(\frac{\rho^{(0)}p^{(1)}}{\gamma(p^{(0)})^2} - \frac{\rho^{(1)}}{\gamma p^{(0)}}\right)
\end{aligned} \tag{6.3.19}$$

In the completely steady case, the constant k_1 was set to the negative of the velocity at the shock, i.e. $k_1 = -u_{n0} = -u_n^{(0)}$, so as to define $n = -1$ to be the end of the induction zone. Therefore keeping this convention, to leading order:

$$\frac{\partial\lambda_1^{(0)}}{\partial n} = -\exp\left(\frac{\rho^{(0)}p^{(1)}}{\gamma(p^{(0)})^2} - \frac{\rho^{(1)}}{\gamma p^{(0)}}\right). \tag{6.3.20}$$

The salient fact is that the $O(\epsilon)$ perturbations have an $O(1)$ effect on the reaction progress variable spatial derivative, $\partial\lambda_1^{(0)}/\partial n$, which in turn has an order $O(1)$ affect on the location of the interface between the reaction and induction zones.

6.3.4 Finding the first order perturbations

The leading order analysis showed that $\rho^{(0)} = \rho_0$, $u_n^{(0)} = u_{n0}$, and $p^{(0)} = p_0$, i.e. a steady constant base state. This simplifies the $\mathcal{O}(\epsilon)$ equations since the terms involving derivatives in n of the leading order quantities are all zero. For example, the continuity equation at $\mathcal{O}(\epsilon)$ is

$$\rho^{(0)}\frac{\partial u_n^{(1)}}{\partial n} + \rho^{(1)}\underbrace{\frac{\partial u_n^{(0)}}{\partial n}}_{=0} + u^{(0)}\frac{\partial\rho^{(1)}}{\partial n} + (u^{(1)} - D_n^{(1)})\underbrace{\frac{\partial\rho^{(0)}}{\partial n}}_{=0} + \underbrace{\frac{\partial\rho^{(0)}}{\partial\tau}}_{=0} = 0. \tag{6.3.21}$$

The term that is a derivative in τ is zero since $\rho^{(0)} = \rho_0$ which is a constant with respect to both n and τ. Therefore, one arrives at a a vastly simpler equation,

$$\rho^{(0)}\frac{\partial u_n^{(1)}}{\partial n} + u^{(0)}\frac{\partial \rho^{(1)}}{\partial n} = 0. \tag{6.3.22}$$

The additional equations obtained from the momentum and energy equations are

$$\begin{aligned}(u_n^{(0)})^2\frac{\partial \rho^{(1)}}{\partial n} + 2u_n^{(0)}\rho^{(0)}\frac{\partial u_n^{(1)}}{\partial n} + \frac{\partial p^{(1)}}{\partial n} = 0,\\ -\frac{\gamma p^{(0)}}{(\gamma-1)(\rho^{(0)})^2}\frac{\partial \rho^{(1)}}{\partial n} + u_n^{(0)}\frac{\partial u_n^{(1)}}{\partial n} + \frac{1}{(\gamma-1)\rho^{(0)}}\frac{\partial p^{(1)}}{\partial n} = 0.\end{aligned} \tag{6.3.23}$$

These equations can be placed into matrix form:

$$\begin{pmatrix} u_{n0} & \rho_0 & 0 \\ u_{n0}^2 & 2u_{n0}\rho_0 & 1 \\ -\dfrac{\gamma p_0}{(\gamma-1)\rho_0} & u_{n0} & \dfrac{\gamma}{(\gamma-1)\rho_0}\end{pmatrix}\frac{\partial}{\partial n}\begin{pmatrix}\rho^{(1)}\\ u_n^{(1)}\\ p^{(1)}\end{pmatrix} = \begin{pmatrix}0\\0\\0\end{pmatrix}. \tag{6.3.24}$$

As before the matrix has a non-zero determinant and more importantly is constant and therefore the solution for each perturbation is a constant state with respect to n, specifically

$$\frac{\partial \rho^{(1)}}{\partial n} = 0 \Rightarrow \rho^{(1)} = \rho_0^{(1)} = k_\rho D_n^{(1)}, \tag{6.3.25}$$

and similarly,

$$u_n^{(1)} = u_{n0}^{(1)} = k_{u_n} D_n^{(1)},\ p^{(1)} = p_0^{(1)} = k_p D_n^{(1)}. \tag{6.3.26}$$

The first order perturbations in the induction zone are steady with respect to n but are slowly varying in time due to the factor $D_n^{(1)}$ in each.

The reaction progress evolution is now prescribed and depends on the the steady flow and also crucially, on $D_n^{(1)}$,

$$\begin{aligned}\frac{\partial \lambda_1^{(0)}}{\partial n} &= -\exp\left(\frac{\rho^{(0)}p^{(1)}}{\gamma(p^{(0)})^2} - \frac{\rho^{(1)}}{\gamma p^{(0)}}\right) = -\exp\left(\left(\frac{\rho^{(0)}k_p}{\gamma(p^{(0)})^2} - \frac{k_\rho}{\gamma p^{(0)}}\right)D_n^{(1)}\right)\\ &= -\exp(-bD_n^{(1)}) \ \text{ with } b = -\left(\frac{\rho^{(0)}k_p}{\gamma(p^{(0)})^2} - \frac{k_\rho}{\gamma p^{(0)}}\right).\end{aligned} \tag{6.3.27}$$

The exponential factor is a slow function of time, therefore one can integrate the equation over n to obtain the first reaction progress variable

$$\lambda_1^{(0)} = -n \exp(-bD_n^{(1)}) \tag{6.3.28}$$

where it is utilized that $\lambda_1^{(0)}(n = 0) = 0$. Since the end of the induction zone is signaled when $\lambda_1^{(0)} = 1$ it is straightforward to solve for the dimensionless distance at which this occurs,

$$1 = -n \exp(-bD_n^{(1)}) \Rightarrow n = F(\tau) = -\exp(bD_n^{(1)}). \tag{6.3.29}$$

The constant b can be simplified using the Rankine-Hugoniot derived post-shock quantities,

$$b = -\frac{4\gamma(\gamma-1)}{(\gamma+1)^2 c_0^4 (D_n^{(0)})^3}\left((D_n^{(0)})^4 + \frac{\delta^2}{\gamma}\right) \tag{6.3.30}$$

and the sound speed at the shock front, c_0^2, as well:

$$c_0^2 = ((\gamma-1)D_n^{(0)} + 2\delta/D_n^{(0)})(2\gamma D_n^{(0)} - (\gamma-1)\delta/D_n^{(0)})/(\gamma+1)^2. \tag{6.3.31}$$

At this point, the position, $F(\tau)$, of the transition from induction to reaction zone is dependent on the $\mathcal{O}(\epsilon)$ deviation in the shock velocity, i.e. $D_n^{(1)}$ and thus is a slow function of time as well. The object of these derivations ultimately is an evolution equation for $D_n^{(1)}$ and this will be obtained by analyzing the perturbation expansion in the main heat release layer subject to the solution found in the induction zone.

6.3.5 Main reaction zone analysis

To begin the asymptotic analysis in the reaction zone, the coordinate measuring the distance from the interface of the induction and reaction zones i.e. at $n = F(\tau)$ is defined as l,

$$l = n - F(\tau). \tag{6.3.32}$$

In the current work however, the characteristic length of the reaction zone is considered to be significantly longer than the induction zone length. To achieve this, one holds that the second reaction rate constant should be small since the length of the reaction zone is roughly inversely proportional to the rate constant. In order to produce this desired regime then it is specifically held that

$$k_2 = \mathcal{O}(\epsilon/\omega) \ll 1, \text{ with } \epsilon \ll \omega \ll 1. \tag{6.3.33}$$

The parameter ω serves to set the relative ratio between the main reaction layer length to the short induction zone length. A more appropriate length scale is chosen such that such that $m = \epsilon l/\omega$ where ω is eventually absorbed into the modified reaction rate constant. Utilizing then that $m = (\epsilon/\omega)(n - F(\tau))$ one can obtain the modified derivatives,

$$\frac{\partial}{\partial n} \to \frac{\partial m}{\partial n}\frac{\partial}{\partial m}, \ \frac{\partial}{\partial t} \to \frac{\partial m}{\partial t}\frac{\partial}{\partial m} + \frac{\partial}{\partial t} \tag{6.3.34}$$

$$\frac{\partial m}{\partial n} = \frac{\epsilon}{\omega}, \ \frac{\partial m}{\partial t} = -\frac{\epsilon}{\omega}\frac{\partial F(\tau)}{\partial t} = -\frac{\epsilon^2}{\omega}F_\tau, \ F_\tau = \frac{\partial F}{\partial \tau}, \tag{6.3.35}$$

$$\frac{\partial}{\partial n} \to \frac{\epsilon}{\omega}\frac{\partial}{\partial m}, \ \frac{\partial}{\partial t} \to -\frac{\epsilon^2 F_\tau}{\omega}\frac{\partial}{\partial m} + \frac{\partial}{\partial t} \tag{6.3.36}$$

The whole system of equations can then be written as

$$\omega\frac{\partial \rho}{\partial t} + \epsilon\frac{\partial}{\partial m}\big(\rho(u - \epsilon(D_n^{(1)} + F_\tau))\big) = 0 \tag{6.3.37}$$

$$\omega\frac{\partial \rho u}{\partial t} + \epsilon\frac{\partial}{\partial m}\big(\rho u(u - \epsilon(D_n^{(1)} + F_\tau) + p\big) = 0 \tag{6.3.38}$$

$$\begin{aligned}\omega\left(\frac{\partial e}{\partial t} - \frac{p}{\rho^2}\frac{\partial \rho}{\partial t} + (u - \epsilon(D_n^{(1)} + F_\tau))\frac{\partial u}{\partial t}\right)\ldots \\ + \epsilon(u - \epsilon(D_n^{(1)} + F_\tau))\frac{\partial}{\partial m}\left(\frac{p}{\rho} + e + \frac{(u - \epsilon(D_n^{(1)} + F_\tau))^2)}{2}\right) = 0\end{aligned} \tag{6.3.39}$$

$$\omega\frac{\partial \lambda}{\partial t} + \epsilon(u - \epsilon(D_n^{(1)} + F_\tau))\frac{\partial \lambda_2}{\partial m} = \omega r_2 \tag{6.3.40}$$

Under the slowly varying assumption, one obtains

$$\omega\frac{\partial\rho}{\partial\tau}+\frac{\partial}{\partial m}\big(\rho(u-\epsilon(D_n^{(1)}+F_\tau))\big)=0 \tag{6.3.41}$$

$$\omega\frac{\partial\rho u}{\partial\tau}+\frac{\partial}{\partial m}\big(\rho u(u-\epsilon(D_n^{(1)}+F_\tau)+p\big)=0 \tag{6.3.42}$$

$$\begin{aligned}\omega\left(\frac{\partial e}{\partial\tau}-\frac{p}{\rho^2}\frac{\partial\rho}{\partial\tau}+(u-\epsilon(D_n^{(1)}+F_\tau))\frac{\partial u}{\partial\tau}\right)\dots\\ +(u-\epsilon(D_n^{(1)}+F_\tau))\frac{\partial}{\partial m}\left(\frac{p}{\rho}+e+\frac{(u-\epsilon(D_n^{(1)}+F_\tau))^2)}{2}\right)=0\end{aligned} \tag{6.3.43}$$

$$\omega\frac{\partial\lambda_2}{\partial\tau}+(u-\epsilon(D_n^{(1)}+F_\tau))\frac{\partial\lambda_2}{\partial m}=\bar{r}_2 \tag{6.3.44}$$

with $\bar{r}_2=(\omega k_2/\epsilon)(1-\lambda_2)^\nu=\bar{k}(1-\lambda_2)^\nu$. Recall that $r_2=k_2(1-\lambda_2)^\nu$ for $\lambda_1=1$, and so the factor $\omega k_2/\epsilon$ is $O(1)$ when $k_2=O(\epsilon/\omega)$.

Solving this explicitly nonlinear system of PDE's requires a full numerical treatment for a general ω. In lieu of this more time consuming numerical approach, an evolution equation can be obtained analytically for $D_n^{(1)}$ that avoids the need to develop a solution for the full PDE system by expanding the solution in the reaction zone.

6.4 Evolution equation for the system of equations

In Ref. [69], an evolution equation was developed for the specific case of a Chapman-Jouguet detonation wave ($D=1$) for the two-step model contained in the present work but limited to the reaction order $\nu=1/2$. The evolution equation was obtained by introducing an asymptotic series for the solution in (6.3.41) in two parameters, inverse activation energy, ϵ, and the parameter ω which ultimately controls the influence of the time derivatives in the perturbation equations for the main reaction layer which are order $\mathcal{O}(\omega)$.

The analysis is simplified if one uses the steady state reaction progress variable

λ_2. For ease of notation, one uses that $\lambda = \lambda_2$ and $r = \bar{r}_2$,

$$\frac{\partial}{\partial m} \rightarrow \frac{\partial \lambda}{\partial m}\frac{\partial}{\partial \lambda} = \frac{r}{u}\frac{\partial}{\partial \lambda}. \tag{6.4.1}$$

One then arrives at the following equations for the perturbations:

$$\frac{\partial}{\partial \lambda}(\rho(u - \epsilon(D_n + F_\tau)) + \omega\frac{u}{r}\frac{\partial \rho}{\partial \tau} = 0, \tag{6.4.2}$$

$$\frac{\partial}{\partial \lambda}(p + \rho u(u - \epsilon(D_n + F_\tau))) + \omega\frac{u}{r}\frac{\partial \rho u}{\partial \tau} = 0, \tag{6.4.3}$$

$$\begin{aligned}\frac{\partial}{\partial \lambda}(\gamma p/(\gamma - 1)\rho + (u - \epsilon(D_n + F_\tau))^2/2 - \beta\lambda) + \\ \omega\frac{u}{r}\left(\frac{\partial u}{\partial \tau} + \frac{1}{(\gamma - 1)u\rho}\frac{\partial p}{\partial \tau} - \frac{\gamma p}{(\gamma - 1)u\rho^2}\frac{\partial \rho}{\partial \tau} - \frac{\beta}{u}\frac{\partial \lambda}{\partial \tau}\right) = 0.\end{aligned} \tag{6.4.4}$$

The following asymptotic expansion is introduced

$$\rho \rightarrow \rho_0 + \epsilon\rho^{(1)} + \omega\epsilon\rho^{(2)},\ u \rightarrow u_0 + \epsilon u^{(1)} + \omega\epsilon u^{(2)}, \tag{6.4.5}$$

$$p \rightarrow p_0 + \epsilon p^{(1)} + \omega\epsilon p^{(2)}, \lambda \rightarrow \lambda_0 + \epsilon\lambda^{(1)} + \omega\epsilon\lambda^{(2)}. \tag{6.4.6}$$

At first order, the solution is independent of the slow time variable τ as is assumed in the induction zone,

$$\begin{aligned}&\frac{\partial}{\partial \lambda}\big(\rho_0 u_0\big) = 0,\\ &\frac{\partial}{\partial \lambda}\big(\rho_0 u_0^2 + p_0\big) = 0,\\ &\frac{\partial}{\partial \lambda}\left(\frac{u_0^2}{2} + \frac{\gamma}{\gamma - 1}\frac{p_0}{\rho_0} - \beta\lambda\right) = 0.\end{aligned} \tag{6.4.7}$$

These equations are algebraically solved for $u_0(\lambda), \rho_0(\lambda)$ and $p_0(\lambda)$. The result of this expansion for the perturbations of order $\mathcal{O}(\epsilon)$ and $\mathcal{O}(\omega\epsilon)$ can be greatly simplified if one defines the following vector functions,

$$\hat{\mathbf{y}}^{(1)} = (\hat{\rho}^{(1)}, \hat{u}^{(1)}, \hat{p}^{(1)})^T = (\rho^{(1)} + \rho_0\tilde{\beta}\lambda^{(1)}, u^{(1)} - u_0\tilde{\beta}\lambda^{(1)}, p^{(1)} + u_0^2\rho_0\tilde{\beta}\lambda^{(1)})^T,$$

$$\& \tag{6.4.8}$$

$$\hat{\mathbf{y}}^{(2)} = (\hat{\rho}^{(2)}, \hat{u}^{(2)}, \hat{p}^{(2)})^T = (\rho^{(2)} + \rho_0\tilde{\beta}\lambda^{(2)}, u^{(2)} - u_0\tilde{\beta}\lambda^{(2)}, p^{(2)} + u_0^2\rho_0\tilde{\beta}\lambda^{(2)})^T.$$

It leads to the following equation where the derivative terms can be grouped together in a very convenient form,

$$\begin{aligned}&\frac{\partial}{\partial\lambda}(\mathbf{B}(\hat{\mathbf{y}}^{(1)}+\omega\hat{\mathbf{y}}^{(2)}))=(D_n+F_\tau)\frac{d\mathbf{g}}{d\lambda}\\&\mathbf{g}(\lambda)=(\rho_0(\lambda),0,u_0(\lambda))^T.\end{aligned}\tag{6.4.9}$$

Integrating this equation from 0 to λ yields

$$\mathbf{B}(\hat{\mathbf{y}}^{(1)}+\omega\hat{\mathbf{y}}^{(2)}))=\mathbf{C}_0(\lambda)D_n+\mathbf{C}_1(\lambda)F_\tau+\omega\mathbf{C}_2(\lambda)\tag{6.4.10}$$

where

$$\mathbf{B}=\begin{pmatrix}u_0 & \rho_0 & 0\\ u_0^2 & 2u_0\rho_0 & 1\\ -\frac{c_0^2}{(\gamma-1)\rho_0} & u_0 & \frac{\gamma}{(\gamma-1)\rho_0}\end{pmatrix},\tag{6.4.11}$$

$$\mathbf{C}_0(\lambda)=\begin{pmatrix}\rho_0(\lambda)-1\\ 0\\ u_0(\lambda)+D\end{pmatrix},\mathbf{C}_1(\lambda)=\begin{pmatrix}\rho_0(\lambda)-\rho_0(0)\\ 0\\ u_0(\lambda)-u_0(0)\end{pmatrix},\tag{6.4.12}$$

and

$$\mathbf{C}_2(\lambda)=\begin{pmatrix}N_1(\lambda)\\ N_2(\lambda)\\ N_3(\lambda)\end{pmatrix}\tag{6.4.13}$$

where

$$N_1(\lambda)=-\int_0^\lambda\frac{u_0}{r_0}\frac{\partial\rho^{(1)}}{\partial\tau}d\lambda\tag{6.4.14}$$

$$N_2(\lambda)=-\int_0^\lambda\frac{u_0}{r_0}\left(u_0\frac{\partial\rho^{(1)}}{\partial\tau}+\rho_0\frac{\partial u^{(1)}}{\partial\tau}\right)d\lambda\tag{6.4.15}$$

$$N_3(\lambda)=-\int_0^\lambda\frac{u_0}{r_0}\left(-\frac{c_0^2}{(\gamma-1)u_0\rho_0}\frac{\partial\rho^{(1)}}{\partial\tau}+\frac{\partial u^{(1)}}{\partial\tau}+\frac{1}{u_0\rho_0}\frac{\partial p^{(1)}}{\partial\tau}-\frac{\beta}{u_0}\frac{\partial\lambda^{(1)}}{\partial\tau}\right)d\lambda.\tag{6.4.16}$$

Inverting the matrix $\mathbf{B}$ is required to resolve the ultimate solutions for the perturba-

tions. This is given by $\mathbf{B}^{-1}(\lambda) = (\gamma-1)/\eta_0 \times \mathbf{A}$ where

$$\mathbf{A} = \begin{pmatrix} u_0\dfrac{\gamma+1}{\gamma-1} & -\dfrac{\gamma}{\gamma-1} & \rho_0 \\ -\dfrac{\gamma}{(\gamma-1)\rho_0}(u_0^2+c_0^2/\gamma) & \dfrac{\gamma u_0}{(\gamma-1)\rho_0} & -u_0 \\ u_0\left(u_0^2+\dfrac{2c_0^2}{\gamma-1}\right) & -\left(u_0^2+\dfrac{c_0^2}{\gamma-1}\right) & u_0^2\rho_0 \end{pmatrix}. \tag{6.4.17}$$

The solution for both orders can be obtained simultaneously as

$$\hat{\mathbf{y}}^{(1)} + \omega\hat{\mathbf{y}}^{(2)} = (\mathbf{B}^{-1}\mathbf{C}_0)D_n + (\mathbf{B}^{-1}\mathbf{C}_1)F_\tau + \omega\mathbf{B}^{-1}\mathbf{C}_2(\lambda) \tag{6.4.18}$$

with the first order solution for the $\mathcal{O}(\epsilon)$ modified solution

$$\begin{cases} \hat{\rho}^{(1)} &= \frac{\gamma-1}{\eta_0}(A_1D_n + A_2F_\tau) + A_3(\lambda)D_n + A_4(\lambda)F_\tau \\ \hat{u}^{(1)} &= \frac{\gamma-1}{\eta_0}(B_1D_n + B_2F_\tau) + B_3(\lambda)D_n + B_4(\lambda)F_\tau \\ \hat{p}^{(1)} &= \frac{\gamma-1}{\eta_0}(C_1D_n + C_2F_\tau) + C_3(\lambda)D_n + C_4(\lambda)F_\tau \end{cases} \tag{6.4.19}$$

where $A_{1,2}, B_{1,2}$ and $C_{1,2}$ are constants and $A_{3,4}, B_{3,4}$ and $C_{3,4}$ are functions of λ that are explicitly bounded as $\lambda \to 1$. Specifically then, it is found that

$$A_1 = \left[\mathbf{A}\mathbf{C}_0\right]_1\Big|_{\lambda=1}, \; A_3(\lambda) = \frac{\gamma-1}{\eta_0}\left(\left[\mathbf{A}\mathbf{C}_0\right]_1\Big|_{\lambda} - \left[\mathbf{A}\mathbf{C}_0\right]_1\Big|_{\lambda=1}\right) \tag{6.4.20}$$

$$A_2 = \left[\mathbf{A}\mathbf{C}_1\right]_1\Big|_{\lambda=1}, \; A_4(\lambda) = \frac{\gamma-1}{\eta_0}\left(\left[\mathbf{A}\mathbf{C}_1\right]_1\Big|_{\lambda} - \left[\mathbf{A}\mathbf{C}_1\right]_1\Big|_{\lambda=1}\right) \tag{6.4.21}$$

where $[\cdot]_i$ refers to the i-th element of the indicated vector. Similar structure holds for B_i and C_i.

6.4.1 Chapman-Jouguet evolution equation

First order problem. For $D = 1$ (CJ case), the sonic parameter $\eta_0 = u_0^2 - c_0^2$ approaches zero at the end of the reaction zone, i.e. at $\lambda = 1$. This is the case treated in [69] where the regularity of the solution as $\lambda \to 1$ is used to close the system of equations. This is equivalent to eliminating the non-regular or unbounded term in the solution for $\hat{\rho}^{(1)}$ in (6.4.19) which is proportional to $1/\eta_0$,

$$A_1D_n + A_2F_\tau = 0. \tag{6.4.22}$$

This is enough to guarantee the regularity of both $\hat{u}^{(1)}$ and $\hat{p}^{(1)}$ since one can show that specifically for $D = 1$,

$$B_1 = -(u_0(1)/\rho_0(1))A_1,\ B_2 = -(u_0(1)/\rho_0(1))A_2 \tag{6.4.23}$$

$$C_1 = (u_0(1))^2 A_1,\ C_2 = (u_0(1))^2 A_2 \tag{6.4.24}$$

and so the unbounded terms in both $\hat{u}^{(1)}$ and $\hat{p}^{(1)}$ are proportional to the same expression set to zero in (6.4.22). Therefore, imposing the regularity of the solution at the end of the reaction zone leads to a nonlinear evolution equation for $D_n^{(1)}$,

$$A_1 D_n^{(1)} - bA_2 \exp(bD_n^{(1)}) \frac{\partial D_n^{(1)}}{\partial \tau} = 0. \tag{6.4.25}$$

Given the nature of the constants ($A_1 > 0$, $A_2 < 0$, and $b < 0$) for reasonable values of the relevant parameters, the dynamics of the system are simple: $D_n^{(1)} \to \infty$ as $\tau \to \infty$ and also $D_n^{(1)} \to -\infty$ in a finite time. Furthermore, if this equation is linearized by assuming that $D_n^{(1)} \propto \exp(\delta\tau)$, the eigenvalue δ is real and positive, unconditionally so. The pulsating dynamics are therefore absent at this level of analysis. Ultimately then, the dynamics produced by the evolution equation in (6.4.22) dictate perturbations which are always unstable at any chosen heat release Q and γ.

Initially defining $\epsilon \ll \omega \ll 1$ has the effect of setting the reaction zone length,

$$l_r = \mathcal{O}(\omega/\epsilon) \ll \mathcal{O}(1/\epsilon) \gg 1 \tag{6.4.26}$$

The leading order analysis shows the quasi-steady dynamics encapsulated in (6.4.22) are unconditionally unstable in this regime. The numerical simulations described in [72] show that the transition from stable to unstable behavior occurs when the reaction zone length is long when compared with the induction zone which implies that $\omega = 1$ or $k_2 = \mathcal{O}(\epsilon)$. However, setting $\omega = 1$ has the effect of excluding a further analytical expansion exploiting the previously small ω and it becomes necessary to numerically solve the PDE system in (6.3.41). Nevertheless, an approximate asymptotic procedure can be performed where additional corrective terms are added to the evolution equation (6.4.22).

Including higher order effects. The preceding leading order analysis fails to produce (through the evolution equation) the pulsating behavior that is observed in numerical simulations [64] and [71]. In fact the relevant range for the parameter ω is $\omega \to 1$, or equivalently when $k_2 = \mathcal{O}(\epsilon)$. Following Ref. [69], an approximate iterative procedure is used to incorporate the $\mathcal{O}(\omega\epsilon)$ problem into the evolution equation. The process is essentially equivalent to including higher order acoustic effects. The strategy employed therein ([69]) is to use the "regular" part of the solutions for $\rho^{(1)}, u^{(1)}$ and $p^{(1)}$ to solve the higher order problem for $\hat{\mathbf{y}}^{(2)}$ encapsulated in (6.4.10). The procedure is summarized as follows,

1. The leading order (regular) solution for the perturbation i.e. $\rho^{(1)}, p^{(1)}, u_n^{(1)}$ and $\lambda^{(1)}$ is obtained.

2. The $\mathcal{O}(\epsilon)$ solution is then used as input for the vector function $\mathbf{C}_2(\lambda)$ that defines the $\mathcal{O}(\omega\epsilon)$ solution in (6.4.18).

3. The first and second order solution is summed and evaluated at the end reaction state.

4. The irregular term then depends on $D_n^{(1)}$ and its time derivatives and this expression is set equal to zero in order to enforce the regularity condition for the now summed expression in lieu of separating each component in the formal expansion.

5. The resulting ordinary differential equation for $D_n^{(1)}$ is derived assuming $\omega \ll 1$ but it is nevertheless taken to the limit $\omega \to 1$.

Following this outlined procedure, the sum of $\mathcal{O}(\epsilon)$ and $\mathcal{O}(\omega\epsilon)$ perturbations are calculated, i.e. $\hat{\mathbf{y}}^{(1)} + \omega\hat{\mathbf{y}}^{(2)}$ as in (6.4.18) and (6.4.19). Specifically for the density perturbation as $\lambda \to 1$ one has for example

$$\rho^{(1)} + \omega\rho^{(2)} \to \frac{\gamma - 1}{\eta_0}\left(A_1 D_n + A_2 F_\tau + \omega\left[\alpha_3 D_{n\tau} + \alpha_4 F_{\tau\tau}\right]\right) \tag{6.4.27}$$

where the coefficients $\alpha_{3,4}$ involve the integrals $N_{1,2,3}$ evaluated at $\lambda = 1$. The expression in parenthesis in (6.4.27) is set equal to zero in order to impose the regularity condition. Note that in the case where it was considered that $\omega \ll 1$ one recovers the previously obtained evolution equation in (6.4.38). Additionally, though the expression was derived for $\omega \ll 1$, the final step of this approximate procedure is to set $\omega = 1$. It produces

$$A_1 D_n + \left(\alpha_3 - bA_2 e^{bD_n^{(1)}}\right)\frac{\partial D_n^{(1)}}{\partial \tau} - b^2\alpha_4 e^{bD_n^{(1)}}\left(\frac{\partial D_n^{(1)}}{\partial \tau}\right)^2 - b\alpha_4 e^{bD_n^{(1)}}\frac{\partial^2 D_n^{(1)}}{\partial \tau^2}. \quad (6.4.28)$$

The validity of the obtained approximate evolution equation lies in its ability to mimic the numerical results. The dynamics of this second-order autonomous differential equation for $D_n^{(1)}$ include the sought-after pulsating dynamics and this is illustrated in Fig. 6.3. The evolution equation that appears in (6.4.28) was derived originally in [69] for explicitly CJ detonation with a reaction order exclusively considered to be $\nu = 1/2$. The main objective of the current work was to generalize this result to any reaction order and also to overdriven detonation where the regularity condition no longer applies.

6.4.2 Overdriven case

The regularizing condition used in the CJ case is not appropriate for overdriven detonation since $1/\eta_0(1)$ is finite for $D > 1$ as $\lambda \to 1$, thus removing the condition that results from the regularization of the solution. However, as in other studies of detonation stability, an algebraic relationship ensuring that no perturbation travels towards the shock must be applied to achieve closure as $\lambda \to 1$ i.e. the so-called "radiation boundary condition":

$$-\frac{c_0(1)D}{u_0(1)}u' + p' = 0 \quad (6.4.29)$$

which was obtained based on the asymptotic analysis used in Ref. [50]. The closure provided by this relationship is necessary to avoid the mechanical attenuation of the

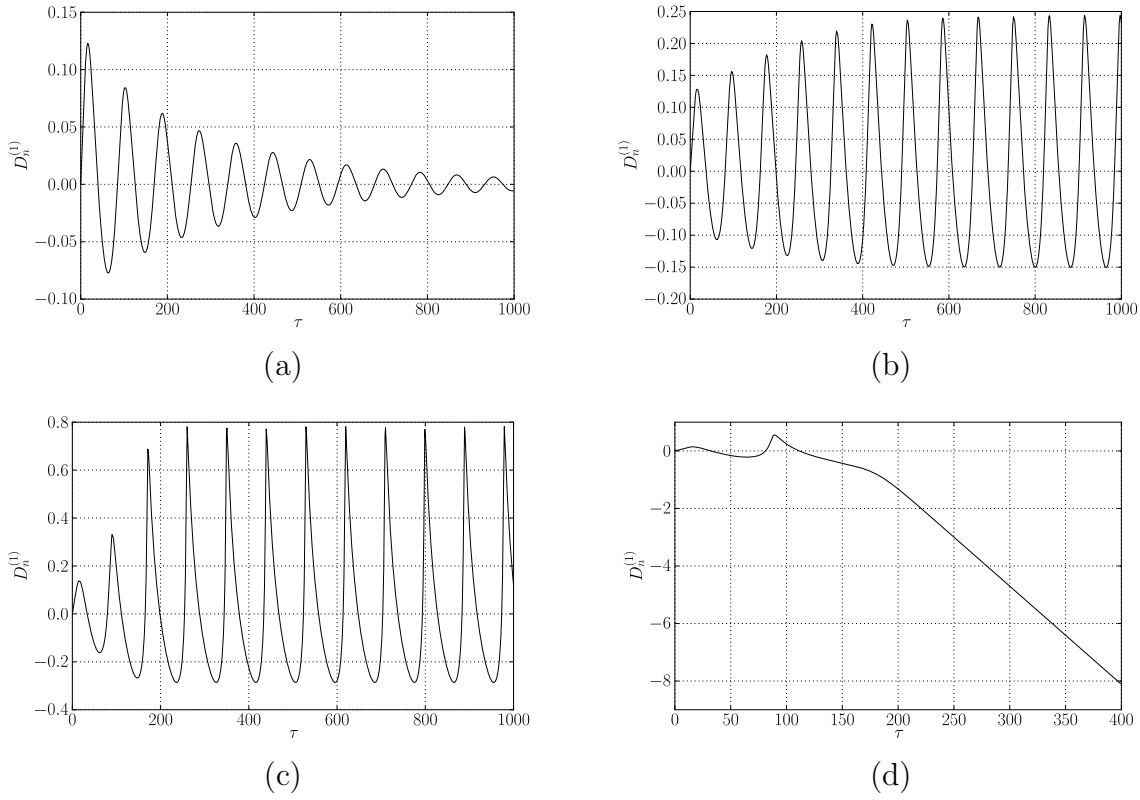

FIGURE 6.3. The different dynamic range of behavior of the evolution equation (6.4.28) including the case of perturbation decay, stable limit cycle, steepening limit cycle and unstable behavior. The tuned parameter here is the rate constant $\tilde{k}$ in the main reaction layer and the stability threshold is around $\tilde{k} = 0.29411$. Here, $D = 1$, $\nu = 1/2$, $\gamma = 1.4$ and $Q = 4$. (a) $\tilde{k} = 0.2777$, (b) $\tilde{k} = 0.3125$, (c) $\tilde{k} = 0.3571$, (d) $\tilde{k} = 0.3846$.

detonation shock front. This condition can be adapted to the modified variables in question i.e. $\hat{\rho}^{(1)}$, $\hat{u}^{(1)}$ and $\hat{p}^{(1)}$ and the corresponding second order variables $\hat{\rho}^{(2)}$, $\hat{u}^{(2)}$ and $\hat{p}^{(2)}$.

Leading order problem. For the order $\mathcal{O}(\epsilon)$ perturbations, the radiation condition is applied as $\lambda \to 1$,

$$-\frac{c_0(1)D}{u_0(1)}u^{(1)}(1,\tau) + p^{(1)}(1,\tau) = 0 \tag{6.4.30}$$

and one then finds that since $\lambda^{(1)}(1,\tau)=0$,

$$u^{(1)}(1,\tau)=\hat{u}^{(1)}(1,\tau)-u_0(1)\tilde{\beta}(1)\lambda^{(1)}(1,\tau)=\hat{u}^{(1)}(1,\tau). \tag{6.4.31}$$

Similarly, $\rho^{(1)}(1,\tau)=\hat{\rho}^{(1)}(1,\tau)$ and $p^{(1)}(1,\tau)=\hat{p}^{(1)}(1,\tau)$. The solution for the first order perturbations in (6.4.19) is:

$$\begin{cases}\hat{\rho}^{(1)} &= \frac{\gamma-1}{\eta_0}(A_1D_n+A_2F_\tau)+A_3(\lambda)D_n+A_4(\lambda)F_\tau\\ \hat{u}^{(1)} &= \frac{\gamma-1}{\eta_0}(B_1D_n+B_2F_\tau)+B_3(\lambda)D_n+B_4(\lambda)F_\tau\\ \hat{p}^{(1)} &= \frac{\gamma-1}{\eta_0}(C_1D_n+C_2F_\tau)+C_3(\lambda)D_n+C_4(\lambda)F_\tau.\end{cases} \tag{6.4.32}$$

Substituting the above for the end of the reaction zone in the radiation condition, one obtains the modified evolution equation for overdriven detonation,

$$\Big(-\frac{c_0(1)D}{u_0(1)}B_1+C_1\Big)D_n+\Big(-\frac{c_0(1)D}{u_0(1)}B_2+C_2\Big)F_\tau=0, \tag{6.4.33}$$

where

$$B_1=-\frac{u_0(1)}{\rho_0(1)}A_1+\frac{\eta_0(1)}{(\gamma-1)\rho_0(1)}(\rho_0(1)-1), \tag{6.4.34}$$

$$B_2=-\frac{u_0(1)}{\rho_0(1)}A_2+\frac{\eta_0(1)}{(\gamma-1)\rho_0(1)}(\rho_0(1)-\rho_0(0)) \tag{6.4.35}$$

$$C_1=u_0(1)^2A_1-\frac{2\eta_0(1)u_0(1)}{\gamma-1}(\rho_0(1)-1), \tag{6.4.36}$$

$$C_2=u_0(1)^2A_2-\frac{2\eta_0(1)u_0(1)}{\gamma-1}(\rho_0(1)-\rho_0(0)). \tag{6.4.37}$$

The evolution equation can then be written in the form

$$\big(A_1+\tilde{A}_1\big)D_n+\big(A_2+\tilde{A}_2\big)F_\tau=0 \tag{6.4.38}$$

$$\tilde{A}_1=\frac{\eta_0(1)(c_0(1)-2u_0(1))}{(\gamma-1)(u_0(1)-c_0(1))u_0(1)}(\rho_0(1)-1) \tag{6.4.39}$$

$$\tilde{A}_2=\frac{\eta_0(1)(c_0(1)-2u_0(1))}{(\gamma-1)(u_0(1)-c_0(1))u_0(1)}(\rho_0(1)-\rho_0(0)). \tag{6.4.40}$$

Note that if $D=1$ the expression above collapses to the original condition that $A_1D_n+A_2F_\tau=0$, the exact evolution equation obtained for the CJ case since $\eta_0(1)\to 0$ implies that $\tilde{A}_1=0$ and $\tilde{A}_2=0$.

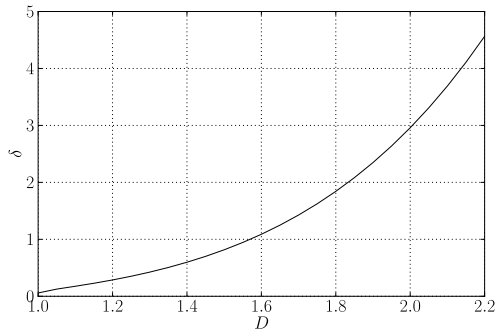

FIGURE 6.4. A linearized growth rate for $D_n^{(1)}$ can be obtained from the leading order evolution equation found in (6.4.38) by assuming $D_n^{(1)} \propto e^{\delta t}$. The linearized growth rate appears here as a function of D. The clear influence of the radiation condition is to destabilize the detonation with respect to the CJ case.

The first order evolution equation derived for the CJ case was found to produce the same sort of dynamics as those found for the corresponding the one-step Arrhenius model in the asymptotic high activation energy limit ($1/\epsilon \to \infty$) otherwise know as the "square wave model" of detonation. The linear perturbations for the square wave profile evolve according to a single non-oscillatory unstable mode. In the current more general formulation, Fig. 6.4 shows that the linearized growth rate of the perturbation governed by (6.4.38) remains positive and real and additionally, increases with higher degrees of overdrive. Generally, higher overdrive tends to stabilize detonations with an apparent exception: detonation with high activation energy. In Ref. [72], a linear stability analysis of high though finite activation energies within the context of Arrhenius one-step planar detonation was performed and a slowly evolving non-oscillatory mode mode was found and examined at various degrees of overdrive. Specifically, it was found to have a growth rate that monotonically increased as the overdrive was increased from $f = D^2 = 1$ to $f = 1.6$. Buckmaster and Ludford [73] predict that this unstable non-oscillatory mode will be present for all degrees of overdrive. Therefore, the increase of the linearized growth rate of this unstable mode derived from the leading order evolution equation (see Fig. 6.4) as overdrive is

increased seems to be in agreement with these previous observations.

Including second-order problem. As in the CJ case, the approximate iterative procedure outlined therein is again used in the overdriven case as well with some modification. Specifically in Ref. [69], the authors used only the "regularized part" of the first order perturbations as input for the second order or $\mathcal{O}(\epsilon\omega)$ corrections. In the overdriven case the input into the $\mathcal{O}(\epsilon\omega)$ problem incorporates the evolution equation in a similar way, i.e. the term proportional to $1/\eta_0$ is replaced given the appropriate evolution equation, i.e.

$$A_1 D_n + A_2 F_\tau = \begin{cases} -(\tilde{A}_1 D_n + \tilde{A}_2 F_\tau) & , \ D > 1 \\ 0 & , \ D = 1 \end{cases} \tag{6.4.41}$$

This implies the input into the $\mathcal{O}(\epsilon\omega)$ problem from the $\mathcal{O}(\epsilon)$ is as follows,

$$\hat{\rho}^{(1)}(\lambda) = \begin{cases} -\frac{\gamma-1}{\eta_0}(\tilde{A}_1 D_n + \tilde{A}_2 F_\tau) + A_3(\lambda) D_n + A_4(\lambda) F_\tau, \ D > 1 \\ A_3(\lambda) D_n + A_4(\lambda) F_\tau, \ D = 1 \end{cases} \tag{6.4.42}$$

Similar constructs hold for $\hat{p}^{(1)}$ and $\hat{p}^{(1)}$ for the purposes of calculating the vector $\mathbf{C}_2(\lambda)$ which introduce higher order derivatives in time for $D_n^{(1)}$. Calculating $N_{1,2,3}(\lambda)$ and summing these leads to the second order solutions. As an example, the first component of $\mathbf{C}_2$ has the integral N_1 and one substitutes as follows for $D > 1$,

$$N_1(\lambda) = -\int_0^\lambda \frac{u_0}{r_0}\frac{\partial \rho^{(1)}}{\partial \tau} d\lambda = -\int_0^\lambda \frac{u_0}{r_0}\left(\frac{\partial \hat{\rho}^{(1)}}{\partial \tau} + \rho_0(\lambda)\tilde{\beta}(\lambda)\frac{\partial \lambda^{(1)}}{\partial \tau}\right) d\lambda \tag{6.4.43}$$

which is calculated using (6.4.42),

$$\begin{aligned} N_1(\lambda) = -\int_0^\lambda \frac{u_0}{r_0}\frac{\partial}{\partial \tau}\Bigg(&\frac{\gamma-1}{\eta_0}(A_1 D_n + A_2 F_\tau) + A_3(\lambda) D_n + A_4(\lambda) F_\tau + \\ &\rho_0(\lambda)\tilde{\beta}(D_1(\lambda) D_n + D_2(\lambda) F_\tau)\Bigg) d\lambda \end{aligned} \tag{6.4.44}$$

$$\begin{aligned} = -\int_0^\lambda \frac{u_0}{r_0}\frac{\partial}{\partial \tau}\Big(&-(\tilde{A}_1 D_n + \tilde{A}_2 F_\tau)\Big) d\lambda - \int_0^\lambda \frac{u_0}{r_0}\frac{\partial}{\partial \tau}\Bigg(A_4(\lambda) D_n + \\ &A_3(\lambda) F_\tau + \rho_0(\lambda)\tilde{\beta}(D_1(\lambda) D_n + D_2(\lambda) F_\tau)\Bigg) d\lambda \end{aligned} \tag{6.4.45}$$

Again, for $D = 1$, the first integral above vanishes. Also, there is a need to define $\lambda^{(1)}$ and this is done in the appendix for general D and ν and this process is similarly repeated for N_2 and N_3 (see Section E.1). The relevant evolution equation results from the radiation condition using both relevant order perturbation solutions,

$$-\frac{c_0(1)D}{u_0(1)}\big(u^{(1)}+\omega u^{(2)}\big)+\big(p^{(1)}+\omega p^{(2)}\big)=0. \tag{6.4.46}$$

One can then include the results of calculating the $N_i(\lambda)$ as in (6.4.44) to obtain

$$\begin{aligned}&\frac{\gamma-1}{\eta_0(1)}\bigg[-\frac{c_0(1)D}{u_0(1)}\Big(B_1D_n+B_2F_\tau+\omega\big[\beta_3D_{n\tau}+\beta_4F_{\tau\tau}\big]\Big)+\\&\qquad\Big(C_1D_n+C_2F_\tau+\omega\big[\xi_3D_{n\tau}+\xi_4F_{\tau\tau}\big]\Big)\bigg]=0\end{aligned} \tag{6.4.47}$$

$$\begin{aligned}&\Big(-\frac{c_0(1)D}{u_0(1)}B_1+C_1\Big)D_n+\Big(-\frac{c_0(1)D}{u_0(1)}B_2+C_2\Big)F_\tau+\\&\qquad\omega\Big(-\frac{c_0(1)D}{u_0(1)}\beta_3+\xi_3\Big)D_{n\tau}+\omega\Big(-\frac{c_0(1)D}{u_0(1)}\beta_4+\xi_4\Big)F_{\tau\tau}=0\end{aligned} \tag{6.4.48}$$

where

$$\beta_3=a_2(1)R_1(1)+b_2(1)U_1(1)+c_2(1)P_1(1) \tag{6.4.49}$$

$$\beta_4=a_2(1)R_2(1)+b_2(1)U_2(1)+c_2(1)P_2(1) \tag{6.4.50}$$

$$\xi_3=a_3(1)R_1(1)+b_3(1)U_1(1)+c_3(1)P_1(1) \tag{6.4.51}$$

$$\xi_4=a_3(1)R_2(1)+b_3(1)U_2(1)+c_3(1)P_2(1) \tag{6.4.52}$$

and $a_2(\lambda)=\mathbf{A}_{2,1}, b_2(\lambda)=\mathbf{A}_{2,2}, c_2(\lambda)=\mathbf{A}_{2,3}$ and $a_3(\lambda)=\mathbf{A}_{3,1}, b_3(\lambda)=\mathbf{A}_{3,2}, c_3(\lambda)=\mathbf{A}_{3,3}$ and these integral functions are given in Section E.1. The approximate evolution equation analysis is complete by setting $\omega=1$. Using that

$$F_\tau=bFD_{n\tau},\ F_{\tau\tau}=b^2D_{n\tau}^2F+bFD_{n\tau\tau}. \tag{6.4.53}$$

This second order ordinary differential equation can be made into a first order system by holding that $u=D_n$ and $v=D_{n\tau}$:

$$\begin{aligned}&\frac{d}{d\tau}\big(u\big)=v\\&\frac{d}{d\tau}\big(v\big)=-\frac{1}{\alpha_4b_FF}\big(\alpha_1u+\alpha_3v+\alpha_2b_FFv+\alpha_4b_F^2Fv^2\big)\end{aligned} \tag{6.4.54}$$

where

$$\alpha_1 = -\frac{c_0(1)D}{u_0(1)}B_1 + C_1,\ \alpha_2 = -\frac{c_0(1)D}{u_0(1)}B_2 + C_2 \tag{6.4.55}$$

$$\alpha_3 = -\frac{c_0(1)D}{u_0(1)}\beta_3 + \xi_3,\ \alpha_4 = -\frac{c_0(1)D}{u_0(1)}\beta_4 + \xi_4. \tag{6.4.56}$$

6.5 Numerical results for the evolution equations

The evolution equation (6.4.54) is integrated presented according to $D_n = 0$ and $D_{n\tau} = 0.01$ at $\tau = 0$. Again, the formulation here allows one to use different values of ν,k, and D. For the cases presented in the following $Q = 4.0$ and $\gamma = 1.4$.

6.5.1 Chapman-Jouguet and $\nu > 1/2$

The evolution equation obtained with help of the radiation condition reproduces the dynamics found in the CJ case (Fig. 6.3) that was found through a regularity condition in [71] at the end of the reaction zone but the two approaches are exactly equivalent. One can then test the basic intuition obtained in [71] via the numerical simulation, i.e. that longer reaction zones (in relation to the induction zone) tend to attenuate the detonation instability. Since higher ν tends to increase the reaction zone length, one expects that the stability boundary between stable and unstable cases will increase. This is confirmed in Fig. 6.5 where the instability threshold in k and ν is plotted and the stable region is increased as ν increases.

Figs. 6.6 and 6.7 show the evolution of D_n in time. Fig. 6.6 shows the dampening effect on the solution in time of a modest increase in ν, i.e. from $\nu = 0.5$ to $\nu = 0.55$ for set values of k. In Fig. 6.7, one sees that relatively high values of k are needed in order to transition into instability with respect to the $\nu = 0.5$ case treated previously.

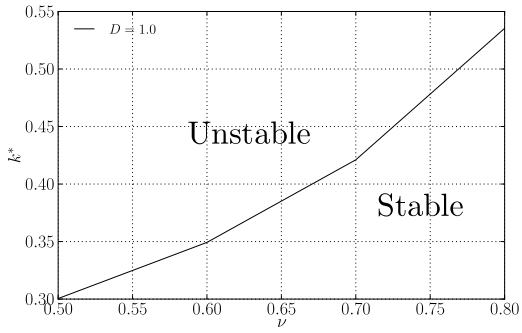

FIGURE 6.5. Stability boundary as a function of ν. The threshold k^* increases which signals that the stable zone increases for higher ν.

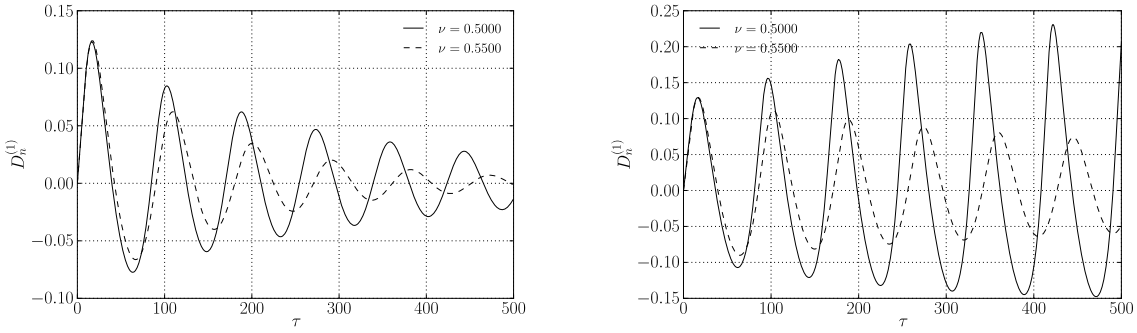

(a) (b)

FIGURE 6.6. Shows effect of increasing ν from 0.5 to 0.55 for different values of k. (a) For $k = 0.2777$, the decay rate is increased as ν increases modestly. (b) For $k = 0.3125$, an unstable case for $\nu = 0.5$ transitions to a stable one for $\nu = 0.55$.

6.5.2 Overdriven detonation

The effect of the overdrive parameter $D = \bar{D}/\bar{D}_{CJ}$ on the evolution of the system is destabilizing i.e. the threshold in k for instability is lowered. This is shown in Fig. 6.8 for various reaction orders. Increasing the overdrive of the underlying detonation flow has a shortening and lengthening effect on the reaction zone but for moderate values of D the effect is to shorten the reaction zone length. This is shown in Fig. 6.9. For a specific D, increases in ν invariably cause an increase in the length of the reaction zone (See Fig. 6.9). The hypothesis that decreasing the length of the

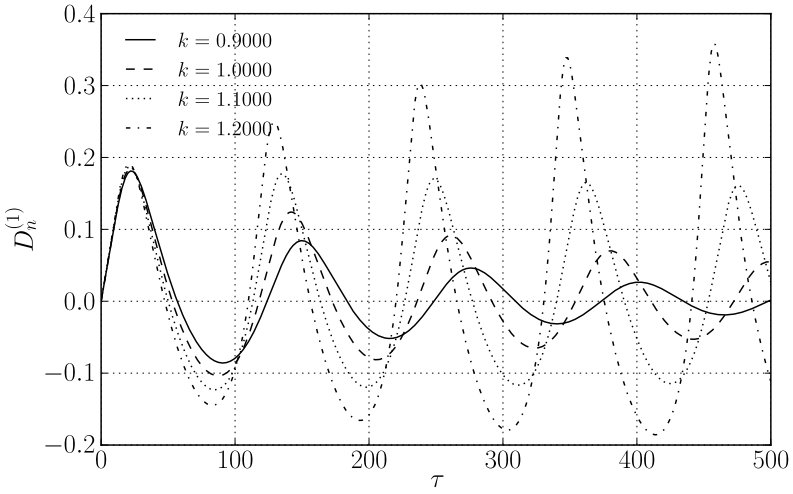

FIGURE 6.7. The effect of increasing the reaction order to $\nu = 1$ in the solution obtained for $D_n(\tau)$ for various values of k.

reaction zone causes a destabilizing effect seems to explain the results for increasing D at least for moderate overdrive, i.e. $D < 2$. The linearized growth rate and frequency of the perturbation is plotted in Fig. 6.10 and it shows that higher overdrive tends to increase the frequency of the perturbations. In Fig. 6.11, the evolution for $D_n^{(1)}$ is shown for various degrees of overdrive, rate constant and reaction order.

6.6 Conclusion

For CJ detonation, the generalized evolution equation results show that increasing reaction order ν does indeed have a stabilizing effect as shown by the complete numerical studies performed in [71]. The reaction zone length increases with ν so this tends to support the idea that increasing the reaction zone length in relation to the induction zone does stabilize the detonation.

For overdriven detonation, the evolution equation derived here was based on the radiation condition rather than a simple regularity condition as in CJ detonation. The results show that increasing D actually increases the instability. For a set reaction

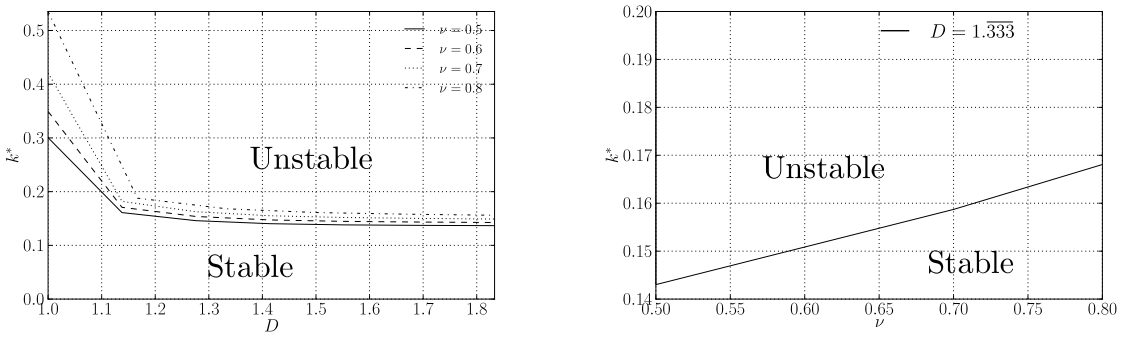

FIGURE 6.8. (a) The effect of increased overdrive turns the detonation for unstable as shown via the lowering of the threshold k^*. (b) The threshold value k^* versus ν for $D = 1.\overline{333}$. Increasing reaction order is stabilizing for overdriven detonation in addition to the CJ case.

order increases in D cause an increase in both growth rate and frequency of the perturbations Fig. 6.10. As the overdrive increases, the frequency of the perturbation increases as well and therefore this is at odds with the explicit slow-time evolution assumption. Furthermore, it is expected that high overdrive eventually must stabilize the detonation [23]. A more detailed asymptotic procedure is necessary to obtain reliable results for high overdrive.

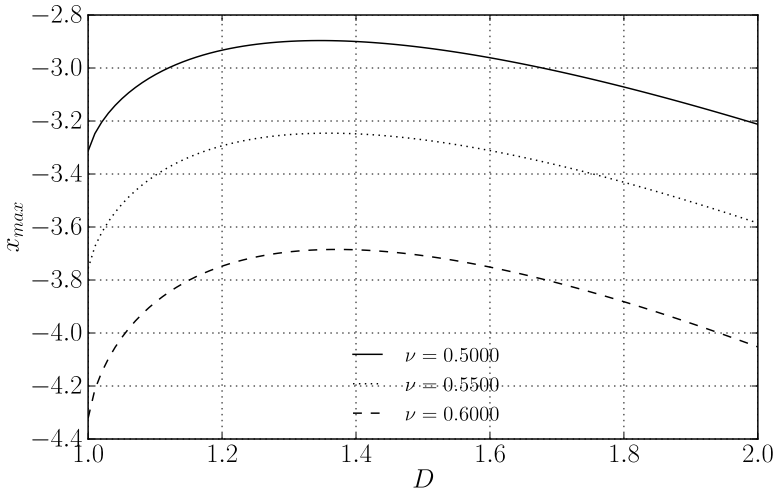

FIGURE 6.9. The effect of increasing D on the extent of the reaction zone. The reaction zone length is greater than the CJ value for moderate overdrive.

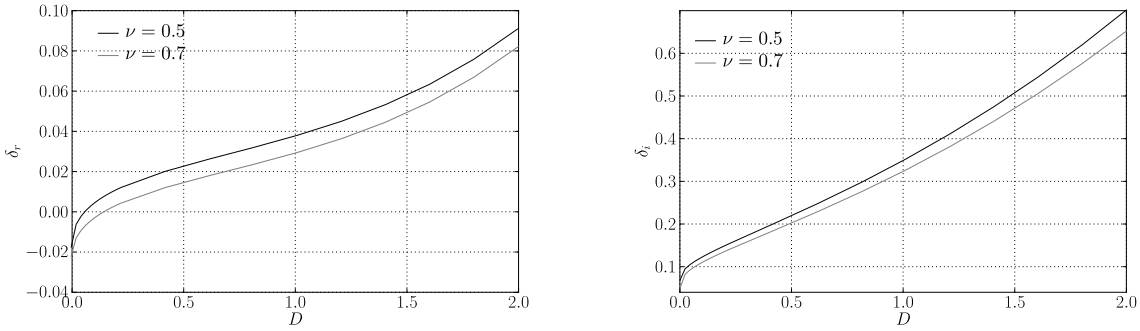

FIGURE 6.10. The variation of the linearized eigenvalue δ for (left) real and (right) imaginary part. Note that as D increases, both growth rate and frequency of oscillations increase. In this case $k = 0.2$ was used.

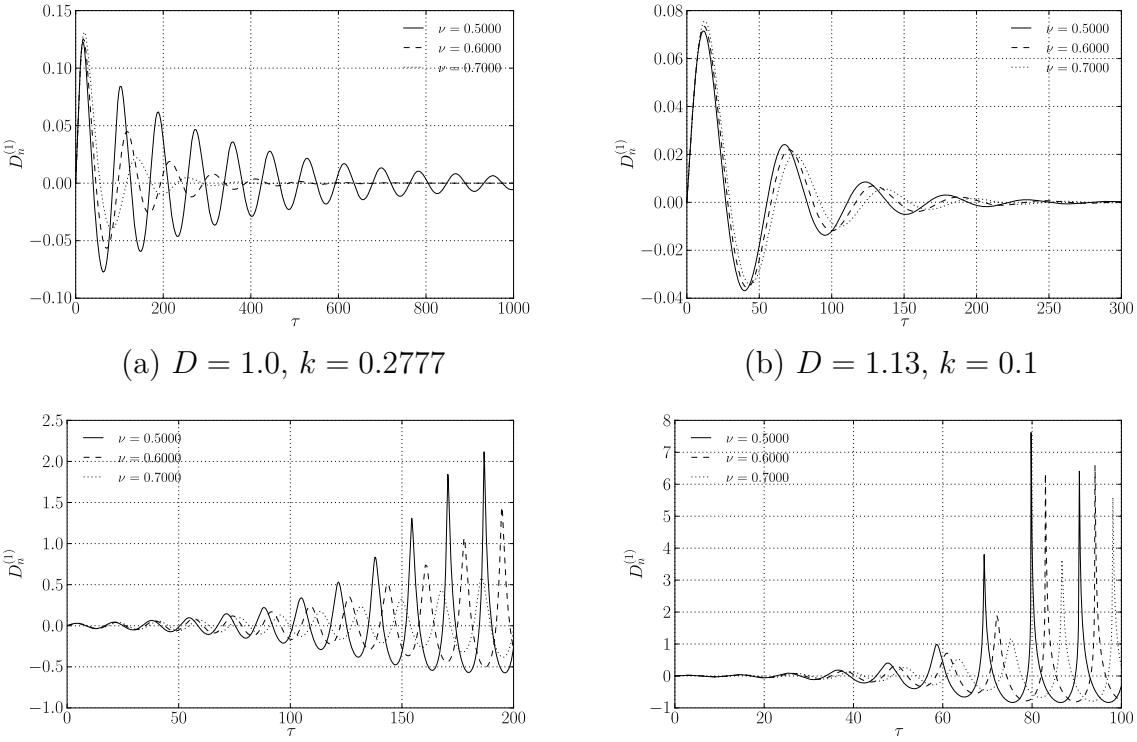

(a) $D = 1.0$, $k = 0.2777$

(b) $D = 1.13$, $k = 0.1$

(c) $D = 1.55$, $k = 0.2$

(d) $D = 1.68$, $k = 0.3$

FIGURE 6.11. Comparison of D_n evolution for various values of ν, k and D. The figures show dampening effect of increasing reaction order for CJ detonation and increasing overdrive as well the stable limit cycles that result.

Chapter 7
Conclusion

The initial value problem approach for 3D perturbations was revisited for an idealized overdriven detonation and the receptivity analysis is completed for this configuration. Several examples of the receptivity analysis were carried out and the three-dimensional nature of the excited unstable modes is confirmed. Additionally, the IVP approach is extended to the special CJ case which leads to a similar solution structure to the overdriven case as well.

A multi-domain spectral collocation method is also used to solve the stability problem for 3D perturbations for a detonation having a generalized condensed phase reaction kinetic model. The method allows for the computation of the eigenspectrum in one calculation and without the need for initial guesses. The method is efficient for 3D perturbations in CJ detonation for the modeled condensed phase explosives. The linear stability analysis is also extended to the case of a detonation propagating in a circular pipe having slightly porous walls. The porous walls are modeled through the use of an acoustic boundary condition and the growth rate and frequency of the unstable modes are dampened with respect to the solid or impenetrable wall case.

Finally, a non-linear evolution equation is obtained through an asymptotic procedure for a detonation having a two-step reaction rate kinetic model. The length ratio between the initial temperature sensitive zone and the longer main reaction layer serves a predictor for the asymptotic stability of the detonation. This is encapsulated in the threshold value between instability in the scaled second reaction rate constant parameter. The result of the evolution reproduces the 1D pulsating dynamics observed in the full numerical simulations of the model. Higher reaction order tends to stabilize and higher overdrive tends to destabilize the slow time pulsating dynamics.

Appendix A
Receptivity of 3D perturbations supplement

A.1 Matrices and vectors

A.1.1 Vectors and matrices in Eq. (2.2.15)

$$\mathbf{A}_1 = \begin{pmatrix} u_1^* & -v^* & 0 & 0 & 0 & 0 \\ 0 & u_1^* & 0 & 0 & v^*/\gamma & 0 \\ 0 & 0 & u_1^* & 0 & 0 & 0 \\ 0 & 0 & 0 & u_1^* & 0 & 0 \\ 0 & \gamma p^* & 0 & 0 & u_1^* & 0 \\ 0 & 0 & 0 & 0 & 0 & u_1^* \end{pmatrix}$$

$$\mathbf{A}_2 = \begin{pmatrix} 0 & 0 & -v^* & 0 & 0 & 0 \\ 0 & 0 & 0 & 0 & 0 & 0 \\ 0 & 0 & 0 & 0 & v^*/\gamma & 0 \\ 0 & 0 & 0 & 0 & 0 & 0 \\ 0 & 0 & \gamma p^* & 0 & 0 & 0 \\ 0 & 0 & 0 & 0 & 0 & 0 \end{pmatrix}, \quad \mathbf{A}_3 = \begin{pmatrix} 0 & 0 & 0 & -v^* & 0 & 0 \\ 0 & 0 & 0 & 0 & 0 & 0 \\ 0 & 0 & 0 & 0 & 0 & 0 \\ 0 & 0 & 0 & 0 & v^*/\gamma & 0 \\ 0 & 0 & 0 & \gamma p^* & 0 & 0 \\ 0 & 0 & 0 & 0 & 0 & 0 \end{pmatrix}$$

$$\mathbf{C} = \begin{pmatrix} -\partial u^*/\partial x_1 & \partial v^*/\partial x_1 & 0 & 0 & 0 & 0 \\ \frac{1}{\gamma}\partial p^*/\partial x_1 & \partial u^*/\partial x_1 & 0 & 0 & 0 & 0 \\ 0 & 0 & 0 & 0 & 0 & 0 \\ 0 & 0 & 0 & 0 & 0 & 0 \\ \kappa\left(r^*/v^* - \partial r^*/\partial v^*\right) & \partial p^*/\partial x_1 & 0 & 0 & \gamma\partial u^*/\partial x_1 - \kappa\partial r^*/\partial p^* & -\kappa\partial r^*/\partial\lambda^* \\ -\partial r^*/\partial v^* & \partial\lambda^*/\partial x_1 & 0 & 0 & \partial r^*/\partial p^* & -\partial r^*/\partial\lambda^* \end{pmatrix}$$

where $\kappa = \beta(\gamma - 1)/v^*$.

$$\mathbf{g}_t = \begin{pmatrix} \partial v^*/\partial x_1 \\ \partial u^*/\partial x_1 \\ 0 \\ 0 \\ \partial p^*/\partial x_1 \\ \partial\lambda^*/\partial x_1 \end{pmatrix}, \quad \mathbf{g}_2 = \begin{pmatrix} 0 \\ 0 \\ \frac{v^*}{\gamma}\partial p^*/\partial x_1 \\ 0 \\ 0 \\ 0 \end{pmatrix}, \quad \mathbf{g}_3 = \begin{pmatrix} 0 \\ 0 \\ 0 \\ \frac{v^*}{\gamma}\partial p^*/\partial x_1 \\ 0 \\ 0 \end{pmatrix}$$

A.1.2 Vectors and matrices in Eq. (2.4.7)

$$Y = \begin{pmatrix} \frac{4}{D^2(\gamma+1)} + \frac{\gamma-1}{\gamma+1} & -\frac{4}{D^2(\gamma+1)M_s} & 0 & 0 & \frac{2}{M_s^2(\gamma+1)} & 0 \\ \frac{2M_s}{D^2(\gamma+1)} & -\frac{2}{D^2(\gamma+1)} + \frac{\gamma-1}{\gamma+1} & 0 & 0 & \frac{2}{(\gamma+1)M_s} & 0 \\ 0 & 0 & 1 & 0 & 0 & 0 \\ 0 & 0 & 0 & 1 & 0 & 0 \\ -\frac{2\varphi M_s^2}{(\gamma+1)} & \frac{4\gamma M_s}{(\gamma+1)} & 0 & 0 & -\frac{\gamma-1}{\gamma+1} & 0 \\ 0 & 0 & 0 & 0 & 0 & 1 \end{pmatrix}$$

$$\mathbf{h}_t = \begin{pmatrix} \frac{4}{(\gamma+1)D^2M_s} \\ \frac{2\left(D^2+1\right)}{(\gamma+1)D^2} \\ 0 \\ 0 \\ -\frac{4\gamma M_s}{(\gamma+1)} \\ 0 \end{pmatrix}, \ \mathbf{h}_2 = \begin{pmatrix} 0 \\ 0 \\ D_s - M_s \\ 0 \\ 0 \\ 0 \end{pmatrix}, \ \mathbf{h}_3 = \begin{pmatrix} 0 \\ 0 \\ 0 \\ D_s - M_s \\ 0 \\ 0 \end{pmatrix}$$

A.2 The discrete spectrum

In this section, it will be demonstrated that the discrete spectrum stemming from Erpenbeck's approach (2.4.16) is equivalent to the unstable modes obtained via the conventional normal-mode approach. Via the assumptions outlined previously, this latter approach can be formulated in the shock-attached coordinate system as the following inhomogeneous system of ordinary differential equations:

$$\mathbf{A}_1 \frac{d\zeta}{dx_1} + \left(i\alpha\mathbf{A}_2 + i\beta\mathbf{A}_3 + \mathbf{C} + \tau\mathbf{I}\right)\zeta = \left(\tau\mathbf{g}_t + i\alpha\mathbf{g}_2 + i\beta\mathbf{g}_3\right) \tag{A.2.1}$$

with initial conditions at the shock

$$\zeta\left(0\right) = \left(\tau\mathbf{h}_t + i\alpha\mathbf{h}_2 + i\beta\mathbf{h}_3\right). \tag{A.2.2}$$

One has to have a constraint at $x_1 \to \infty$ defining a bounded solution of Eq. (A.2.1) in order to complete formulation of the eigenvalue problem. One can utilize the following

transformation for components of vector ζ

$$\begin{aligned}
\zeta_1 &= z_{MS1} \\
\zeta_2 &= z_{MS2} \\
\alpha\zeta_3 + \beta\zeta_4 &= k z_{MS3} \\
\zeta_5 &= z_{MS4} \\
\zeta_6 &= z_{MS5} \\
k &= \sqrt{\alpha^2 + \beta^2}
\end{aligned} \tag{A.2.3}$$

and reduce the system of equations (A.2.1) to the system of five ordinary differential equations considered in normal mode studies Refs. [25] and [26]:

$$\frac{d\mathbf{z}_{MS}}{dx_1} + \mathbf{A}_{1MS}^{-1}\left(ik\mathbf{B}_{MS} + \mathbf{C}_{MS} + \tau\mathbf{I}\right)\mathbf{z}_{MS} = \mathbf{A}_{1MS}^{-1}\left(\tau + ik\mathbf{B}_{MS}\right)\mathbf{z}_x^*. \tag{A.2.4}$$

One can find the 5×5 matrices and vector $\mathbf{z}_x^*$ as follows:

$$\mathbf{A}_{1MS} = \begin{pmatrix} u_1^* & -v^* & 0 & 0 & 0 \\ 0 & u_1^* & 0 & v^*/\gamma & 0 \\ 0 & 0 & u_1^* & 0 & 0 \\ 0 & \gamma p^* & 0 & u_1^* & 0 \\ 0 & 0 & 0 & 0 & u_1^* \end{pmatrix}$$

$$\mathbf{B}_{MS} = \begin{pmatrix} 0 & 0 & -v^* & 0 & 0 \\ 0 & 0 & 0 & 0 & 0 \\ 0 & 0 & 0 & v^*/\gamma & 0 \\ 0 & 0 & \gamma p^* & 0 & 0 \\ 0 & 0 & 0 & 0 & 0 \end{pmatrix}$$

$$\mathbf{C}_{MS} = \begin{pmatrix} -\partial u^*/\partial x_1 & \partial v^*/\partial x_1 & 0 & 0 & 0 \\ \frac{1}{\gamma}\partial p^*/\partial x_1 & \partial u^*/\partial x_1 & 0 & 0 & 0 \\ 0 & 0 & 0 & 0 & 0 \\ \kappa\left(r^*/v^* - \partial r^*/\partial v^*\right) & \partial p^*/\partial x_1 & 0 & \gamma\partial u^*/\partial x_1 - \kappa\partial r^*/\partial p^* & -\kappa\partial r^*/\partial\lambda^* \\ -\partial r^*/\partial v^* & \partial\lambda^*/\partial x_1 & 0 & \partial r^*/\partial p^* & -\partial r^*/\partial\lambda^* \end{pmatrix}$$

$$\mathbf{z}_x^* = \begin{pmatrix} \partial v^*/\partial x_1 \\ \partial u^*/\partial x_1 \\ 0 \\ \partial p^*/\partial x_1 \\ \partial\lambda^*/\partial x_1 \end{pmatrix}$$

The perturbation shock conditions are recast as follows:

$$\mathbf{z}_{MS}(0)=\left[\frac{4\tau}{(\gamma+1)D^2M_s},\frac{2(D^2+1)\tau}{(\gamma+1)D^2},ik(D_s-M_s),-\frac{4\gamma M_s}{(\gamma+1)},0\right]^T \tag{A.2.5}$$

Similarly, one can use transformation of dependent variables for the adjoint system (2.4.12)

$$\begin{aligned} y_1&=y_{MS1}\\ y_2&=y_{MS2}\\ \alpha y_3+\beta y_4&=ky_{MS3}\\ y_5&=y_{MS4}\\ y_6&=y_{MS5} \end{aligned} \tag{A.2.6}$$

and to recast it as

$$\frac{d\mathbf{y}_{MS}}{dx_1}-\left\{\mathbf{A}_{1MS}^{-1}\left(ik\mathbf{B}_{MS}+\mathbf{C}_{MS}+\tau\mathbf{I}\right)\right\}^T\mathbf{y}_{MS}=0 \tag{A.2.7}$$

One can find the asymptotics of fundamental solutions of Eq. (A.2.7) at $x_1\to\infty$ as

$$\mathbf{y}_{MSj}(x_1)=\mathbf{y}_{MSj\infty}\exp(-\mu_j x_1) \tag{A.2.8}$$

The interest here lies only in the bounded fundamental solution $\mathbf{y}_{MS1}(x_1)$. For this fundamental solution, it is found that

$$\mathbf{y}_{MS1\infty}=\begin{pmatrix} 0\\ \tau\\ -iku_\infty^*\\ -\frac{v_\infty^*}{\gamma c_\infty}\sqrt{\tau^2+c_\infty^2(1-M_\infty^2)k^2}\\ \frac{C_{56}u_\infty^*v_\infty^*\left[\tau^2-u_\infty^{*2}k^2\right]}{\gamma\left[u_\infty^{*2}c_\infty^2k^2-\tau c_\infty^2C_{66}-\tau^2c_\infty^2+C_{66}u_\infty^*c_\infty\sqrt{\tau^2+c_\infty^2(1-M_\infty^2)k^2}\right]} \end{pmatrix} \tag{A.2.9}$$

In order to prove equivalence of the discrete spectrum stemming from Eq. (2.4.16) and the spectrum in the normal-mode approach, the dot product of Eq. (A.2.4) and $\mathbf{y}_{MS1}(x_1)$ is considered and integrated with respect to x_1. Using integration by parts and that $\mathbf{y}_{MS1}(x_1)$ satisfies Eq. (A.2.7), one arrives at

$$\mathbf{z}_{MS}(0)\cdot\mathbf{y}_{MS1}(0)+\int_0^\infty\left[\mathbf{A}_{1MS}^{-1}\left(\tau+ik\mathbf{B}_{MS}\right)\mathbf{z}_x^*\right]\cdot\mathbf{y}_{MS1}(x_1)\,dx_1=0 \tag{A.2.10}$$

Using the shock conditions, Eq. (A.2.5), and transformations (A.2.3) and (A.2.6), it is concluded that Eq. (A.2.10) is equivalent to Eq. (2.4.16).

A.3 Receptivity to incoming quiescent gas perturbations

The case of incoming perturbations from the quiescent gas is treated in this section. In particular one supposes that there is an isobaric density perturbation in the quiescent gas in front of the shock. This variation is proportional to $\sin(kx^l)$, and therefore in the shock frame this transforms to a periodic in time disturbance of the form $\sin(\omega t)$ with frequency $\omega = kD_s$ which in the transformed system can be written as

$$\overline{\mathbf{z}}(0_-, \tau) = \frac{\omega}{\omega^2 + \tau^2} \begin{pmatrix} 1 \\ 0 \\ 0 \\ 0 \\ 0 \\ 0 \end{pmatrix} \delta(\alpha)\delta(\beta)$$

Therefore this induces a particular amplitude for the receptivity coefficient (2.4.18) for the discrete modes indexed by k i.e.,

$$R_k = -\frac{(\mathbf{y}_1(0), \mathbf{Y}\overline{\mathbf{z}}(0_-, \tau))|_{\tau_k}}{\partial V/\partial\tau|_{\tau_k}}$$

where any pre-existing initial perturbations behind the shock in either burnt or reaction zone are negligible, i.e. $\mathbf{F}_1 = 0$. The dot product in the receptivity coefficient can be rewritten

$$R_k = -\frac{\omega}{\omega^2 + \tau_k^2} \frac{(\mathbf{y}_1(0), \mathbf{Y}_1)|_{\tau_k}}{\partial V/\partial\tau|_{\tau_k}}$$

where $\mathbf{Y}_1$ denotes the entire first column of the matrix $\mathbf{Y}$ given in Appendix B. The solution (in α and β space) has therefore contribution from both discrete and continuous spectra,

$$\hat{\mathbf{z}}(x_1, \alpha, \beta, t) = \sum_k R_k \hat{\mathbf{z}}_{dmk} e^{\tau_k t} + \frac{1}{2\pi i} \int_{-i\infty}^{i\infty} \overline{\mathbf{z}}(x_1, \alpha, \beta, \tau) e^{\tau t} d\tau$$

One can see that if τ_j is close to the imaginary axis then $\omega/(\omega^2+\tau_j^2)$ might become large and lead to resonance if in addition ω is close to the imaginary part of τ_j.

However, physically it is expected that the solution will compensate for this resonance in some form. This resonance phenomena must also has an effect on the continuous spectrum (the remaining portion of the solution). The vector $\overline{\mathbf{z}}$ is rewritten in the following way,

$$\overline{\mathbf{z}}(x_1,\alpha,\beta,\tau) = -\frac{\omega}{\omega^2+\tau^2}\frac{(\mathbf{y}_1(0,\tau),\mathbf{Y}_1)}{V(\tau)}\mathbf{z}'(x_1,\alpha,\beta,\tau).$$

where

$$\mathbf{z}' = \left(\int_{\infty}^{x_1}(\mathbf{y}_1,\mathbf{F}_2)dx_1\right)\overline{\mathbf{z}}_1 + \sum_{k=2}^{6}\left(\int_0^{x_1}(\mathbf{y}_k,\mathbf{F}_2)dx_1 - c_k\right)\overline{\mathbf{z}}_k$$

and

$$c_k = V(\tau)\frac{(\mathbf{y}_k(0,\tau),\mathbf{Y}_1)}{(\mathbf{y}_1(0,\tau),\mathbf{Y}_1)} + (\mathbf{y}_k(0,\tau),\mathbf{q})$$

The contribution from the continuous spectrum (CS) can be written in the following way:

$$CS = -\frac{1}{2\pi i}\int_{-i\infty}^{i\infty}\frac{e^{\tau t}\omega}{\omega^2+\tau^2}\frac{(\mathbf{y}_1(0,\tau),\mathbf{Y}_1(0))}{V(\tau)}\mathbf{z}'(x_1,\tau)d\tau$$

It will be shown that at leading order the continuous spectrum provides (through Taylor expansions) a contribution that balances the unstable mode.

The unstable modes are symmetric about the real axis so the focus is on the upper half of the imaginary axis integral (CS_+) for now. One deforms the path around the pole at $\tau = i\omega$ with a half circle of radius ϵ that maintains $\mathrm{Re}(\tau) > 0$. Requiring that $\mathrm{Re}(\tau) > 0$ is crucial to maintain the principle of causality as shown in Ref. [32]. In the limiting procedure as $\epsilon \to 0$,

$$CS_+ = -\frac{1}{2\pi i}\lim_{\epsilon\to 0}\left(\int_{C_\epsilon+i\omega}(\dots)d\tau + \int_{i\omega+i\epsilon}^{i\infty}(\dots)d\tau + \int_0^{i\omega-i\epsilon}(\dots)d\tau\right)$$

The first integral over the half circle of radius ϵ keeping the real part of τ positive gives half of the residue due to the pole at $\tau = i\omega$. This residue is evaluated in the

usual way as

$$-\lim_{\epsilon\to 0}\frac{1}{2\pi i}\left(\int_{C_\epsilon+i\omega}(\dots)d\tau\right) = -\frac{1}{2}\lim_{\tau\to i\omega}\left(\frac{(\tau-i\omega)\omega}{\omega^2+\tau^2}\frac{(\mathbf{y}_1(0,\tau),\mathbf{Y}_1)}{V(\tau)}\mathbf{z}'(x_1,\tau)e^{\tau t}\right)$$
$$= -\frac{1}{2}\lim_{\tau\to i\omega}\left(\frac{\omega}{\tau+i\omega}\frac{(\mathbf{y}_1(0,\tau),\mathbf{Y}_1)}{V(\tau)}\mathbf{z}'(x_1,\tau)e^{\tau t}\right)$$

Given that $i\omega$ will be close to the eigenvalue τ_j, then the limit point can be written $\tau \to i\omega = \tau_j + \delta$, with $\delta = i\omega - \tau_j$ small in magnitude. It is obtained that

$$-\lim_{\epsilon\to 0}\frac{1}{2\pi i}\left(\int_{C_\epsilon+i\omega}(\dots)d\tau\right) =$$
$$-\frac{1}{2}\left(\frac{\omega}{\tau_j+i\omega+\delta}\frac{(\mathbf{y}_1(0,\tau_j+\delta),\mathbf{Y}_1)}{V(\tau_j+\delta)}\mathbf{z}'(x_1,\tau_j+\delta)e^{(\tau_j+\delta)t}\right)$$

The resulting function above is regular, so it can be expanded in Taylor series around τ_j:

$$-\lim_{\epsilon\to 0}\frac{1}{2\pi i}\left(\int_{C_\epsilon+i\omega}(\dots)d\tau\right) = \frac{1}{2}\left(\frac{\omega}{\tau_j^2+\omega^2}\frac{(\mathbf{y}_1(0,\tau_j),\mathbf{Y}_1)}{\partial V/\partial\tau|_{\tau_j}}\mathbf{z}'(x_1,\tau_j)e^{(\tau_j)t}\right)+O(\delta)$$

where $V(\tau_j+\delta) = V(\tau_j) + \partial V/\partial\tau|_{\tau_j}\delta + \cdots = \partial V/\partial\tau|_{\tau_j}\delta + \dots$ since $V(\tau_j) = 0$ and also $(\tau_j+i\omega)\delta = (\tau_j+i\omega)(i\omega-\tau_j) = -(\tau_j^2+\omega^2)$. Examining $\mathbf{z}'(x_1,\tau_j)$ closely it is seen that it is exactly equal to $\hat{\mathbf{z}}_{dmj}(x_1,\tau_j)$ since the first term in the coefficient c_k is identically zero at τ_j. To leading order then, the contribution from the pole on the imaginary axis is negative one half the contribution from the discrete mode associated with τ_j.

Physically one expects that the contribution from the unstable discrete mode above can be balanced further. Recall the form of the remaining integral over the imaginary axis, and consider the new parameter $A > 0$ to split this integral in the following way:

$$\int_{i\omega+i\epsilon}^{i\infty}(\dots)d\tau + \int_0^{i\omega-i\epsilon}(\dots)d\tau = \int_{i\omega+iA}^{i\infty} + \int_0^{i\omega-iA} + \int_{i\omega+i\epsilon}^{i\omega+iA} + \int_{i\omega-iA}^{i\omega-i\epsilon} \tag{A.1}$$

Only the second two integrals on the right-hand side depend on ϵ. Closing of the path of those two integrals is shown in Figure A.1. Introducing the change of variable

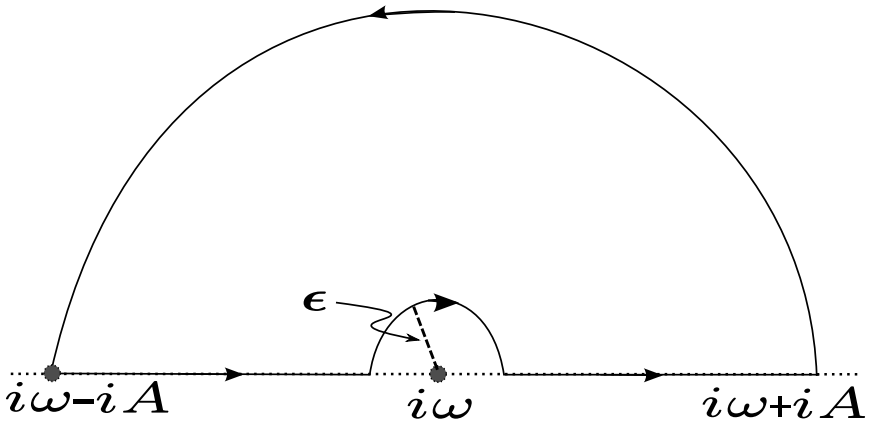

FIGURE A.1. The scheme for closing the integral in (A.1).

$\tau = i\omega + iu$ produces the following:

$$\int_{i\omega+i\epsilon}^{i\omega+iA} + \int_{i\omega-iA}^{i\omega-i\epsilon} = \left(\int_{-A}^{-\epsilon} \frac{e^{iut}}{u}\mathbf{f}(u)du + \int_{\epsilon}^{A} \frac{e^{iut}}{u}\mathbf{f}(u)du \right)$$

where

$$\mathbf{f}(u) = \frac{\omega e^{i\omega t}(\mathbf{y}_1(0, iu + i\omega), \mathbf{Y}_1)}{(iu + 2i\omega)V(iu + i\omega)}\mathbf{z}'(x_1, iu + i\omega)$$

Now imagine that A is sufficiently small such that the vector function $\mathbf{f}(u)$ is well approximated by its Taylor series about $u = 0$ such that $\mathbf{f}(\mathbf{u}) = \mathbf{f}(0) + O(A)$, then to leading order,

$$\int_{i\omega+iA}^{i\omega+i\epsilon} + \int_{i\omega-i\epsilon}^{i\omega-iA} \approx \mathbf{f}(0)\left(\int_{-A}^{-\epsilon} \frac{e^{iut}}{u}du + \int_{\epsilon}^{A} \frac{e^{iut}}{u}du \right)$$

Using the contour shown in Figure A.1:

$$\int_{-A}^{-\epsilon} \frac{e^{iut}}{u}du + \int_{\epsilon}^{A} \frac{e^{iut}}{u}du = -\int_{C_\epsilon} \frac{e^{iut}}{u}du - \int_{C_A} \frac{e^{iut}}{u}du$$

the inner half-circle integral is evaluated in the limit as $\epsilon \to 0$ so one obtains half the negative residue since the path is traversed clockwise. Therefore,

$$\lim_{\epsilon\to 0} \int_{C_\epsilon} \frac{e^{iut}}{u}du = -\pi i \text{Sign}(t)$$

Next the contribution from the integral over C_A is bounded. Firstly one rescales $u = z/t$, so that $At = R$ and thus replace $z = R\exp(i\theta)$,

$$\int_{C_A} \frac{e^{iut}}{u} du = \int_{C_R} \frac{e^{iz}}{z} dz = i \int_0^{\pi} e^{-R\sin\theta} e^{iR\cos\theta} d\theta.$$

Taking the magnitude of this integral and using the symmetry about $\theta = \pi/2$,

$$\left| \int_{C_A} \right| \leq \int_0^{\pi} e^{-R\sin\theta} d\theta = 2\int_0^{\pi/2} e^{-R\sin\theta} d\theta.$$

Changing variables once again $w = \sin\theta$ and integrating by parts,

$$\begin{aligned} 2\int_0^1 \frac{e^{-Rw}}{\sqrt{1-w^2}} dw &= 2\big(e^{-Rw}\sin^{-1}(w)\big)|_0^1 + 2R\int_0^1 e^{-Rw}\sin^{-1}(w) dw \\ &\leq \pi e^{-R} + \pi R \int_0^1 w e^{-Rw} dw \\ &= \pi e^{-R} + \pi R\bigg(-\frac{e^{-R}}{R} - \frac{e^{-R}}{R^2} + \frac{1}{R^2}\bigg) = \frac{\pi}{R}(1 - e^{-R}) \approx \frac{\pi}{R}. \end{aligned}$$

Therefore to leading order the contribution from this small section of the integral across the imaginary axis of τ gives,

$$\begin{aligned} -\frac{1}{2\pi i}\lim_{\epsilon\to 0}\int_{i\omega+i\epsilon}^{i\omega+iA} + \int_{i\omega-iA}^{i\omega-i\epsilon} \approx -\frac{1}{2}\lim_{\tau\to i\omega} \mathbf{f}(\tau - i\omega) = \\ -\frac{1}{2}\lim_{\tau\to i\omega} \frac{\omega e^{\tau t}(\mathbf{y}_1(0,\tau), \mathbf{Y}_1)\mathbf{z}'(x_1,\tau)}{(\tau + i\omega)V(\tau)} \end{aligned}$$

As in the previous case we write that in the limit $\tau \to i\omega = \tau_j + \delta$ using that $|\delta| \ll 1$ to obtain at leading order:

$$-\frac{1}{2\pi i}\lim_{\epsilon\to 0}\int_{i\omega+iA}^{i\omega+i\epsilon} + \int_{i\omega-i\epsilon}^{i\omega-iA} \approx \frac{1}{2}\bigg(\frac{\omega}{\tau_j^2+\omega^2}\frac{(\mathbf{y}_1(0,\tau_j), \mathbf{Y}_1)}{(\tau_j)\partial V/\partial\tau|_{\tau_j}}\mathbf{z}'(x_1,\tau_j)e^{(\tau_j)t}\bigg)$$

In total we can write the contribution from the upper half of the continuous spectrum as

$$\begin{aligned} CS_+ = &\left(\frac{\omega}{\tau_j^2+\omega^2}\frac{(\mathbf{y}_1(0,\tau_j), \mathbf{Y}_1)}{(\tau_j)\partial V/\partial\tau|_{\tau_j}}\mathbf{z}'(x_1,\tau_j)e^{(\tau_j)t}\right) + O(A) + O(1/(At)) + O(\delta) \\ &- \left(\frac{1}{2\pi i}\int_{i\omega+iA}^{i\infty}(\dots)d\tau + \int_0^{i\omega-iA}(\dots)d\tau\right) \end{aligned}$$

At leading order, the contribution from the continuous spectrum integral balances the contribution from the unstable mode that is resonant with the incoming perturbation of prescribed frequency ω. However, there are two competing temporal processes at play. In order to balance the unstable mode, time must be large to produce the approximation above to leading order due to the $O(1/At)$ term. Related to this, there is growth in the resonant unstable mode as t grows which will cause a growing discrepancy between the continuous spectrum and the unstable mode. However, the growth rate of the unstable mode is itself very small as a requirement to produce the resonance phenomena.

Appendix B
Initial value problem in CJ detonation supplement

B.1 Matrices and vectors

Linearized Euler and reaction equations

In the following, the subscript 0 refers to the steady state solution for the appropriate quantity and the prime represents a derivative in x. The matrix $\mathbf{A}_x$,

$$\mathbf{A}_x = \begin{pmatrix} u_0 & -\dfrac{1}{u_0} & 0 & 0 & 0 \\ 0 & -1 & 0 & 1 & 0 \\ 0 & 0 & -1 & 0 & 0 \\ \dfrac{a_0^2 u_0^2}{\gamma(\gamma-1)} & \dfrac{a_0^2}{\gamma} & 0 & -\dfrac{u_0^2}{\gamma-1} & 0 \\ 0 & 0 & 0 & 0 & u_0 \end{pmatrix}. \tag{B.1.1}$$

The matrix $\mathbf{A}_y$ has very few non-zero components,

$$(\mathbf{A}_y)_{13} = \frac{1}{u_0},\ (\mathbf{A}_y)_{34} = 1,\ \text{and}\ (\mathbf{A}_y)_{43} = a_0^2/\gamma. \tag{B.1.2}$$

The matrix $\mathbf{A}_t$,

$$\mathbf{A}_t = \begin{pmatrix} 1 & 0 & 0 & 0 & 0 \\ 0 & -\dfrac{1}{u_0} & 0 & 1 & 0 \\ 0 & 0 & -\dfrac{1}{u_0} & 0 & 0 \\ \dfrac{a_0^2 u_0}{\gamma(\gamma-1)} & 0 & 0 & -\dfrac{u_0}{\gamma-1} & 0 \\ 0 & 0 & 0 & 0 & 1 \end{pmatrix}. \tag{B.1.3}$$

The matrix $\mathbf{B}$ is not sparse,

$$\mathbf{B} = \begin{pmatrix} u_0' & \frac{u_0'}{u_0^2} & 0 & 0 & 0 \\ u_0 u_0' & -\frac{u_0'}{u_0} & & 0 & 0 \\ 0 & 0 & 0 & 0 & 0 \\ \frac{a_0^2 u_0 u_0'}{\gamma(\gamma-1)} - Q u_0 W_{0\rho} & -\frac{u_0 u_0'}{\gamma-1} + \frac{a_0^2 u_0'}{u_0(\gamma-1)\gamma} & 0 & -\frac{\gamma u_0 u_0'}{\gamma-1} - Q u_0 W_{0p} & -Q u_0 W_{0\lambda} \\ u_0 W_{0\rho} - u_0^2 \lambda_0' & \lambda_0' & & u_0 W_{0p} & u_0 W_{0\lambda} \end{pmatrix} \tag{B.1.4}$$

where the subscript p, λ and ρ refers to the partial derivative with respect to the subscript, i.e. $W_{0\rho} = \partial W_0 / \partial \rho$, and a prime refers to a full derivative in x.

Finally, the relevant vectors are given as follows:

$$\mathbf{s}_t = \left(0, \frac{1}{u_0}, 0, 0, 0\right)^T \tag{B.1.5}$$

and the remaining vector $\mathbf{s}_y$ is

$$\mathbf{s}_y = \left(0, 0, u_0', 0, 0\right)^T. \tag{B.1.6}$$

Linearized Rankine-Hugoniot equations

First the coefficient vectors. There is only one component to $\mathbf{h}_y$,

$$\mathbf{h}_y = \left(0, 0, \frac{2(\gamma P - 1)}{\gamma + 1}, 0, 0\right)^T \tag{B.1.7}$$

The time derivative vector has more non-zero components

$$\mathbf{h}_t^T = \left(\frac{4P\gamma(\gamma+1)}{(2P\gamma+\gamma-1)^2}, \frac{2P\gamma - \gamma + 1}{\gamma+1}, 0, \frac{4}{\gamma+1}, 0\right)^T \tag{B.1.8}$$

and finally the matrix $\mathbf{Y}$,

$$\mathbf{Y} = \begin{pmatrix} \frac{(\gamma+1)(4P\gamma+\gamma-1)}{(2P\gamma+\gamma-1)^2} & -\frac{4P\gamma(\gamma+1)}{(2P\gamma+\gamma-1)^2} & 0 & -\frac{2\gamma(\gamma+1)}{(2P\gamma+\gamma-1)^2} & 0 \\ \frac{2P\gamma}{\gamma+1} & -\frac{2P\gamma-\gamma+1}{\gamma+1} & 0 & -\frac{2\gamma}{\gamma+1} & 0 \\ 0 & 0 & 1 & 0 & 0 \\ \frac{2}{\gamma+1} & -\frac{4}{\gamma+1} & 0 & -\frac{\gamma-1}{\gamma+1} & 0 \\ 0 & 0 & 0 & 0 & 1 \end{pmatrix}. \tag{B.1.9}$$

B.2 Shearing transformation to obtain Eq. (3.3.27)

The modification of the eigenvalues of the leading order matrix in Eq. (3.3.24) comes about due to the properties of the employed transformation $\mathbf{q} = (\mathbf{S}^{-1})^2\mathbf{p}$ given that $\mathbf{S}$ depends on w. Inserting $\mathbf{q} = (\mathbf{S}^{-1})^2\mathbf{p}$ into Eq. (3.3.24) produces

$$w\frac{d}{dw}\big[(\mathbf{S}^{-1})^2\mathbf{p}\big] = (\mathbf{E}_1 + w\mathbf{E}_2 + w^2\mathbf{E}_3 + \dots)(\mathbf{S}^{-1})^2\mathbf{p} \tag{B.2.1}$$

and so the LHS of Eq. (B.2.1) becomes

$$w\frac{d}{dw}\big[(\mathbf{S}^{-1})^2\mathbf{p}\big] = w(\mathbf{S}^{-1})^2\frac{d\mathbf{p}}{dw} + w\frac{d}{dw}\Big[(\mathbf{S}^{-1})^2\Big]\mathbf{p}. \tag{B.2.2}$$

Multiplying both sides by $\mathbf{S}^2$ in Eq. (B.2.1) and solving for $wd\mathbf{p}/dw$, one obtains

$$w\frac{d\mathbf{p}}{dw} = \mathbf{S}^2(\mathbf{E}_1 + w\mathbf{E}_2 + w^2\mathbf{E}_3 + \dots)(\mathbf{S}^{-1})^2\mathbf{p} - w\mathbf{S}^2\frac{d}{dw}\Big[(\mathbf{S}^{-1})^2\Big]\mathbf{p}. \tag{B.2.3}$$

Particularly, the last term in the above equation,

$$\begin{aligned} -w\mathbf{S}^2\frac{d}{dw}\Big[(\mathbf{S}^{-1})^2\Big]\mathbf{p} &= -w\begin{pmatrix} 1 & & & \\ & 1 & & \\ & & 1 & \\ & & & w^2 \end{pmatrix} \times \begin{pmatrix} & & & \\ & & & \\ & & & \\ & & & -2/w^2 \end{pmatrix}\mathbf{p} \\ -w\mathbf{S}^2\frac{d}{dw}\Big[(\mathbf{S}^{-1})^2\Big]\mathbf{p} &= \begin{pmatrix} & & & \\ & & & \\ & & & \\ & & & 2 \end{pmatrix}\mathbf{p}. \end{aligned} \tag{B.2.4}$$

Therefore this matrix has an effect on the order w^0 matrix in the transformed problem and the shearing transformation reduces the eigenvalue $-h_1 - 2$ to $-h_1$. This matrix will clearly affect only $\mathbf{F}_1$, the leading order matrix in the transformed problem, and especially only the element on column and row number 4. Thus the fourth component of the matrix $\mathbf{F}_1$ is $-h_1 - 2 + 2 = -h_1$. Finally then, no two eigenvalues differ by a positive integer of this matrix.

Additionally, the matrices of the form, $\mathbf{S^2 E}_i(\mathbf{S}^{-1})^2$, will break down in the following manner,

$$\begin{aligned}\mathbf{S^2 E}_i(\mathbf{S}^{-1})^2 = w^2 &\begin{pmatrix} & & & \\ & & & \\ & & & \\ (\mathbf{E}_i)_{41} & (\mathbf{E}_i)_{42} & (\mathbf{E}_i)_{43} & \end{pmatrix} \\ + w^0 &\begin{pmatrix} (\mathbf{E}_i)_{11} & (\mathbf{E}_i)_{12} & (\mathbf{E}_i)_{13} & \\ (\mathbf{E}_i)_{21} & (\mathbf{E}_i)_{22} & (\mathbf{E}_i)_{23} & \\ (\mathbf{E}_i)_{31} & (\mathbf{E}_i)_{32} & (\mathbf{E}_i)_{33} & \\ & & & (\mathbf{E}_i)_{44} \end{pmatrix} \\ + w^{-2} &\begin{pmatrix} & & (\mathbf{E}_i)_{14} & \\ & & (\mathbf{E}_i)_{24} & \\ & & (\mathbf{E}_i)_{34} & \\ & & & \end{pmatrix}.\end{aligned} \tag{B.2.5}$$

Evidently, each $\mathbf{E}_i$ will have a contribution to a different order matrix in the transformed problem (i.e. $\mathbf{F}_i$). In particular since the matrix $\mathbf{E}_3$ is multiplied by w^2, it will have an order zero effect on the transformed system and hence the form of $\mathbf{F}_1$. One could think that $w\mathbf{E}_2$ would then have a term proportional to w^{-1} but in that case the rightmost column is zero so it has no effect.

Most importantly, then, the leading order matrix is upper diagonal and has eigenvalues $-h_1, -h_2, -h_1, -h_1$ though it is no longer exactly diagonal due to the contribution of the higher order matrix $\mathbf{E}_3$.

the RHS of (3.3.24) to obtain $wd\mathbf{p}/dw = \ldots$. Therefore adding the following to the RHS,

B.3 Convergence of integrals in Eq. (3.4.3)

The following is a discussion of the convergence of the integrals that arise in the definition of the IVP solution. Specifically, integrals of the type that appear in Eq. (3.4.3) will converge due to the exponential decay of the first linearly independent solution $\overline{\mathbf{z}}_1$. In the following, one can redefine V as

$$\begin{aligned} V &= ikV_k + \sigma V_\sigma \\ V_\sigma &= (\mathbf{y}_1(0)\cdot\mathbf{h}_t) + \sigma I_t, \\ V_k &= (\mathbf{y}_1(0)\cdot\mathbf{h}_y) + I_y. \end{aligned} \tag{B.3.1}$$

with

$$I_y = \int_0^{-\infty} (\mathbf{y}_1\cdot\mathbf{A}_x^{-1}\mathbf{s}_y)\,dx,\ I_t = \int_0^{-\infty} (\mathbf{y}_1\cdot\mathbf{A}_x^{-1}\mathbf{s}_t)\,dx. \tag{B.3.2}$$

Evidently, the matrix $\mathbf{A}_x^{-1}$ becomes singular since the flow becomes locally sonic at the end of reaction zone ($x\to-\infty$). In other words, in the CJ case,

$$\begin{gathered} \eta_0 = u_0^2 - c_0^2 \to 0 \text{ as } x\to-\infty \Rightarrow \\ \det(A_x^{-1}) \propto 1/\eta_0 \to \infty. \end{gathered} \tag{B.3.3}$$

However the singular nature of this matrix is compensated by the stronger exponential decay of the first adjoint eigenfunction as detailed previously. Specifically we know that as $x\to-\infty$,

$$\mathbf{y}_1 \to \mathbf{d}_0^1 \exp\left(-\frac{2\sigma}{\beta(\gamma+1)w}\right) w^\phi \tag{B.3.4}$$

where $w\to\exp(\beta x)$. Therefore the exponential factor above decays at a *doubly* exponential rate. To ease the development of a more rigorous approach to this issue it is advantageous to switch independent variables, i.e. from x to w. Recall that $w = u_0 - u_0^\infty$. Referring to both integrals at once by choosing t or y as the subscript on the vector $\mathbf{s}$ and then allowing that $w(0) = u_0(0) - u_0^\infty = u_0^+ - u_0^\infty > 0$,

$$I_{y,t} = \int_{w(0)}^{0} \frac{\mathbf{y}_1\cdot\mathbf{A}_x^{-1}\mathbf{s}_{y,t}}{dw/dx} dw. \tag{B.3.5}$$

This is convenient since we have obtained asymptotic representations of the functions above in terms of w, i.e.

$$\begin{aligned}\mathbf{A}_x^{-1}\mathbf{s}_y &= -(0,0,dw/dx,0,0)^T,\\ \mathbf{A}_x^{-1}\mathbf{s}_t &= -\frac{1}{\eta_0}(1/u_0,u_0,0,a_0^2/u_0,0)^T\end{aligned} \tag{B.3.6}$$

with

$$\begin{aligned}a_0^2 &= -\gamma(w^2+((\gamma-1)u_0^\infty/\gamma)w-u_0^{\infty 2}/\gamma),\\ \eta_0 &= (\gamma+1)w^2+(\gamma+1)u_0^\infty w\\ dw/dx &= -\exp\left(\frac{\tau}{(w+u_0^\infty)(w-u_0^\infty/\gamma)}\right)\frac{\alpha w}{2(w+u_0^\infty)}.\end{aligned} \tag{B.3.7}$$

The integrals in question have been converted to bounded intervals though they may be improper depending on the behavior of the integrand as $w \to 0$. Specifically from the above equation it is clear that $\eta_0 \to K_1 w$ and $dw/dx \to K_2 w$ where are K_1 and K_2 are constants. This results in the conclusion that

$$\mathbf{A}_x^{-1}\mathbf{s}_y/(dw/dx) \to 1,\ \mathbf{A}_x^{-1}\mathbf{s}_t/(dw/dx) \to K_3 w^{-2}. \tag{B.3.8}$$

As can seen above the singular nature of the matrix causes the second quantity above to explode since $1/\eta_0$ appears as a factor. Also, the conversion factor $1/(dw/dx)$ adds another power to w in the denominator.

The integrand is bounded for all $w > 0$ or equivalently for any finite x and so as a result, the question of the convergence of integrals depends exclusively on the asymptotic behavior as $w \to 0$ or $x \to -\infty$. The correct classification is clear if we analyze the (exact) asymptotic form of the integrands

$$\begin{aligned}\mathbf{y}_1\cdot\mathbf{A}_x^{-1}\mathbf{s}_y/(dw/dx) &\to K_4\exp\left(-\frac{2\sigma}{\beta(\gamma+1)w}\right)w^{D_{11}^1} \to 0\\ \mathbf{y}_1\cdot\mathbf{A}_x^{-1}\mathbf{s}_t/(dw/dx) &\to K_5\exp\left(-\frac{2\sigma}{\beta(\gamma+1)w}\right)w^{D_{11}^1-2} \to 0.\end{aligned} \tag{B.3.9}$$

If we hold that $\mathrm{Re}(\sigma) > 0$, then the exponential decay beats any growth due to a negative power of w in both cases. Since the integrand function is effectively 0 as

$w \to 0$ in both cases, then the integral itself must be a well defined constant since we know the function itself is bounded throughout this finite interval, i.e.

$$\text{if } |\mathbf{y}_1 \cdot \mathbf{A}_x^{-1}\mathbf{s}_{y,t}/(dw/dx)| < C_{t,y} \tag{B.3.10}$$

then

$$|I_{y,t}| \leq w(0)C_{t,y} \tag{B.3.11}$$

so I_y and I_t converge and are well defined even though the matrix $\mathbf{A}_x^{-1}$ is singular as $x \to -\infty$.

Appendix C

Multi-domain spectral collocation supplement

C.1 Matrices and vectors

Linearized Euler and reaction equations

In the following, the subscript 0 refers to the steady state solution for the appropriate quantity and the prime represents a derivative in x. The matrix $\mathbf{A}_0$ from (4.2.11),

$$\mathbf{A}_0 = \begin{pmatrix} (\alpha\eta_0 - W_0 u_0 u_{0,\beta})/u_0 + 2\beta Q(\gamma-1)W_{0,v_0} & -\alpha u_0^2 + (W_0 u_{0,\beta_0}(c_0^2 - 3u_0^2))/u_0 \\ c_0^2 W_0 u_{0,\beta}/u_0^2 - 2\beta Q(\gamma-1)W_{,v_0} & u_0(\alpha + 2W_0 u_{0,\beta_0}/u_0) \\ 0 & 0 \\ -W_0 u_{0,\beta}(u_0^2 - 2c_0^2)/u_0^2 - 2\beta Q(\gamma-1)W_{0,v_0} & (\alpha c_0^2 + W_0 u_{0,\beta_0}(c_0^2 + u_0^2)/u_0)/u_0 \\ -W_{0,v_0}\eta_0/u_0 & W_0\eta_0/u_0^2 \end{pmatrix}$$

$$\begin{pmatrix} iku_0^2 & -u_0(\alpha + \gamma W_0 u_{0,\beta_0}/u_0) + 2\beta_0 Q(\gamma-1)W_{0,p_0} \\ -ic_0^2 k & u_0(\alpha + \gamma W_0 u_{0,\beta_0}/u_0) - 2\beta_0 Q(\gamma-1)W_{0,p_0} \\ \alpha\eta_0/u_0 & -ik\eta_0 \\ -ic_0^2 k & u_0(\alpha + \gamma W_0 u_{0,\beta_0}/u_0) - 2\beta_0 Q(\gamma-1)W_{0,p_0} \\ 0 & -W_{0,p_0}\eta_0/u_0 \end{pmatrix}$$

$$\begin{pmatrix} 2Q(\gamma-1)(W + \beta W_{0,\beta_0}) \\ -2Q(\gamma-1)(W + \beta W_{0,\beta_0}) \\ 0 \\ -2Q(\gamma-1)(W + \beta W_{0,\beta_0}) \\ \alpha\eta_0/u_0 - W_{0,\beta_0}\eta_0/u_0 \end{pmatrix}$$

Finally, the relevant vector $\mathbf{s}_0$ that appears in the governing equation (4.2.11) is given as follows:

$$\mathbf{s}_0 = -\begin{pmatrix} \alpha W_0 u_{0,\beta}(3u_0^2 - c_0^2)/u_0^2 \\ -2W_0\alpha u_{0,\beta} \\ ikW_0 u_{0,\beta}\eta_0/u_0 \\ -\alpha W_0 u_{0,\beta}(c_0^2 + u_0^2)/u_0^2 \\ -\alpha W_0\eta_0/u_0^2 \end{pmatrix}$$

Linearized Rankine-Hugoniot equations

First the coefficient vectors for the boundary condition at $x = 0$ or $\beta = 1$ is

$$\mathbf{h} = \left(\frac{2(1+\delta)}{\gamma+1}, \frac{4}{\gamma+1}, -ik\frac{2(1-\delta)}{\gamma+1}, -\frac{4\delta}{\gamma+1}, 0 \right)^T$$

Appendix D
Porous wall stability analysis supplement

D.1 Model problem for eigenfunction expansion method

The radial eigenfunction dependence found in the impenetrable wall stability problem is crucial in defining the stability problem as a two-point boundary value problem with ODE's depending only the axial variable z. The Bessel function structure leads to a simple relation governing the radial wave numbers of each perturbation. In order to ascertain the leading order effect of the slight porosity on the resulting modified stability problem, an eigenfunction expansion utilizing the impenetrable wall eigenfunctions was used to represent the radial dependence of the perturbation in the modified problem. The "non-diagonal" terms were assumed to be higher order terms in the governing equations since in the limit, the expansion collapses to a single distinguished member.

D.1.1 The exact eigenfunction

In the following, a model problem is defined to clarify and illustrate the concept. The chosen problem is the classic wave equation in a finite spatial domain,

$$u_{tt} = u_{xx} \tag{D.1.1}$$

$$u_x(t,0) = 0,\ u_x(t,\pi) = \beta u(t,\pi), \tag{D.1.2}$$

with β assumed small. This model is meant to mimic the structure encountered in the porous wall stability problem where it is the impedance that is assumed small. The boundary condition chosen here is similar to the structure found in the full problem since in that context, the normal velocity is related to the pressure in our boundary condition, i.e. $u = p/Z$. From the normal coordinate momentum equation,

the normal pressure gradient is proportional to the normal velocity component in the frequency domain, i.e. $d\hat{p}/dr \propto \hat{u} \Rightarrow d\hat{u}/dr = \hat{u}/Z$ where $1/Z \to 0$.

The task is to obtain a reduction to ODE's in t that determines "amplitude" of each spatial eigenfunction. This can be done exactly in the current instance by assuming that the spatial eigenfunction be of the form $A\cos(kx) + B\sin(kx)$ where k is to be determined from the boundary conditions. Therefore,

$$u_x(0) = 0 \Rightarrow 0 = -Ak\sin(0) + Bk\cos(0) \Rightarrow B = 0 \tag{D.1.3}$$

and

$$\begin{aligned} u_x(\pi) = \beta u(\pi) \Rightarrow A\beta\cos(k\pi) = -Ak\sin(k\pi) \Rightarrow & \beta\cos(k\pi) + k\sin(k\pi) = 0 \\ & \beta + k\tan(k\pi) = 0 \end{aligned} \tag{D.1.4}$$

Therefore the wave numbers are obtained from a transcendental equation. In the limit of course, $\beta = 0$, the wave numbers are simple, i.e. $\tan(k\pi) = 0 \Rightarrow k \in \mathbb{Z}$. One can obtain through Taylor expansion, the deviation from the $\beta = 0$ case through the following procedure, assuming that $k \to k_0 + \beta k_1$,

$$\begin{aligned} \beta + k\tan(k\pi) \to & \beta + (k_0 + \beta k_1)(\tan(k_0\pi + \beta k_1\pi)) = 0 \\ = & \beta + (k_0 + \beta k_1)\left(\tan(k_0\pi) + (\beta k_1\pi)\frac{1}{\cos^2(k_0\pi)}\right) = 0 \\ = & \big[k_0\tan(k_0\pi)\big] + \beta\left[1 + k_1\tan(k_0\pi) + \frac{k_0k_1\pi}{\cos^2(k_0\pi)}\right] + \mathcal{O}(\beta^2) = 0. \end{aligned} \tag{D.1.5}$$

Therefore one can obtain that

$$k_0\tan(k_0\pi) = 0 \Rightarrow k_0 = m,\ m \in \mathbb{Z} \tag{D.1.6}$$

as expected. At $\mathcal{O}(\beta)$ one obtains k_1 as follows:

$$k_1 = -\frac{1}{m\pi} \tag{D.1.7}$$

The wave number is modified in the following way for small β along with the frequency ω_m if one assumes $u_m \propto \exp(i\omega_m t)$,

$$\tilde{k}_m = m - \beta/(\pi m),\ \tilde{\omega}_m = \pm\tilde{k}_m = \pm[m - \beta/(\pi m)]. \tag{D.1.8}$$

This was obtained through Taylor expansion on the exact transcendental equation governing the wave numbers of the general β problem.

D.1.2 The eigenfunction expansion

In the present detonation stability study an approximate procedure is set down in order to obtain the ODE system in z that determines stability. The concept will be illustrated within the context of the present modeled wave equation problem. In the following, an eigenfunction expansion for the spatial dependence is proposed for the model problem in order to compare with the exact spatial eigenfunctions and the resulting time dependence (i.e. $\bar{\omega}_m$ from (D.1.8)).

In the special limiting case where $\beta = 0$, the eigenfunctions are simple, i.e.

$$u_m \propto \cos(mx), \ m \in \mathbb{Z}. \tag{D.1.9}$$

Therefore for non-zero β, one proposes the expansion for the m-th eigenfunction

$$u_m \sim \sum_n^{\infty} \hat{u}_n^m(t) \cos(nx) \tag{D.1.10}$$

To obtain the governing equations for $\hat{u}_n^m(t)$, the governing equation is multiplied by $\cos(mx)$ and integrated. On the right hand, one incorporates integration by parts,

$$\begin{aligned}
\int_0^{\pi} u_{tt} \cos(mx) dx &= \int_0^{\pi} u_{xx} \cos(mx) dx \\
&= u_x \cos(mx)\Big|_0^{\pi} + m \int_0^{\pi} u_x \sin(mx) dx \\
&= u_x \cos(mx)\Big|_0^{\pi} + m \left[u \sin(mx)\Big|_0^{\pi} - m \int_0^{\pi} u \cos(mx) dx \right] \\
&= u_x \cos(mx)\Big|_0^{\pi} + mu \sin(mx)\Big|_0^{\pi} - m^2 \int_0^{\pi} u \cos(mx) dx
\end{aligned} \tag{D.1.11}$$

At this point one can incorporate the explicit boundary conditions when determining

the non-integral terms above,

$$\begin{aligned} u_x \cos(mx)\Big|_0^\pi &= u_x(t,\pi)\cos(m\pi) - u_x(t,0)\cos(0) = \beta u(t,\pi)\cos(m\pi) \\ mu\sin(mx)\Big|_0^\pi &= mu(t,\pi)\sin(m\pi) - mu(t,0)\sin(0) = 0 \end{aligned} \tag{D.1.12}$$

Then, one has

$$\frac{d^2}{dt^2}\left[\int_0^\pi u\cos(mx)dx\right] = \beta u(t,\pi)\cos(m\pi) - m^2\int_0^\pi u\cos(mx)dx \tag{D.1.13}$$

Now one incorporates the expansion for u in (D.1.10), so

$$\int_0^\pi u\cos(mx)dx = \int_0^\pi \sum_n^\infty \hat{u}_n^m(t)\cos(nx)\cos(mx)dx = \sum_n^\infty u_n^m \int_0^\pi \cos(nx)\cos(mx)dx \tag{D.1.14}$$

$$= \sum_n^\infty \hat{u}_n^m \frac{\pi}{2}\delta_{nm} = \frac{\pi}{2}\hat{u}_m^m \tag{D.1.15}$$

Therefore the governing equation is formally given by

$$\frac{d^2}{dt^2}\hat{u}_m^m = \frac{2\beta}{\pi}\cos(m\pi)\sum_n^\infty \hat{u}_n^m(t)\cos(n\pi) - m^2\hat{u}_m^m \tag{D.1.16}$$

If it is so that $u_m \to \cos(mx)$ as $\beta \to 0$ then the "off-diagonal" weights $u_n^m(t)$ individually must vanish in the limit as well. Furthermore, the infinite sum above collapses to one term if their cumulative sum is higher order in β, i.e. only $\hat{u}_m^m$ survives. The consequence of this hypothesis is as follows, a reduced finite set of terms with a perturbation proportional to β,

$$\begin{aligned} \frac{d^2}{dt^2}\hat{u}_m^m &= \left[\frac{2\beta}{\pi}\cos^2(m\pi) - m^2\right]\hat{u}_m^m \\ \frac{d^2}{dt^2}\hat{u}_m^m &= -\left[m^2 - \frac{2\beta}{\pi}\right]\hat{u}_m^m \end{aligned} \tag{D.1.17}$$

As a result if one proposes $\hat{u}_m^m(t) \propto \exp(i\bar{\omega}_m t)$, one obtains that

$$\bar{\omega}_m = \pm\sqrt{m^2 - \frac{2\beta}{\pi}} \tag{D.1.18}$$

β	ω_1	ω_2	ω_3	$\bar{\omega}_1$	$\bar{\omega}_2$	$\bar{\omega}_3$
10^{-1}	0.967206	1.983969	2.989355	0.967645	1.984020	2.989370
10^{-2}	0.996806	1.998407	2.998938	0.996811	1.998408	2.998939

TABLE D.1. First three frequencies ω_m derived from the wave numbers defined by $\beta + k\tan(k\pi)$. The same quantities $\bar{\omega}_m$ calculated using the approximate procedure, i.e. using (D.1.18), also appear.

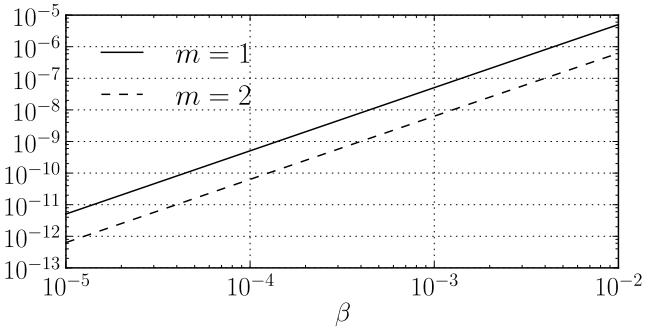

FIGURE D.1. The comparison between ω_m exact and the prediction obtained from the eigenfunction expansion. The error is $\mathcal{O}(\beta^2)$ as $\beta \to 0$.

In the limit as $\beta \to 0$, this function can be expanded in Taylor series to produce:

$$\bar{\omega}_m \to \pm\left[m - \frac{2\beta}{\pi}\frac{1}{2m}\right] = \pm\left[m - \frac{\beta}{m\pi}\right] \tag{D.1.19}$$

It is clear that this derived frequency is the same that is predicted via the Taylor expansion of the exact result, i.e. (D.1.8). A specific comparison appears in Table D.1. It would seem then that it is a safe assumption to consider the non-diagonal terms negligible in the eigenfunction expansion in determining the time dependence of each perturbation. The leading order effect on the frequency of the m-th eigenfunction for the small non-zero β problem is retained via the approximate eigenfunction expansion method. A plot of the difference between the presently derived predicted frequency, $\bar{\omega}_m = \pm\sqrt{m^2 - 2\beta/\pi}$, and the exact frequency calculated numerically appears in Fig. D.1. One can assume the discarded terms are order β^2 in the limit from the slope of the lines.

D.2 Derivation of ODE's

D.2.1 Derivation of continuity

Two of the linearized equations contain radial derivative terms in radial velocity, and therefore, incorporate a boundary condition in r. In the non-porous case, this term is exactly zero, but in the following, one explicitly incorporates the acoustic boundary condition. From the matrix-vector equation in (5.2.7) one obtains the continuity equations with r, z variables:

$$\rho^*\left(\frac{\partial u_n}{\partial r}+\frac{u_n}{r}+\frac{in}{r}w_n\right)+\tau\rho_n+\rho^*\frac{\partial v_n}{\partial z}+\frac{d\rho^*}{dz}v_n+v^*\frac{\partial \rho_n}{\partial z}+\frac{dv^*}{dz}\rho_n-\frac{d\rho^*}{dz}\tau\psi_n=0 \tag{D.2.1}$$

parametrized by n, the azimuthal frequency. In the absence of the acoustic boundary condition one would substitute the expansion of each of the unknown dependent variables $\rho_n, u_n, \ldots$ in terms of the appropriate Bessel function form. However, for the eigenfunction expansion which does not explicitly meet the new boundary condition we first multiply by $J_n(k_{nj}r)r$ and integrate from $r \in [0, a]$ (as suggested in the eigenfunction expansion problem described by Zauderer [59]). The following is produced:

$$\begin{aligned}&\int_0^a J_n(k_{nj}r)r\left(\rho^*\frac{\partial u_n}{\partial r}\right)dr+\int_0^a \rho^* J_n(k_{nj}r)r\left(\frac{u_n}{r}+\frac{in}{r}w_n\right)dr+\\&\int_0^a J_n(k_{nj}r)r\left(\tau\rho_n+\rho^*\frac{\partial v_n}{\partial z}+\frac{d\rho^*}{dz}v_n+v^*\frac{\partial \rho_n}{\partial z}+\frac{dv^*}{dz}\rho_n-\frac{d\rho^*}{dz}\tau\psi_n\right)dr=0\end{aligned} \tag{D.2.2}$$

The first term above includes a derivative in r inside the integral. In order to incorporate the boundary condition into the eventual ODE system in z, one must integrate

by parts. Therefore,

$$\begin{aligned}\int_0^a J_n(k_{nj}r)r\left(\rho^*\frac{\partial u_n}{\partial r}\right)dr &= -\rho^*\int_0^a\left(\frac{d}{dr}\big[J_n(k_{nj}r)r\big]u_n\right)dr + \rho^*\left(u_nJ_n(k_{nj}r)r\right)\Big|_0^a \\ &= -\rho^*\int_0^a\left(\frac{d}{dr}\big[J_n(k_{nj}r)r\big]u_n\right)dr + \rho^*u_n(z,r)\Big|_{r=a}J_n(k_{nj}a)a \\ &= -\rho^*\int_0^a\left(\frac{d}{dr}\big[J_n(k_{nj}r)r\big]u_n\right)dr + \frac{\rho^*J_n(k_{nj}a)a}{Z}\left[p_n(z,r)+\frac{v^*}{\tau}\frac{\partial}{\partial z}p_n(z,r)\right]\Big|_{r=a}\end{aligned} \tag{D.2.3}$$

where as a consequence of the acoustic BC, it is held that $u_n(z,r)\big|_{r=a} = -p_n(z,r)\big|_{r=a}/Z$. In the non-acoustic BC case, the second term above disappears due to $1/|Z| \to 0$. The eigenfunction expansion has not been implemented at this step quite yet since $p_n(r,z)$ has not yet been broken down into constituents. More on that later.

The second term in (D.2.2) bears deeper scrutiny as it bears a direct relation to the axial vorticity of the perturbation flow. As Shalaev outlines, the axial vorticity perturbation Ω_z is nothing but

$$\Omega_z = \frac{1}{r}\left(\frac{\partial(rw)}{\partial r} - \frac{\partial u}{\partial \phi}\right) \tag{D.2.4}$$

which has a ready solution, reflecting the fact that the axial vorticity perturbation travels along a particle path defined by v^*, the steady state axial vorticity[1]. Manipulation of the relevant governing equations yields that Ω_z satisfies the following PDE,

$$\frac{\partial\Omega_z}{\partial t} + v^*\frac{\partial\Omega_z}{\partial z} = 0 \tag{D.2.5}$$

Clearly, after proposing the time dependence: $\Omega_z \propto \exp(\tau u)$ and ϕ-dependence: $\Omega_z = \sum_n^\infty (\Omega_z)_n \exp(in\phi)$,

$$\tau(\Omega_z)_n + v^*\frac{\partial(\Omega_z)_n}{\partial z} = 0 \tag{D.2.6}$$

This equation for $(\Omega_z)_n$ can be readily solved

$$(\Omega_z)_n = K_0(r)\exp\left(-\tau\int_0^z\frac{dz'}{v^*}\right) \tag{D.2.7}$$

[1]Note that normal modes carry no axial vorticity

where $K_0(r)$ is determined from the correspondingly transformed boundary condition (i.e. function of τ and n) at the front ($z = 0$). This is the input from the quiescent gas. Now note here that Kasimov and Stewart [27] essentially hold that there is no vorticity present in the quiescent or reaction zones, i.e. $K_0(r) = 0$. This brings the consequence that

$$(\Omega_z)_n = \frac{1}{r}\left(\frac{\partial(rw_n)}{\partial r} - inu_n\right) \Rightarrow (\Omega_z)_n \to 0 \Rightarrow \frac{\partial(rw_n)}{\partial r} - inu_n = 0$$
$$\frac{\partial(rw_n)}{\partial r} = inu_n \tag{D.2.8}$$

At this point it is necessary to incorporate the relevant eigenfunction expansions, which specifically state that

$$\rho_n^j = \sum_m^N \rho_{nm}^j(z) J_n(k_{nm}r),\ u_n = \sum_m^N u_{nm}^j(z) k_{nm} J_n'(k_{nm}r),\ w_n = \sum_m^N w_{nm}^j(z) J_n(k_{nm}r)/r,$$
$$v_n = \sum_m^N v_{nm}^j(z) J_n(k_{nm}r),\ p_n = \sum_m^N p_{nm}^j(z) J_n(k_{nm}r),\ \text{and}\ \lambda_n = \sum_m^N \lambda_{nm}^j(z) J_n(k_{nm}r) \tag{D.2.9}$$

where the weight functions $u_{nm}^j, w_{nm}^j, \ldots$ are functions of z only, and ODE's are sought for their evolution. Using this scheme produces the modified set of equations:

$$\begin{aligned}
&\sum_m^N \frac{\rho^* J_n(k_{nj}a)a}{Z} J_n(k_{nm}a)\left[p_{nm}^j(z) + \frac{v^*}{\tau}\frac{d}{dz}p_{nm}^j(z)\right] - \\
&\sum_m^N \rho^* u_{nm}^j \int_0^a \frac{d}{dr}\big[J_n(k_{nj}r)r\big]\frac{d}{dr}[J_n(k_{nm}r)]dr + \\
&\sum_m^N \int_0^a \rho^* J_n(k_{nj}r) r\left(\frac{u_{nm}^j}{r}\frac{d}{dr}[J_n(k_{nm}r)] + \frac{in}{r^2}w_{nm}^j J_n(k_{nm}r)\right)dr + \\
&\sum_m^N \int_0^a J_n(k_{nj}r) r J_n(k_{nm}r)\left(\tau\rho_{nm}^j + \rho^*\frac{dv_{nm}^j}{dz} + \frac{d\rho^*}{dz}v_{nm}^j + v^*\frac{d\rho_{nm}^j}{dz} + \right. \\
&\qquad \left. \frac{dv^*}{dz}\rho_{nm}^j - \frac{d\rho^*}{dz}\tau\psi_{nm}^j\right)dr = 0
\end{aligned} \tag{D.2.10}$$

Incorporating the vorticity equation appropriate to the eigenfunction expansion leads

to

$$\frac{\partial(rw_n)}{\partial r} = inu_n \Rightarrow \sum_m^N w_{nm}^j \frac{\partial(rJ_n(k_{nm}^j r)/r)}{\partial r} = \sum_m^N inu_{nm}^j \frac{\partial J_n(k_{nm}r)}{\partial r} \Rightarrow w_{nm}^j = inu_{nm}^j. \tag{D.2.11}$$

This equation above is incorporated to the eigenfunction expanded Eq. (D.2.2):

$$\begin{aligned}
&\sum_m^N \rho^* u_{nm}^j \Bigg[\int_0^a J_n(k_{nj}r) r \left(\frac{1}{r}\frac{d}{dr}[J_n(k_{nm}r)] - \frac{n^2}{r^2} J_n(k_{nm}r) \right) dr \\
&- \int_0^a \left(\frac{d}{dr}\big[J_n(k_{nj}r)r\big] \frac{d}{dr}[J_n(k_{nm}r)] \right) dr \Bigg] + p_{nj} \frac{\rho^* J_n(k_{nj}a)a}{Z} J_n(k_{nj}a) \\
&+ \sum_m^N \int_0^a J_n(k_{nj}r) r J_n(k_{nm}r) \Bigg(\tau\rho_{nm}^j + \rho^* \frac{dv_{nm}^j}{dz} + \frac{d\rho^*}{dz} v_{nm}^j + \\
&\qquad v^* \frac{d\rho_{nm}^j}{dz} + \frac{dv^*}{dz}\rho_{nm}^j - \frac{d\rho^*}{dz}\tau\psi_{nm}^j \Bigg) dr = 0
\end{aligned} \tag{D.2.12}$$

The first terms proportional to u_{nj} in (D.2.12) can be transformed using the Bessel function equation to substitute for $dJ_n/dr = k_{nj}J_n'/r$, i.e.

$$\frac{k_{nj}J_n'}{r} = -k_{nj}^2 J_n'' - k_{nj}^2 J_n + \frac{n^2}{r^2} J_n \tag{D.2.13}$$

so that

$$\begin{aligned}
&\sum_m^N u_{nm}^j(z) \Bigg[- \int_0^a \left(\frac{d}{dr}\big[J_n(k_{nj}r)r\big] J_n'(k_{nm}r) k_{nm} \right) dr + \\
&\qquad \int_0^a J_n(k_{nj}r) r \left(\frac{J_n'(k_{nj}r)k_{nj}}{r} - \frac{n^2}{r^2} J_n \right) dr \Bigg] \\
&= \sum_m^N u_{nm}^j(z) \Bigg[- \int_0^a \left(\frac{d}{dr}\big[J_n(k_{nj}r)r\big] J_n'(k_{nj}r) k_{nj} \right) dr + \\
&\qquad \int_0^a J_n(k_{nj}r) r \Big(- k_{nm}^2 J_n'' - k_{nm}^2 J_n + \frac{n^2}{r^2} J_n - \frac{n^2}{r^2} J_n \Big) dr \Bigg] \\
&= \sum_m^N u_{nm}^j(z) \Bigg[- \int_0^a \left(\frac{d}{dr}\big[J_n(k_{nj}r)r\big] J_n'(k_{nm}r) k_{nm} + J_n(k_{nj}r) r (k_{nm}^2 J_n'') \right) dr - \\
&\qquad \int_0^a r J_n(k_{nj}r) k_{nm}^2 J_n(k_{nm}r) dr \Bigg]
\end{aligned} \tag{D.2.14}$$

At this point it is useful to note that the first includes a perfect derivative in the integrand so that,

$$\int_0^a \left[\frac{d}{dr}\big[J_n(k_{nj}r)r\big]J_n'(k_{nm}r)k_{nm} + J_n(k_{nj}r)r(k_{nm}^2 J_n'')\right] = \int_0^a \frac{d}{dr}\Big[rJ_n(k_{nj}r)k_{nm}J_n'(k_{nm}r)\Big]dr = \big[rJ_n(k_{nj}r)k_{nm}J_n'(k_{nm}r)\big]\Big|_0^a = 0 \tag{D.2.15}$$

and the second term is reducible through the orthogonality condition

$$\int_0^a rJ_n(k_{nj}r)J_n(k_{nj}r)dr = Q_j = \frac{k_{nj}^2a^2 - n^2}{2k_{nj}^2}J_n^2(k_{nj}a) \tag{D.2.16}$$

Therefore one can show that

$$u_{nj}(z)\Bigg[-\int_0^a \left(\frac{d}{dr}\big[J_n(k_{nj}r)r\big]J_n'(k_{nj}r)k_{nj}\right)dr + \int_0^a J_n(k_{nj}r)r\left(\frac{J_n'(k_{nj}r)k_{nj}}{r} - \frac{n^2}{r^2}J_n\right)dr\Bigg] = -k_{nj}^2Q_ju_{nm}^j(z) \tag{D.2.17}$$

One can then combine the above with (D.2.12) and incorporating the fact that:

$$-\rho^*k_{nj}^2Q_ju_{nj}^j(z) + \sum_m^N \frac{\rho^*J_n(k_{nj}a)a}{Z}J_n(k_{nm}a)\left[p_{nm}^j(z) + \frac{v^*}{\tau}\frac{d}{dz}p_{nm}^j(z)\right] + Q_j\left(\tau\rho_{nj}^j(z) + \rho^*\frac{dv_{nj}^j}{dz} + \frac{d\rho^*}{dz}v_{nj}^j + v^*\frac{d\rho_{nj}^j}{dz} + \frac{dv^*}{dz}\rho_{nj}^j - \frac{d\rho^*}{dz}\tau\psi_{nj}^j\right) = 0 \tag{D.2.18}$$

One notices that this is equivalent to the equation found by Kasimov and Stewart [27] but for one crucial difference, that is the term proportional to $1/Z$. All the transformations that were obtained to arrive at this final equation can be summarized as follows:

$$\int_0^a J_n(k_{nj}r)r\left(\frac{\partial u_n^j}{\partial r} + \frac{u_n^j}{r} + \frac{in}{r}w_n^j\right)dr = -k_{nj}^2Q_ju_{nj}^j(z) + \sum_m^N \frac{J_n(k_{nj}a)J_n(k_{nm}a)a}{Z}\left[p_{nm}^j(z) + \frac{v^*}{\tau}\frac{d}{dz}p_{nm}^j(z)\right] \tag{D.2.19}$$

This relation will prove useful in transforming the energy equation specifically.

D.2.2 Energy equation

The energy equation requires a similar treatment to the continuity equation. It is given by

$$\gamma p^*\left[\frac{\partial u_n^j}{\partial r}+\frac{in}{r}w_n^j+\frac{1}{r}u_n^j\right]+\tau_j p_n^j+v^*\frac{\partial p_n^j}{\partial z}+\gamma p^*\frac{\partial v_n^j}{\partial z}+ C_{51}\rho_n^j+\frac{dp^*}{dz}v_n^j+C_{55}\psi_n^j+C_{56}\lambda_n^j-\tau_j\frac{dp^*}{dz}\psi_n^j=0 \tag{D.2.20}$$

Multiplying by $rJ_n(k_{nj}r)$ and integrating over $r\in[0,a]$ produces:

$$\int_0^a rJ_n(k_{nj}r)\gamma p^*\left[\frac{\partial u_n^j}{\partial r}+\frac{in}{r}w_n^j+\frac{1}{r}u_n^j\right]dr+\int_0^a rJ_n(k_{nj}r)\Bigg(\tau p_n^j+v^*\frac{\partial p_n^j}{\partial z}+\gamma p^*\frac{\partial v_n^j}{\partial z}+ C_{51}\rho_n^j+\frac{dp^*}{dz}v_n^j+C_{55}p_n^j+C_{56}\lambda_n^j-\tau\frac{dp^*}{dz}\psi_n^j\Bigg)=0 \tag{D.2.21}$$

Firstly, the first term in the above is exactly reducible using (D.2.19). Secondly, via the eigenfunction expansion, the second term after substitution will be proportional to $\int_0^a rJ_n(k_{nm}r)J_n(k_{nj}r)dr=Q_j\delta_{mj}$ and so one obtains:

$$-\gamma p^*k_{nj}^2Q_ju_{nj}(z)+\gamma p^*\sum_m^N\frac{J_n(k_{nj}a)a}{Q_jZ}J_n(k_{nm}a)\left[p_{nm}^j(z)+\frac{v^*}{\tau}\frac{d}{dz}p_{nm}^j(z)\right]+\Bigg(\tau_jp_{nj}^j+ v^*\frac{dp_{nj}^j}{dz}+\gamma p^*\frac{dv_{nj}^j}{dz}+C_{51}\rho_{nj}^j+\frac{dp^*}{dz}v_{nj}^j+C_{55}p_{nj}^j+C_{56}\lambda_{nj}^j-\tau_j\frac{dp^*}{dz}\psi_{nj}^j\Bigg)=0 \tag{D.2.22}$$

D.2.3 Radial momentum equation

The radial momentum equation is as follows:

$$\tau_ju_n^j+v^*\frac{\partial u_n^j}{\partial z}+\frac{1}{\gamma\rho^*}\frac{\partial p_n^j}{\partial r}-\frac{1}{\gamma\rho^*}\frac{dp^*}{dz}\frac{d\psi_n^j}{dr}=0 \tag{D.2.23}$$

Following Shalaev's method in the context of the IVP approach [52], one integrates the above from 0 to r, then multiplies by $rJ_n(k_{nj}r)$ and then integrate the result over $[0,a]$:

$$\int_0^a rJ_n(k_{nj}r)\int_0^r\left(\tau_ju_n^j+v^*\frac{\partial u_n^j}{\partial z}+\frac{1}{\gamma\rho^*}\frac{\partial p_n^j}{\partial r}-\frac{1}{\gamma\rho^*}\frac{dp^*}{dz}\frac{d\psi_n^j}{dr}\right)dr'\Bigg)dr=0 \tag{D.2.24}$$

After replacing the eigenfunction expansion scheme on the left hand side one finds that

$$\sum_m^N \int_0^a r J_n(k_{nj}r)\Bigg(\tau_j u_{nm}^j + v^* \frac{du_{nm}^j}{dz} + \frac{1}{\gamma\rho^*} p_{nm}^j - \frac{1}{\gamma\rho^*}\frac{dp^*}{dz}\psi_{nm}^j\Bigg)\int_0^r \frac{dJ_n(k_{nm}r)}{dr'}dr'\Bigg)dr = 0$$

$$\sum_m^N \int_0^a r J_n(k_{nj}r)\Bigg(\tau_j u_{nm}^j + v^* \frac{du_{nm}^j}{dz} + \frac{1}{\gamma\rho^*} p_{nm}^j - \frac{1}{\gamma\rho^*}\frac{dp^*}{dz}\psi_{nm}^j\Bigg)\big[J_n(k_{nm}r) - J_n(0)\big] = 0$$

$$\sum_{j=1}^\infty \Bigg(\tau_j u_{nm}^j + v^* \frac{du_{nm}^j}{dz} + \frac{1}{\gamma\rho^*} p_{nm}^j - \frac{1}{\gamma\rho^*}\frac{dp^*}{dz}\psi_{nm}^j\Bigg)\int_0^a r J_n(k_{nm}r)J_n(k_{nj}r)dr -$$

$$J_n(0)\int_0^a r J_n(k_{nj}r)dr \sum_{j=1}^\infty \Bigg(\tau_j u_{nm}^j + v^* \frac{du_{nm}^j}{dz} + \frac{1}{\gamma\rho^*} p_{nm}^j - \frac{1}{\gamma\rho^*}\frac{dp^*}{dz}\psi_{nm}^j\Bigg) = 0 \tag{D.2.25}$$

As Shalaev [52] details, $J_n(0) = 0$ for $n > 0$ and through the properties of Bessel functions

$$\int_0^a r J_0(k_{0j}r)dr = \frac{a}{k_{0j}} J_1(k_{0j}a) = -\frac{a}{k_{0j}} J_0'(k_{0j}a) = 0 \tag{D.2.26}$$

the equation becomes:

$$\tau u_{nj}^j + v^* \frac{du_{nj}^j}{dz} + \frac{1}{\gamma\rho^*} p_{nj}^j - \frac{1}{\gamma\rho^*}\frac{dp^*}{dz}\psi_{nj}^j = 0 \tag{D.2.27}$$

No modification of the underlying equations is found for the conservation of radial momentum (at least in the current implementation).

D.2.4 Azimuthal, axial and reaction equations

Transforming these equations is very straightforward. Specifically one has the azimuthal, axial and reaction rate equations, respectively, :

$$\begin{aligned}
&\tau_j w_n^j + v^* \frac{\partial w_n^j}{\partial z} + \frac{in}{r}\frac{1}{\gamma\rho^*} p_n^j - \frac{1}{\gamma\rho^*}\frac{in}{r}\frac{dp^*}{dz}\psi_n^j = 0 \\
&\tau_j v_n^j + \frac{dv^*}{dz} v_n^j + v^* \frac{\partial v_n^j}{\partial z} + \frac{1}{\gamma\rho^*}\frac{\partial p_n^j}{\partial z} + \frac{v^*}{\rho^*}\frac{dv^*}{dz}\rho_n^j - \tau_j \frac{dv^*}{dz}\psi_n^j = 0 \\
&\tau_j \lambda_n^j + v^* \frac{\partial \lambda_n^j}{\partial z} + C_{61}\rho_n^j + \frac{d\lambda^*}{dz} v_n^j + C_{65} p_n^j - \frac{d\lambda^*}{dz}\tau_j \psi_n^j + C^{66}\lambda_n^j = 0
\end{aligned} \tag{D.2.28}$$

Again, multiplying by $r^2 J_n(k_{nj}r)$, $rJ_n(k_{nj}r)$, and $rJ_n(k_{nj}r)$, respectively, and integrating each equation over $[0, a]$ one finds

$$\begin{aligned}
&\int_0^a \left(\tau_j w_n^j + v^* \frac{\partial w_n^j}{\partial z} + \frac{in}{r}\frac{1}{\gamma\rho^*} p_n^j - \frac{1}{\gamma\rho^*}\frac{in}{r}\frac{dp^*}{dz}\psi_n^j\right) r^2 J_n(k_{nj}r)dr = 0 \\
&\int_0^a \left(\tau_j v_n^j + \frac{dv^*}{dz} v_n^j + v^* \frac{\partial v_n^j}{\partial z} + \frac{1}{\gamma\rho^*}\frac{\partial p_n^j}{\partial z} + \frac{v^*}{\rho^*}\frac{dv^*}{dz}\rho_n^j - \tau_j \frac{dv^*}{dz}\psi_n^j\right) rJ_n(k_{nj}r)dr = 0 \\
&\int_0^a \left(\tau_j \lambda_n^j + v^* \frac{\partial \lambda_n^j}{\partial z} + C_{61}\rho_n^j + \frac{d\lambda^*}{dz} v_n^j + C_{65} p_n^j - \frac{d\lambda^*}{dz}\tau_j \psi_n^j + C^{66}\lambda_n^j\right) rJ_n(k_{nj}r)dr = 0
\end{aligned} \tag{D.2.29}$$

After substitution one finds that each left hand integral above is proportional to the Bessel equation orthogonality integral, so that one obtains, cleanly,

$$\begin{aligned}
&\tau_j w_{nj}^j + v^* \frac{dw_{nj}^j}{dz} + \frac{in}{\gamma\rho^*} p_{nj}^j - \frac{in}{\gamma\rho^*}\frac{dp^*}{dz}\psi_{nj}^j = 0 \\
&\tau_j v_{nj}^j + \frac{dv^*}{dz} v_{nj}^j + v^* \frac{dv_{nj}^j}{dz} + \frac{1}{\gamma\rho^*}\frac{dp_{nj}^j}{dz} + \frac{v^*}{\rho^*}\frac{dv^*}{dz}\rho_{nj}^j - \tau \frac{dv^*}{dz}\psi_{nj}^j = 0 \\
&\tau_j \lambda_{nj}^j + v^* \frac{d\lambda_{nj}^j}{dz} + C_{61}\rho_{nj}^j + \frac{d\lambda^*}{dz} v_{nj}^j + C_{65} p_{nj}^j - \frac{d\lambda^*}{dz}\tau \psi_{nj}^j + C^{66}\lambda_{nj}^j = 0
\end{aligned} \tag{D.2.30}$$

For this set of equations, there is no effect of the porous wall boundary condition.

D.3 Matrices and vectors

D.3.1 The matrices for the PDE system

$$\mathbf{A}_z = \begin{pmatrix} v^* & 0 & 0 & \rho^* & 0 & 0 \\ 0 & v^* & 0 & 0 & 0 & 0 \\ 0 & 0 & v^* & 0 & 0 & 0 \\ 0 & 0 & 0 & v^* & 1/\gamma\rho^* & 0 \\ 0 & 0 & 0 & \gamma p^* & v^* & 0 \\ 0 & 0 & 0 & 0 & 0 & v^* \end{pmatrix}, \mathbf{A}_r = \begin{pmatrix} 0 & \rho^* & 0 & 0 & 0 & 0 \\ 0 & 0 & 0 & 0 & 1/(\gamma\rho^*) & 0 \\ 0 & 0 & 0 & 0 & 0 & 0 \\ 0 & 0 & 0 & 0 & 0 & 0 \\ 0 & \gamma p^* & 0 & 0 & 0 & 0 \\ 0 & 0 & 0 & 0 & 0 & 0 \end{pmatrix}, \tag{D.3.1}$$

$$\mathbf{A}_\phi = \begin{pmatrix} 0 & 0 & \rho^* & 0 & 0 & 0 \\ 0 & 0 & 0 & 0 & 0 & 0 \\ 0 & 0 & 0 & 0 & 1/(\gamma\rho^*) & 0 \\ 0 & 0 & 0 & 0 & 0 & 0 \\ 0 & 0 & \gamma p^* & 0 & 0 & 0 \\ 0 & 0 & 0 & 0 & 0 & 0 \end{pmatrix}, \tag{D.3.2}$$

$$\mathbf{C} = \begin{pmatrix} dv^*/dz & \rho^*/r & 0 & d\rho^*/dz & 0 & 0 \\ 0 & 0 & 0 & 0 & 0 & 0 \\ 0 & 0 & 0 & 0 & 0 & 0 \\ i(v^*/\rho^*)dv^*/dz & 0 & 0 & dv^*/dz & 0 & 0 \\ -\kappa\big(\omega^* + \rho^*\frac{\partial\omega^*}{\partial\rho^*}\big) & \gamma p^*/r & 0 & dp^*/dz & \gamma dv^*/dz - \kappa\rho^*\frac{\partial\omega^*}{\partial p^*} & -\kappa\rho^*\frac{\partial\omega^*}{\partial\lambda^*} \\ -\frac{\partial\omega^*}{\partial\rho^*} & 0 & 0 & d\lambda^*/dz & -\frac{\partial\omega^*}{\partial p^*} & -\frac{\partial\omega^*}{\partial\lambda^*} \end{pmatrix} \tag{D.3.3}$$

and the vectors:

$$\mathbf{g}_t = \begin{pmatrix} d\rho^*/dz \\ 0 \\ 0 \\ dv^*/dz \\ dp^*/dz \\ d\lambda^*/dz \end{pmatrix}, \mathbf{g}_r = \begin{pmatrix} 0 \\ (dp^*/dz)/(\gamma\rho^*) \\ 0 \\ 0 \\ 0 \\ 0 \end{pmatrix}, \mathbf{g}_\phi = \begin{pmatrix} 0 \\ 0 \\ (dp^*/dz)/(\gamma\rho^*) \\ 0 \\ 0 \\ 0 \end{pmatrix} \tag{D.3.4}$$

D.3.2 The matrices and vectors pertaining to the ODE system

$$
\mathbf{A} = \begin{pmatrix} v^* & 0 & 0 & \rho^* & 0 & 0 \\ 0 & v^* & 0 & 0 & 0 & 0 \\ 0 & 0 & v^* & 0 & 0 & 0 \\ 0 & 0 & 0 & v^* & 1/\gamma\rho^* & 0 \\ 0 & 0 & 0 & \gamma p^* & v^* & 0 \\ 0 & 0 & 0 & 0 & 0 & v^* \end{pmatrix}
$$

$$
\mathbf{B}_n^m = \begin{pmatrix} \tau + \frac{dv^*}{dz} & -\rho^* k_{nm}^2 & 0 & \frac{d\rho^*}{dz} & 0 & 0 \\ 0 & \tau & 0 & 0 & 1/\gamma\rho^* & 0 \\ 0 & 0 & \tau & 0 & in/\gamma\rho^* & 0 \\ \frac{v^*}{\rho^*}\frac{dv^*}{dz} & 0 & 0 & \tau + \frac{dv^*}{dz} & 0 & 0 \\ C_{51} & -\gamma p^* k_{nj}^2 & 0 & \frac{dp^*}{dz} & \tau + C_{55} & C_{56} \\ C_{61} & 0 & 0 & \frac{d\lambda^*}{dz} & C_{65} & \tau + C_{66} \end{pmatrix}
$$

$$
\mathbf{h} = -\begin{pmatrix} \rho^* \\ 0 \\ 0 \\ 0 \\ \gamma p^* \\ 0 \end{pmatrix}, \quad \mathbf{g}_n = \begin{pmatrix} \tau\frac{d\rho^*}{dz} \\ \frac{1}{\gamma\rho^*}\frac{dp^*}{dz} \\ \frac{in}{\gamma\rho^*}\frac{dp^*}{dz} \\ \tau\frac{dv^*}{dz} \\ \tau\frac{dp^*}{dz} \\ \tau\frac{d\lambda^*}{dz} \end{pmatrix}, \quad (\mathbf{q_0})_n^m = \int_0^a r J_n(k_{nj} r) \begin{pmatrix} \rho_0(r,z) \\ \int_0^r u_0(r',z)dr' \\ r w_0(r,z) \\ v_0(r,z) \\ p_0(r,z) \\ \lambda_0(r,z) \end{pmatrix} dr \tag{D.3.5}
$$

Appendix E
Two-step reaction asymptotic analysis supplement

E.1 Evolution equation integral functions

$$R_1(\lambda) = -\int_0^\lambda \frac{u_0}{r_0}\left(-\frac{\gamma-1}{\eta_0(\lambda)}\tilde{A}_1 + A_3(\lambda) + \rho_0\tilde{\beta}D_1(\lambda)\right)d\lambda \tag{E.1.1}$$

$$R_2(\lambda) = -\int_0^\lambda \frac{u_0}{r_0}\left(-\frac{\gamma-1}{\eta_0(\lambda)}\tilde{A}_2 + A_4(\lambda) + \rho_0\tilde{\beta}D_2(\lambda)\right)d\lambda \tag{E.1.2}$$

$$U_1(\lambda) = -\int_0^\lambda \frac{u_0}{r_0}\left(\frac{\gamma-1}{\eta_0(\lambda)}\left(-u_0(\lambda)\tilde{A}_1 + \rho_0(\lambda)\tilde{B}_1\right) + u_0(\lambda)A_3(\lambda) + \rho_0(\lambda)B_3(\lambda)\right)d\lambda \tag{E.1.3}$$

$$U_2(\lambda) = -\int_0^\lambda \frac{u_0}{r_0}\left(\frac{\gamma-1}{\eta_0(\lambda)}\left(-u_0(\lambda)\tilde{A}_2 + \rho_0(\lambda)\tilde{B}_2\right) + u_0(\lambda)A_4(\lambda) + \rho_0(\lambda)B_4(\lambda)\right)d\lambda \tag{E.1.4}$$

$$\begin{aligned} P_1(\lambda) = -\int_0^\lambda \frac{u_0}{r_0}\Bigg(&\frac{\gamma-1}{\eta_0(\lambda)}\left(-\frac{c_0^2}{(\gamma-1)D}\tilde{A}_1 + \tilde{B}_1 - \frac{1}{(\gamma-1)D}\tilde{C}_1\right) + \\ &\frac{c_0^2}{(\gamma-1)D}A_3(\lambda) + B_3(\lambda) - \frac{1}{(\gamma-1)D}C_3(\lambda) - u_0(\lambda)\tilde{\beta}D_1(\lambda)\Bigg)d\lambda \end{aligned} \tag{E.1.5}$$

$$\begin{aligned} P_2(\lambda) = -\int_0^\lambda \frac{u_0}{r_0}\Bigg(&\frac{\gamma-1}{\eta_0(\lambda)}\left(-\frac{c_0^2}{(\gamma-1)D}\tilde{A}_2 + \tilde{B}_2 - \frac{1}{(\gamma-1)D}\tilde{C}_2\right) + \\ &\frac{c_0^2}{(\gamma-1)D}A_4(\lambda) + B_4(\lambda) - \frac{1}{(\gamma-1)D}C_4(\lambda) - u_0(\lambda)\tilde{\beta}D_1(\lambda)\Bigg)d\lambda \end{aligned} \tag{E.1.6}$$

with

$$\tilde{B}_1 = \frac{u_0(1)}{\rho_0(1)}\tilde{A}_1 + \frac{\eta_0(1)(\rho_0(1)-1)}{(\gamma-1)\rho_0(1)} \tag{E.1.7}$$

$$\tilde{B}_2 = \frac{u_0(1)}{\rho_0(1)}\tilde{A}_2 + \frac{\eta_0(1)(\rho_0(1)-\rho_0(0))}{(\gamma-1)\rho_0(1)} \tag{E.1.8}$$

$$\tilde{C}_1 = -u_0(1)^2\tilde{A}_1 - \frac{2\eta_0(1)u_0(1)(\rho_0(1)-1)}{\gamma-1} \tag{E.1.9}$$

$$\tilde{C}_2 = -u_0(1)^2\tilde{A}_2 - \frac{2\eta_0(1)u_0(1)(\rho_0(1)-\rho_0(0))}{\gamma-1} \tag{E.1.10}$$

E.2 Obtaining $\lambda^{(1)}$

The governing equation for the reaction progress perturbation is

$$\frac{\partial \lambda^{(1)}}{\partial \lambda} + \frac{\nu}{1-\lambda}\lambda^{(1)} = -\frac{u^{(1)} - D_n - F_\tau}{u_0} \tag{E.2.1}$$

Using the modified velocity perturbation such that $\hat{u}^{(1)} = u^{(1)} - \beta(\gamma-1)(u_0/\eta_0)\lambda^{(1)}$, one obtains:

$$\frac{\partial \lambda^{(1)}}{\partial \lambda} + \frac{\nu}{1-\lambda}\lambda^{(1)} - \frac{\gamma-1}{\eta_0(\lambda)}\beta\lambda^{(1)} = -\frac{\hat{u}^{(1)} - D_n - F_\tau}{u_0} \tag{E.2.2}$$

Multiplying by a currently unknown function $U(\lambda)$, integrating from 0 to λ, and using integration by parts, one obtains

$$\begin{aligned}
&\int_0^\lambda U\frac{\partial \lambda^{(1)}}{\partial \lambda} + \int_0^\lambda U(\lambda)\lambda^{(1)}\left(\frac{\nu}{1-\lambda} - \frac{\gamma-1}{\eta_0(\lambda)}\beta\right)d\lambda = \\
&\qquad\qquad - \int_0^\lambda U(\lambda)\frac{\hat{u}^{(1)} - D_n - F_\tau}{u_0}d\lambda \\
&U(\lambda)\lambda^{(1)}\Big|_0^\lambda - \int_0^\lambda \lambda^{(1)}\frac{\partial U}{\partial \lambda}d\lambda + \int_0^\lambda U(\lambda)\lambda^{(1)}\left(\frac{\nu}{1-\lambda} - \frac{\gamma-1}{\eta_0(\lambda)}\beta\right)d\lambda = \\
&\qquad\qquad - \int_0^\lambda U(\lambda)\frac{\hat{u}^{(1)} - D_n - F_\tau}{u_0}d\lambda \\
&U(\lambda)\lambda^{(1)}\Big|_0^\lambda + \int_0^\lambda \lambda^{(1)}\left[U(\lambda)\left(\frac{\nu}{1-\lambda} - \frac{\gamma-1}{\eta_0(\lambda)}\beta\right) - \frac{dU(\lambda)}{d\lambda}\right]d\lambda = \\
&\qquad\qquad - \int_0^\lambda U(\lambda)\frac{\hat{u}^{(1)} - D_n - F_\tau}{u_0}d\lambda
\end{aligned} \tag{E.2.3}$$

Holding that

$$dU/d\lambda = U(\lambda)\left[\frac{\nu}{1-\lambda} - \frac{\gamma-1}{\eta_0(\lambda)}\right] \tag{E.2.4}$$

one can eliminate the integral on the left hand side. Therefore, solving the separable ODE above one finds

$$\int_0^\lambda \frac{dU}{U} = \nu\int_0^\lambda \frac{1}{1-\lambda}d\lambda - (\gamma-1)\beta\int_0^\lambda \frac{1}{\eta_0(\lambda)}d\lambda, \tag{E.2.5}$$

$$U(\lambda) = (1-\lambda)^{-\nu}(p_0(\lambda) - (\gamma+1)a),\ a = D^2 + \delta/\gamma \tag{E.2.6}$$

so that, finally,

$$\lambda^{(1)} = -\frac{(1-\lambda)^{\nu}}{p_0(\lambda) - a(\gamma+1)} \int_0^{\lambda} \frac{\hat{u}^{(1)} - D_n - F_{\tau}}{u_0(\lambda)(1-\lambda)^{\nu}} (p_0(\lambda) - a(\gamma+1)) d\lambda \tag{E.2.7}$$

References

[1] F. Abel, "Contributions to the history of explosive agents," *Philosophical Transactions of the Royal Society of London*, pp. 489–516, 1869.

[2] M. Berthelot and P. Vieille, "Sur la vitesse de propagation des phenomenes explosifs dans les gaz," *CR Acad. Sci., Paris*, vol. 94, pp. 101–108, 1883.

[3] E. Mallard and H. Le Chatelier, "On the propagation velocity of burning in gaseous explosive mixtures," *CR Hebd. Sceances Acad. Sci*, vol. 93, pp. 145–148, 1881.

[4] D. Chapman, "On the rate of explosion in gases," *Philos. Mag*, vol. 47, pp. 90–104, 1899.

[5] E. Jouguet, "On the propagation of chemical reactions in gases," *J. de Mathematiques Pures et Appliquees*, vol. 1, pp. 347–425, 1905.

[6] W. Rankine, "On the thermodynamic theory of waves of finite longitudinal disturbance," *Philosophical Transactions of the Royal Society of London*, vol. 160, pp. 277–288, 1870.

[7] H. Hugoniot, "Sur la propagation du movement dans les corps et spécialement dans les gaz parfaits," *J. Ecole Polytechnique*, vol. 58, pp. 1–125, 1889.

[8] V. Mikhelson, "The normal velocity of ignition of combustible gaseous mixtures," *Transactions of Moscow University*, vol. 10, pp. 1–92, 1893.

[9] W. Fickett and W. Davis, *Detonation: Theory and Experiment*. Mineola, NY: Dover, 2000.

[10] J. von Neumann, "Theory of detonation waves," in *John von Neumann, Collected Works* (A. Taub and A. Taub, eds.), vol. 2, MacMillan, 1942.

[11] Y. Zel'Dovich, "On the theory of detonation propagation in gaseous systems," *Sov. J. Exp. Theor. Phys*, vol. 10, no. 5, pp. 542–568, 1940.

[12] W. Döring, "The detonation process in gases," *Ann. Physik*, vol. 43, p. 421, 1943.

[13] G. Schott, "Observations of the structure of spinning detonation," *Physics of Fluids*, vol. 8, p. 850, 1965.

[14] C. Campbell and D. Woodhead, "The ignition of gases by an explosion wave. Part I. carbon monoxide and hydrogen mixtures," *J. chem. Soc*, vol. 4, pp. 1572–1578, 1927.

[15] J. H. Lee, *The Detonation Phenomenon*. New York: Cambridge University Press, 2008.

[16] K. Shchelkin, "Two cases of unstable combustion," *Zh. eksp. teor. Fiz*, vol. 36, pp. 600–6, 1959.

[17] R. Zaidel, "Stability of detonation waves in gas mixtures," *Doclady Academii Nauk SSSR(in Russian)*, vol. 136, no. 5, pp. 1142–1145, 1961.

[18] J. Erpenbeck, "Stability of steady-state equilibrium detonations," *Physics of Fluids*, vol. 5, pp. 604–614, 1962.

[19] J. Erpenbeck, "Stability of idealized one-reaction detonations," *Physics of Fluids*, vol. 7, pp. 684–696, 1964.

[20] F. A. Williams, *Combustion Theory*. Boulder, CO: Westview Press, 2nd ed., 1994.

[21] G. Abouseif and T. Toong, "Theory of unstable one-dimensional detonations," *Combustion and Flame*, vol. 45, pp. 67–94, 1982.

[22] R. Alpert and T. Toong, "Periodicity in exothermic hypersonic flows about blunt projectiles," *Acta Astron*, vol. 17, pp. 538–560, 1972.

[23] H. Lee and D. Stewart, "Calculation of linear detonation stability: one-dimensional instability of plane detonation," *Journal of Fluid Mechanics*, vol. 216, pp. 103–132, 1990.

[24] V. Pukhnachev, "The stability of chapman-jouget detonations," *Dokl. Akad. Nauk SSSR*, vol. 149, pp. 798–801, 1963.

[25] M. Short, "Multidimensional linear stability of detonation wave at high activation energy," *SIAM Journal on Applied mathematics*, vol. 57, no. 50, pp. 307–326, 1997.

[26] M. Short and D. Stewart, "Cellular detonation stability. part 1. a normal-mode linear analysis," *Journal of Fluid Mechanics*, vol. 368, pp. 229–262, 1998.

[27] A. Kasimov and D. Stewart, "Spinning instability of gaseous detonations," *Journal of Fluid Mechanics*, vol. 406, pp. 179–203, 2002.

[28] D. Stewart and A. Kasimov, "State of detonation stability theory and its application to propulsion," *Journal of Propulsion and Power*, vol. 22, no. 6, pp. 1230–1244, 2006.

[29] M. Morkovin, "Critical evaluation of transition from laminar to turbulent shear layers with emphasis on hypersonic traveling bodies," Tech. Rep. AFRL Report AFF DL-TR-68-149, Air Force Flight Dynamics laboratory, Wright-Patterson AFB, OH, USA, 1969.

[30] E. Reshotko, "Boundary-layer stability and transition," *Annual Reviews in Fluid Mechanics*, vol. 8, pp. 311–349, 1976.

[31] E. Forgoston and A. Tumin, "Initial value problem for three-dimensional disturbances in a hypersonic boundary layer," *Physics of Fluids*, vol. 17, no. 083106, 2005.

[32] A. Tumin, "Initial-value problem for small disturbances in an idealized one-dimensional detonation," *Physics of Fluids*, vol. 19, no. 106105, 2007. See also: Tumin, A., Stability of idealized one-reaction detonations revisited, AIAA Paper 2007-0897, January 2007.

[33] C. Chiquete, I. Shalaev, and A. Tumin, "Receptivity of plane idealized one-reaction detonations to three- dimensional perturbations," 46th. AIAA Meeting and Exhibit, January 2008. Paper No. 2008-1038.

[34] G. Sharpe, "Linear stability of idealized detonations," *Proc. R. Soc. Lond. A*, vol. 453, pp. 2603–2625, 1997.

[35] C. Chiquete and A. Tumin, "Initial value problem for small perturbations in an idealized cj detonation," Proceedings of the 6th U.S. National Combustion Meeting, May 2009. Paper # 32F1.

[36] G. Namah, C. Brauner, J. Buckmaster, and C. Schmidt-Laine, "Linear stability of one-dimensional detonations," in *Dynamical Issues in Combustion Theory* (A. Friedman and W. M. Jr., eds.), vol. 35, pp. 229–239, New York: Springer-Verlag, 1991.

[37] J. Buckmaster and J. Neves, "One-dimensional detonation stability: the spectrum for infinite activation energy," *Physics of Fluids*, vol. 31, no. 12, pp. 3571–3576, 1988.

[38] C. Chiquete and A. Tumin, "Multidomain spectral collocation method for three-dimensional perturbations in idealized cj detonations," Proceedings of the Western States Sections of the Combustion Institute, October 2009. Paper # 09F-41.

[39] M. Radulescu and J. Lee, "The failure mechanism of gaseous detonations: experiments in porous wall tubes," *Combustion and Flame*, vol. 131, no. 1-2, pp. 29–46, 2002.

[40] A. Teodorczyk and J. Lee, "Detonation attenuation by foams and wire meshes lining the walls," *Shock Waves*, vol. 4, no. 4, pp. 225–236, 1995.

[41] J. Austin, *The role of instability in gaseous detonation*. PhD thesis, PhD thesis, California Institute of Technology, Pasadena, California, 2003.

[42] C. Chiquete and A. Tumin, "A normal mode stability analysis of an idealized detonation in a cylindrical pipe with slightly porous walls," Proceedings of the 7th U.S. National Combustion Meeting, March 2011. Paper # 2F14.

[43] C. Chiquete and M. Short, "Asymptotic study of pulsating evolution of overdriven and cj detonation with a chain-branching kinetics model s," 23rd ICDERS Meeting, July 2011. Paper # 295.

[44] P. Drazin and W. Reid, *Hydrodynamic stability*. Cambridge Univ Pr, 2004.

[45] M. Goldstein, "Scattering of acoustic waves into tollmien-schlichting waves by small streamwise variations in surface geometry," *Journal of Fluid Mechanics*, vol. 154, no. -1, pp. 509–529, 1985.

[46] J. Buckmaster and C. Ludford, "The effect of structure on the stability of detonations i. role of the induction zone," in *Twenty-first Symposium on Combustion*, pp. 1669–1676, The Combustion Institute, 1986.

[47] E. Kamke, *Differentialgleichungen. Losungsmethoden und Losungen*. Leipzig: Akademische Verlagsgesellschaft Geest & Portig, 1959.

[48] A. Tumin, "Multi-domain spectral collocation method of stability of detonations," *AIAA Journal*, vol. 45, pp. 2356–2359, 2007.

[49] W. Wasow, *Asymptotic expansions for ordinary differential equations*. New York: Interscience, 1965.

[50] M. Short, I. Anguelova, T. Aslam, J. Bdzil, A. Henrick, and G. Sharpe, "Stability of detonations for an idealized condensed-phase model," *Journal of Fluid Mechanics*, vol. 595, pp. 45–82, 2008.

[51] C. Canuto, M. Hussaini, A. Quaternoni, and T. Zang, *Spectral Methods in Fluid Dynamics*. Berlin: Springer-Verlag, 1988.

[52] I. Shalaev and A. Tumin, "Initial-value problem for perturbations of idealized detonations in circular pipes," *Combustion Theory and Modelling*, vol. 14, no. 1, pp. 1–22, 2010.

[53] A. Pierce, *Acoustics: an introduction to its physical principles and applications*. Acoustical Society of Amer, 1989.

[54] A. Webster, "Acoustical Impedance and the Theory of Horns and of the Phonograph," *Proceedings of the National Academy of Sciences of the United States of America*, vol. 5, no. 7, p. 275, 1919.

[55] A. Kennelly and K. Kurokawa, "Acoustic Impedance," in *Proc. Am. Ac. Arts and Sc*, vol. 56, pp. 1–42, 1921.

[56] K. Taylor, "Acoustic generation by vibrating bodies in homentropic potential flow at low mach number," *Journal of Sound and Vibration*, vol. 65, no. 1, pp. 125–136, 1979.

[57] M. Myers, "On the acoustic boundary condition in the presence of flow," *Journal of Sound and Vibration*, vol. 71, no. 3, pp. 429–434, 1980.

[58] F. Farassat and M. Dunn, "A simple derivation of the acoustic boundary condition in the presence of flow," *Journal of sound and vibration*, vol. 224, pp. 384–386, 1999.

[59] E. Zauderer, *Partial differential equations of applied mathematics*. New York: Wiley-Interscience, 1989.

[60] S. Agrawal and C. Patel, "On convergence of Fourier-Bessel series," *Bull. Acad. Polon. Sci., Ser. Sci. Math., Astronom. et Phys*, vol. 23, pp. 1255–1263, 1975.

[61] M. Stinson and Y. Champoux, "Propagation of sound and the assignment of shape factors in model porous materials having simple pore geometries," *The Journal of the Acoustical Society of America*, vol. 91, p. 685, 1992.

[62] V. Kozlov, A. Fedorov, and N. Malmuth, "Acoustic properties of rarefied gases inside pores of simple geometries," *The Journal of the Acoustical Society of America*, vol. 117, p. 3402, 2005.

[63] W. Gordon, A. Mooradian, and S. Harper, "Limit and spin effects in hydrogen-oxygen detonations," in *Symposium (International) on Combustion*, vol. 7, pp. 752–759, Elsevier, 1958.

[64] M. Short and J. Quirk, "On the nonlinear stability and detonability limit of a detonation wave for a model three-step chain-branching reaction," *Journal of Fluid Mechanics*, vol. 339, pp. 89–119, 1997.

[65] J. McVey and T. Toong, "Mechanism of instabilities of exothermic hypersonic blunt-body flows(Exothermic hypersonic blunt body flow periodic instability mechanism, using ballistic range with schlieren photographic equipment)," *Combustion Science and Technology*, vol. 3, no. 2, pp. 63–76, 1971.

[66] H. Lehr, "Experiments on shock-induced combustion," *Astronautica Acta*, vol. 17, pp. 589–597, 1972.

[67] M. Kaneshige and J. Shepherd, "Oblique detonation stabilized on a hypervelocity projectile," in *Symposium (International) on Combustion*, vol. 26, pp. 3015–3022, Elsevier, 1996.

[68] E. Oran and J. Boris, *Numerical simulation of reactive flow*, vol. 275. Elsevier New York, 1987.

[69] M. Short, "A nonlinear evolution equation for pulsating Chapman-Jouguet detonations with chain-branching kinetics," *Journal of Fluid Mechanics*, vol. 430, pp. 381–400, 2001.

[70] M. Short and J. B. Bdzil, "Propagating laws for steady curved detonations with chain-branching kinetics," *Journal of Fluid Mechanics*, vol. 479, pp. 39–64, 2003.

[71] M. Short and G. J. Sharpe, "Pulsating instability of detonations with a two-step chain-branching reaction model: theory and numerics," *Combution Theory and Modeling*, vol. 7, pp. 401–416, 2003.

[72] M. Short, "Multidimensional linear stability of a detonation wave at high activation energy," *SIAM Journal on Applied Mathematics*, vol. 57, pp. 307–326, 1997.

[73] J. Buckmaster and G. Ludford, "The effect of structure on the stability of detonations I. Role of the induction zone," in *Symposium (International) on Combustion*, vol. 21, pp. 1669–1676, Elsevier, 1988.